Printable Green RFID Antennas for Embedded Sensors

YASAR AMIN

Doctoral Thesis in Electronic and Computer Systems
Stockholm, Sweden 2013

TRITA-ICT/ECS AVH 12:12
ISSN 1653-6363
ISRN KTH/ICT/ECS/AVH-12/12-SE
ISBN 978-91-7501-619-1

KTH School of Information and
Communication Technology
SE-164 40 Kista
Sweden

Akademisk avhandling som med tillstånd av Kungl Tekniska högskolan framlägges till offentlig granskning för avläggande av teknologie doktorsexamen 2013-02-25, klockan 13:00 i Sal E, Forum, Isafjordsgatan 39, Kista.

Tryck: Universitetsservice US AB

In The Name of God

I would like to dedicate this thesis to my ***family***

Abstract

In the recent years, radio-frequency identification (RFID) technology has been widely integrated into modern society applications, ranging from barcode successor to retail supply chain, remote monitoring, detection and healthcare, for instance. In general, an RFID tag or transponder is composed of an antenna and an application-specific integrated circuit chip. In a passive UHF RFID system (which is the focus of presented research), the communication between the transponder tag and the reader is established by modulating the radar cross section (RCS) of the transponder tag. The need for flexible RFID tags has recently been increased enormously; particularly the RFID tags for the UHF band ensure the widest use but in the meantime face considerable challenges of cost, reliability and environmental friendliness.

The multidimensional focus of the aforementioned research encompasses the production of low-cost and reliable RFID tags. The state-of-the-art fabrication methods and materials for proposed antennas are evaluated in order to surmount the hurdles for realization of flexible green electronics. Moreover, this work addresses the new rising issues interrelated to the field of economic and eco-friendly tags comprising of paper substrate. Paper substrates offer numerous advantages for manufacturing RFID tags, not only is paper extensively available, and inexpensive; it is lightweight, recyclable and can be rolled or folded into 3D configurations.

The most important aspect of an RFID system's performance is the reading range. In this research several pivotal challenges for item-level tagging, are resolved by evolving novel structures of progressive meander line, quadrate bowtie and rounded corner bowtie antennas in order to maximize the reading distance with a prior selected microchip under the various constraints (such as limited antenna size, specific antenna impedance, radiation pattern requirements). This approach is rigorously evolved for the realization of innovative RFID tag antenna which has incorporated humidity sensor functionality along with calibration mechanism due to distinctiveness of its structural behavior which will be an optimal choice for future ubiquitous wireless sensor network (WSN) modules.

The RFID market has grown in a two-dimensional trend, one side constitutes standalone RFID systems. On the other side, more ultramodern approach is paving its way, in which RFID needs to be integrated with broad operational array of distinct applications for performing different functions including sensors, navigation, broadcasting, and personal communication, to mention a few. Using different antennas to include all communication bands is a straightforward approach, but at the same time, it leads to increase cost, weight, more surface area for installation, and above all electromagnetic compatibility issues. The indicated predicament is solved by realization of proposed single wideband planar spirals and sinuous antennas which covers several bands from 0.8–3.0GHz. These antennas exhibit exceptional performance throughout the operational range of significance, thus paving the way for developing eco-friendly multi-module RF industrial solutions.

Acknowledgements

The highest praise is God's for supporting me during this and all other steps of my life. One of the joys of completion is to look over the journey past and remember all the friends and family who have helped and supported me along this long but fulfilling road.

I would like to express my heartfelt gratitude to Professor Hannu Tenhunen, Professor Li-Rong Zheng, and Dr. Qiang Chen, who are not only mentors but dear friends. I could not have asked for better role models, each inspirational, supportive, and patient. I could not be prouder of my academic roots and hope that I can in turn pass on the research values, and the dreams that they have given to me.

My colossal thanks to Professor Axel Jantsch for his help and generous support during my PhD work. I would also like to thank Professor Urban Westergren who provided encouraging and constructive feedback. It is no easy task, reviewing a thesis, and I am grateful for his thoughtful and comprehensive comments. It gives me great pleasure in acknowledging the support and help of Professor Elena Dubrova. To the many anonymous reviewers of the various conferences and journals, thanks for helping to shape and guide the direction of the work with your careful and instructive comments. I would like to thank all former and current administrative staff at KTH, especially Alina Munteanu for her brilliant administrative work. Thanks IT service groups at KTH to keep servers and computers alive.

As a member of iPack VINN Excellence Center and Electronic Systems department, I have been surrounded by glorious colleagues; both communities have provided a rich and fertile environment to study and explore new ideas. I acknowledge valuable discussion with all of my friends and colleagues at KTH; Botao Shao, Ana Lopez Cabezas, Geng Yang, Yi Feng, Awet Yemane Weldezion and Liu Zhiying for being working as an impressive team member throughout my PhD studies. I appreciate my dear friends, Muhammad Ali Shami, Omar Malik and Muhammad Adeel Tajammul for their excellent support throughout my MBA and PhD studies. I would like to thank Dr. Fredrik Jonsson, Dr. Majid Baghaei Nejad and Dr. Julius Hållstedt for always welcoming me as a friend and helping to develop the ideas in this thesis. Professor Antti Paasio, Professor Pasi Malinen, Professor Pasi Liljeberg, Rajeev Kumar Kanth, Sari Stenvall-Virtanen, colleagues at the TSE and TUCS, Turku University, thank you.

My personal thanks to the Higher Education Commission (HEC), Pakistan,

and University of Engineering and Technology, Taxila, Pakistan for awarding me a scholarship and an opportunity to pursue my education towards PhD in Sweden which ultimately blended with MBA programme for PhD students. I also appreciate the financial support provided by iPack center for the PhD research work.

My special thanks to my father who shares my passions and rekindling dreams. My profound thankfulness to my mother, and my parents-in-law for their infinite patience and love.

I also appreciate my brothers especially Saad Amin and my beloved sister and also my brothers-in-law and sisters-in-law for their love and prayers. Finally, but most importantly, I would like to give my deepest gratitude to Aiysha, my dear wife, for her enormous help and support. All of my achievements have an invisible part of your contribution.

Yasar Amin, 2013

Contents

List of Figures

List of Tables

List of Acronyms

2D Two Dimensional

3D Three Dimensional

3G Third-Generation Cell-Phone Technology

4G 4th Generation (wireless/mobile communications)

AB Aktiebolag

AIDC Automatic Identification and Data Capture

Al Aluminum

ASIC Application-Specific Integrated Circuit

AUT Antenna Under Test

CAD Computer-Aided Design

CAGR Cumulative Average Growth Rate

CLIP Conductive Low-cost Ink Project

CW Continuous-wave

dB Decibel

dBi Decibels referenced to Isotropic gain

DC Direct Current

DCB Dichlorobenzene

DMP Dimatix Materials Printer

DOD Drop On Demand

DPI Dots Per Inch

DPP Dry Phase Patterning

EIRP Equivalent Isotropically Radiated Power

EM Electromagnetic(s)

EPC Electronic Product Code

ETSI European Telecommunications Standards Institute

EU European Union

FCC Federal Communications Commission

FDTD Finite Difference Time Domain

FEM Finite Element Method

FESEM Field Emission Scanning Electron Microscope

FLEXO Flexography

FR-4 Flame Retardant 4

GND Ground

HF High Frequency

HFSS High Frequency Structure Simulator

HP Hewlett Packard

IC Integrated Circuit

ICT Information and Communication Technology

IoT Internet-of-Things

ISM Industrial, Scientific and Medical (Radio Bands)

ISO International Organization for Standardization

IT Information Technology

KTH Kungliga Tekniska Högskolan

LF Low Frequency

LHCP Left Hand Circular Polarization

LTE Long Term Evolution

MEMS Micro-Electro-Mechanical Systems

MRO Maintenance, Repair and Overhaul

MWF Microwave Frequency

NA North America

NTS Nano Technology Systems

NXP Next Experience

OE-A Organic Electronics Association

OLED Organic Light Emitting Display

PC Personal Computer

PEC Perfect Electrical Conductor

PEN Polyethylene Naphthalate

PET Polyethylene Terepthalate

PTF Polymer Thick Film

RF Radio Frequency

RFID Radio Frequency Identification

RHCP Right Hand Circular Polarization

SEM Scanning Electron Microscope

SICS Swedish Institute of Computer Science

SMA SubMiniature Version A

SOL Short-Open-Load

SOLT Short-Open-Load-Through

TI Texas Instruments

UHF Ultra High Frequency

USN Ubiquitous Sensor Network

VNA Vector Network Analyzer

VTT Valtion Teknillinen Tutkimuskeskus

WEB World Electronic Broadcast

WiFi Wireless Fidelity

XWB Extra Wide Body

List of Publications

Papers included in this thesis:

1. Y. Amin, Q. Chen, H. Tenhunen, and L.-R. Zheng, "Evolutionary versatile printable RFID antennas for "green" electronics," *Journal of Electromagnetic Waves and Applications*, vol. 26, nos. 2-3, pp. 264-273, 2012.

2. Y. Amin, Q. Chen, H. Tenhunen, and L.-R. Zheng, "Performance-optimized quadrate bowtie RFID antennas for cost-effective and eco-friendly industrial applications," *Progress in Electromagnetics Research*, vol. 126, pp. 49-64, 2012.

3. Y. Amin, Q. Chen, L.-R. Zheng, and H. Tenhunen, "Development and analysis of flexible UHF RFID antennas for "green" electronics," *Progress in Electromagnetics Research*, vol. 130, pp. 1-15, 2012.

4. Y. Amin, J. Hållstedt, H. Tenhunen, and L.-R. Zheng, "Design of novel paper-based inkjet printed rounded corner bowtie antenna for RFID applications," *Sensors & Transducers Journal*, vol. 115, no. 4, pp. 160-167, 2010.

5. Y. Amin, R. K. Kanth, P. Liljeberg, Q. Chen, L.-R. Zheng, and H. Tenhunen, "Performance-optimized printed wideband RFID antenna and environmental impact analysis," *ETRI Journal*, submitted for publication, 2012.

6. Y. Amin, R. K. Kanth, P. Liljeberg, Q. Chen, L.-R. Zheng, and H. Tenhunen, "Green wideband RFID tag antenna for supply chain applications," *IEICE Electronics Express*, vol. 9, no. 24, pp. 1861-1866, 2012.

7. Y. Amin, Q. Chen, L.-R. Zheng, and H. Tenhunen, "Design and fabrication of wideband archimedean spiral antenna based ultra-low cost "green" modules for RFID sensing and wireless applications," *Progress in Electromagnetics Research*, vol. 130, pp. 241-256, 2012.

8. Y. Amin, Q. Chen, L.-R. Zheng, and H. Tenhunen, ""Green" wideband log-spiral antenna for RFID sensing and wireless applications," *Journal of Electromagnetic Waves and Applications*, vol. 26, nos. 14-15, pp. 2043-2050, 2012.

9. Y. Amin, Q. Chen, L.-R. Zheng, and H. Tenhunen, "Two-arm sinuous antenna for RFID ubiquitous sensors and wireless applications," *Journal of Electromagnetic Waves and Applications*, vol. 26, nos. 17-18, pp. 2365-2371, 2012.

10. Y. Amin, Y. Feng, Q. Chen, L.-R. Zheng, and H. Tenhunen, "RFID antenna humidity sensor co-design for USN applications," *IEICE Electronics Express*, submitted for publication, 2013.

Related publications not included in this thesis:

11. Y. Amin, Q. Chen, B. Shao, J. Hållstedt, H. Tenhunen, and L.-R. Zheng, "Design and analysis of efficient and compact antenna for paper based UHF RFID tags," in *IEEE International Symposium on Antennas, Propagation and EM Theory (ISAPE 2008)*, China, pp. 62-65.

12. Y. Amin, S. Prokkola, B. Shao, J. Hållstedt, H. Tenhunen, and L.-R. Zheng, "Inkjet printed paper based quadrate bowtie antennas for UHF RFID tags," in 11^{th} *IEEE International Conference on Advanced Communication Technology (ICACT 2009)*, Korea, pp. 109-112.

13. Y. Amin, B. Shao, J. Hållstedt, S. Prokkola, H. Tenhunen, and L.-R. Zheng, "Design and characterization of efficient flexible UHF RFID tag antennas," in *IEEE European Conference on Antennas and Propagation (EUCAP 2009)*, Germany, pp. 2784-2786.

14. B. Shao, Q. Chen, Y. Amin, J. Hållstedt, R. Liu, H. Tenhunen, and L.-R. Zheng, "Process-dependence of inkjet printed folded dipole antenna for 2.45 GHz RFID tags," in *IEEE European Conference on Antennas and Propagation (EUCAP 2009)*, Germany, pp. 2338-2339.

15. Y. Amin, S. Prokkola, B. Shao, J. Hållstedt, Q. Chen, H. Tenhunen, and L.-R. Zheng, "Low cost paper based bowtie tag antenna for high performance UHF RFID applications," in *Proceedings of Nanotech 2009*, USA, vol. 1, pp. 538-541.

16. Y. Amin, J. Hållstedt, S. Prokkola, H. Tenhunen, and L.-R. Zheng, "Robust flexible high performance UHF RFID tag antenna," in *IEEE Electronic Packaging Technology Conference (EPTC 2009)*, Singapore, pp. 235-239.

17. B. Shao, Q. Chen, Y. Amin, D. S. Mendoza, R. Liu and L.-R. Zheng, "An ultra-low-cost RFID tag with 1.67 Gbps data rate by ink-jet printing on paper substrate," in *IEEE Solid State Circuits Conference (A-SSCC 2010)*, China, pp. 1-4.

18. R. K. Kanth, W. Ahmad, Y. Amin, P. Liljeberg, L.-R. Zheng, and H. Tenhunen, "Analysis, design and development of novel, low profile 2.487 GHz microstrip antenna," in *IEEE Symposium on Antenna Technology*

and Applied Electromagnetics & the American Electromagnetics Conference 2010, Canada, pp. 1-4.

19. R. K. Kanth, P. Liljeberg, H. Tenhunen, H. Kumar, Y. Amin, Q. Chen and Li-Rong Zheng, "Quantifying the environmental footprint of rigid substrate printed antenna," in *IEEE International conference on Technology and Society in Aisa 2012*, Singapore, pp. 1-5.

20. R. K. Kanth, P. Liljeberg, H. Tenhunen, Q. Wan, Y. Amin, B. Shao, Q. Chen, L.-R. Zheng, and H. Kumar, "Evaluating sustainability, environmental assessment and toxic emissions during manufacturing process of RFID based systems," in *IEEE* 9^{th} *International Conference on Dependable, Autonomic and Secure Computing (DASC 2011)*, Australia, pp. 1066-1071.

21. R. K. Kanth, P. Liljeberg, H. Tenhunen, Y. Amin, Q. Chen, and L.-R. Zheng, "Comparative end-of-life study of polymer and paper based radio frequency devices," *International Journal of Environmental Protection (IJEP)*, vol. 2, no. 8, pp.1-5, 2012.

22. Y. Amin, B. Shao, Q. Chen, L.-R. Zheng, and H. Tenhunen, "Electromagnetic analysis of RFID antennas for "green" electronics," *Electromagnetics*, accepted for publication, 2012.

Summary of the included papers

Paper I Y. Amin, Q. Chen, H. Tenhunen, and L.-R. Zheng, "Evolutionary versatile printable RFID antennas for "green" electronics," *Journal of Electromagnetic Waves and Applications*, vol. 26, nos. 2-3, pp. 264-273, 2012.

The development of low cost directly printable RFID tag antennas is essential for item-level tracking. In this paper evolutionary design approach to achieve robust extremely versatile RFID antennas on paper/flexible substrates which allow a simple integration directly on e.g. paperboard in a roll-to-roll production line is presented. Fully integrated printed tags for "green" electronics are designed for operability in frequencies 866–868MHz & 902–928MHz. Moreover, we have presented benchmarking results for various challenges of antennas in terms of ruggedness, reliability and flexing performance.

The author's contribution: The author is responsible for all related work in this publication including antennas designing, inkjet fabrication, performance & measurement analysis, and writing the manuscript.

Paper II Y. Amin, Q. Chen, H. Tenhunen, and L.-R. Zheng, "Performance-optimized quadrate bowtie RFID antennas for cost-effective and eco-friendly industrial applications," *Progress in Electromagnetics Research*, vol. 126, pp. 49-64, 2012.

In this paper, an in-depth efficient optimization for high performance tag antenna designs for operability in frequencies 866–868MHz & 902–928MHz is presented. Fully integrated printed RFID antennas show potential solution for item level labeling applications. In order to accommodate the antenna during the package printing process, it is vastly preferred that antenna structures are printed on paper substrates. However, the electromagnetic properties and thickness of paper substrates are susceptible to change due to various environmental effects. Thus, adequately consistent in performance and material insensitive printed Quadrate Bowtie RFID antennas are proposed. It is demonstrated that the proposed antennas can tolerate a considerable variation in the permittivity on thin paper substrates, and present excellent results when n across metal and water containing objects.

The author's contribution: The author is responsible for all related work in this publication including antennas designing, inkjet fabrication, performance & measurement analysis, and writing the manuscript.

Paper III Y. Amin, Q. Chen, L.-R. Zheng, and H. Tenhunen, "Development and analysis of flexible UHF RFID antennas for "green" electronics," *Progress in Electromagnetics Research*, vol. 130, pp. 1-15, 2012.

In this paper, novel Bowtie antennas which cover complete UHF RFID band (860–960MHz), fabricated on various ultra-low-cost substrates using state-of-the-art printing technologies are investigated as an approach that aims to accommodate the antenna during the package printing process whilst faster production on commercially available paper. The proposed antenna structures are evaluated in reference to circuit and field concepts, to exhibit extreme degree of functional versatility. These antennas are developed to cater the variations which appear in electromagnetic properties and thickness of paper substrate due to various environmental effects. Computed (simulated) and well-agreed measurement results confirm a superior performance of the tag modules while stepping towards next generation of "green" tags.

The author's contribution: The author is responsible for all related work in this publication including antennas designing, inkjet fabrication, performance & measurement analysis, and writing the manuscript.

Paper IV Y. Amin, J. Hållstedt, H. Tenhunen, and L.-R. Zheng, "Design of novel paper-based inkjet printed rounded corner bowtie antenna for RFID applications," *Sensors & Transducers Journal*, vol. 115, no. 4, pp. 160-167, 2010.

This paper presents a novel inkjet printed rounded corner bowtie antenna with T-matching stubs on paper substrate, which is the cheapest and widest available substrate. The antenna exhibits compact size with outstanding read range and complete coverage of UHF RFID band (860–960MHz). The design criteria are discussed; challenges outlined generic design process with a focus on inkjet printing, and analyzed the results due to variation in paper dielectric constant. The antenna has a wider bandwidth for catering the fabrication disparity. The results show extreme immunity of the proposed antenna against paper dielectric constant variation.

The author's contribution: The author is responsible for all related work in this publication including antennas designing, inkjet fabrication, performance & measurement analysis, and writing the manuscript.

Paper V Y. Amin, R. K. Kanth, P. Liljeberg, Q. Chen, L.-R. Zheng, and H. Tenhunen, "Performance-optimized printed wideband RFID antenna and environmental impact analysis," *ETRI Journal*, submitted for publication, 2012.

This paper presents performance optimized RFID tag antenna, developed by using commercially accessible paper substrates and advanced inkjet printing

process to guarantee mechanical flexibility and ultra-low production costs. The proposed antenna structure can endure the variations which emerge in electromagnetic properties of paper substrate due to varying environmental effects. Hole-matching technique is implemented to eliminate the matching network for reducing the consumption of conductive ink. The proposed structure is uniquely evaluated by demonstrating, sustainability and environmental impact analysis that validate the potential for ultra-low cost mass production of RFID tags for future generation of organic electronics. The antenna performance is assessed for cardboard cartons exclusively containing metal cans and water bottles. The experimental characterization of the proposed antenna endorses the wider bandwidth to cover UHF RFID ISM band (860–960MHz), which empowers its usage throughout the globe for supply chain applications. The improved design effectuates return loss of better than –15dB over a wide frequency range while exhibiting outstanding readability from 10.1 meters.

The author's contribution: The author is responsible for all related work in this publication including antennas designing, inkjet fabrication, performance & measurement analysis, and writing the manuscript except the sustainability and environmental impacts analysis.

Paper VI Y. Amin, R. K. Kanth, P. Liljeberg, Q. Chen, L.-R. Zheng, and H. Tenhunen, "Green wideband RFID tag antenna for supply chain applications," *IEICE Electronics Express*, vol. 9, no. 24, pp. 1861-1866, 2012.

In this paper, we demonstrated an RFID tag antenna manufactured by advanced inkjet printing technology on paper substrate using novel hole-matching technique for reducing the consumption of substrate material and conductive ink while attaining green RFID tags. In-depth electromagnetic analysis is performed methodologically for optimizing the parameters that effectuate the antenna dimensions. The antenna design is optimized for consistent wideband performance and extended read range throughout the complete UHF RFID band (860–960MHz), while exhibiting benchmarking results when n across cardboard cartons filled with metal or water containing objects.

The author's contribution: The author is responsible for all related work in this publication including antennas designing, inkjet fabrication, performance & measurement analysis.

Paper VII Y. Amin, Q. Chen, L.-R. Zheng, and H. Tenhunen, "Design and fabrication of wideband archimedean spiral antenna based ultra-low cost "green" modules for RFID sensing and wireless applications," *Progress in Electromagnetics Research*, vol. 130, pp. 241-256, 2012.

In this paper, a parametric analysis is performed for a wideband Archimedean spiral antenna in recognition of an emerging concept to integrate RFID along with several applications by using a single antenna. The antenna is fabricated using state-of-the-art inkjet printing technology on various commercially available paper substrates to provide the low-cost, flexible RF modules

for the next generation of "green" electronics. The effects on electromagnetic characteristics of the planar Archimedean spiral antenna, due to the use of paper are investigated besides other parameters. The proposed antenna is evaluated and optimized for operational range from 0.8–3.0GHz. It exhibits exceptional coverage throughout numerous RFID ISM bands so do for other wireless applications.

The author's contribution: The author is responsible for all related work in this publication including antennas designing, inkjet fabrication, performance & measurement analysis, and writing the manuscript.

Paper VIII Y. Amin, Q. Chen, L.-R. Zheng, and H. Tenhunen, ""Green" wideband log-spiral antenna for RFID sensing and wireless applications," *Journal of Electromagnetic Waves and Applications*, vol. 26, nos. 14-15, pp. 2043-2050, 2012.

In this paper, the novel idea of integrating RFID with sensors along with other wireless applications by using single tag antenna is implemented, by fabricating proposed antenna using state-of-the-art inkjet printing technology on commercially available paper substrates. For the first time, a parametric analysis is performed for realization of planar log-spiral antenna on paper for operational range from 0.8–3.0GHz, which also exhibits excellent coverage throughout numerous RFID ISM bands, and for other wireless applications. The ANSYS HFSS™ tool is used to design and predict the performance of the proposed antenna in terms of radiation pattern and input impedance.

The author's contribution: The author is responsible for all related work in this publication including antennas designing, inkjet fabrication, performance & measurement analysis, and writing the manuscript.

Paper IX Y. Amin, Q. Chen, L.-R. Zheng, and H. Tenhunen, "Two-arm sinuous antenna for RFID ubiquitous sensors and wireless applications," *Journal of Electromagnetic Waves and Applications*, vol. 26, nos. 17-18, pp. 2365-2371, 2012.

In this paper, two-arm planar sinuous antenna is demonstrated to realize the emerging concept of integrating RFID functionalities along with sensors and other wireless applications for "green" electronics. In-depth, parametric analysis is performed for the proposed antenna which is fabricated on paper substrate using revolutionary inkjet printing technology to develop a system-level solution for ultra-low cost mass production of multi-purpose wireless tags in an approach that could be easily expanded to other microwave and wireless "cognition" applications. The proposed antenna exhibits excellent performance throughout several RFID ISM bands, and for other wireless applications in its operational range from 0.8–3.0GHz.

The author's contribution: The author is responsible for all related work in this publication including antennas designing, inkjet fabrication, performance & measurement analysis, and writing the manuscript.

Paper X Y. Amin, Y. Feng, Q. Chen, L.-R. Zheng, and H. Tenhunen, "RFID antenna humidity sensor co-design for USN applications," *IEICE Electronics Express*, submitted for publication, 2013.

In this letter, an RFID tag antenna which has incorporated humidity sensor functionality along with calibration mechanism due to distinctiveness of its structural behavior, is proposed. The sensor-enabled antenna is directly printed on paper substrate using state-of-the-art inkjet printing technology for realizing the eco-friendly and ultra-low cost Ubiquitous Sensor Network (USN) module. The antenna has reduced profile that paves the way for small item-level tagging and monitoring. The effect of humidity on paper-based antenna characteristics along with other electromagnetic parameters is investigated to evaluate the antenna performance under realistic operating conditions. The proposed antenna exhibits wider operational bandwidth and extended read range while at the same time provides an additional degree of freedom for sensor calibration.

The author's contribution: The author is responsible for all related work in this publication including antennas designing, inkjet fabrication, performance & measurement analysis, and writing the manuscript.

Chapter 1

Introduction

1.1 Background

1.1.1 Ubiquitous Sensor Networks

The next wave in the era of intelligent sensing and processing will be outside the realm of the traditional desktop. In the Internet-of-Things paradigm (IoT) [198], selective information from any item of a certain value is on the network in one form or another. Radio frequency IDentification (RFID) and sensor network technologies are giving fuel to this evolving standard, in which information and communication are invisibly embedded in our surroundings. In this context, everyday objects, such as cars, packages of food beverages, refrigerator items, medical equipments, logistics, and more advanced, loosely coupled, computational and information services will not merely be in the range of each other's interaction but also communicate with one another [65, 1]. This signifies the futurity internet will be object-to-object communication rather than machine-to-machine communication [94].

Significant amounts of information from sensor enabled devices will flow in order to furnish smart, and proactive environments that will expressively meliorate both work and leisure experiences of people. Smart interacting physical object that conform to the current situation, without any human participation will become the next ratiocinative step to hoi polloi already linked up anytime and anywhere [159]. With the growing presence of WiFi, 3G and 4G LTE wireless Internet access, the evolution towards **U**biquitous **S**ensor **N**etworks (Figure 1.1) is already discernible today [220]. However, the Internet-of-Things[1] vision for successfully emerging demands:

1. The computing standard to go beyond traditional mobile computing scenarios that employ smartphones and portables [224], and develop into connecting conventional existing objects and embedding intelligence into our environs.

[1] Internet-of-Things denotes to a ubiquitous network society in which a vast collection of objects is "connected."

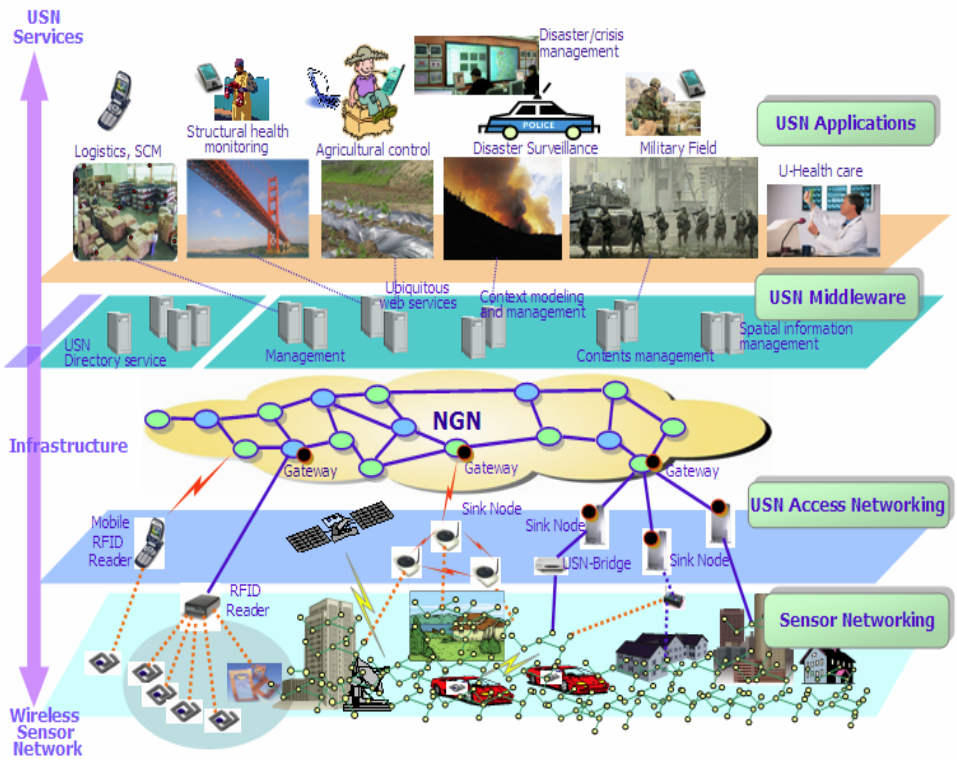

Figure 1.1: The vision of Ubiquitous Sensor Networks. (Courtesy: ITU NGN-GSI)

2. The sensor based technology to disappear from the cognizance of the user while at the same time incorporated in every item for being detected.

1.1.2 Evolution of RFID-Enabled Ubiquitous Sensing

The significant advantages and wide applicability of RFID systems and Wireless sensor networks (WSNs) elevated them as the most ubiquitous computing technologies in contemporary literature [50, 89, 149, 116]. It is highly anticipated by analyzing the consumer and technology trends that, in the near future, a number of devices such as wireless tags, and sensors especially in embedded form will increase by manifold as compared to the current scenario. These devices collect and transmit information about people, wildlife, livestock, objects and their ambient environment, which corresponds to identification, sensing and information processing. In the current 2011 report of IDTechEx, the economic value related to RFID market is anticipated as $5.84 billion, up from $5.63 billion recorded in 2010. This is the accumulative impact of RFID tags, readers, software services related with

RFID cards, labels, fobs and all other form factors. These all factors will lead to an estimated growth of USN/WSN market by 2021 to $2 billion as compared to $0.45 billion in 2011 [23].

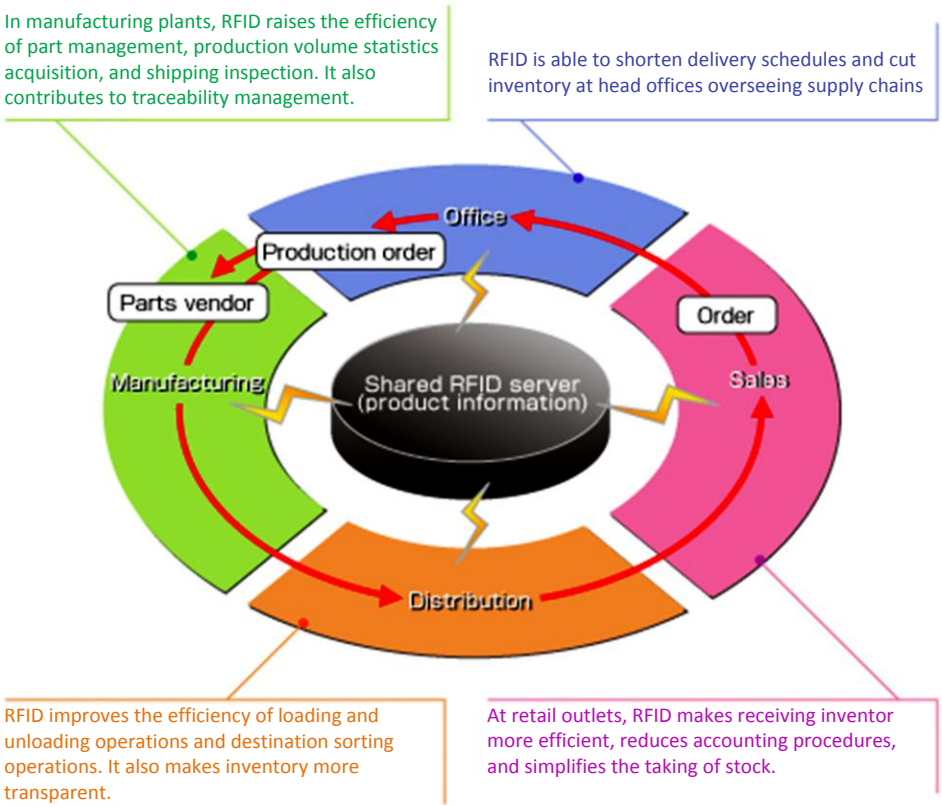

Figure 1.2: RFID bridging the gap between digital and physical worlds. (Courtesy: Toshiba Tec Corp.)

RFID due to its vast practice has drawn considerable press and scientific community attention in recent years, and for compelling reasons: RFID not only supplants traditional line-of-sight dependent barcode technology [3], it also delivers additional benefits of removing boundaries that aggressively limited the use of prior alternatives. In contrast to the barcode, with RFID, however, a reader can process the encoded information even when the tag is concealed for either aesthetic or security reasons. The early impact of the clandestine nature of RFID technology led the privacy advocates to raise concerns. One of the main objection states that common products equipped with such tags can be tracked beyond the intended use of manufacturers and retail stores. For example, some apprehensions that advertising agencies might influence the technology for directed selling or security agencies

might furtively practice it to monitor the individuals. Thanks to latterly updated RFID ASIC variant for providing another layer of protection in which the readability or detection can be authorized to only intended readers. The implementation of RFID in the areas of supply-chain management, asset tracking, manufacturing and retail automation, bridged the growing gap between the digitally networked world and the physical world (Figure 1.2). In the future, RFID tags will probably be used and recycled as environmental sensors on an unprecedented scale [207].

Succinctly, RFID systems are comprised of two main components: wireless tags and readers. A tag has an identification (ID) number and a memory bank that stores additional information such as manufacturer, product type, and environmental factors such as temperature and humidity. The reader can read and/or write data to tags via wireless transmissions. In most of the RFID implementation cases, the tags are either attached or embedded into the objects that need to be identified or detected [126]. The reader can observe the existence of the corresponding objects by foremost reading tag IDs in the vicinity and then accessing a record database that provides a mapping between IDs and objects [200].

Another area which is budding with the growing demand of RFID applications is its impact on eco-systems. However, so far mainly cost insensitive niche areas have utilized this new technology [151, 194]. The requirement for RFID tags to survive against harsh environments adds further complexity to the implementation horizon [46]. The material of the objects on which the tags are attached can influence the capacitive characteristics and radiation pattern of the tag antenna [106, 125]. Some experience has suggested that there is a need to take precautionary measures to prevent the likely negative results from the final disposal of RFID labels [192]. Currently, most of the RFID tags are neither biodegradable [21] nor recyclable [34].

The convergence of MEMS technology, wireless communications and digital electronics, provided energy to WSN potentiality [171, 85]. Thus, WSN emerged as a system which has abilities of self-networking, self-configuring, self-diagnosing and self-healing. These attributes made it an especially attractive solution for a wide range of environmental monitoring, distributed surveillance, healthcare and control applications [143]. Nowadays, the primary use of RFID systems is to identify the objects or to track their position without transmitting any information about the physical conditions of the target. On the other hand, WSNs constitute the networks of small, cost effective devices that can collaborate and convey information by sensing the ambient environmental conditions such as light intensity, temperature, pressure, humidity, sound and vibration.

WSN and RFID possibly will play a pivotal role in the generation of pervasive/ubiquitous computing [113]. The WSN has a distinct applicability on monitoring such as environmental and habitat monitoring, while the RFID is commonly applied for identifying tasks in such as logistics and industrial manufacturing processes. Even though, each has significant applicability, some already existing applications can be imposingly enriched by the integration of both technologies [80, 212].

1.2 RFID Classification and Principles of Operation

Over the various stages of RFID system development, numerous types of RFID systems have emerged. The systems distinguish from each other by system utilization, operating frequency, reading distance, protocol, power supplied to the tag, and the process for sending data from the tag to the reader [84]. RFID systems can be categorized as 'near-field' RFID and 'far-field' RFID in terms of the method of transmitting power from the reader to the tag. The other classification is based on the process of powering up the tags: RFID systems can be classified as 'passive', 'active' and 'semi-active' [64].

The outer space around the reader antenna can be split into two main regions as represented in Figure 1.3: far-field and near-field. In the far-field, electric and magnetic fields propagate outward as an electromagnetic wave whereas both are perpendicular to each other and to the direction of propagation. The angular field distribution is independent of the distance from the antenna. The fields are uniquely related to each other via free-space impedance and decay as $1/r$. In the near-field, the field components have different angular and radial dependence (e.g. $1/r^3$). The near-field region is further composed of two sub-regions: radiating, where the angular field distribution is dependent on the distance, and reactive, where the energy is stored but not radiated.

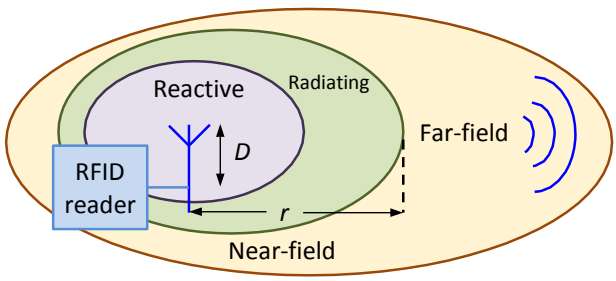

Figure 1.3: Antenna near and far-field regions. (Figure adopted from [146])

The antenna whose size is comparable to wavelength (UHF RFID), the estimated boundary between the far-field and the near-field region is often given as $r = 2D^2/\lambda$ where D is the maximum antenna dimension and is the wavelength. For electrically small antennas (LF/HF RFID), the radiating near-field region is small, and the boundary between the far-field and the near-field regions is commonly given as $(r = c/2\pi f)$ [37, 27, 117]. It is noteworthy to commemorate that reference point of antenna structure (also referred as phase center of antenna) depends on antenna geometry and its electrical size [20, 146].

1.2.1 Near-field Coupling

Electromagnetic field in the near zone is reactive and quasi-static in nature. Electric field is decoupled from magnetic fields, and which one will prevail is determined by the type of antenna employed: the electric field dominates when a dipole antenna is used, whereas the magnetic field dominates in the case of a small-loop antenna. The coupling between tag and reader antennas can be achieved through interaction with the electric or magnetic fields (Figure 1.4). In near-field RFID systems, inductive coupling systems are practically more widely available than capacitive coupling systems [54].

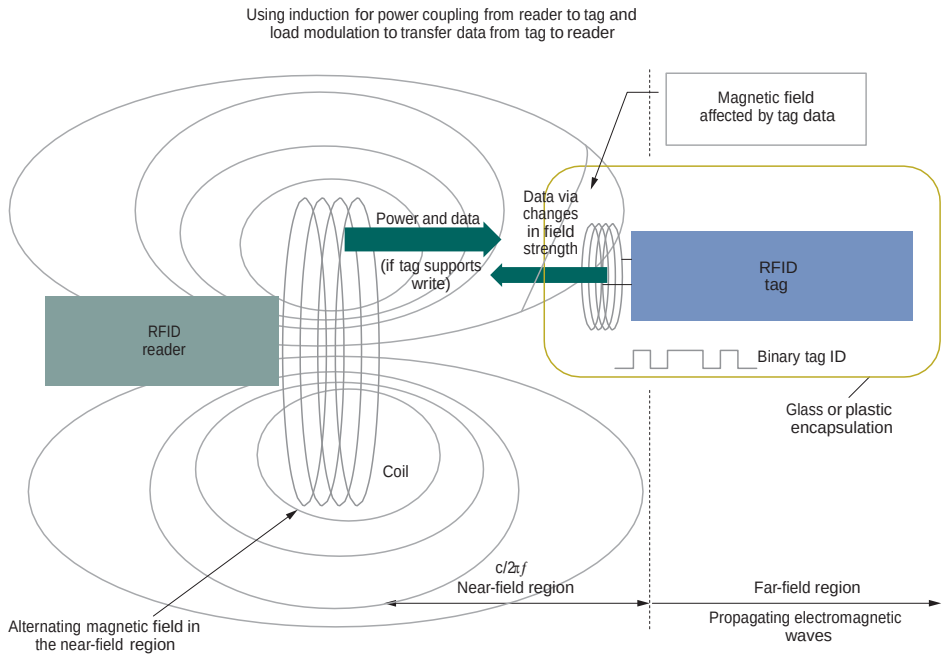

Figure 1.4: Near-field RFID communication mechanism. (Figure adopted from [208])

1.2.2 Far-field Coupling

In far-field RFID systems, the EM waves radiating from the reader antenna are captured by the tag antenna which then develops an alternating potential difference that appears across the ports of the microchip. A diode can rectify this potential and link it to a capacitor, which results in an accumulation of energy in order to power up its electronics [214]. The tags are located beyond the near-field zone of the reader in order to prevent the information is transmitted back to the reader

by using load modulation. Thus, in far-field RFID systems the communication between the reader and tag is comprehended by using a backscattering principle.

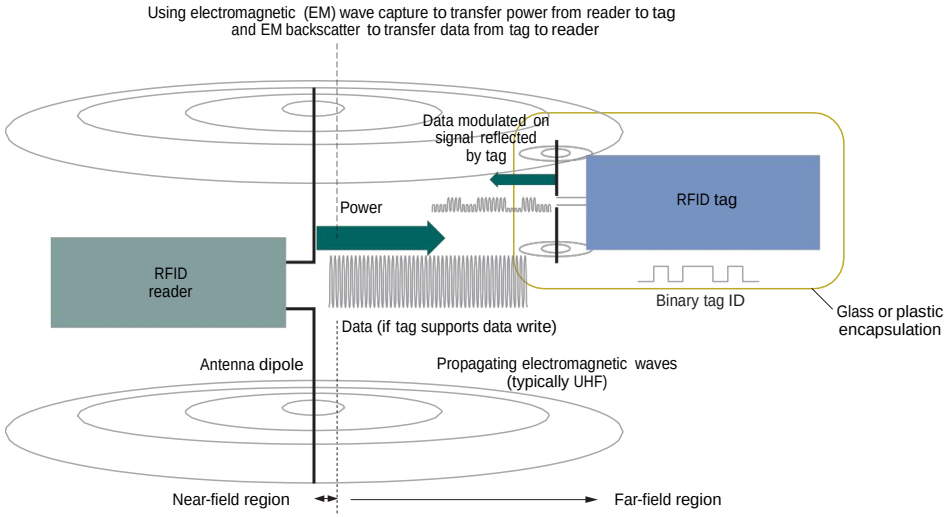

Figure 1.5: Far-field RFID communication mechanism. (Figure adopted from [208])

The reader antenna emits energy as showed in Figure 1.5, which is received by the tag antenna, and some of the incident energy is then reflected from the tag and detected by the reader. The variation of the tag's load (microchip) impedance causes the envisioned impedance mismatch between the tag antenna and the load. As a consequence, the varying impedance mismatch produces variation in (amplitude of) the reflected signals. Therefore, by changing the tag antenna's load over time, the tag can reflect incoming signal (with fluctuations in amplitude) back to the reader in a pattern that encodes the tag's ID. This category of communication is called 'backscattering modulation' [79, 40].

1.2.3 Active RFID Systems

In active RFID systems, tags have an on-board power source (e.g., a battery) and electronics for performing specialized tasks [216]. An active tag uses its on-board power supply to support microchip operation and transmit data to a reader. It does not require the power emitted from the reader for data transmission. The on-board electronics incorporate microprocessors, sensors, and input/output ports, and so on. In an active RFID system, the tag always communicates first, followed by the reader. As the presence of a reader is unnecessary for the data transmission, an active tag can broadcast its information to surroundings even in the absence of a reader. This type of active tag, which continuously transmits data with or without the presence of a reader, is also called a transmitter. Another type of active tag

enters into a sleep or low-power state in the absence of interrogation by a reader. A reader wakes the tag from its sleep state by issuing an appropriate command. The ability to enter into a sleep state conserves battery power, and consequently this type of tag generally has a longer battery life than an active transmitter tag. This type of active tag is called a transmitter/receiver [9]. The reading distance of an active RFID system can be 30m or more [134, 147].

1.2.4 Passive RFID Systems

In passive RFID systems, the RFID tag has no on-board power source, and instead uses the power emitted from the reader to activate itself and transmit its stored information to the reader [188, 196, 63]. Compared to active or semi-active tags, passive tags, therefore, are simpler in structure, lighter in weight, less expensive, more generally resistant to harsh environmental conditions, and offer a virtually unlimited operational lifetime. Several commercially available passive RFID tags are shown in Figure 1.6. The trade-off is that passive tags have shorter reading distances than active tags and require higher-power readers. They are also constrained in their capacity to store information and their ability to perform well in electromagnetically noisy environments [182, 55]. The reading range of passive RFID systems can be usually up to 10 meters.[2] In tag-to-reader communication for this type of tag, the reader always communicates first, followed by the tag. The presence of a reader is necessary for such a tag to transmit its data. A passive tag usually consists of a microchip and an antenna fabricated on a substrate.

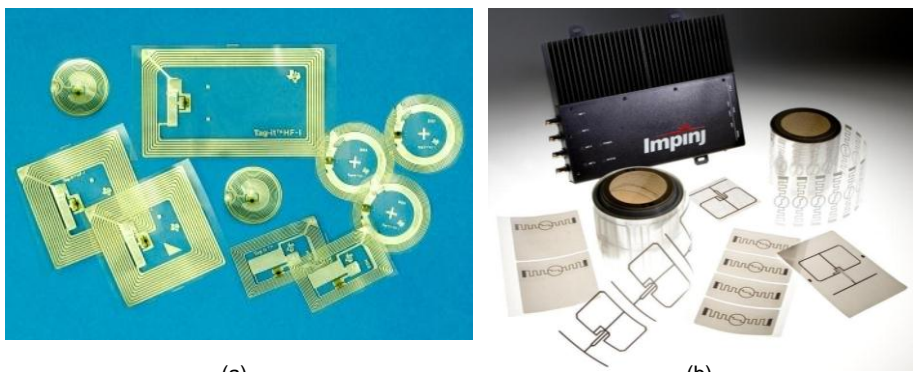

Figure 1.6: Commercial passive RFID tags: (a) HF tags from TI Inc., (b) UHF tags from Impinj Inc.

[2]The reported RFID integrated circuits for UHF tags can attain a sensitivity better that –12dBm to –18dbm [100, 29, 91, 150, 6], which can significantly improve the read range.

1.3 Components of Passive RFID Tag

Antenna Passive RFID tags can have different shapes, dimensions as well as distinct capabilities, but all passive tags are comprised of Tag antenna, Integrated circuit (microchip) and Substrate. The first thing that can be clearly distinguished while looking at a tag is the tag antenna. The size of the tag antenna not only influences the overall size but also contributes to roughly one third of tag's cost [178, 165]. The antenna is accounted for transmitting and receiving RF waves while enabling the communication with the reader.

Integrated Circuit *(Microchip)* The IC (microchip) is the central processing element of the RFID tag. It is a silicon chip with dimensions usually less than one square millimeter[3]. The IC of an RFID tag functions like a microprocessor but in a much less complex approach. Unlike microprocessor, the IC has a single main purpose of transmitting the tag's unique ID. The unique ID is stored/embedded in the IC's memory. Whenever the IC is activated by the energy captured and processed from the tag antenna [36], its logic circuit will retrieve the ID number stored in the memory, and then broadcasts it by using the backscattering modulation. There are several types of ICs are available depending upon the particular applications [57, 119, 32]. The RFID IC is usually equipped with an extra memory, which can be written by the user for embedding additional information with the help of the reader [66].

Substrate The substrate is the material that supports the tag components together. The substrate can be rigid (usually FR-4) or flexible (usually PET) depending upon the particular application [123], and can be manufactured through several different types of materials. For instance, RFID tags utilized for document tracking need a flexible substrate in order to bend in accordance with attached paper sheet. The most volatile but potential candidate for such use is paper substrate because of its abundant availability, environmental friendliness, and above all, it can be printed together with the target document. In some special cases, the space to place RFID tags is exceedingly limited, and tag dimensions become the prime concern. Special industrial substrates [73, 25, 30], such as a flexible magnetic composite substrate, can help in trimming the antenna form factor around two to three times but at higher overall cost of the tag [133]. In depth analysis, and design examples of RFID tags fabricated on various substrates will follow throughout the text, while concentrating on the sensing pertinency and state-of-the-art fabrication technologies employed for these tags.

[3]Hitachi's super-mini wireless automatic recognition mu-Chip is only $0.4mm^2$

1.4 Future Trends and Challenges

Technology trends in RFID are not only evolved through new inventions, advancements and improvements of already running businesses, but also by social, economic and political factors play a key role towards the realization of futuristic RFID sensors networks. By considering all these complexities EPCglobal projected, the roadmap from RFID to IoT whose one of significant driving force is ubiquitous sensing as showed in Figure 1.7. In the roadmap, top emerging trends associated with RFID are identified that are expected to drive its ubiquitous adoption. These RFID trends are emphasizing technological advancements, business process innovations, evolving standards and legislation and consumer application innovations that focus on:

- low-cost and reliable production of RFID tags, the fabrication methods and materials for antennas are considered to be challenges [155, 96]. Moreover, the research area appears deserted while addressing the new rising issues interrelated to the field of economic and eco-friendly tags comprising of paper substrate [7, 118].
- The substrate material and the associated integration techniques which are becoming more than a basic research topic, due to the ever growing demand for affordable and power-efficient broadband wireless electronics virtually in a ubiquitous manner [154].

1.4.1 Design Challenges for RFID Tag Antennas

The most important aspect of an RFID system's performance is the reading range– the maximum distance at which an RFID reader can detect the backscattered signal from the tag [165]. For a specific application with prior selected reader (including reader antenna), the reading distance depends on the performance of the tag. As typical passive RFID tag consists of an antenna and a microchip or strap. The characteristics of the microchip are quantified by IC manufacturers and cannot be modified by the users. The key challenge for tag antenna design is to maximize the reading distance with a prior selected microchip under the various constraints (such as limited antenna size, specific antenna impedance & radiation pattern, and cost).

Generally, the requirements for RFID tag antennas with prior selected microchips can be summarized as follows [72]:

- good impedance matching for receiving maximum signals from the reader to power up the microchip;
- small enough for being attached or embedded into the specified object;
- insensitive to the attached object to keep performance consistent;

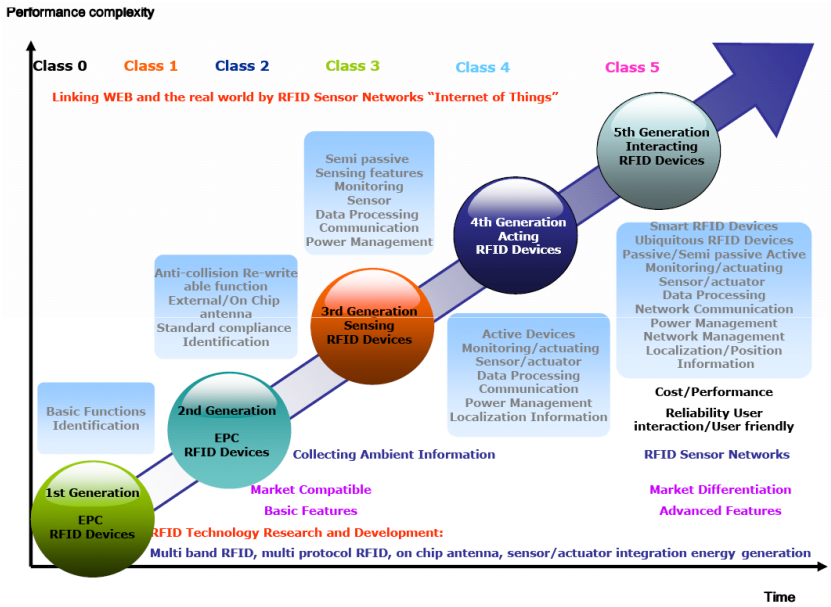

Figure 1.7: A roadmap to RFID sensor networks for IoT. (Figure adopted from [92])

- required radiation patterns (omnidirectional, directional or hemispherical);
- robust in mechanical structure; and
- low cost in both materials and fabrication.

Under the different limitations for particular RFID applications, various aspects should be considered in RFID tag antenna design [139, 165]:

Frequency band: The antenna type is dependent on the operating frequency. In LF and HF RFID applications, spiral coil antennas are most commonly employed [31, 101] to harvest the energy from the reader by coupling. At UHF and MWF frequencies, dipole antennas [88], meander line antennas [132], slot antennas [223, 2], and patch antennas [206] are widely utilized [122].

Size: Tags are demanded to be small so that they can be embedded into or bonded to a specific object such as a cardboard box, airline baggage strip, identification card or printed label. The size limitation is one of the challenges for RFID tag antenna designing [173, 172]. Small size limits the coupling capacity of the loop antenna peculiarly at LF and HF, and results in low efficiency of the antenna at UHF and MWF. As a result, the reading range of RFID systems will be reduced substantially [24].

Radiation patterns: Some applications demand a specific directivity pattern of the tag antenna such as omnidirectional, directional or hemispherical coverage.

Sensitivity to objects: The performance of a tag will be altered when it is placed on different objects such as cardboard boxes with variant contents, and demeaned on lossy objects such as plastic bottles containing water and oil, or metallic cans [51]. The tag antenna is required to be tuned for optimal performance on a particular item, or designed to be less sensitive to the assorted types of object on which the tag is placed [45, 166, 148].

Cost: An RFID tag must be a low-cost device for large scale applications. This enforces limitations on both the antenna design and the choice of materials for fabricating the tag, including the microchip. The materials used for the fabrication of the tag antenna are conducting strip/wire and supporting dielectric. The dielectrics usually include flexible polyester for LF and HF and rigid printed circuit board substrates like FR-4 for UHF and MWF. For further reducing the cost, all-printed RFID tags have been reported that use screen printing or inkjet printing techniques [184, 168].

Reliability: An RFID tag must be a reliable device that can deal with fluctuation in temperature, humidity, and mechanical stress, and survive procedure such as label insertion, printing, and lamination [98, 197, 163].

Eco-Friendliness: The lately emerged demand for RFID antenna is its operability on substrates which can be easily recycled such as paper substrate [213]. In order for businesses to minimize their antagonistic impact on the green environment, there is a need to evaluate this challenging factor [39].

1.5 Author's Contribution and Thesis Organization

1.5.1 Contributions

The main theme of the presented research is the development of versatile, low-cost RFID tags with a focus on exploring design techniques, and printing technologies for realizing performance optimized eco-friendly tag antennas. In this context, the research is divided into four parts, which are explored in parallel with the first part while the concept and knowledge achieved, constitute the key ingredients in improvement of the next area focused in this research. In the first part, innovative large scale production technologies are explored and analyzed with several types of electrically conductive inks and extremely flexible substrate materials. The inks are further evaluated on the basis of flexibility, annealing temperature, sintering time, and conductivity. Various ultra-low-cost substrates are investigated as an approach that has ultimate aim to accommodate the antenna during the package printing process, whilst faster production on commercially available paper substrate.

In the second part, the paramount design and print parameters that an RFID tag can accommodate are investigated in design evolution process in order to realize narrow-band (EU & NA bands) progressive meander line antennas. The antennas are optimized for reducing ink usage and innovative shunt stub meandering technique is applied for further improving the antenna performance. The evolution process is applied to get robust tags, which must show less sensitivity to the variation of dielectric permittivity environment. As a result, novel quadrate bowtie passive RFID tag antennas are developed. The quadrate bowtie antenna profile modification and T-matching network are used to match the antenna input impedance to tag's chip impedance, and the effects of metal and water on the proposed antennas are also categorically investigated. The objective is to stabilize the antenna on the entire frequency band of interest. However, even if it is not possible to eliminate it completely, it is made possible in the proposed antennas to strongly limit this phenomenon.

In the third part, the newfangled set of parameters emerging in RFID antennas are addressed, while entering the era of green RFID revolution by evaluating and optimizing the key design parameters which are affected by the utilization of paper substrate. The semi-rounded corner, full-rounded corner, straight-corner bowtie antennas are developed by using innovative conjugately impedance matching techniques with the RFID chip, thus implementing or eliminating the use of matching network in order to improve the stability or reduction in ink usage, respectively. The antennas exhibit wideband characteristics for their entire coverage of UHF RFID band (860–960MHz). The proposed tags are a perfect choice for far-field industrial applications due to their eco-friendliness, flexibility and substantially extended read range, especially for large items-level tracking in supply chain (cardboard cartons containing water & metal objects) and freight (wood or metal pallet) transportation.

In the fourth part, several design parameters of planar spirals and sinuous antennas are optimized while demonstrating an emerging concept of integrating RFID functionalities along with sensors and other wireless applications for green electronics. The wideband nature of the proposed antennas is exploited to accommodate several modules for sensing and wireless applications, in addition to an RFID tag. In-depth, parametric analysis is performed for the proposed antennas which are fabricated on paper substrates to develop a system-level solution for ultra-low cost mass production of multi-purpose wireless tags in an approach that could be easily expanded to other microwave and wireless "cognition" applications. The antennas exhibit excellent performance throughout several RFID ISM bands, and for other wireless applications in their operational range from 0.8–3.0GHz. These directly printable antennas are intended for cardboard cartons level tagging, where size is not an issue but high performance with increased functionality at low cost is desired so that valuable goods can be tracked in any orientation and transported safely.

In the final part of this research, an innovative RFID antenna with integrated humidity sensor and calibration functionality for wireless sensor network is developed. The antenna is composed of series & shunt stubs and capacitive tip-loading

is employed for impedance matching and reliability for near & far-field communication. The innovative structure plays the key role for humidity sensing, and sensor calibration. The prototypes of the antenna are fabricated and tested: antenna effectively senses the ambient humidity levels while demonstrating stable behavior for RFID communication. The antenna has a compact size of 1×10cm for 902–928MHz RFID band.

1.5.2 Thesis Organization

Chapter 1 introduces RFID systems, their classification and principles of operation with a focus on RFID's potential in ubiquitous sensor networks and future trends.

Chapter 2 evaluates state-of-the-art fabrication technologies for organic and printed electronics, and provides analysis of manufacturing technologies with a focus on low cost RFID solutions available for industrial applications.

Chapter 3 presents the novel structures of narrow-band antennas which cover the EU and NA RFID bands along with performance optimization techniques for green electronics.

Chapter 4 provides the in-depth analysis on design and development of wideband RFID antennas, which cover complete UHF RFID ISM band with innovative performance enhancement techniques without limiting the bandwidth of operation that ranges from matching techniques to structural optimizations for achieving optimal effective aperture.

Chapter 5 describes the implementation of an emerging concept of antennas which can accommodate multiple wireless modules, and provide stable broadband multimode feature in near and far-fields. The focus is then extended to innovative sensor-enabled RFID antenna which provides humidity sensing along with calibration functionality.

Chapter 6 concludes the presented research along with discussion on future work and possibilities of RFID applications in emerging trends of flexible and organic electronics.

1.6 Thesis Navigation

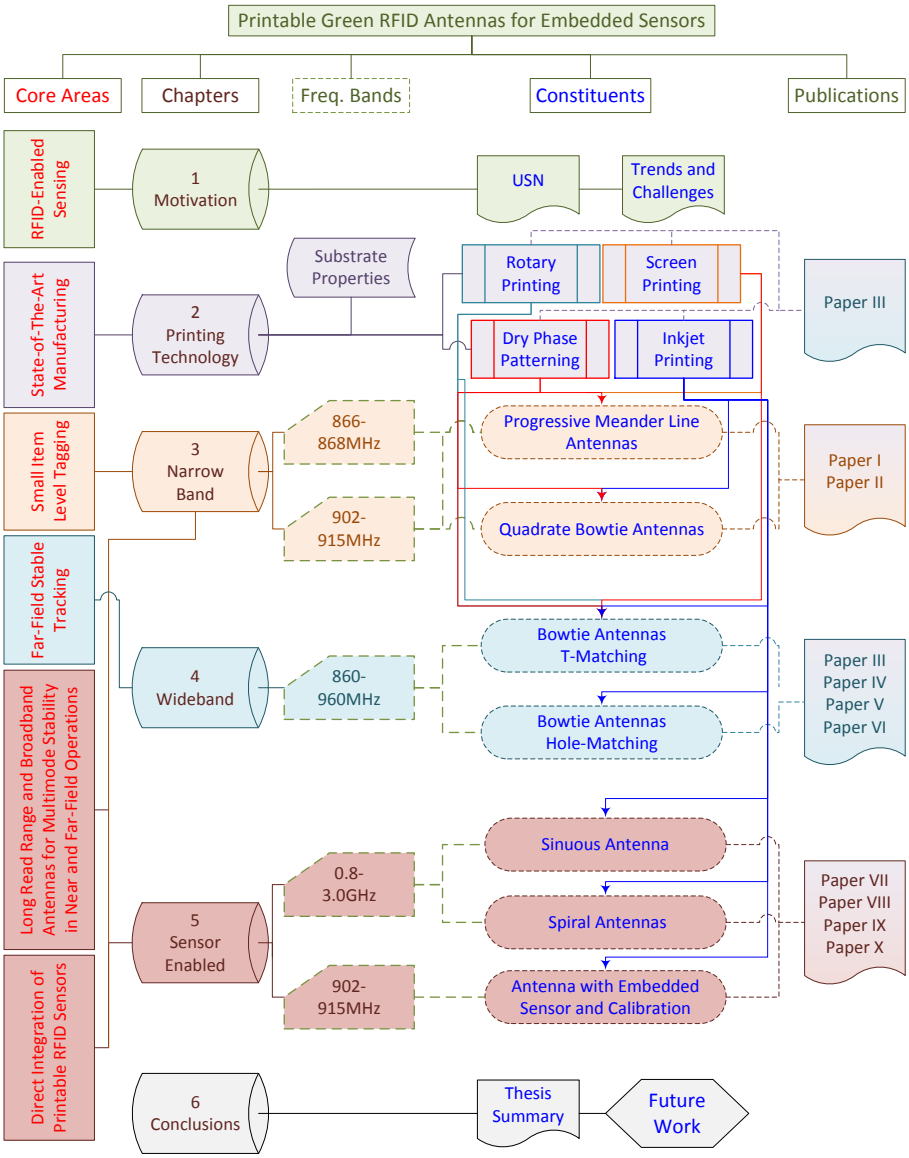

Figure 1.8: Navigation of the dissertation.

Chapter 2

State-of-the-Art Technology for RFID

Flexible and low-cost RFID (radio frequency identification) transponder is one of the auspicious applications for organic printed electronics which is based on innovative large scale production technologies, electrically conductive inks and extremely flexible substrate materials. This chapter provides an overview of the cardinal constituents driving the printed electronics into the era of digital-lifestyle. Later on, an in-depth analysis of state-of-the-art printing technologies for organic electronics is conducted in coaction with different inks and substrate materials for realization of eco-friendly RFID antennas.

2.1 Organic and Printed Electronics for RFID

RFID tags manufactured by applying printed electronics have been well-thought-out to be distant from commercialisation; nevertheless they are proceeding into the zone of mass production. The market for printed tags has seen a Cumulative Average Growth Rate (CAGR) of 16.1% from 2007 to 2015. The pace at which the printed RFID is developing renders luculent indications that the printed electronics market is likewise in its growing stages. Conventional manufacturing of displays and electronic components involves larger expensive, vacuum-based equipment and facilities for performing steps that involve high temperatures. In Photolithography, a resist mask is defined, enabling the antecedently deposited material to be removed and thrown away as electronic waste, which results into the required pattern by taking away the mask. These ingredients amass not only towards immense capital investments to commit such fabrication capacity, but also there are high material costs required to manufacture such products.

The Printed Electronics in direct contrast demands the conductive material to be deposited on the predefined position. Therefore, this process requires fewer steps and lower temperature, which is desirable for organic or inorganic flexible

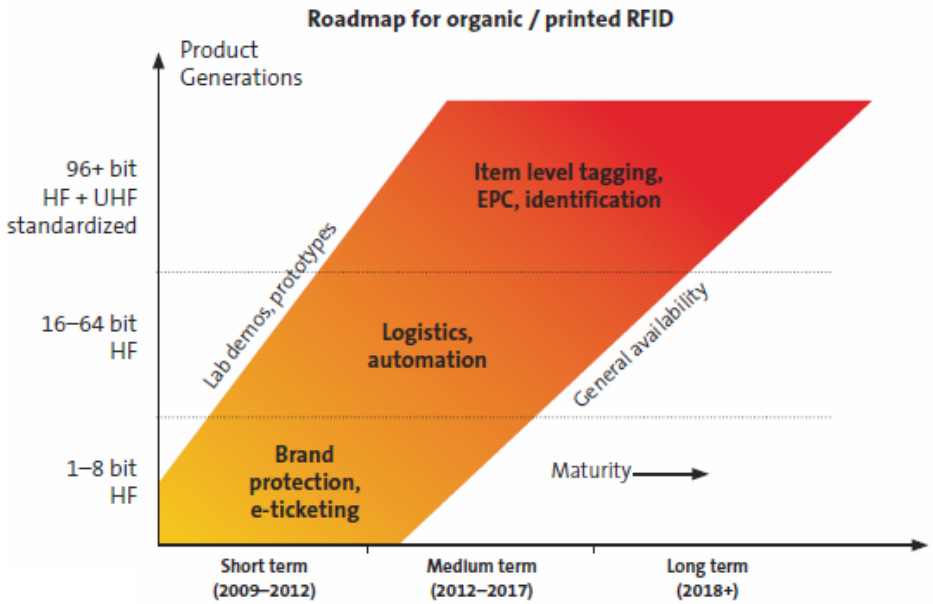

Figure 2.1: Roadmap of organic/printed RFID. (Figure adopted from [22])

substrates. The flexible nature of the technology makes use of large roll-to-roll manufacturing possible without highly sophisticated production environments. The possibility of deploying low cost materials and their utilization can drastically reduce the manufacturing cost. Printed electronics along with its customizable feasibleness envision tremendous potential in a wide range of revolutionary applications that are lightweight, and robust and above all the production costs are acceptable for disposable electronics.

Printed electronics is an emerging technology that enables fabrication of electronic components and devices by employing standard printing processes. IDTechEx [61] discovers that the market for printed and potentially printed electronics, including organic, inorganic and composites, will increase from $1.92 billion in 2009 to $57.16 billion in 2019. The majority of the market in 2009 (71%) is for electronics which are comparatively developed and conductive inks for RFID tags, sensors and Organic Light Emitting Displays (OLEDs) have enormous potentiality. The incomparable feature of this technology is its ability to manufacture a large number of devices or components at an ultra-low cost as depicted in the roadmap of organic/printed RFID in Figure 2.1 by Organic Electronics Association (OE-A) [22]. RFID tags with printed electronics are available at a lower price, as standard printing processes are practiced to produce the integrated circuits (ICs) that are used for these tags.

2.1.1 Materials and Inks

Organic electronics relies on electrically active materials that can be employed as conductors, semiconductors, dielectrics, luminescent, electrochromic, electrophoretic or encapsulation materials. The required dielectrics and encapsulation materials for a specific application have to be cautiously selected since process conditions, and interaction with other printed layers can influence the performance and the stability of the resultant organic electronic product.

Table 2.1: Characterized/evaluated substrate parameters [13].

Substrate Material	Thickness(μm)/ Permittivity(ε_r)/*Loss Tangent*	RFID Applications
Kodak U-P Photopaper	250 / 3.3(avg.) / *0.077 (1GHz@25℃)*	Packaging
Kodak Photopaper	280 / 3.3(avg.) / *0.077 (1GHz@25℃)*	Packaging
HP Adv. Photopaper	250 / 3.3(avg.) / *0.04 (1GHz@25℃)*	Packaging
Paper (p_e:smart)	250 / 3.2(avg.) / *0.077 (1GHz@25℃)*	Packaging
Paper (Korsnäs)	375 / 3.3(avg.) / *0.077 (1GHz@25℃)*	Packaging
Teonex Q51	25 / 2.9 / *0.005 (1GHz@25℃)*	Harsh environment
Kapton HN	125 / 3.5 / *0.0026(1KHz@25℃)*	Harsh environment
Metal coated PET	50 / 3.3 / *0.003 (0.9GHz@25℃)*	Fully wrapable

Thus, inks and coatings are key drivers in printed electronics, with technologies straddling from metals such as silver, copper and carbon nanotubes. By viewing the potential of the market, large and small scale ink manufacturers are developing products, with big multi-national companies such as Cabot [59], DuPont [67] and Sun Chemical [60] to fast growing start-ups like Kovio [108], Plextronics [156] and PolyIC [102]. In this research antennas are fabricated on various ultra-low-cost substrates (characterized & evaluated for the proposed antennas in Table 2.1), in distinct combinations of conductive inks with the state-of-the-art printing technologies (Screen Printing, Rotary Printing (Flexo), Inkjet printing & Dry Phase Patterning) are mentioned in Table 2.2.

The other major challenges for printed electronics applications are the choice of the substrate material for integration with these revolutionary fabrication technologies [47]. The possibility of implementation of inorganic materials such as polyimide (e.g., PET) and organic substrates such as paper can lead to manifold advantages. It is proven that organic substrates have lower cost and property of easily being biodegradable, which make them most promising materials for UHF & MWF RFID applications. These features make organic substrates an outstanding candidate for eco-friendly electronics and as a step towards the realization of “green” electronics.

Table 2.2: Printing technology/ink/substrate/speed combinations [13].

Inkjet Printing	**Rotary Printing**	**Screen Printing**	**DPP**
Cabot Ink (CCI-300)	*Asahi*	*Asahi*	*Al Coated*
Xerox Ink (AG-120I)	*Paste (LS-411AW)*	*Paste (LS-411AW)*	
Harima Ink (NPS-JL)			
Kodak Photopaper	Kapton HN	Kapton HN	PET
HP Photopaper	Teonex Q51 (2&4m/min)	Paper (Korsnäs)	
Paper (p_e:smart)	Paper (Korsnäs)		

2.1.2 Paper as an Economical Environmentally Friendly RF Substrate

Paper is an ultra-low cost, widely available, environmentally friendly material [116], which is extremely flexible and can sustain high temperatures than plastic inlays. In contrast to plastics, paper does not stretch in rough environments, which implies that RFID-enabled paper tickets and labels can maintain their form for a prolonged period. The selfsame roll-to-roll or screen printing processing previously employed for paper cards, banners, tickets and labels can also be applied for mass production of RFID tags for various applications. Accordingly, mass fabrication of RFID inlays on paper is becoming more effective by the use of inkjet printing technology for RFID tag antennas, which is followed by flip chip mounting of ICs and/or aboard more microelectronic devices. The integration of paper with an additive printing process signifies that the production cost is remarkably scaled down, whereas the end product is robust as well as dedicated.

There are additional characteristics of paper that brands it an economical substrate [28]. Its low surface profile is highly suitable for coating purposes such as a different kind of coatings similar to photopaper. Thus, the fast and revolutionary inkjet printing technology can be employed in conjunction with appropriate bonding methods for producing multilayer electronic circuits e.g., by integrating antenna, IC, and flexible battery along with addition circuitry to facilitate ubiquitous sensor networks [34, 116]. Nevertheless, this prospect is in early research stage which may appear in the near future with more useful printed components [154]. Moreover, the inclusion of certain textile to paper make it hydrophobic or fire-retardant, consequently, for specific application it prevents the paper substrate for absorbing the moisture [169].

Paper substrate due to its long history of evolution has a wide variety of types in terms of different density, coating material, texture and dielectric properties [213]. These dielectric properties (dielectric constant and dielectric loss tangent) are the foundation of RF parameters needed for the design engineer before proceeding to develop an RF circuit ‘on-paper’ design. In this research, the characterization of

electrical and dielectric properties of paper substrate (mentioned in Table 2.1 are performed by utilizing Acreo[1] AB, VTT[2] and in-house facilities.

2.2 Manufacturing Technologies Analysis

The manufacturing processes are analyzed primarily with a focus on low cost solutions available for industrial applications at present. In general, the comparison of the exact cost for each printing process depends upon the number of factors which make such analysis out of scope of this research. However, relative comparison of cost per tag is carried out while implementing each technology and on the basis of this study (which is reflected from included Paper III), each fabrication technology is given the scale value from (1) to (4), where (4) corresponds to the cheapest solution. The succeeding analysis is simplified for the purpose of focusing mainly on the performance and capabilities of the printing technologies by taking into consideration the upshots demonstrated for one of our designed antennas.

2.2.1 Screen Printing – (2)

One of the recent areas, where screen has made itself welcome is in the printing of RFID antennas. The technological advancements have made it possible to print antennas through the process of screen printing, by using conventional substrates or materials. The proposed antennas are screen printed with the semi-automatic screen printer (Figure 2.2(a)) in VTT on Kapton HN and Korsnäs paper, as showed in Figure 2.2(b) & (c), respectively. The 25μm thick layer is printed using Asahi paste in order to exploit its outstanding mechanical performance [93], while remarkably stable ink distribution all over the printed patterns is achieved. Robust proposed RFID tag antennas are achieved by this process, which can maintain their performance even being bent several times, this is demonstrated with detail in Paper III. The characterization and measurements of the printed traces are carried out using Veeco profilometer, which are presented in Figures 2.2(d)–(g). The samples are post-annealed for 2 hours at 140°C to achieve improved conductivity.

2.2.2 Rotary Printing – (4)

Rotary printing, is a finer resolution printing (flexo) technology, it is rapidly gaining importance by RFID antenna printing providers as a manufacturing choice that offers higher throughput than screen printing.

The rotary screen printing of antennas is studied here using VTT's ROKO pilot line showed in Figure 2.3(a). PEN, polyimide and paper substrates are used with two silver PTF - (Polymer Thick Film) inks and one silver nanoparticle ink.

[1] Acreo AB is part of Swedish ICT together with Interactive Institute, Santa Anna, SICS and Viktoria Institute.

[2] Technical Research Centre of Finland.

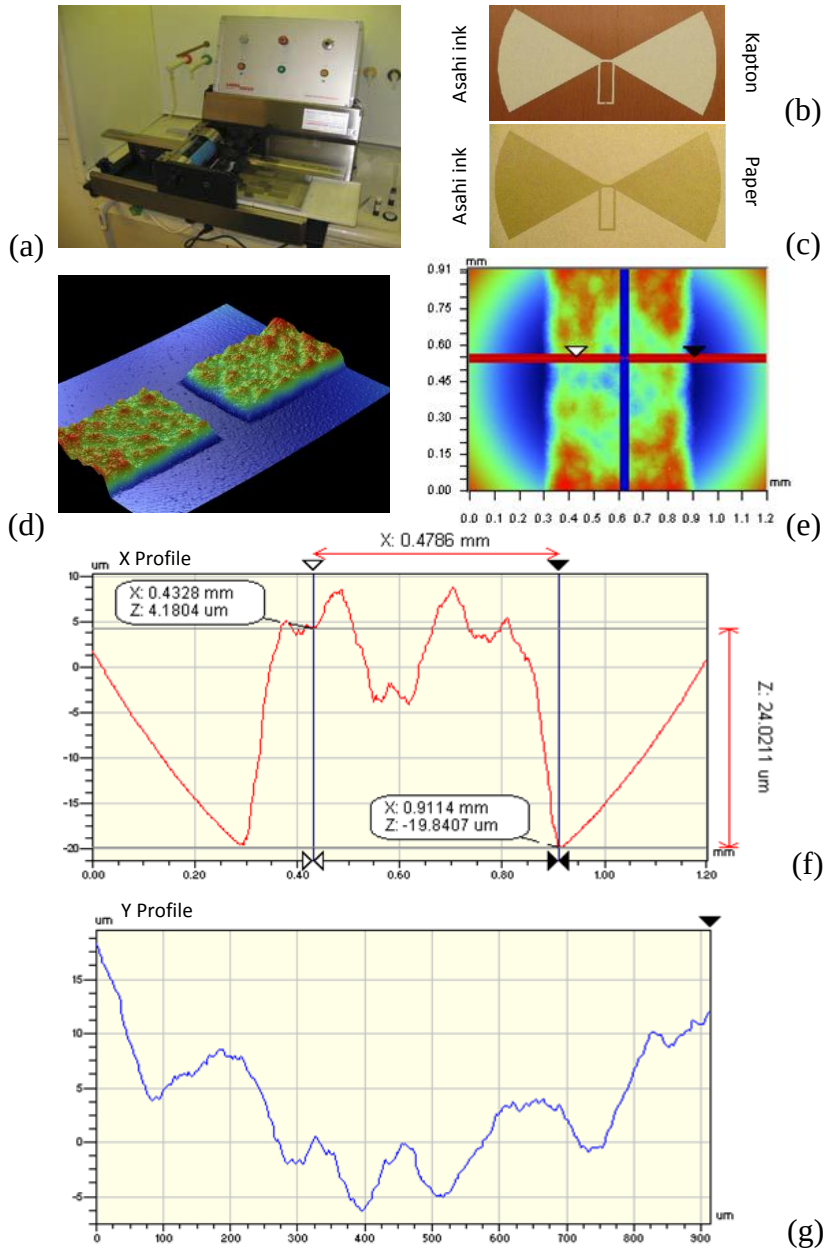

Figure 2.2: (a) Screen printing setup; screen printed antenna on: (b) Kapton HN, (c) Korsnäs paper; profilometer measurement of printed layer: (d) roughness, (e) surface topography, (f) thickness X-Profile, (g) thickness Y-Profile. (Reproduced courtesy of The Electromagnetics Academy [13])

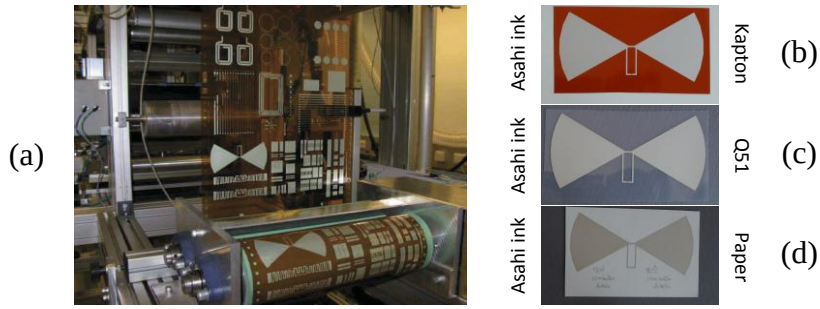

Figure 2.3: (a) Rotary printing setup at VTT; Rotary printed antenna on: (b) Kapton HN, (c) Q51, (d) Korsnäs paper. (Reproduced courtesy of The Electromagnetics Academy [13])

Additionally, the printing screen mesh size is varied in these test runs to study its effects on e.g., layer thickness. A hot air drying oven having length of 4m is used. The performance of rotary printed antennas showed in Figures 2.3(b)–(d) depend on several parameters. The line thickness is typically 10–15μm, and sheet resistance 50mΩ/square, which can be further decreased to 30mΩ/square by additional oven drying. The best print quality is obtained using a printing speed of 2m/min.

2.2.3 Dry Phase Patterning – (3)

The proposed antennas are also developed using Dry Phase Patterning (DPP) for comparison and validation of the concept (in Acreo AB, Sweden), a method for patterning metal layers on flexible substrates. The laminate of Aluminum/PET is patterned for proposed antennas showed in Figure 2.4(c). Process speed up to 150m/min and line pitch down to 250μm has been demonstrated, which made DPP a better choice for cost effective RFID tags.

Figure 2.4: (a) DPP setup at Acreo, (b) antenna patterning, (c) aluminum patterned antenna on PET. (Reproduced courtesy of The Electromagnetics Academy [13])

Laboratory production line showed in Figures 2.4(a) & (b) is used for the test

trials. One of the main benefits of employing DPP method for the fabrication of proposed antennas is the reduced load on the environment which embraces the concept of "green" tags. This is mainly because of reduced energy consumption; no washing, brushing or drying is required. Since, no chemicals are used, the residual product is in a dry and easily recyclable form.

2.2.4 Inkjet Printing – (1)

Inkjet printing is a direct-write mechanism by which the desired design outline is transferred directly to the (flexible) substrate. This technology requires no masks compared with the conventional etching technique, which has been commonly used in industry. During inkjet printing, the single ink droplet is jetted from the nozzle to the desired position, therefore, creating no waste, ensuing in an economical and eco-friendly production choice [195].

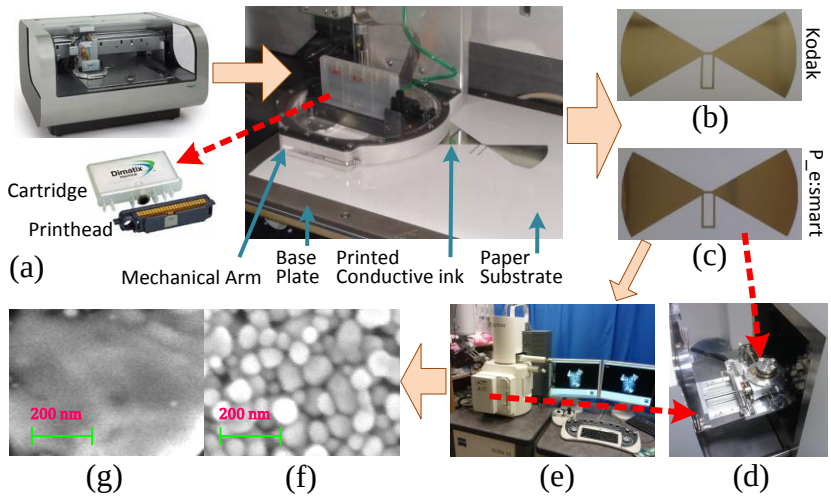

Figure 2.5: (a) Inkjet printing setup; inkjet printed antenna on: (b) Kodak photopaper, (c) Felix Schoeller paper; (d) SEM sample holder, (e) ULTRA-55 FESEM Carl Zeiss setup; SEM images of three layers of printed silver nanoparticle ink, after curing 2hr at: (f) 100℃ (g) 150℃. (Reproduced courtesy of The Electromagnetics Academy [13])

The inkjet printing setup used in the present research is showed in Figure 2.5(a) and is based on a Fujifilm Dimatix DMP2800 printer. It uses one user fillable piezo-based inkjet print cartridge with 16 nozzles in a single row and 254μm nozzle spacing, to eject 1pl or 10pl drops (depending upon the choice of cartridge). The printed structures in this particular demonstration on Kodak photopaper and (p_e:smart) from Felix Schoeller are showed in Figure 2.5(b) & (c), respectively. These are printed using 10pl cartridge (DMC-11610) filled with Cabot conductive

Ink (CCI-300 from Cabot Corp.), having viscosity of 11–15cP, with silver solid loading of 19–21wt% and density of 1.23–1.24g/ml is jetted with printing resolution of 1270dpi. The printing was carried out in a standard laboratory environment to determine the extent to which useable devices could be fabricated on a commercial scale printing method.

Two different sintering processes are evaluated as a whole in this research after drying of ink on the substrate, first one is the prevalent method and the other is "PulseForge Technology" [190]. In the first approach the sintering process is carried out for 2 hr at 150℃ for sufficiently curing, to remove the excess solvent and material impurities from the depositions. The characterization of the printed structures is carried out under ULTRA-55 Field Emission Scanning Electron Microscope from Carl Zeiss NTS showed in Figures 2.5(d) & (e). Figures 2.5(f) & (g) show the SEMs for elaborating the difference between the heating temperature after a 2hr curing at 100℃ and 150℃, respectively [12].

At high temperature, an almost solid metal conductor is formed so providing a percolation channel for the conduction of electrons throughout the material without obstruction. The printed samples of antennas with multi-functional capabilities are also sintered through "PulseForge Technology" by Novacentrix USA, in order to demonstrate sintering and annealing for high-speed roll-to-roll manufacturing often in ambient air (and is capable of up to 1000 feet per minute). This approach enables the use of ultra low temperature and flexible substrates such as paper substrate, which cannot be annealed at high temperatures. The sintering process also presents the derived benefit of increasing the bonding of the deposition with the paper substrate [12].

2.3 Summary

Traditional RFID antennas, which are fabricated by the use of engraved copper or copper wire, is only suitable for small scale production, and in scenarios where higher cost is not a primary concern. In contrast to the subtractive process of etching into a copper layer, screen, rotary (flexo) and inkjet printing are additive processes, thusly realizing more cost-effective and eco-friendly products because these processes consume lower proportion of raw materials [186], and limit the wastage of material. Furthermore, it is well demonstrated that directly printed antennas using silver ink with screen and rotary (flexo) printing technologies can withstand twisting, bending and mechanical stresses in harsh environments. The direct printing process is more appropriate in combination with ultra-low-cost paper substrate because the conductive ink penetrates into the fibers of the paper structure and enhances the flexibility. These market driven solutions for organic and printed electronics are more effective for rapid and stable fabrication which ensues into robust and reliable products. Screen, Rotary (Flexo) printing and DPP, are well-tested industrial processes, compatible with high speed reel-to-reel manufacturing, which can easily be scaled to meet any production demands. The accuracy and repeata-

bility of these processes along with existing mathematical models and extensive knowledge of the electrical and mechanical characteristics of silver ink, newfangled antennas can be reliably developed in much shorter time than ever before.

Chapter 3

RFID Antennas: Narrow-Band

Radio frequency identification (RFID) has been increasingly used in many applications such as supply chain management, inventory control, security management, and logistics [225, 26]. This chapter which is profound reorganization of included paper I and II, presents fully integrated printed RFID progressive meander line antennas as a potential solution for small item-level labeling in these applications. In order to accommodate the antenna during the package printing process, it is vastly preferred that antenna structures are printed on paper substrates. However, the electromagnetic properties and thickness of paper substrates are susceptible to change due to various environmental effects. Thus, adequately consistent in performance and material insensitive printed quadrate bowtie RFID antennas are proposed. This chapter also includes in-depth efficient optimization for small & high performance tag antenna designs for operability in frequencies 866–868MHz & 902–928MHz.

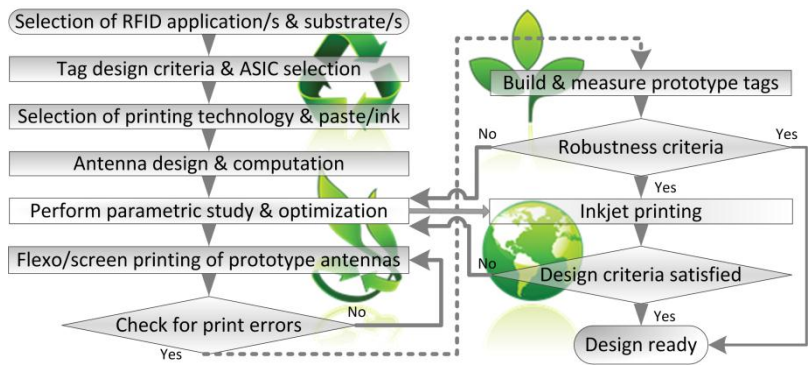

Figure 3.1: Evolution process for robust & "green" RFID tags. (Reproduced courtesy of Taylor & Francis [10])

3.1 Progressive Meander Line Antennas

This section expounds the design process for evolution of progressive meander line RFID tag antennas for FCC (North America) and ETSI (EU) bands. The design and computations are performed using ANSYS HFSS™. These antennas are printed on several substrates using state-of-the-art printing technologies (screen printing, flexography and inkjet printing. The measurements are carried out in an anechoic chamber owing to an experimental set up dedicated to antenna characterization. The small size, low cost, convenient aspect ratio and exceptional read range of these antennas make them an ideal choice for far-field case, carton and pallet applications. The focus is extended to eco-friendly tags, which can be a milestone for the next generation of printable "green" electronics.

3.1.1 Antennas Design Evolution & Geometry

The paramount design and print parameters that an RFID tag can accommodate are investigated in design evolution process which is proposed in Figure 3.1. Each antenna is designed for flexible and "green" electronics utilizing most commonly available substrates (Table 2.1). Several conductive inks are used for trial printing of these antenna structures which are summarized in Table 2.2.

The evolution process is applied to get robust tags which must show less sensitivity to the variation of dielectric permittivity environment. The objective is to stabilize the antenna on the entire frequency band of interest. The variations of the environment inevitably impact the tag performance [87] e.g., usage on metallic objects; however, even if it is not possible to eliminate it completely [52], it is made possible in the proposed antennas to strongly limit this phenomenon. The NXP ucode g2xm (TSSOP8, e.g., the target IC impedance at 915MHz is 22-j191Ω) is selected in flip-chip package. The main goal of optimization at each stage is to maximize the feeding power to the load (RFID IC) while at the same time the antenna area is minimized in order to employ these tags on small objects.

In the first phase novel meander line antenna is developed which is a natural choice when the size and tuning is considered [209]. Unique progressive meandering technique is deployed to realize the antenna for 866–868MHz band showed in Figure 3.2(a). The whole structure measures only 9cm x 0.8cm and is smaller than previously published results [46, 132, 165].

In the second evolution phase the antennas with higher stability against environmental effects are realized. The major challenge at this stage is to maintain the gain and smaller size while improving the stability factor. The other ingredient that governed the design modifications is the low ink usage to reduce the manufacturing cost. Thus an innovative technique of also meandering the matching stub is introduced to rectify the issues of low gain, stability and matching. Furthermore, rigorous optimization is performed which is resulted into two distinctive antenna structures presented in Figures 3.2(b) & (c) cover EU and North American UHF RFID band, respectively. These compact antennas are extremely suitable for tags

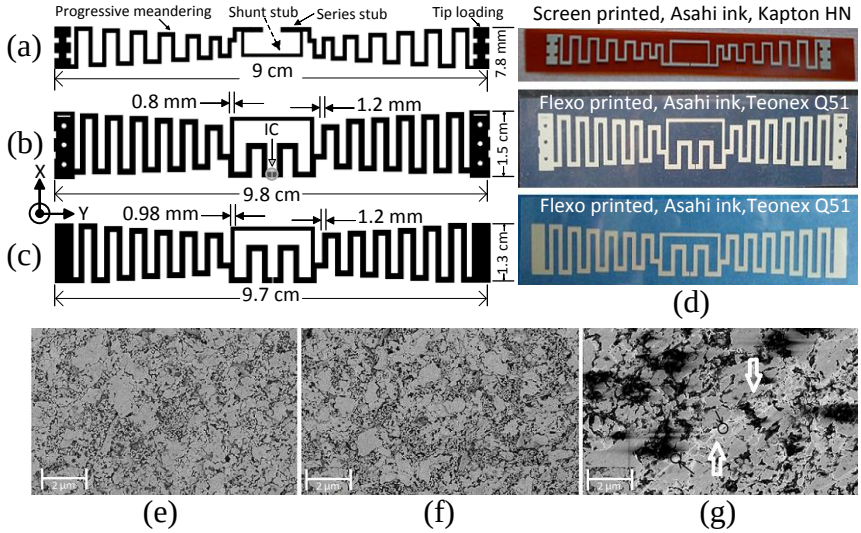

Figure 3.2: (a) The smallest proposed antenna, (b) enhanced EU band antenna, (c) optimized NA band antenna, (d) antennas printed on flexible substrates, (e) SEM of asahi printed antenna trace, (f) SEM after bending 50 times, (g) SEM after scratch test. (Reproduced courtesy of Taylor & Francis [10])

attached to articles which are prone to be bent or folded several times during their life cycle and are far more superior than formerly published results [46, 132, 165]. The final evolution stage comprises of realizing these antennas on different types of paper substrate as showed in Figure 3.3(f).

3.1.2 Antennas Fabrication Parameters

During transportation it is likely that items get scratches. Therefore, for solving this problem antennas are manufactured using flexo and screen printing with Asahi paste in order to exploit its outstanding mechanical performance [93]. We have tested the mechanical toughness after printing these antennas showing excellent scratch resistance, i.e. no change in conductivity or antenna efficiency. Figures 3.2(e) & (g) show scanning electron microscope (SEM) photos of antenna traces before and after getting scratches (by metal object of sharp edge 400μm x 100μm with an applied force of one Newton), respectively. These proposed antennas are extremely flexible and perform without retardation after being bent several times and results are shown in Figures 3.3 & 3.4 along with bending test setup in Figure 3.3(d).

The first step in the process of evolutional development of the “green” tags involves inkjet printing utilizing DMP2800 inkjet printer which is a table-top printer available from Dimatix Inc. and is shown in Figure 3.3(f). To ensure good RF

properties, an in-house recipe was developed. The print head is adjusted to achieve high print resolution, which ensures good RF conductivity throughout the frequency band of interest. The silver nanoparticle based ink mentioned in Table 2.2, is then jetted at a temperature of 40℃, while the paper substrate mentioned in Table 2.1 (p_e:smart from Felix Schoeller & 280g photopaper) is maintained at 60℃ (cabot ink) & at 30℃ (harima ink). In order to achieve better conductivity each structure is printed with multi-layers [136] e.g. 3–4 layers to provide better analysis about the printing technique. Each printed structure is then cured in a thermal oven for two hours at 120℃ (cabot ink) and for 1.5 hours at 90℃ (harima ink).

In the final step, these "green" tags are realized with roll-to-roll printing arrangement (using Korsnäs flexo printing paper of 375μm thickness) to add tremendous scale of industrial usage for these antennas. The measurement analysis in Figures 3.3 & 3.4 illustrate surpassing performance of these environmentally friendly tags.

3.1.3 Parametric Analysis

RFID Tags (based on far-field communication and the physical property of backscattering or "reflected" power), with different sizes, presented in Figures 3.2(a)–(d) with manufacturing combinations mentioned in Table 2.2 are measured in a rigorous measurement approach. Firstly for each antenna structure ten identical prototypes are printed (with same combination of printing material & technology) and are measured across the frequency band of interest using half mirror method. Maximum deviated value at a particular point among ten samples is reported here which provides in depth view for worst case analysis to project more realistic data. This technique is adopted to thoroughly investigate the reliability criteria of each designed structure.

One of the most important tag performance characteristics is read range. Read range is also sensitive to the tag orientation, the material which the tag is placed on, and to the propagation environment. The read range can be obtained from the Friis equation as explained in [165], but it gives the maximum distance at which RFID reader can read the tag in free space. Thus this calculation of read range is invalid at near-field distances. In most UHF RFID systems, this distance extends well into the far-field zone. While some tag application scenarios involve near-field tag scanning, it can be expected that in most cases the tag which can operate in the far-field should receive more than adequate power to operate when brought closer to RFID reader antenna into the near-field. Hence, the read range of most UHF RFID tags is determined by the tag performance in far-field [144]. The read range of the proposed antenna of Figure 3.2(a) is from 3.5m(paper/inkjet) – 4m(optimal). However, the optimized antennas of Figures 3.2(b) & (c) exhibits exceptional read range from 5.5 – 6.5 meters with different manufacturing combinations, which is better in comparison with reported results [46, 132, 165].

Moreover, the near-field performance testing is carried out inside the anechoic chamber with Impinj's UHF RFID reader Kit. The transition from near-field to

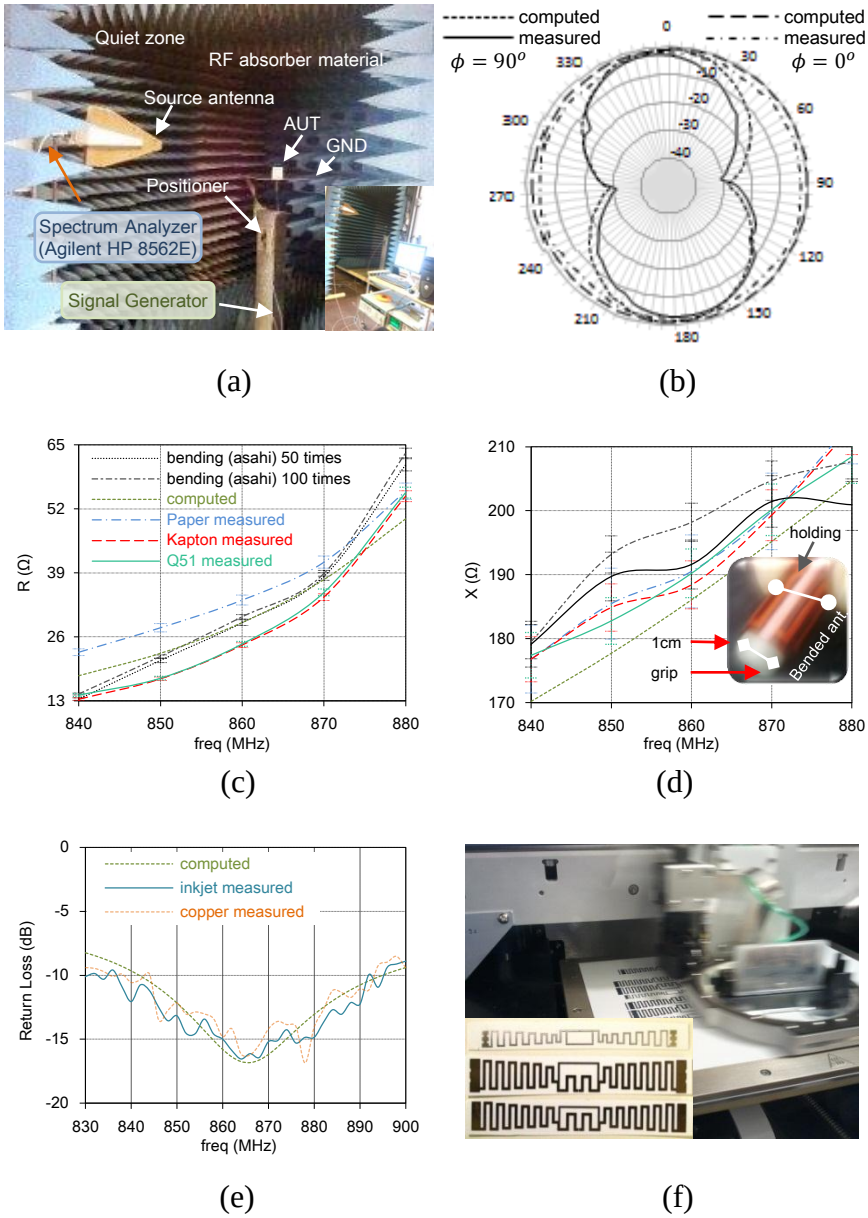

Figure 3.3: (a) Experiment setup in the anechoic chamber, The smallest ETSI band antenna: (b) 2D far-field radiation plots, (c) input resistance variation, (d) input reactance variation & bending test setup, (e) return loss analysis, (f) inkjet printing setup & antennas printed on paper substrate. (Reproduced courtesy of Taylor & Francis [10])

far-field is not abrupt and the far-field distance is determined by $(2D^2/\lambda)$. The D (maximum dimension of the radiating structure) of reader antenna used is 0.3m (1 foot), thus in one of the measurement cases the far-field distance at 915MHz (λ=0.33m) is estimated to be 0.56m. The proposed antennas exhibit flawless readability with in reactive near-field region. It is worth noting in this region, that the antenna pattern is taking shape but is not fully formed, and the antenna gain measurements vary with distance.

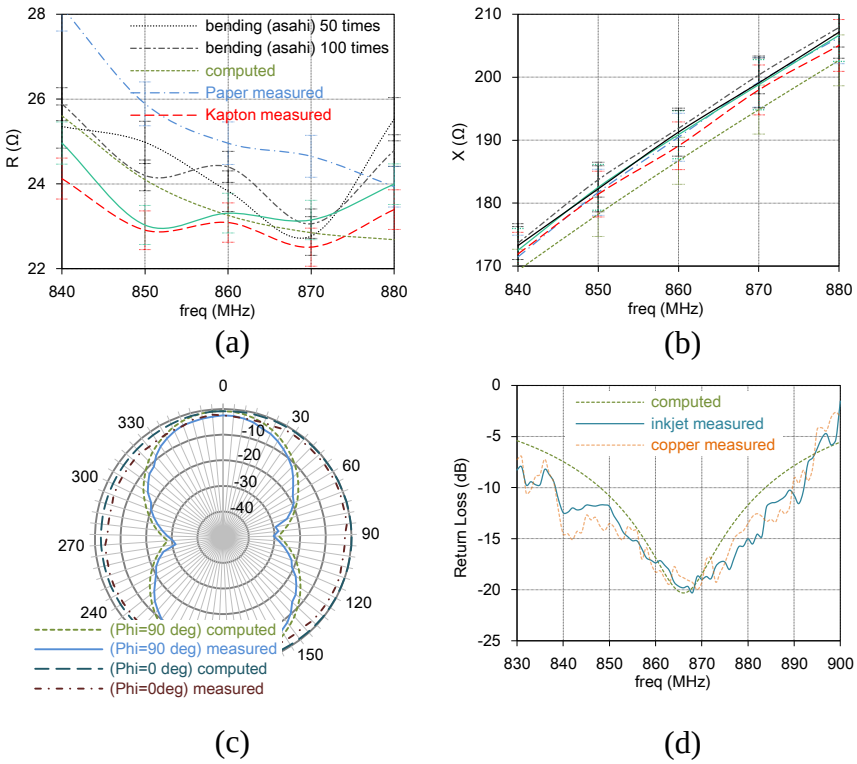

Figure 3.4: ETSI band antennas: (a) input resistance variation, (b) input reactance variation, (c) 2D far-field radiation plots, (d) return loss analysis. (Reproduced courtesy of Taylor & Francis [10])

Impedance measurements are taken using vector network analyzer (MS2026B, Anritsu [58]). The standard calibration method short-open-load (SOL) is used. The impedance variation of antenna in Figure 3.2(a) is shown in Figures 3.3(c) & (d). It is depicted from Figure 3.3(c) that the antenna has maintained the resistance around 35Ω in a linear manner with frequency. This design has the constrain of higher resistance value which evolutes towards the design showed in Figure 3.2(b), so that the resistance can be maintained closer to the desired value of around

23Ω. Figures 3.4(a) & (b) show the impedance analysis of the proposed antenna in Figure 3.2(b). There is very small variation observed among the curves for different antennas which is elaborated in Figure 3.4(a).

The reactance of antenna in Figure 3.2(a) is shown in Figure 3.3(d) which features a positive value but with disparities among different curves. If this design is realized with different combinations mentioned in Table 2.1 instead of only one combination then these disparities have adverse effects on reliability. Figures 3.2(b) & 3.3(f) show more robust proposed structures which have linear and stable reactance behavior despite the variation especially in the dielectric constant of substrate material which is shown in Figure 3.4(b). This pertained to an inductance that conjugately matched or, equivalently cancelled the effect of the IC capacitance. Fairly good agreement is found between the computed and measured results.

In order to verify the performance of the inkjet printed RFID antennas Figure 3.3(f), measurements are also executed on standard copper clad antenna prototypes. These have the same dimensions and fabricated using lpkf ProtomatC30. The return loss results of antennas in Figures 3.2(a) & (b) are shown in Figures 3.3(e) & 3.4(d) respectively. It is pragmatic that the return loss of the inkjet printed antennas is vaguely larger than the return loss of copper antenna. However, by analyzing the results in Figure 3.4(d) the optimized antenna structure in Figure 3.2(b) has better return loss agreement with computed values. Overall, good agreement between the standard copper based and the inkjet printed antennas is observed, regardless of the higher metal loss of the silver based conductive ink. The distortion is possibly due to the effect of metal ground fixture used for half mirror method [114].

The most challenging in measurement steps, the radiation pattern of antennas is measured in an anechoic chamber setup [103] that replicate absolute free space which is presented in Figure 3.3(a). The antenna under test (AUT) is mounted over the positioner assembly in the center of the chamber which is set to rotate the antenna in small steps of 5 degrees to obtain a 360° radiation pattern. A continuous-wave (CW) signal from the signal generator excites the AUT. The receiver antenna is connected to the spectrum analyzer (Agilent HP 8562E [189]) and a PC running the test automation software controls the measurement setup. The antennas with paper substrate are attached to the test terminal with CW2400 silver conductive epoxy, cured at 24℃ for 4 hours to get maximum conductivity and adhesion. The normalized computed radiation pattern and the microwave chamber measurement, are plotted. As shown in Figures 3.3(b) & 3.4(c), the radiation patterns are almost uniform (omnidirectional) at 866MHz, with directivity around 1.9dBi (for antenna in Figure 3.2(a)) – 2.1dBi (for antennas in Figures 3.2(b) & (c)). They show very good agreement between computations and measurements, which also could be verified for other frequencies within the antenna's bandwidth. Similar parametric behavior is depicted by antennas for North American band which are photographed in Figures 3.2(c) & 3.3(f).

3.2 Quadrate Bowtie RFID Antennas

In this section, novel quadrate bowtie passive RFID tag antennas on paper/PET substrates are presented with the introduction of impedance matching approach to improve the reliability against environmental diversities as well as increase the maximum reading distance. The quadrate bowtie antenna [161] profile modification and T-matching network are used to match the antenna input impedance to tag's chip impedance, and the effects of metal and water on the proposed antennas are also categorically investigated. These antennas are printed on different substrates (Table 2.1) using **D**ry **P**hase **P**atterning and Inkjet Printing technologies.

3.2.1 Antenna Dimensions and Parametric Optimization

The proposed quadrate bowtie antennas are optimized on a methodical basis for minimizing the effects of environmental adversities on RFID tags. The main purpose of enhancement is to maximize the feeding power to the load and reduce the antenna area, while realizing the highly efficient structures on paper substrate for eco-friendly tags. Figure 3.5 shows the Thevenin equivalent circuit of the IC tag, from which the consumption power at the load is evaluated assuming the incident plane waves. In Figure 3.5, v_o is received open voltage, $Z_a = R_a + jX_a$ the input impedance of the tag antenna, $Z_c = R_c + jX_c$ the impedance of the load, I the current flowing at the load. I and the consumption power of the load P_c are obtained from (3.1) & (3.2):

$$I = \frac{v_o}{Z_a + Z_c} \tag{3.1}$$

$$P_c = Re\{Z_c I I^*\} \tag{3.2}$$

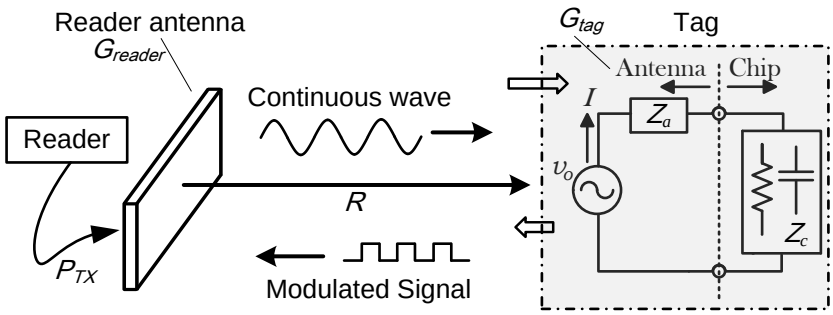

Figure 3.5: Far-field RFID mechanism & equivalent circuit of an IC tag. (Reproduced courtesy of The Electromagnetics Academy [11])

It is worth mentioning here that throughout the text onwards whenever input impedance of antenna is referred it will be meant that the real part R_a of the

antenna input impedance Z_a consists of the radiation resistance and the antenna losses or loss resistance. Hence, one of the optimization criteria is defined as (3.3),

$$kP_c + \left(1 - \frac{S}{S_{max}}\right) \rightarrow max \tag{3.3}$$

where S is the antenna size and S_{max} the maximum size, and k in the first term is the weighting constant to offset the first and second terms. If the effect of the second term in the objective function is trivial, the impedance matching between Z_a and Z_c will stand for the optimal antenna, that is, Z_a of the optimized antenna will be the complex conjugate of Z_c. Note that the input voltage v_o depends on the antenna structure in this problem [128]. Thus, it requires a conjugate matching technique such as series or parallel stubs. The matching network of the tag has to ensure the maximum power delivered to the chip. To achieve these design goals, a T-matched quadrate bowtie antenna (half wavelength dipole antenna) with rounded corners, is designed and fabricated. This design is used for the matching of the passive antenna terminals to the NXP ucode g2xm (TSSOP8, e.g. the target IC impedance at 915MHz is 22-j191Ω). The prototype antenna structures for UHF RFID European (EU) band and North American (NA) are shown along with dimensions in Figures 3.6(a) & (b) respectively. The T-match arms are liable for impedance matching of the antenna terminals to that of the RFID chip through the fine tuning of the series and shunt stubs.

3.2.2 Antenna Effective Aperture

A commonly disregarded issue about an (RFID) antenna is how directivity and gain are correlated to its physical dimensions. Since the field/current, on the antenna aperture is not uniform, the concept of antenna effective aperture is established to serve this purpose. The effective aperture A_e is less than the physical aperture A_p [90]. The directivity D can also be articulated in expressions of the aperture size and aperture efficiency η_{ap}:

$$D = \frac{4\pi}{\lambda^2} A_e = \frac{4\pi}{\lambda^2} \eta_{ap} A_p \tag{3.4}$$

where λ is the wavelength of the radio waves. By knowing the power density S at the receiving antenna, we can approximate the received power P_r:

$$P_r = SA_e \tag{3.5}$$

Thus during optimization course of action, much effort is devoted to improving the effective aperture to increase the gain while maintaining the low profile of the proposed antennas showed in Figure 3.6.

3.2.3 Skin Depth Effect and Antenna Performance

The skin depth and ohmic losses of the printed conductive layer set the boundary conditions for the manufacturing methods, and parameters such as the amount of

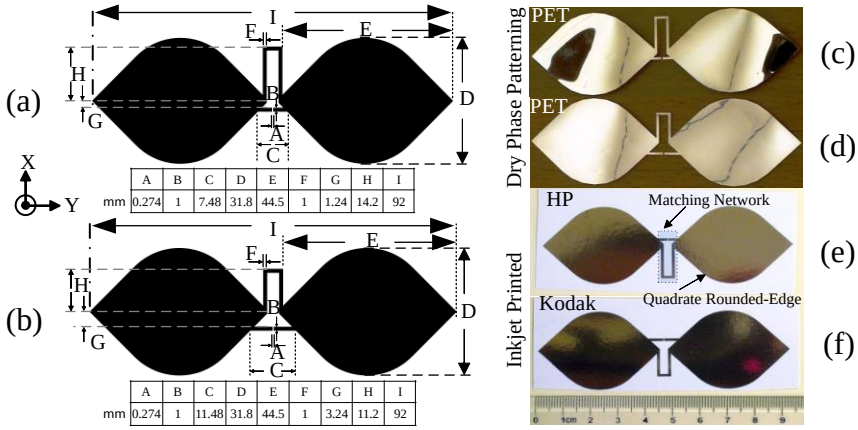

Figure 3.6: The geometry of RFID quadrate bowtie antenna for: (a) EU band, (b) NA band; DPP of antenna on PET for: (c) EU band, (d) NA band; inkjet printed antenna on: (e) HP photopaper for EU band, (f) Kodak photopaper for NA band. (Reproduced courtesy of The Electromagnetics Academy [11])

silver ink and the thickness of the printed layers. Skin depth is one of the significant factors that lead to achieve a certain thickness of the conductive layer/s [180]. Due to the skin effect at high frequencies, e.g., at UHF, the current density is crowded in the region near the surface of a good conductor. More precisely the skin depth is the depth below the surface of the conductor at which the amplitude of the incident electric field decays to 0.37% of the amplitude at the surface of the conductor. Mathematically, the skin depth δ in case of a good conductor is, therefore [90], expressed as:

$$\delta \approx \sqrt{\frac{1}{\pi f \mu \sigma}} \tag{3.6}$$

where f is the frequency, μ is the permeability and σ is the conductivity of the conductor material. Thus from above we can deduce three key conclusions that surround the manufacturing process of the proposed antennas:

1. The higher the frequency, (in this particular case, 860–960MHz), the smaller the skin depth.

2. The higher the permeability (in case, it is not that high, which needs attention while printing process), the smaller the skin depth. However, for a good conductor, the permittivity has little effect on the skin depth.

3. The higher the conductivity (in case, the conductivity of the printed structure is almost 5 times lower than that of bulk silver due to several parametric constrains in manufacturing), the smaller the skin depth.

3.2.4 Result Analysis and Discussion

Passive RFID tags for European and North American UHF RFID bands are manufactured with different substrates mentioned in Table 2.1, are measured across the frequency band of interest using half mirror method to investigate the reliability aspects of the proposed antennas for commercial grade practices. Ten identical prototypes of proposed structures are manufactured on an each paper substrate in order to determine the worst case analysis ingredients. Thus, each curve in Figure 3.7 represents the highest deviated values at a certain point among identical samples.

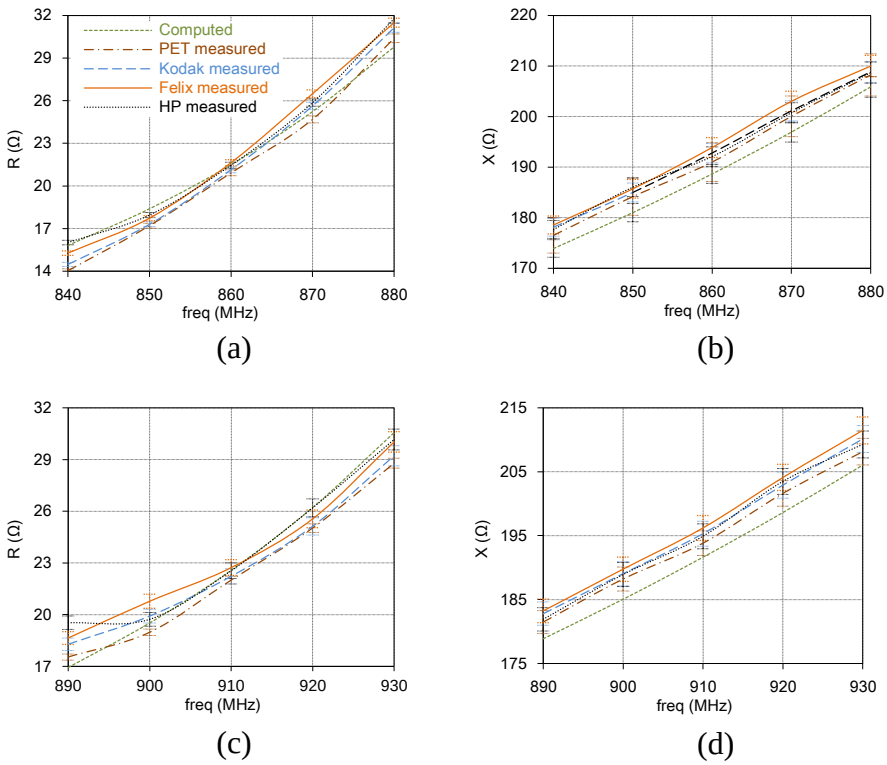

Figure 3.7: EU band's quadrate bowtie antenna input: (a) (radiation & loss) resistance variation, (b) reactance variation; NA band's antenna input: (c) (radiation & loss) resistance variation, (d) reactance variation. (Reproduced courtesy of The Electromagnetics Academy [11])

In order to verify the performance of the inkjet printed antennas of Figures 3.6(e) & (f), measurements are also executed using standard antenna prototypes fabricated on Aluminum coated PET substrate as showed in Figures 3.6(c) & (d). These standard prototypes have the same dimensions as

that of proposed antennas and are fabricated using DPP process at Acreo AB. The impedance variation of antenna in Figure 3.6(a) is shown in Figures 3.7(a) & (b). Whereas, input impedance plots of antenna in Figure 3.6(b) are shown in Figures 3.7(c) & (d). The resistive parts of impedance as showed in Figures 3.7(a) & (c) for EU and NA band antennas respectively, printed on different photopapers demonstrate consistency to the DPP antennas & simulated results throughout frequency band of interest which is a primary concern for antennas stable behavior. However, slightly greater drift is observed in the resistive part of the antennas printed on paper (p_e:smart) from Felix Schoeller as compared to the others but the difference remains within the acceptable range. Similarly, fairly coherent trend of reactance curves is depicted in Figures 3.7(b) & (d) for both proposed structures. The formation of round corners is used to obtain wider impedance band. Round corners at the sharp vertexes decreases the reflection of incident current near the edges and changes the current distribution on radiation surfaces. Thus, flatter impedance within the frequency band of interest with much stable real and imaginary parts is demonstrated in Figure 3.7.

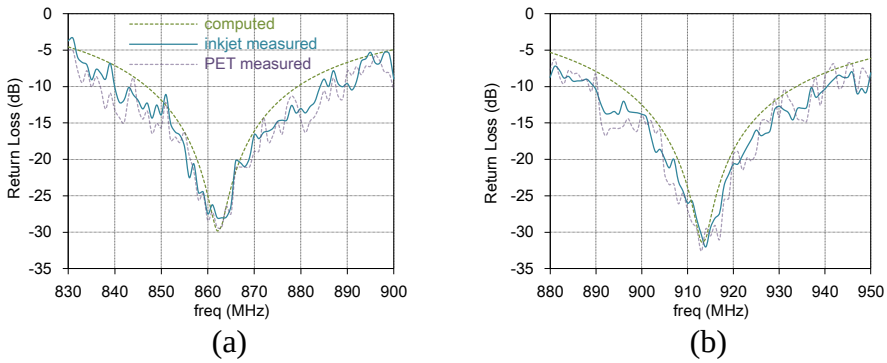

Figure 3.8: Return loss of quadrate bowtie antennas for: (a) EU band, (b) NA band. (Reproduced courtesy of The Electromagnetics Academy [11])

Using the Friis equation, the read range can be estimated by Equation (3.7) defining forward-link-limited range and Equation (3.8) defining reverse-link-limited range. Read range is also susceptible to the tag orientation, the object which the tag is placed on, path loss, spatial and temporal fading statistics of the propagation environment [145].

$$R_{forward} = \left(\frac{\lambda}{4\pi}\right)\sqrt{\frac{P_{TX}G_{reader}G_{tag}}{P_{min,tag}}} \tag{3.7}$$

and defining the minimum signal power for demodulation at the reader as $P_{min,rdr}$

we obtain the reverse-link-limited range:

$$R_{reverse} = \left(\frac{\lambda}{4\pi}\right)\sqrt[4]{\frac{P_{TX,reader}T_b G^2_{reader}G^2_{tag}}{P_{min,rdr}}} \tag{3.8}$$

where the output power of the reader is P_{TX}, the gain of the reader antenna is G_{reader}, and the gain of the tag antenna is G_{tag}. λ is the wavelength in free space at the operating frequency, P_{min} is the minimum power required to turn on the tag chip and T_b is backscatter transmission loss.

The read range from Equations (3.7) & (3.8) gives the maximum distance at which RFID reader can interpret the tag in free space. The proposed antennas have surpassed read range from 6.5m(HP) – 7.0m depending upon which substrate is utilized. Furthermore, the detailed analysis of read range variation is presented in Table 3.1 & 3.2.

The return loss results of antennas in Figures 3.7(a) & (b) is shown in Figures 3.8(a) & (b) respectively. It is pragmatic that the return loss of the inkjet printed antennas is slightly higher than the return loss of standard PET substrate antennas. Overall, good agreement between the standard PET-based, and the inkjet printed antennas is observed, regardless of the higher metal loss of the silver based conductive ink. The normalized computed radiation pattern and the microwave chamber measurements are plotted in Figure 3.9. The radiation patterns are nearly uniform (omnidirectional) at 915MHz. They show remarkably satisfactory agreement between computations and measurements. The same uniformity in antenna radiation pattern could be demonstrated for other frequencies within the antenna's bandwidth. Similar parametric behavior is depicted by proposed antennas for EU band, which are shown in Figures 3.6(a), (c) & (e).

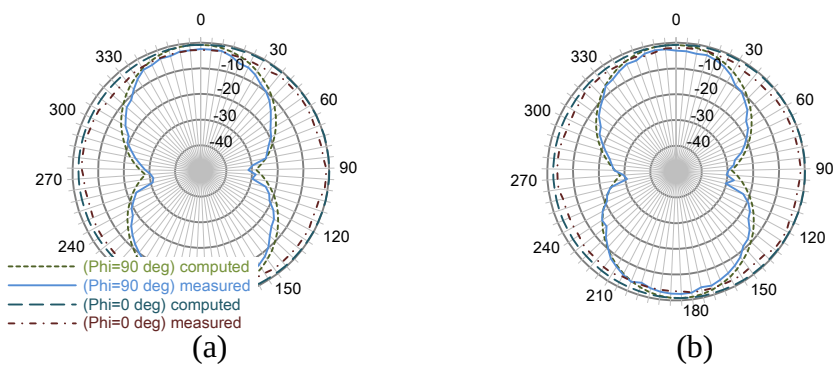

Figure 3.9: Measured & computed 2D far-field radiation plots of quadrate bowtie antennas for: (a) EU band, (b) NA band. (Reproduced courtesy of The Electromagnetics Academy [11])

Table 3.1: Analysis of effect by metal on the proposed tag at 915MHz [11].

Measured • Computed ∗	Input impedance (Ω)•	Rad. eff. (%)∗	Trans. coeff. (dB)∗	Directivity (dBi)∗	Gain (dBi)∗	Reading range, R (m)•
Free space	24.42 + j194.92	83.64	–1.07	1.85	1.97	6.50
d = 1 mm	4.31 + j152.13	1.02	–13.57	7.96	–10.37	0.31
d = 5 mm	5.76 + j173.06	6.61	–9.97	8.26	–1.12	1.14
d = 10 mm	7.75 + j186.55	18.02	–3.53	8.29	0.58	3.22
d = 15 mm	10.17 + j193.10	30.67	–0.67	8.28	2.92	8.10

3.2.5 Analysis for Industrial Applications

Effects of Metal on Tag Antenna Performance

The metal effect is limited in the tag antenna which has its own ground plane [175, 125]. However, the antenna which does not have a ground plane, such as quadrate bowtie, the radiation characteristics and input impedance of the antenna, are distorted when the tag is placed on or near a metal object. Whenever there is an encounter with metal objects these variations certainly impact the tag performance [87]; however, even if it is not possible to eliminate it completely [52]; it is made possible in the proposed antennas to, strongly limit this phenomenon.

The comprehensive data on the metal effect on the proposed RFID tag antenna placed close to a metal plate and reading distance at 915MHz is summarized in Table 3.1. The antenna is positioned parallel to and below a metal plate measuring 30cm × 30cm. The directivity, radiation efficiency, gain, and input impedance, are examined for the different distances from the metal plate. Considering the worst case, i.e., when the antenna is placed extremely close to the metal plate (d = 1mm), the directivity of the antenna enhances significantly to around 8dBi. However, the radiation efficiency plunges drastically to 1.02%, which results in remarkably low gain of –10.37dBi at 915MHz. Particularly, the real part of the input impedance varies severely, as well. This variation in impedance outcome in deprived impedance matching with the RFID tag chip (circuit showed in Figure 3.5), resulting in a transmission loss of –13.57dB at 915MHz. The gain reduction and poor impedance matching results in the reading distance reducing to 0.31m. However, the proposed antenna still exhibited superior reading distance when placed so closer to the metal object in coherence with previously published results [52, 125].

The directivity of the antenna remains virtually unchanged, by moving the antenna further away from the metal plate. In the meantime, the radiation efficiency shows an escalating drift, which domino result in increasing antenna gain. The real part of the input impedance shows modest change, whereas the imaginary part inclined to values close to those in free space. An increasing trend is observed in

Table 3.2: Analysis of effect by water on the proposed tag at 915MHz [11].

Measured • Computed ∗	Input impedance (Ω)•	Rad. eff. (%)∗	Trans. coeff. (dB)∗	Directivity (dBi)∗	Gain (dBi)∗	Reading range, R (m)•
Free space	24.42 + j194.92	83.64	–1.07	1.85	1.97	6.50
d = 1 mm	129.27 + j330.00	8.77	–9.51	4.12	–7.51	0.61
d = 5 mm	23.61 + j201.20	6.29	–1.32	2.67	–10.05	1.15
d = 10 mm	13.77 + j189.04	20.26	–0.33	2.81	–3.02	3.23
d = 15 mm	12.20 + j189.90	27.64	–0.15	3.73	–1.13	4.37
d = 20 mm	10.21 + j190.82	38.31	–0.08	4.93	–0.12	5.26

the reading distance; when the tag is moved away from the metal plate. When the tag is moved to d = 5mm, the reading distance exhibits higher value than that of in free space because the metal plate acts as a reflector which ultimately boosts the tag antenna gain. In conclusion, although the metal object degrades the reading range of the tag significantly when it is directly attached or is placed real close to it, but the proposed antennas are even capable of reasonably communicating under these critical testing conditions.

Effects of Water on Tag Antenna Performance

Table 3.2 shows the complete characteristic analysis of the proposed antenna which is placed close to a water cuboid. The antenna is placed parallel to and above a water cuboid which is measuring 30cm×8cm×8cm; whereas, ε_r = 77.3 and tanδ = 0.048 [211] of water is adopted in this experimentation. The input impedance, radiation efficiency, directivity, and gain are inspected at different distances away from the water cuboid. When the proposed antenna is placed closer to water at a distance of d = 1mm, the directivity of the antenna amplifies while the radiation efficiency reduces considerably, which domino effect in a decrease, in the antenna gain. In dissimilarity with the metal plate effect, it is pragmatic that the water always causes a decrease in the gain regardless of the distance between the water and the proposed antenna. When the antenna is moved further away at a distance of d = 15–20mm, the antenna gain achieves the value roughly equal to that in free space. The input impedance displays a smoother variant with the exception of the situation once the antenna is extremely close to the water i.e.; d = 1mm. If the tag antenna is placed extremely close to water (that means almost touching the cuboid), the reading distance reduces considerably to 0.61m but not that much as observed in the case of metal plate. When the tag is moved further away, the effect of the water is declined; resulting in read range enhancement. Therefore, exhibiting the graceful degradation in functionality for suitability in high performance industrial applications. The proposed antennas exhibit improved performance and

are in accordance with commercially available RFID tags and previously published results [35].

Furthermore, the metallic plate and water do not degrade the bandwidth of the proposed antennas to such an extent that they become unreadable until the tag is placed closer than $d = 1$mm. The bandwidth degradation behavior is constant, in case the tag is brought nearer to the water containing objects, but in case of metallic plate, the bandwidth degradation is more serious particularly within $d = 5$mm. The proposed antennas are designed with reasonably wideband in order to demonstrate readable bandwidth at the expense of read range (bandwidth vs read range trade-off) which limits their usage to narrow bandwidth operations i.e. either for EU band or NA band. The stabilization of bandwidth can further be achieved by reducing the effect of matching network, but that will induce instability against dielectric variation of paper substrate, so it is trade-off always among optimum values depending upon the applications.

3.3 Summary

The development of extremely versatile eco-friendly antennas for a high robustness level with respect to mechanical stresses and dielectric environment is demonstrated. The novel quadrate bowtie antennas for UHF RFID industrial applications have been proposed and fabricated on paper and PET substrates, using inkjet printing and DPP technology, respectively. In addition to categorical optimization of antenna profile, a T-matching network is introduced to develop a novel compact, RFID tag, featuring outstanding overall performance. The quadrate bowtie antennas exhibit exceptional operational characteristics when stumble upon metal and water containing objects. The use of the inkjet printing process in the development of these proficient RFID antennas on different types of paper has also been demonstrated, verifying that paper-based inkjet printing topologies offer a remarkably low-cost, green solution [152] to system-level packaging for UHF, wireless, and microwave applications.

Chapter 4

RFID Antennas: Wideband

This chapter (which is reformation of included Papers III–VI) includes performance optimized wideband RFID tag antennas which cover the entire UHF RFID ISM band (860–960MHz). The innovative antenna structures can endure the variations which emerge in electromagnetic properties of paper substrate due to varying environmental effects. New antenna design methodologies are developed in an attempt to reduce the consumption of substrate material and conductive ink while achieving optimum read range. This chapter also gives a unique insight into evaluating sustainability that validates the potential for ultra-low cost mass production of RFID tags for green electronics.

4.1 Bowtie Antenna: Rounded Corners with T–Matching

This section presents a thorough review of novel rounded-corner bowtie passive RFID tag antennas, which are fabricated on different ultra-low-cost substrates Table (2.1) in combination with the printing technologies already mentioned in section 2.2 for these particularized antennas as a trial run. The implementation of T-match arms for matching of the antenna to the integrated circuit (IC) is introduced that improves the reliability against environmental diversities as well as increase the maximum reading distance.

4.1.1 Antenna Dimensions and Parametric Optimization

The main purpose of optimization is to maximize the feeding power to the load to achieve the maximum possible read range while preserving the multifaceted nature of the proposed antenna. The NXP UCODE G2XM (Al strap) RFID IC is preferred. The proposed antenna structure is shown in Figure 4.1 along with dimensions and IC terminals placed in the center of the T-match arms. The T-match arms are also responsible for the matching of the antenna impedance to that of the IC through the fine tuning of the length L_4, height h, and width W_2.

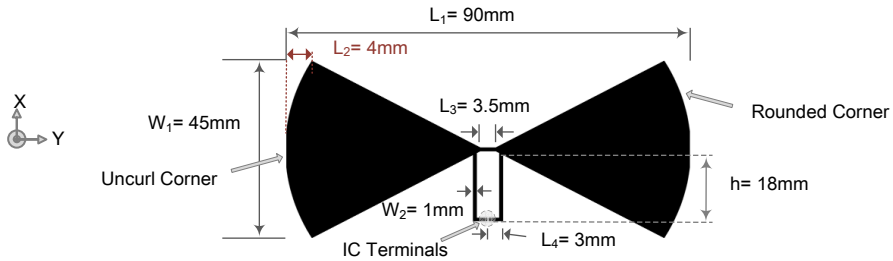

Figure 4.1: T-match folded rounded-corner bowtie RFID tag. (Reproduced courtesy of The Electromagnetics Academy [13])

In the proposed tag, antenna is directly connected to a source (IC or strap) thus, the impedance matching will stand for the optimal antenna. This ultimate goal defines the essence of antenna design in order to control the current distribution, which in turn determines the radiation pattern and input impedance. Therefore, to assess development process thoroughly all relevant parameters of antenna are analysed, which are categorized from the manufacturing, circuit and field point of views as summarized in Figure 4.2.

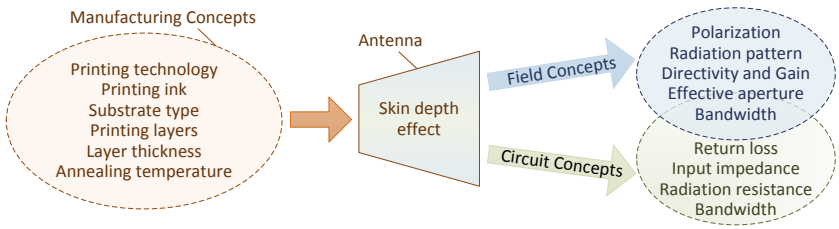

Figure 4.2: An outline of key antenna development parameters. (Reproduced courtesy of The Electromagnetics Academy [13])

4.1.2 Field and Circuit Concepts Parametric Analysis

During the printing process of the proposed antennas, attention is given to fabricate five identical structures with the same combination of printing material, ambient conditions & technology. These prototypes are then measured across the UHF frequency band using half mirror method. Half mirror method is adapted instead of balun usage to eliminate the possibility of error [121]. Furthermore, maximum deviated data value at a frequency among five prototypes is reported here.

Figures 4.3(a) & (b) show the impedance plots. As showed in Figure 4.3(a), the computed resistance for the antenna in the UHF RFID frequency range maintains a value close to 14Ω between the two successive peaks. There is extremely small

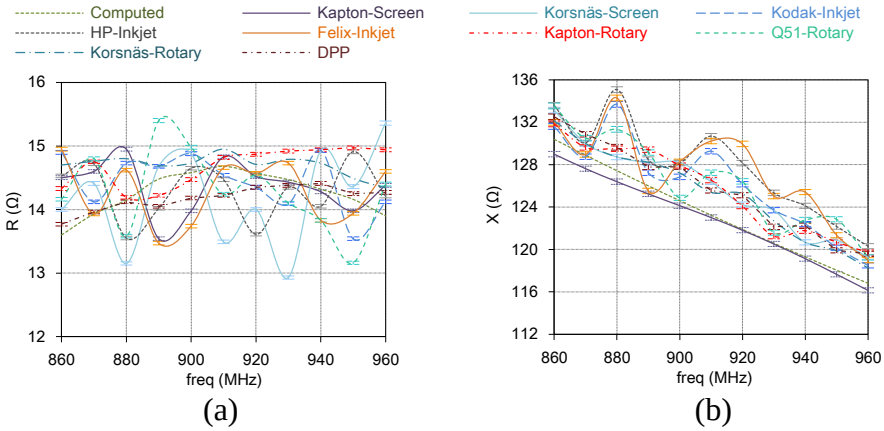

Figure 4.3: Antenna input: (a) resistance variation, (b) reactance variation. (Reproduced courtesy of The Electromagnetics Academy [13])

variation observed among the curves for different antennas, and it can be well illustrated from the Figure 4.3(a), that all the prototype antennas have maintained the resistance around 14Ω in a linear fashion with frequency. The reactance part of the impedance, as showed in Figure 4.3(b), follows a positive value with a linear variation with frequency, pertaining to an inductance that conjugately matches or, equivalently, cancels the effect of the 1.42pF input capacitance (parallel) of the IC. It is observed that a relatively constant concurrence is found between the computed and measured results.

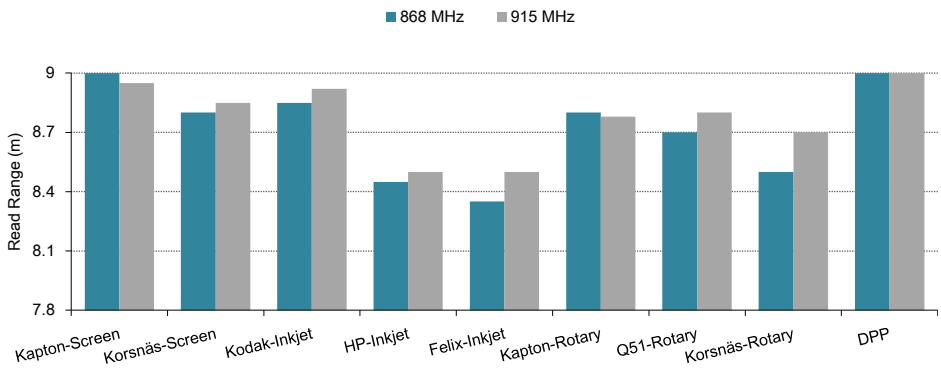

Figure 4.4: Measured read range. (Reproduced courtesy of The Electromagnetics Academy [13])

The RFID IC/strap is attached to the IC terminals on printed structures with

CW2400 silver conductive epoxy. It is observed that the read range can be influenced by the reader antenna in use. The measured and computed results are in close agreement, and the maximum read range achieved is 9 meters. The complete comparison of read range of different printed antennas is analysed in Figure 4.4, which exhibits the improved performance than previously published results [169, 35].

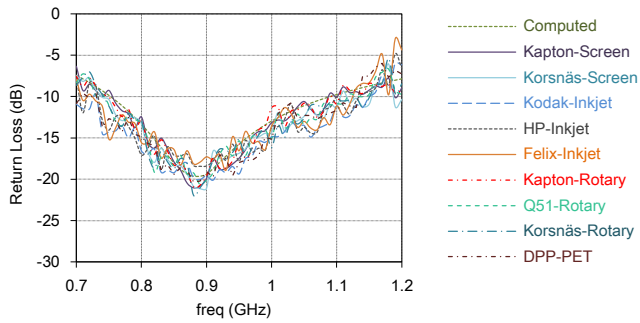

Figure 4.5: Measured and computed return loss. (Reproduced courtesy of The Electromagnetics Academy [13])

The return loss of the antenna structure is calculated based on the power reflection coefficient. The computed return loss is showed along with measured values of the rotary, screen, DPP & inkjet printed antennas in Figure 4.5. On the whole, a good agreement among the computed, and the manufactured antennas is pragmatic despite the higher metal loss of the silver-based conductive ink. Moreover, it is deduced from Figures 4.4 & 4.5 that the proposed antenna design can gracefully cater the variations in the properties of different substrates mentioned in Table 2.1. The characteristics of the bowtie profile of the half-wavelength dipole antenna body allows for a broadband operation. The bandwidth of the proposed antenna is 197MHz, corresponding to 23% around the center frequency 855MHz; so it covers the worldwide UHF RFID bands and can cater greater degree of environmental disparities. Another larger variant of the proposed antenna (Paper IV) with semi-curled corners is developed which demonstrates greater stability against environmental effects. Furthermore, each calculation at a frequency is carried out by considering the variation of the IC reactance, which varies from 130–116Ω from 850–960MHz, respectively. In general, it is sufficient by conjugately matching the antenna input impedance to those provided in the IC specifications by the manufacturer around the center frequency.

The normalized computed radiation pattern and the microwave chamber measurements are plotted in Figure 4.6. The radiation patterns are nearly uniform (omnidirectional) at 915MHz with directivity around 2.1dBi and show extreme agreement between computations and measurements, which can also be verified for other frequencies within the antenna bandwidth and are in coherence with previously published results [52, 169].

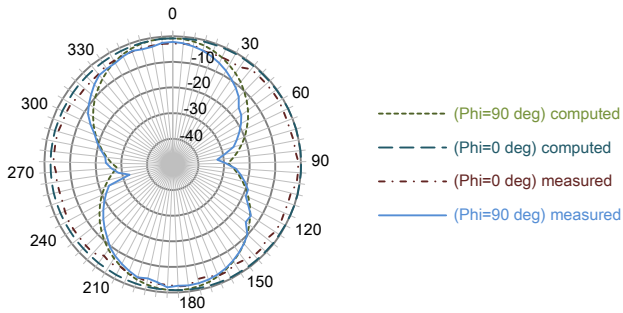

Figure 4.6: Measured & computed 2D far-field radiation plots. (Reproduced courtesy of The Electromagnetics Academy [13])

4.2 Bowtie Antenna: Rounded Corners with Hole–Matching Technique

In this section, a UHF RFID tag antenna using an innovative technique of pattern holes for conjugate impedance matching with the RFID strap, while at the same time saving the expensive ink is discussed. The antenna is designed by eliminating the matching network in order to achieve wideband characteristics and reliability against environmental multifariousness. We have revisited the manufacturing technique in order to achieve extra degree of enhancement in electrical characteristics while utilizing inkjet printing technology. The proposed antenna is directly printed on different commercially available paper substrates which are characterized for flexible printed electronics (Table 2.1). Furthermore, an in-depth sustainability and life cycle analysis is provided, which reveals that the proposed tag provides promising results for large items level tracking in supply chain (cardboard cartons containing water & metal objects) and goods (wood or metal pallet) transportation.

4.2.1 Antenna Design and Optimization

The proposed antenna is optimized for maximizing the read range while minimizing the ink consumption and effects of environmental harsh conditions on RFID tag. One of the critical observations made while field testing (in supply chain industry) of antennas having thinner traces used for matching network, is that the effect of even minor scratches on those tracks can cause loss of RFID tags during transportation. Therefore, it led towards the realization of a structure which can eliminate such risk factors while exhibiting better performance.

The NXP UCODE G2XM (SOT1040AB2 (Al strap), for instance the goal IC impedance at 915MHz is 13.3-j122Ω) is preferred. It is noteworthy here that the proposed design and technique is not restricted to the above mention RFID IC and it can be realized with any other commercially available RFID straps to produce

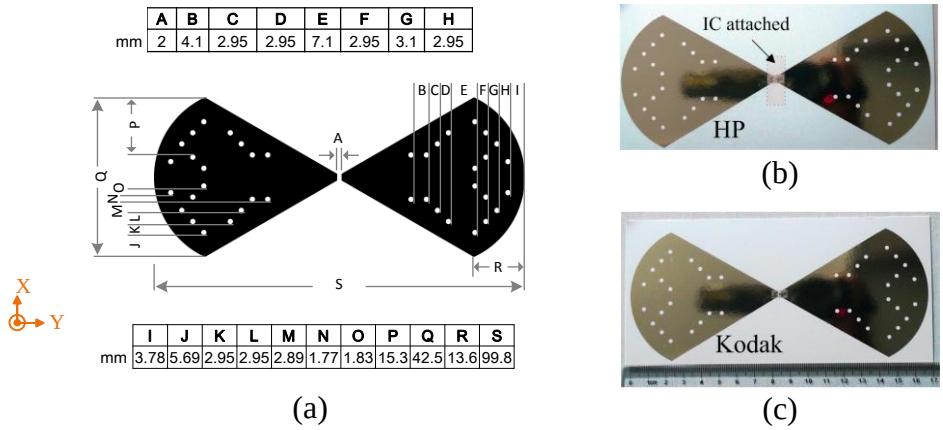

Figure 4.7: (a) The geometry & dimensions of RFID antenna; inkjet printed RFID tag on: (b) HP photopaper, (c) Kodak photopaper. [17]

optimum results accordingly. The proposed rounded corner bowtie antenna structure is shown in Figure 4.7(a), and the printed antenna integrated with RFID strap forming an RFID tag in Figures 4.7(b) & (c). The implementation of pattern holes is responsible for matching of the antenna impedance to that of the IC through the fine tuning of their location and size which is mentioned in Figure 4.7(a). It is observed that earlier efforts [154] to reduce the ink usage led towards lower gain and as a result, the scope of those tags is limited in supply chain industry. In the proposed approach for achieving multidimensional performance benefits, the pattern holes suite these requirements effectively. It is noticed that the inner holes positions *(B–D)* are more persuasive towards antenna efficiency whereas, the outer hole positions *(E–I)* assist more towards fine tuning the impedance. The vertical positions of holes *(J–P)* are critical towards current distribution. Moreover, it is observed that the insertion of more pattern holes can cause the performance degradation. In achieving extended read range while keeping minimum antenna size as possible, an established concept that the effective aperture is less than the physical aperture is accomplished [90], which resulted in predilection of rounded corner structure.

4.2.2 Effect of Annealing Temperature

In addition to manufacturing parameters discussed in section 2.2.4, in this study, effect of annealing temperature is observed in order to achieve a greater degree of conductivity while using the same set of printing parameters. Losses in a conductor and substrate materials are particularly challenging to identify through measurements. Even though, methods for such analysis have been proposed [187], but it is yet more difficult when the conductor under consideration is a radiating antenna [27]. The effect of reduced conductivity is ab initio obtained by simulating

the antenna in free space, which is also verified by mounting the printed antennas on HF51 [170], i.e. virtually with no substrate and then after with the substrate to acquire a complete overview of parameters that need to be optimized for paper printing. It is discovered that the antenna formed by a Perfect Electrical Conductor (PEC) has the widest smith chart impedance loop and is exceptionally tight followed by antennas with sheet resistance of 50–150mΩ. The antennas made with the highest sheet resistances, 1000–2000mΩ, featured narrower loops. A narrower loop, caused by the higher ohmic losses, is an indication of the antenna receiving a lower Q-value.

Thus, higher the sheet resistance; more antenna structure behaves similar to an open end transmission line. From these observations, the annealing parameters are investigated to achieve better curing while, at the same time due to green nature of the proposed antennas, lowest possible energy should be consumed to accomplish optimum manufacturing objectives. After rigorous iterations, it is concluded that each type of paper substrate should be annealed at different temperature in order to attain better conductivity, in spite of the fact that all antennas under test are printed with same conductive ink.

4.2.3 Results Discussion and Parametric Analysis

The measurements are carried out in a multidimensional approach for not only finding out the impedance, return loss, radiation pattern and read range but also determine the reliability parameters, which are extracted by repeatability. Thus, for worst case analysis five identical antennas with the selfsame combination of printing material, ambient conditions and inkjet technology are fabricated. The purpose of using several paper substrates is to verify the performance matrix on a rational basis, because paper substrates from different manufacturers significantly differ in properties exploited by printed electronics. In order to get a better understanding of antenna behavior when printed on paper substrate, maximum deviated data value at a frequency among five prototypes is reported hither.

It is observed from Figure 4.8(a) the computed and measured resistance for the antenna from 860–960MHz maintains a value around 14Ω all over the curves. It is noteworthy, that the proposed structure and design technique are well suitable for adequate tuning of the matching characteristics as depicted in Figure 4.14. The reactance part of the impedance, as showed in Figure 4.8(b), exhibits a positive value with a linear variation with frequency, and slight fluctuation within acceptable values is pragmatic. It is noticed that a reasonably good harmony exists between the computed and measured results. The read range performance testing is conducted with Impinj's UHF RFID reader Kit and in order to make the measurement more edifying, the proposed tag is bonded on a closed-cell rigid foam HF51 from ROHACELL's with 90mm thickness [170, 8]. The foam is based on polymethacrylimide (PMI) chemistry and has extremely low dielectric constant of 1.057@2.5GHz, resembling that of the free space and is especially designed for antenna applications. This setup facilitates to determine the tag read range variation when placed on

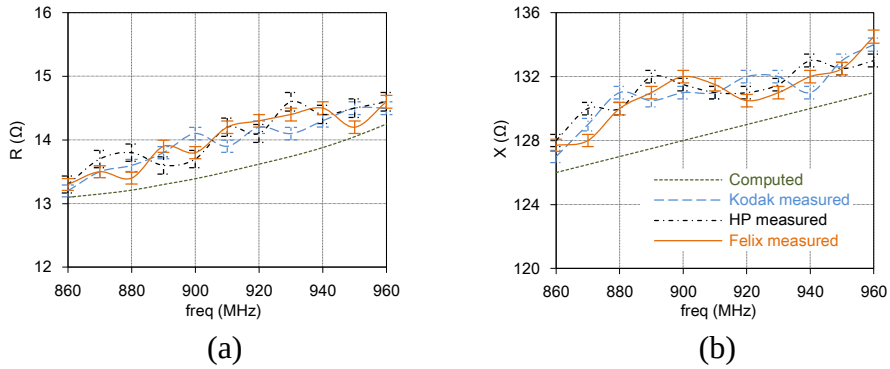

Figure 4.8: Input: (a) resistance variation, (b) reactance variation. [17]

different objects, as analyzed in Figure 4.9(a) for cardboard cartons exclusively containing cola cans and plastic water bottles. The measured read range validates the exceptional performance of the proposed RFID tag.

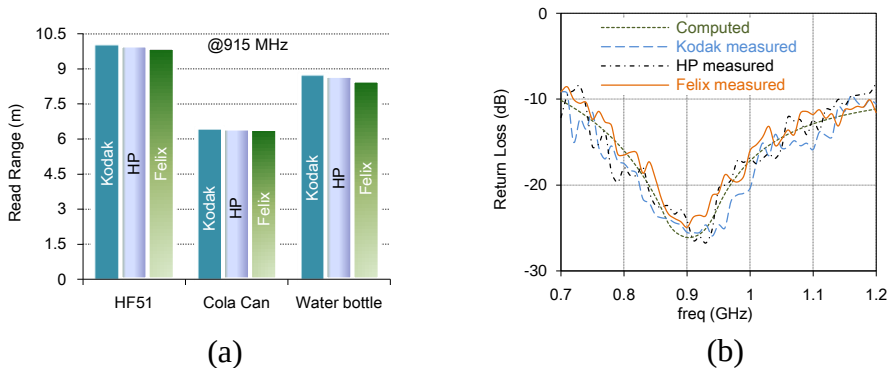

Figure 4.9: (a) Measured read range, (b) measured and computed return loss. [17]

The return loss of the antenna is calculated based on the power reflection coefficient. Figure 4.9(b) shows the measured and computed return loss of the proposed antenna. The distortion in the measured values is due to the ground plate fixture used for half mirror method, which can be reduced or eliminated by using ground plate with more curved edges. The 3D simulated and 2D measured normalized radiation patterns of antenna printed on Kodak photopaper at characteristic frequency of 915MHz are plotted in Figures 4.10(a) & (b), respectively. The antenna exhibits stable gain values throughout the frequency band of interest. The radiation patterns are almost uniform (omnidirectional) at 915MHz and show tremendous match between computations and measurements, which can also be demonstrated for other frequencies (860–960MHz) within the antenna bandwidth, and are in consistency

with earlier published results [169, 215].

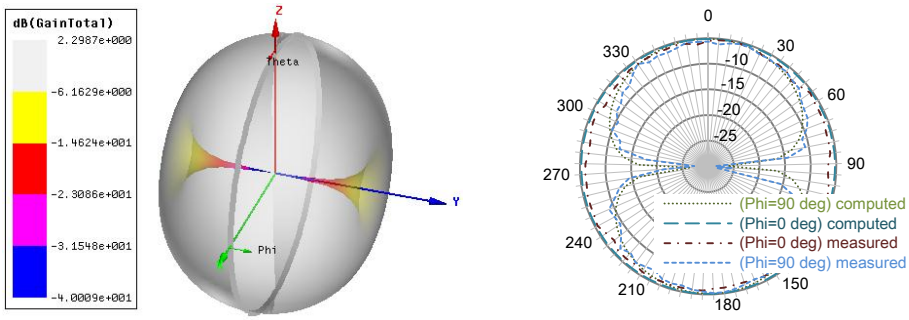

(a) (b)

Figure 4.10: (a) 3D simulated, (b) 2D measured; far-field radiation plots. [17]

4.2.4 Sustainability and Environmental Impacts Analysis

This section emphasis on sustainability and environmental impacts analysis for the proposed antenna to validate that it has the potential to be used in various RFID-based eco-friendly applications. Figure 4.7 explicitly shows the dimension of the antenna which leads to determine the area required to accommodate antenna on the substrate that is 10cm×4.3cm. Inkjet printing is considered for tracing the pattern on the substrate. The environmental impacts model is created as showed in Figure 4.11 by using life cycle assessment software "GaBi" [69].

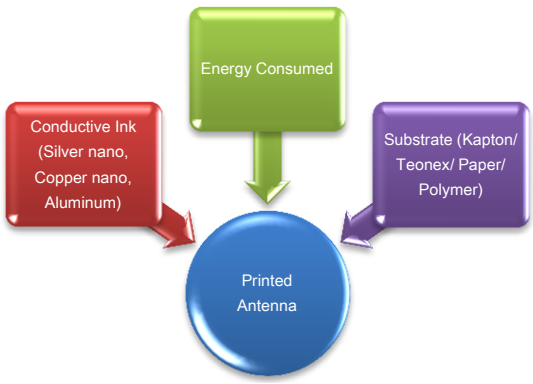

Figure 4.11: Parametric model required for sustainability analysis.[17]

Inkjet printing is accomplished by using Fujifilm Diamatix printer which is operated at 230V AC, 50Hz with maximum power consumed at any moment is 375W.

The estimated time required for printing a pattern is 15 minutes. If the printer operates at its maximum power rating, the energy required to print 1 million patterns is 337500 Mega Joules i.e. ($375\times15\times60\times10^6$). The substrate under test is high gloss inkjet photopaper with standard weight of 280g/m^2 and thus for 1 million tags the required weight of paper substrate is 975.545kg ($230\times99.8\times42.5\times10^{-3}$). The capability of the printer to produce the antenna trace on paper substrate is 4000 structures with 1000ml (1kg) of conductive ink. Therefore, the estimated amount of conductive ink consumed for production of 1 million tags is 250kg. The mass of each component for manufacturing 1 million proposed RFID antennas is summarized in Table 4.1.

Table 4.1: Mass of each component specified in the model.

Material	Mass
Substrate (Paper / Kapton/ Teonex)	976kg
Conductive Ink (Silver nano / Copper nano / Aluminum)	250kg
Energy Consumed	337500MJ

Based on the modeling parameters, possible environmental impacts are explored in terms of global warming potential ($KGCO_2$ equivalent), acidification potential ($KGSO_2$ equivalent), ozone layer depletion potential and human toxicity potentials. The Institute for Environment and Sustainability, European Commission Joint Research Centre, has published the research report [56] that recommends a preferred methodological approach which aims to calculate the environmental footprints of the products and organizations. For product environmental footprint, "ISO 14044: Environmental management - Life Cycle Assessment" is a recommended method. This method is employed to analyze the environmental footprint sustainability analysis of the proposed printed antenna. Life cycle approach takes into consideration the spectrum of resources flows and environmental interventions associated with the product, service, or organization from a supply chain perspective, including all phases from raw material acquisitions through processing, distribution, use and end of life processes [82, 219]. There are different methods such as TRACI (Tools for reduction and Assessment of Chemical and other Environmental Impacts) and CML (Centre for Environmental Studies, University of Leiden) that are employed to perform life cycle impact assessment. In this study, LCIA-CML methodology is considered to achieve the projected research analysis.

Figure 4.12 shows the potential environmental impacts in the manufacturing process of the proposed printed antenna. Four main environmental impacts are demonstrated and in each emission profile, there are four columns that correspond to the quantity of emissions caused by a specific component such as substrate, conductive ink or the associated energy consumptions in manufacturing 1 million printed antennas. $KGCO_2$ and $KGSO_2$ are carbon dioxide and sulphur dioxide equivalent emissions while ozone layer depletion and human toxicity potentials are

computed by the release of trichlorofluoromethane (CFC-11, also known as R11) and dichlorobenzene (DCB), respectively.

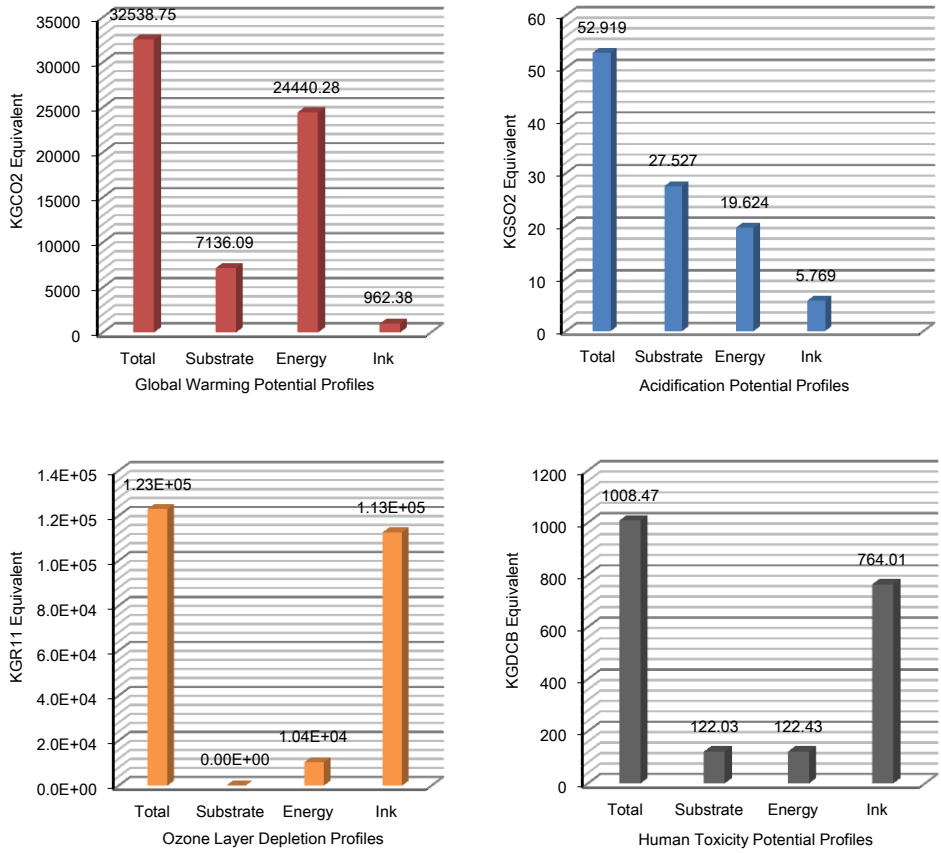

Figure 4.12: Environmental emissions profiles. [17]

4.3 Bowtie Antenna: Square Hole–Matching Technique

The supply chain represents a holistic system and is an efficacious candidate for widespread greening initiatives. In supply chain, RFID tags are used at different levels. Pallet-level tagging illustrates the environment where RFID tags are attached to individual pallets. Pallet-level tagging is characteristically used in full-pallet storage and logistics & transportation applications. In Carton-level tagging, RFID tags are attached to cartons. This level of tagging facilitates mixed-pallet loads. Lastly, in item-level tagging, each manufactured commodity has its sole RFID tag [77, 118].

This section presents electromagnetic analysis of a flexible, planar UHF RFID tag antenna which is optimized for long read range applications. The proposed antenna is manufactured on three different commercially available paper substrates (Table 2.1) with inkjet printing technology. The proposed antenna uses innovative technique of square pattern holes for conjugately impedance matching with the RFID chip, thus eliminating the use of matching network and reduces the ink usage. The antenna exhibits wideband characteristics for its entire coverage of UHF RFID band (860-960MHz). The proposed tag is intended for large items-level tracking in supply chain (cardboard cartons containing water & metal objects) and freight (wood or metal pallet) transportation [16].

4.3.1 Antenna Design Numerical Analysis and Optimization

The proposed antenna is designed and optimized in a methodical approach, explained in Figure 3.1. The concept stage encompasses an antenna design, which can exhibit better read range and smaller size in order to reduce the ink consumption. It is also emphasized that the antenna can cater the environmental variations, which may affect attributes of paper substrate in order to realize eco-friendly economical RFID tags. Bowtie structure having square pattern holes is implemented for conjugately matching the antenna impedance to that of NXP UCODE G2XM (Al strap-SOT1040AB2). The primary aim of iterations and parametric optimization is to maximize the feeding power to the load (RFID IC) which encapsulates the concept of effective aperture. Hence during optimization strategy, much effort is devoted for improving the effective aperture in order to boost the antenna gain which consequently increases the amount of power delivered to the chip of the proposed RFID tag showed in Figure 4.13.

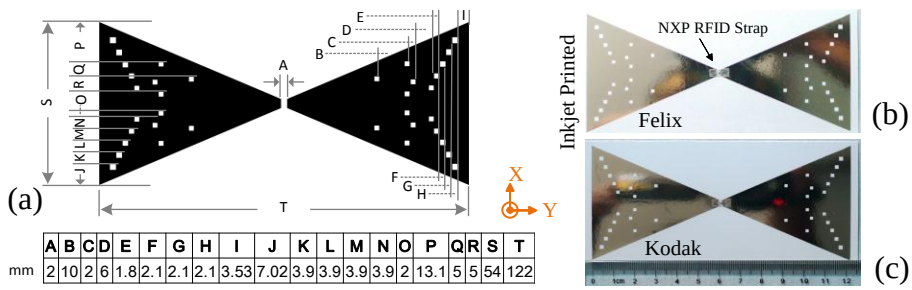

	A	B	C	D	E	F	G	H	I	J	K	L	M	N	O	P	Q	R	S	T
mm	2	10	2	6	1.8	2.1	2.1	2.1	3.53	7.02	3.9	3.9	3.9	3.9	2	13.1	5	5	54	122

Figure 4.13: (a) The geometry & dimensions of RFID antenna; inkjet printed RFID tag on: (b) Felix paper, (c) Kodak photopaper. [16]

Now by achieving maximum effective aperture A_{e-max} of the tag antenna (by using Equations 3.4 & 3.5) located in the field of the reader antenna with the power density S as showed in Figure 4.14. The tag antenna receives the power from the wave and delivers it to the RFID chip (strap) with load impedance Z_c.

Fraction of the power received by the tag antenna is delivered to the chip whereas the remaining portion of power is reflected and re-radiated by the antenna. Thus, the power transmission coefficient, τ is used to calculate the power delivered to the RFID chip. Mathematically, it is expressed as:

$$P_{tag-chip} = \tau P_{tag-ant} \tag{4.1}$$

where $P_{tag-ant}$ is the power antenna received from the incident wave, and $P_{tag-chip}$ is the power delivered to the chip. The power transmission coefficient, τ, is determined by the impedance matching between the tag antenna and the chip. Therefore, good impedance matching between antenna and chip is of paramount importance. It is worth mentioning here that both Z_a and Z_c are frequency-dependent.

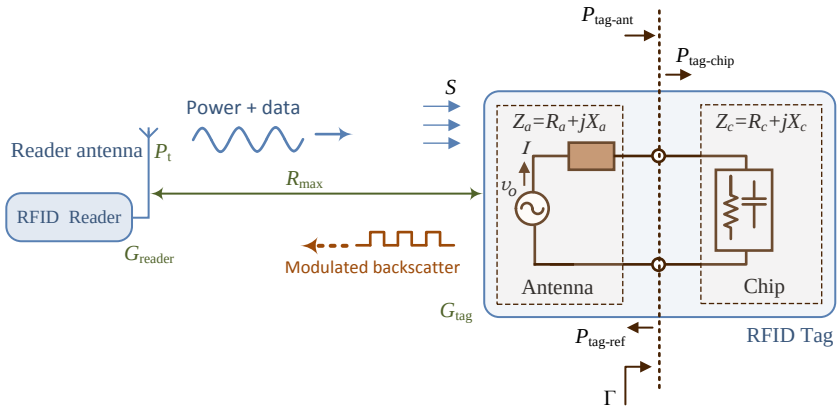

Figure 4.14: Enriched tag equivalent circuit & far-field RFID mechanism. [16]

Power wave reflection coefficient Γ is defined to evaluate the transmission of the power waves as:

$$\Gamma = \frac{Z_c - Z_a^*}{Z_c + Z_a}, \quad 0 \leq |\Gamma| \leq 1 \tag{4.2}$$

Thus, the power delivered to the chip is:

$$P_{tag-chip} = \left(1 - |\Gamma|^2\right) P_{tag-ant} \tag{4.3}$$

Therefore, the power transmission coefficient is calculated by:

$$\tau = \frac{P_{tag-chip}}{P_{tag-ant}} = 1 - |\Gamma|^2 = \frac{4R_aR_c}{(R_a + R_c)^2 + (X_a + X_c)^2}, \quad 0 \leq \tau \leq 1 \tag{4.4}$$

From Equation (4.3) maximum power is transferred when the antenna is conjugately matched to the chip, i.e. $R_c = R_a$ and $X_c = -X_a$, then $|\Gamma| = 0$, $\tau = 1.0$. The matching is tuned by size and number of square pattern holes in the proposed

antenna as showed in Figure 4.13, therefore, after rigorously going through the numerical analysis in recognition of optimum proposed antenna, Equation (3.5) takes the form:

$$P_{tag-chip-max} = P_{tag-ant} = SA_{e-max} \tag{4.5}$$

It is advantageous to relate the power transmission coefficient, τ, to another widely used parameter, return loss (RL), for describing the impedance matching characteristics. The return loss is defined as:

$$RL = 10log_{10}(|\Gamma|) \tag{4.6}$$

The return loss is computed and measured for the proposed antenna which is explained in next section. Moreover, for further analysis, with the return loss, the corresponding reflection coefficient and the power transmission coefficient can be easily calculated.

4.3.2 Results Discussion and Analysis

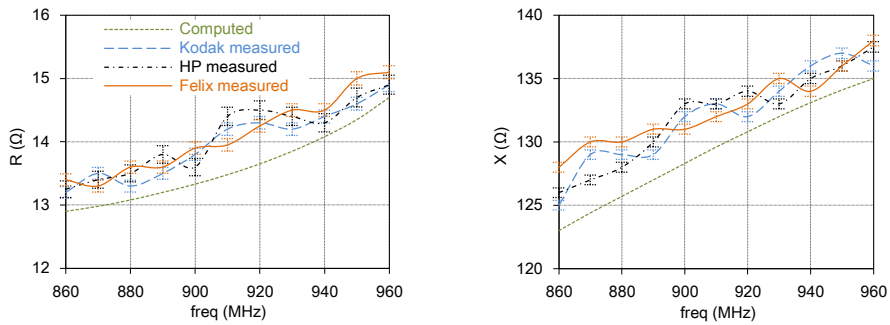

Figure 4.15: Input: (a) resistance variation, (b) reactance variation. (Reproduced courtesy of Taylor & Francis)

The operation frequency of the demonstrated printed UHF RFID tag is 860–960MHz. However, the measurement analysis for read range and far-field radiation patterns are punctuated for EU and North American bands to make the analysis more comparative and elaborative. The characterization of reliability and repeatability is conducted, employing worst case analysis, by manufacturing five selfsame prototypes using the same combination of printing material and ambient conditions.

Figures 4.15(a) & (b) show the impedance plots. It is observed from Figure 4.15(a) the computed and measured resistance for the antenna from 860–960MHz varies between two extremes, from 13–15Ω with mostly measured values maintain around 14Ω. However, fairly constant conformity is obvious among

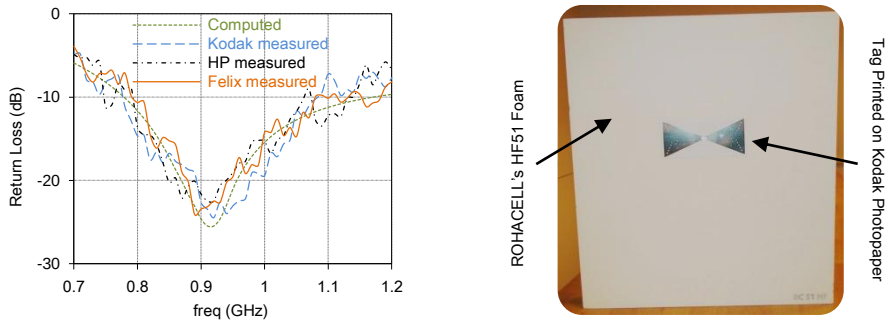

Figure 4.16: (a) Measured and computed return loss, (b) tag attached to semi-rigid foam for read range measurements. (Reproduced courtesy of Taylor & Francis)

the curves of antennas printed on different substrates. The reactance part of the impedance, as showed in Figure 4.15(b), exhibits a positive value with a linear variation against frequency. There are minor fluctuations among the curves with a maximum 5% variation around the targeted value of 131Ω from 860–960MHz. Overall good agreement is pragmatic between computed and measured values, which supports the effectiveness of innovative design technique. Furthermore, by investigating the consistently elevated behavior of the measured results over the computed values reveals that the measurement fixture asserts certain amount of impedance probably through the SMA configuration for the metal plate, which can be eliminated by considering its effect [121] or by utilizing S-parameter method merely for impedance measurement [114, 160]. The return loss of the proposed antenna is calculated based on the power reflection coefficient as mentioned in Equation (4.2). Figure 4.16(a) shows the measured and computed return loss of the proposed antenna with the measured bandwidth of the antenna in the worst case is 260MHz, corresponding to 28% around the center frequency 910MHz; so it covers the global UHF RFID bands and can cater greater degree of environmental disparities.

The critical parameter, which determines the performance of an RFID tag antenna, is the read range [158]. The effective isotropic radiated power referenced for both the RFID reader and reader antenna, or equivalent isotropically radiated power *(EIRP)*, is set to 3.2W and 4W according to ETSI and FCC RFID standards, respectively. The read range performance testing is conducted outside anechoic chamber with Impinj's UHF RFID reader Kit to achieve information for real environment scenario. In order to make the measurement more enlightening, the proposed tag is attached as showed in Figure 4.16(b), on a closed-cell rigid foam HF51 from ROHACELL's with 90mm thickness [170]. Figures 4.17(a) & (b) show the comparative analysis of measured read range for EU & North American bands, respectively, which are covered by the proposed RFID tag along with other UHF RFID bands. In this analysis, proposed tags are attached to cardboard cartons ex-

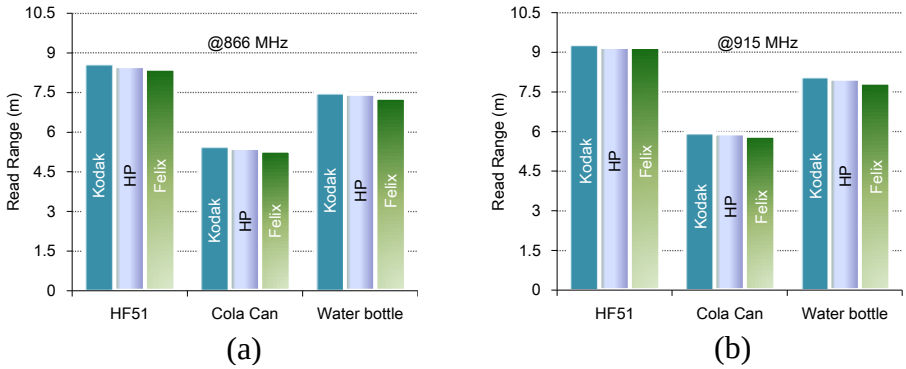

Figure 4.17: Measured read range for UHF RFID: (a) EU band, (b) North American band. (Reproduced courtesy of Taylor & Francis)

clusively containing cola cans, and plastic water bottles. The measured read range validates the outstanding performance of the proposed RFID tag, which can also be demonstrated for other RFID bands within the antenna operational frequencies.

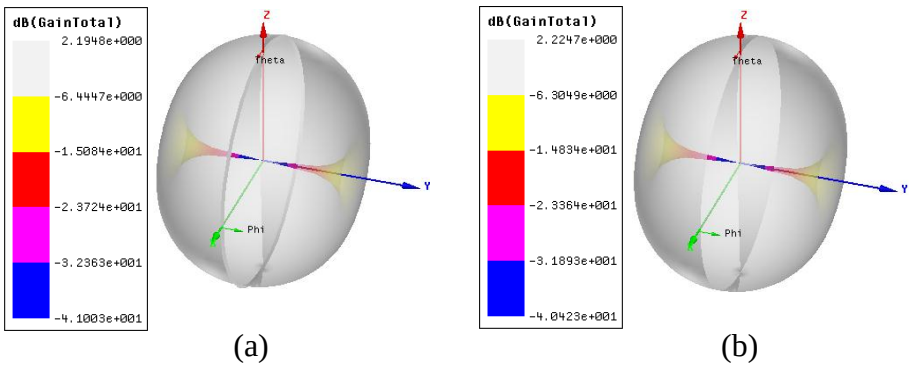

Figure 4.18: 3D simulated far-field radiation plots for UHF RFID: (a) EU band, (b) North American band. (Reproduced courtesy of Taylor & Francis)

Figures 4.18(a) & (b) show 3D simulated radiation pattern of the proposed antenna at 866MHz and 915MHz, respectively. The gain of the realized antenna is about 2.1dBi@866MHz and 2.2dBi@915MHz. Figures 4.19(a) & (b) show the 2D measured normalized radiation patterns of antenna printed on Kodak photopaper at characteristic frequency of 866MHz and 915MHz, respectively. It is observed that radiation patterns are nearly uniform (omnidirectional) and show substantial concurrence between computations and measurements, which can also be established for other frequencies within the antenna bandwidth, and are in well coherence with

earlier published results [169, 52].

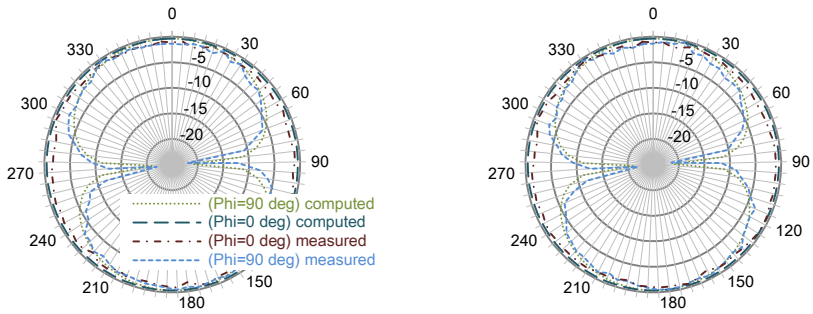

Figure 4.19: 2D measured & computed far-field radiation plots for UHF RFID: (a) EU band [16], (b) North American band. (Reproduced courtesy of Taylor & Francis)

4.4 Summary

In this chapter, we have investigated several key development parameters (from manufacturing, circuit and field point of views) of innovative RFID tag antennas proficient of significantly increasing RFID read range and printed on commercial paper substrates. The measured impedance bandwidth of proposed antennas completely covers the UHF RFID band while exhibiting extraordinary read range of up to 10.1m, thus expands to the global usage of these tags. The robustness, eco-friendliness and flexibility of the proposed antennas make them an excellent choice for far-field industrial applications. The proposed antennas have optimized effective aperture comprising of pattern holes, curled and uncurled corners along with T-matching network, while concurrently reducing the ink consumption which plays a vital role in roll-to-roll fabrication of ultra-low cost green tags. Furthermore, the sustainability and environmental impacts reckoning for the printed antennas can be applied as a manufacturing yield benchmark for future productions.

Chapter 5

RFID Antennas: Sensor-Enabled

In this chapter (which is the reflective restructuring of included Papers VII–X), the novel idea of integrating RFID with sensors along with other wireless applications by using single tag antenna is addressed. The explicit parametric analysis is presented for wideband circularly polarized antennas for operational range from 0.8–3.0GHz, in the realization of the emerging concept to integrate RFID along with several applications. The final section includes development of innovative antenna as a sensor and its calibration technique.

5.1 Introduction

RFID is considered an emerging leading technology in future telecommunications [167, 107, 75]. The RFID market has grown in a two-dimensional trend one side constitutes standalone RFID systems which are commonly found at present [193, 135, 124, 204]. On the other side, more ultramodern approach is paving its way, in which RFID needs to be integrated with broad operational array of distinct applications [5, 95] for performing different functions including navigation, broadcasting, and personal communication [155, 181], to mention a few. Using different antennas to include all communication bands is a straightforward approach, but at the same time, it leads to increase cost, weight, more surface area for installation, and above all electromagnetic compatibility issues [81]. Thus, there is the need for wide-bandwidth antennas [164, 48]. The espousal of a single, wideband antenna is certainly more attractive because of the fact that RFID is replacing other identification methods by whistling about cost-effective more efficient solutions.

Spirals are extensively used circularly polarized wideband antennas [71, 110, 142, 162]. The wideband features of spiral antenna brought it to the limelight in recent literature, particularly for miniaturization [109]. The fundamental inspiration for miniaturization is to slow down the wave traveling within the antenna structure. Numerous approaches have been pursued to achieve it, which includes dielectric [112] or magneto-dielectric loading [111], artificial materials [201], spi-

ral arm shaping [141], distributed reactive loading [120] and arm orienting vertically [81]. Conversely, when using the popular dielectric loading approach, the input impedance is also lowered. On the other hand, when the wave velocity is reduced by meandering of metalized arms, the axial ratio also deteriorates [71]. It has been established that coiling of the spiral arms provides for impedance control [110].

5.2 Archimedean Spiral Antenna

5.2.1 Synthesis of the Antenna Topology

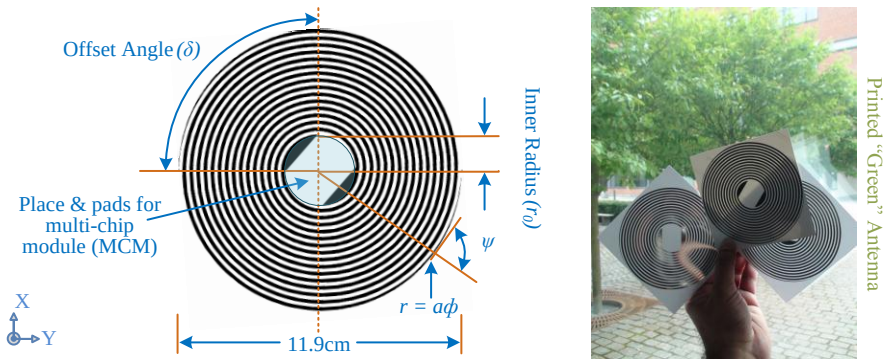

Figure 5.1: Dimensions & green theme of proposed antennas. (Reproduced courtesy of The Electromagnetics Academy [12])

In order to achieve stable broadband [49] multimode feature in far and near-fields planar Archimedean spiral antenna structure is realized. Three designs of a two-arm Archimedean spiral antenna are assessed. The in-depth research proves that the Archimedean spiral is not a frequency-independent antenna structure because the spacing between the arms is specified by a constant, not an angle [99]. However, this is a contentious point because fundamentally frequency-independent performance is achieved over 10:1 bandwidths. The following numerical calculations are exploited to construct the proposed antenna structure in Figure 5.1. The centerline of the proposed Archimedean antenna is defined by:

$$r = a\phi = r_0 + (E)\phi^{(1/S)} \tag{5.1}$$

where,

$$a = \frac{1}{K}\frac{dK}{dC} \tag{5.2}$$

and C is the angle of rotation which depends on K. If the antenna is to be scaled to a frequency that is K times lower than the original frequency, the antenna's physical surface must be made K times greater to maintain the same electrical

dimensions [27]. The Expansion coefficient *(E)* and the Spiral coefficient *(S)* of the proposed antenna are 1 whereas, r_0 is the inner radius which is 1.6cm. The pitch angle ψ varies with radius as:

$$tan\psi = \frac{r}{a} \tag{5.3}$$

When r is large, then the pitch angle approaches 90°. An equivalent design ratio τ_{eq}, which varies with radius, may be defined for the Archimedean spiral that has the same pitch angle ψ at radius r. Therefore,

$$\tau_{eq}(r) = e^{-2\pi/|tan\psi|} = e^{-2\pi|a/r|} \tag{5.4}$$

It is worth noting here that τ_{eq} approaches 1 for large value of r. The sides of a strip may be defined in terms of the rotation angle ϕ of Figure 5.1 and the angle δ (offset angle is 90^o of the proposed structure) to get:

$$r = a\left(\phi \pm \frac{\delta}{2}\right) \tag{5.5}$$

The radial width of the antenna strip W_r is a constant, which is independent of radius and is obtained by:

$$W_r = a\delta \tag{5.6}$$

The actual width of the antenna strip varies to some extent with radius and is calculated by:

$$W = a\delta \sin\psi \tag{5.7}$$

The spacing S_r between the centerlines of the adjacent turns for one arm is specified by:

$$S_r = 2\pi a \tag{5.8}$$

Furthermore, the actual spacing is given by:

$$S = S_r \sin\psi = 2\pi a \sin\psi \tag{5.9}$$

The two-arm spiral antenna proposed in Figure 5.1 for frequency band 0.8–3GHz is self complementary when *W/S = 1/4* or $\delta = \pi/2$ [27]. Given that the strip widths and spacings are defined by constants rather than by angles, Archimedean spiral antenna does not conform to either the frequency-independent or log-periodic principles [99]. Thus, this antenna gives autonomy to those ASIC manufacturers [125, 87] which have frequency dependent modules. In practice, it is observed that frequency independent characteristics are obtained if τ is large enough in the active region (i.e., radiation region), wherein the circumference of the radiation ring is about one length. Alas, diminutive information has been published [81, 53] on the degradation of gain and patterns versus τ. Some published results indicate the loosely wound log-spiral performs as well as the tightly wound Archimedean spirals; however, this analysis is out of scope of this research.

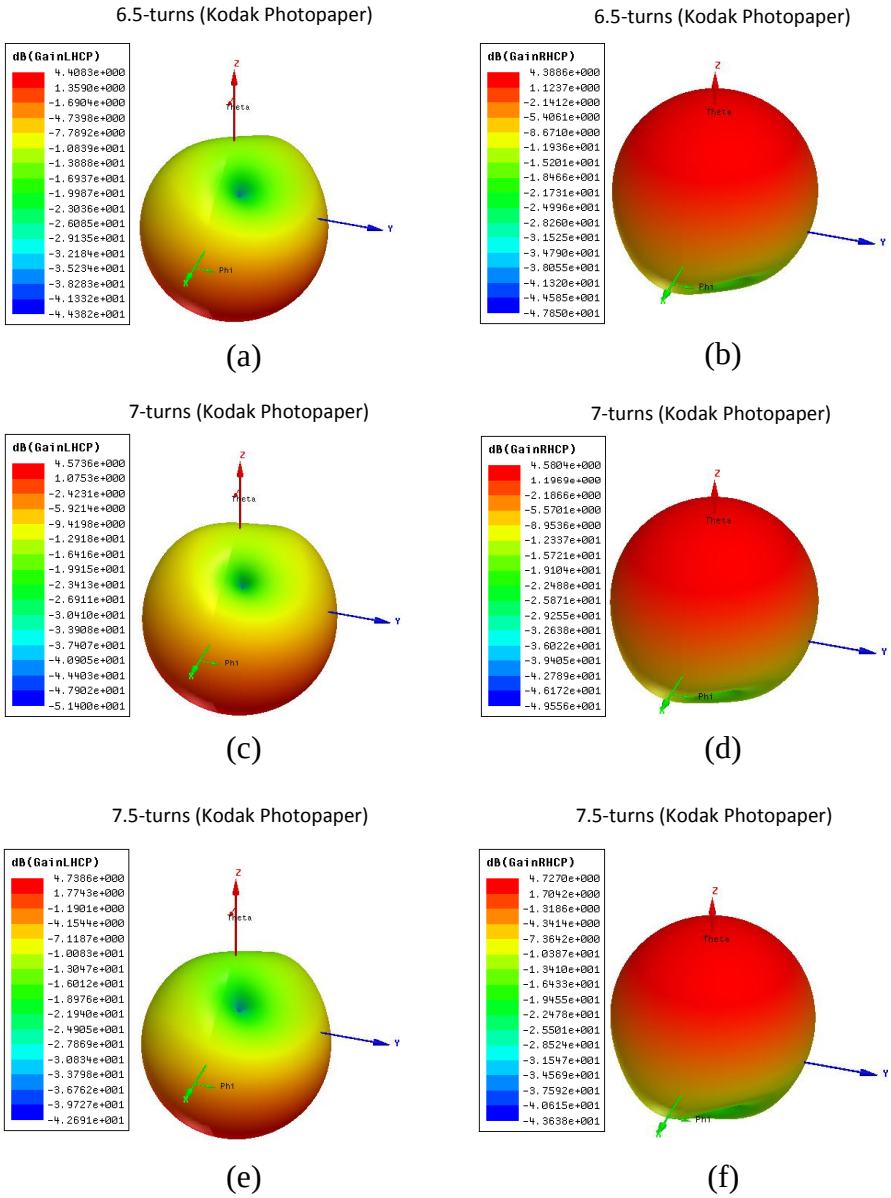

Figure 5.2: Simulated 3D LHCP & RHCP gain radiation patterns of antennas with 6.5, 7 and 7.5–turns. (Reproduced courtesy of The Electromagnetics Academy [12])

5.2.2 Manufacturing Parametric Analysis

The conductivity of the printed traces of silver nano-particle based inks used in this research, after curing, is high enough (for Xerox ink $\approx 0.7 \times 10^7$ S/m and for Cabot ink $\approx 0.9 \times 10^7$ S/m) to be considered as a good conductor, but not as high as bulk silver. The skin depth for traces of the proposed antenna with operational frequency at 800MHz is evaluated using Equation (3.6). The thickness of the printed single layer of ink from the printer used is around 200nm (Nano-AG-120I) – 600nm (CCI-300). It has been found after careful iterations that at least three layers of printing by Cabot ink and four layers of printing by Xerox ink, are sufficient to achieve better performance under the limits imposed by various design factors.

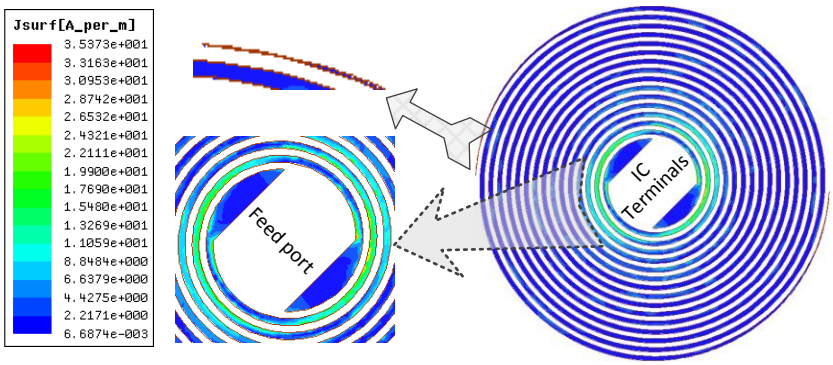

Figure 5.3: The current distribution of proposed antenna at 1.9GHz, (Reproduced courtesy of The Electromagnetics Academy [12])

From Figures 5.2(e) & (f), it is obvious that the proposed antenna with 7.5-turns has improved LHCP (Figure 5.2(e)) and RHCP (Figure 5.2(f)) gain, than antennas with 6.5-turns (Figures 5.2(a) & (b)), and 7-turns (Figures 5.2(c) & (d)). This performance criterion is achieved without enlarging the antenna's physical aperture. Specifically, the antenna with 7.5-turns at approximately 1.9GHz exhibits a 4.7-dB, 4.5-dB and 4.4-dB gain on Kodak, HP and Felix Schoeller paper(p_e:smart) respectively, by printing with Cabot ink. Whereas, by printing with Xerox ink the gain achieved at 1.9GHz is 4.7-dB, 4.6-dB and 4.6-dB on Kodak, HP and Felix Schoeller paper, respectively. It is depicted from Figure 5.2 that by further increasing the number of spiral turns, the gain improves at lower frequencies. It is observed that the antenna impedance also decreases with the increase in number of turns.

On the other hand if the number of turns are reduced, the gain of the antenna decreases to a value which violates the design requirements because these tags are proposed for large items-level tacking and information gathering. So it is mandatory for the antenna to exhibit better gain to achieve higher read range while at the

same time providing readability in the near-field region. Moreover, due to the consumption of expensive conductive ink, the size of the antenna has to be within economical limits for its possible realization on industrial scale. Therefore, the optimal design pattern is achieved while considering the size limits along with other performance factors for attaching to large items in the working range from 0.8–3.0GHz is realized with 7.5-turns, and its current distribution plot is shown in Figure 5.3.

Two different sintering processes are evaluated after drying of ink on the substrate, first one is the prevalent method and the other is "PulseForge Technology" [190]. In the first approach sintering is carried out in the oven with ventilation system at different temperature and time (as mentioned in Table 5.1), depending upon the combination of ink and substrate, for sufficiently curing, removing the excess solvent and material impurities from the depositions. The printed samples are also sintered through "PulseForge Technology" by Novacentrix USA, in order to demonstrate sintering and annealing for high-speed roll-to-roll manufacturing often in ambient air (and is capable of up to 1000 feet per minute). This approach enables the use of ultra low temperature and flexible substrates such as paper substrate, which cannot be annealed at high temperatures.

Table 5.1: Annealing parameters for printed antennas [12].

Substrate	Xerox Ink Nano-AG-120I	Cabot Ink CCI-300	Temperature (°C)	Time (Minutes)
Kodak U-P Photopaper	√	–	140	30
Kodak U-P Photopaper	–	√	150	120
HP Adv. Photopaper	√	–	120	45
HP Adv. Photopaper	–	√	120	120
Felix Schoeller Paper	√	–	110	90
Felix Schoeller Paper	–	√	110	90

5.2.3 Field & Circuit Concepts Parametric Analysis

A set of precise and thorough methods for evaluation of the reliability parameters and characterization of the proposed fabricated antenna on different paper substrates are implemented. Firstly, five identical structures are printed for each arrangement of ink and paper substrate. Secondly, in this study, an experimental methodology for the characterization of the impedance of the balanced tag antenna is implemented along with the balun structure. The balanced tag antenna is considered as a two-port network and the impedance of the antenna is characterized using network parameters. The antenna is connected to the two ports of a vector network analyzer through a test fixture mentioned in detail in [115]. The influence of the test fixture is deembedded by using a port-extension technique and

the antenna impedance can be extracted directly from the measured parameters. Whereas, the broadband balun transforms the unbalanced coaxial mode into balanced two-wire transmission line mode that fed the spiral antenna. The accuracy of the measurements is increased if all errors up to the measuring instrument tip are eliminated [221]. This includes internal VNA errors after the sampler, the cables along with their tips used to connect to the test structure. The reference plane is shifted to the tips by using the standard calibration methods SOLT (short-open-load-through) for two-ports technique and short-open-load (SOL) for balun structure.

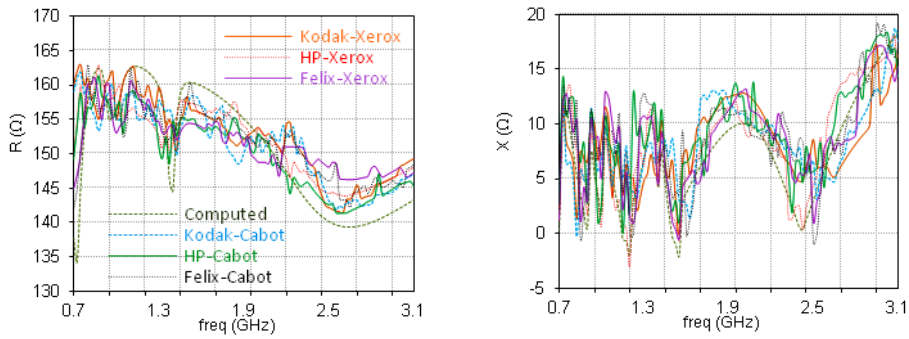

Figure 5.4: (a) Input resistance variation, (b) input reactance variation. (Reproduced courtesy of The Electromagnetics Academy [12])

The impedance graphs are presented in Figure 5.4 with the largest deviated value at a certain frequency which provides information for worst case analysis, in addition to exploration of performance parameters. This method helps in discovering potential variations that can take place due to the use of paper substrate, which is of critical significance. As showed in Figure 5.4(a), the measured resistance for the antenna between 1.1–1.4GHz, fluctuates between 158–144Ω and from 1.41–3.0GHz, the variation of resistance is between 146–154Ω but with much steady manner. However, exceptionally small deviation is pragmatic among the curves of all antennas and this behavior is stable over a much larger frequency range in accordance with published results for spiral structures in [81, 53]. The reactance part of the impedance, as showed in Figure 5.4(b), follows smaller positive values around 15Ω with really small variation with frequency. Moreover, relatively constant harmony exists between the computed and measured results. This conforms to both frequency dependent & independent antennas in some extent; however, this behavior of impedance is deliberately achieved because most of the commercially available ASIC till date have also frequency dependence. More importantly, the impedance of the proposed antenna besides easier to match at lower frequencies.

The computed return loss is showed along with measured values of the Xerox

ink & Cabot ink printed antennas in Figure 5.5(a). From Figure 5.5(a), it is clear that the proposed antenna has better return loss and is less than –15dB throughout the frequency band of interest (and in eloquence with [177, 33]), which is the paramount requirement of antennas for optimal performance. Furthermore, the stable response of paper substrate at higher frequencies, (although with a certain amount of variations but within acceptable values) make it a suitable candidate for broadband antennas. Overall, a good agreement among the computed, Xerox ink printed, and the Cabot ink printed antennas is observed.

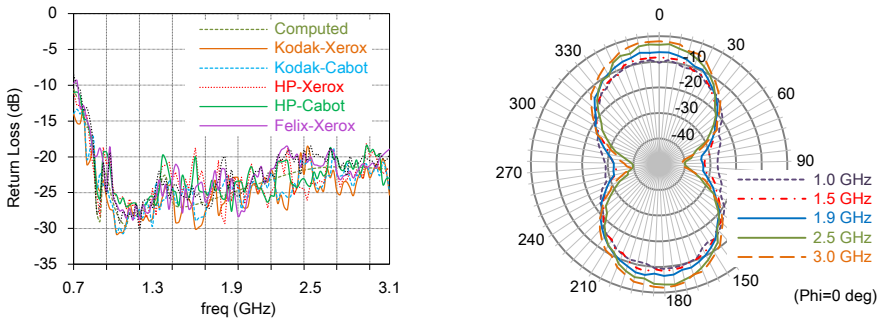

Figure 5.5: (a) Measured & computed return loss, (b) measured & computed 2D far-field radiation plots. (Reproduced courtesy of The Electromagnetics Academy [12])

The measured normalized radiation patterns (of antenna printed on Kodak photopaper using Cabot ink) at characteristic frequencies of (1.0, 1.5, 1.9, 2.5) & 3.0GHz are plotted in Figure 5.5(b). It is observed that all of the radiation patterns have normal shape and show extreme similarity between computations and measurements, which can also be verified for other frequencies within the antenna bandwidth and are in coherence with previously published results [53]. Additionally, the measured radiation patterns exhibit a slight offset due to the feed line connecting to SMA. It can be depicted from Figure 5.5(b) that the radiation pattern does not deteriorate in the whole bandwidth from 0.8–3.0GHz.

5.3 Log-Spiral Antenna

This section presents electromagnetic analysis of a versatile, wideband planar log-spiral antenna, which is one of the extensively, used circularly polarized wideband antennas [185, 123]. The thriving use of the proposed inkjet printed antenna from 0.8–3.0GHz is demonstrated.

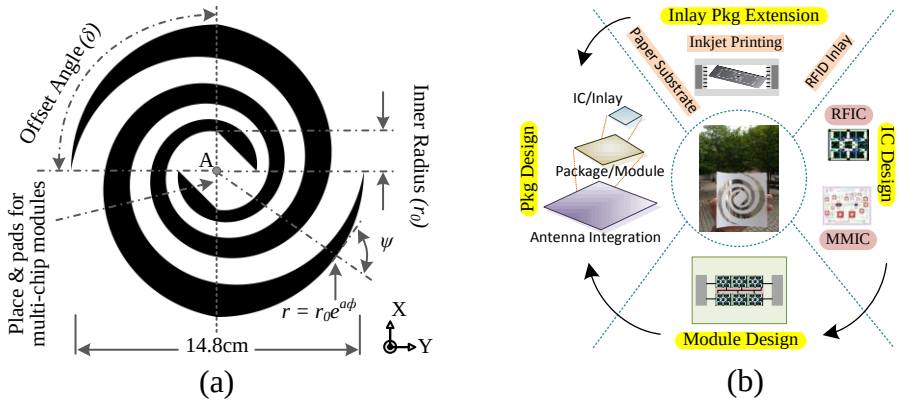

Figure 5.6: (a) Dimensions & (b) integration process of proposed antenna. (Reproduced courtesy of Taylor & Francis [14])

5.3.1 Synthesis of the Antenna Topology

Numerous design topologies of a two-arm log-spiral antenna, which is one of the antenna configurations, that closely parallels the frequency independent concept are assessed. It is worth mentioning here that, the entire shape of proposed antenna cannot be entirely specified by angles it is not exactly frequency independent [27]. However, the construction of the proposed planar log-spiral structure is defined by the angles ψ and δ to obtain as much independence from frequency as possible within limits imposed by different factors mentioned throughout the text. The curve of the antenna in Figure 5.6(a) which has 1.25-turns is calculated by:

$$r = r_0 e^{a\phi} \tag{5.10}$$

Where r_0 is the inner radius which is defined to be 1.36cm in Figure 5.6(a) according to the area and space required for the multi-chip module/s package. The expansion coefficient a (which is governed by Equation (5.11)) of the proposed antenna is 2.88 and is related with the pitch angle ψ.

$$a = \frac{ln(\tau)}{2\pi} \tag{5.11}$$

Where expansion ratio (τ) is defined to be less than 1. The second arm of the proposed log-spiral antenna is obtained by rotating the first arm by 180^o around the starting point A. The constant r_0 in Equation (5.10) can be resolute from the initial value of ϕ, which is arbitrary. The planar structure is self-complementary when $\delta = 90^o$, and Babinet's principle [27] leads to the conclusion that the input impedance is $60\pi\Omega$ for free space (with no dielectric loading), and independent frequency [99].

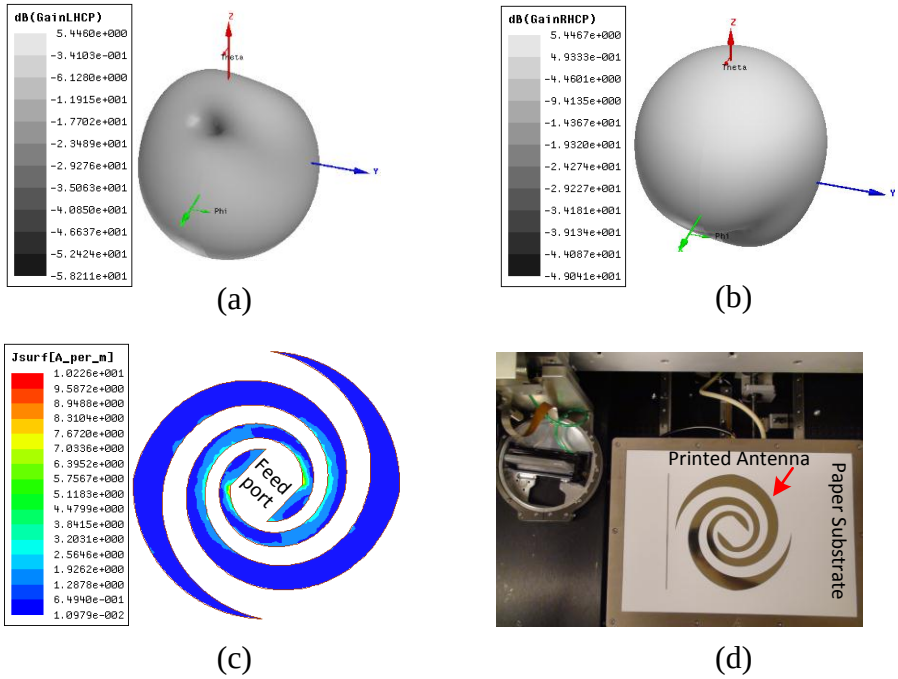

Figure 5.7: Simulated 3D gain: (a) LHCP, (b) RHCP; (c) current distribution at 1.9GHz; (d) inkjet printing setup & antenna printed on paper substrate. (Reproduced courtesy of Taylor & Francis [14])

Figure 5.6(b) explains the integration and development process encapsulating the proposed wireless tag. The proposed structure is optimized without enlarging the antenna's physical aperture. Thus, it is evident from the LHCP (Figure 5.7(a)) and RHCP (Figure 5.7(b)) gain of the proposed antenna that it exhibits improved performance among several other configurations endeavored to achieve an optimal design. Therefore, the optimal design pattern for working range from 0.8–3.0GHz is realized with 1.25-turns and its current distribution plot is shown in Figure 5.7(c).

5.3.2 Field & Circuit Concepts Parametric Analysis

Firstly, five identical structures are printed on each paper substrate. The impedance is measured using S-parameter method (which is the most accurate method reported till date), in which the antenna is connected to the two ports of a vector network analyzer through a test fixture [160, 115].

The principle governing this method is shown in Figure 5.8(a), which shows a distinctive asymmetrical balanced dipole antenna, with two arms of different lengths and excited differentially. The positive and negative ports of the source with a

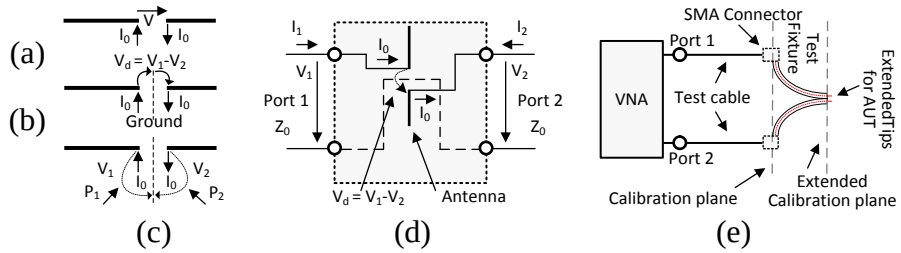

Figure 5.8: Asymmetrical balanced dipole antenna: (a) excitation, (b) virtual ground, (c) ports definition; (d) network representation of the asymmetrical dipole antenna; (e) configuration of measurement setup. (Reproduced courtesy of Taylor & Francis [14])

voltage of V are connected to the input terminals of the radiators of the antenna, respectively. As showed in Figure 5.8(b), the driven voltage can be split as V_1 and V_2 with a virtual ground plane without any disturbance of the current distribution on the antenna. Hence, each terminal of the antenna radiators and the ground plane can be regarded as a "port", which is showed in Figure 5.8(c). The antenna can be equivalent to a "two-port" network, as showed in Figure 5.8(d). The impedance of the antenna is thusly associated to the network parameters of the corresponding two-port network, and can be characterized by measuring the network parameters such as S-parameters [160]. From Figure 5.8(d), the normalized impedance of the antenna can be expressed as follows:

$$\tilde{Z}_d = \frac{V_d}{I_0} = \frac{V_1 - V_2}{I_0} \tag{5.12}$$

Using the impedance matrix, the Equations of a linear two ports (relating voltages and currents) are:

$$V_1 = Z_{11} I_1 + Z_{12} I_2 \tag{5.13}$$

$$V_2 = Z_{21} I_1 + Z_{22} I_2 \tag{5.14}$$

If the two ports are driven by current source i.e., $I_1 = I_0$ and $I_2 = -I_0$, the differential voltage V_d is given by:

$$V_d = V_1 - V_2 = (Z_{11} - Z_{21} - Z_{12} + Z_{22}) I \tag{5.15}$$

and the impedance is given by:

$$\tilde{Z}_d = \frac{V_d}{I_0} = \frac{V_1 - V_2}{I_0} = (Z_{11} - Z_{21} - Z_{12} + Z_{22}) \tag{5.16}$$

Now by transforming the Z-parameters as a function of S-parameters and taking into account $Z_d = Z_0 \cdot \tilde{Z}_d$, we get:

$$Z_d = \frac{2\ Z_0 (1 - S_{11} S_{22} + S_{12} S_{21} - S_{12} - S_{21})}{(1 - S_{11})(1 - S_{22}) - S_{21} S_{12}} \tag{5.17}$$

where Z_0 is the reference impedance, which is mostly 50Ω for measurement systems. Thus, in case of the symmetrical balanced antenna, where $S_{11} = S_{22}$, and $S_{12} = S_{21}$. By substituting these values in Equation (5.17), we get a simplified expression [160], which is as follows,

$$Z_d = \frac{2\ Z_0(1 - S_{11}^2 + S_{21}^2 - 2S_{12})}{(1 - S_{11})^2 - S_{21}^2} \tag{5.18}$$

The constellation of the measurement system is illustrated in Figure 5.8(e). The measurement is carried out by using a two-port VNA (MS2026B, Anritsu) and a test fixture. The test fixture is constructed by using two semi-rigid coaxial cables having a length of 100mm with an outer conductor diameter of 2.2mm. The outer conductors of the coaxial cables are shorted by jointly soldering with the corresponding gap between the tips to accommodate between the two terminals of the antenna. One end of the fixture is with two SMA connectors, which is connected to the VNA through the test cables. The other end of the fixture is opened with the small extension (1.5mm) of inner conductors in order to form the tips for connecting the antenna under test (AUT). Antenna is attached to the test fixture tips with CW2400 silver conductive epoxy, cured at 24℃ for 4 hours for achieving maximum conductivity and adhesion.

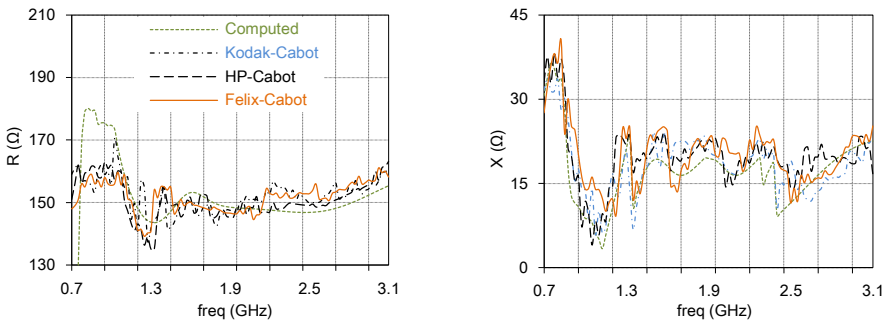

Figure 5.9: Input: (a) resistance variation, (b) reactance variation. (Reproduced courtesy of Taylor & Francis [14])

The impedance graphs are presented in Figure 5.9 with the largest deviated value at a certain frequency which provides information for worst case analysis. As showed in Figure 5.9(a), the measured resistance for the antenna between 1.1–1.4GHz, fluctuates between 158–144Ω and from 1.41–3.0GHz, the variation of resistance is between 146–154Ω but in much steady manner. However, exceptionally small deviation is pragmatic among the curves of all antennas, and this behavior is stable over a much larger frequency range in accordance with the published results for spiral structures in [53]. The reactance part of the impedance, as showed in Figure 5.9(b), follows smaller positive values around 15Ω with exceedingly small

variation with frequency. This performance relates to both frequency dependent & independent antennas to some extent. Moreover, relatively constant harmony exists between the computed and measured results.

The actual transformation between the unbalanced and the balanced mode is achieved by the balun which is exactly the same as well defined in [191], composed of the coplanar waveguide and the coplanar strip line which are only needed to connect the sender/receiver and the antenna. The balanced output from the balun is connected to the antenna using the balanced coplanar strip line. However, due to the additional complexity introduced by attaching Balun using CW2400 and the feed line connecting to SMA, a slight offset/error and distortion is observed in the measured values. The measured return loss is showed along with computed values in Figure 5.10(a). It is clear that the proposed antenna has better return loss and is less than –15dB throughout the frequency band of interest, which is the paramount necessity of antennas for optimal performance. Furthermore, the stable response of paper substrate at higher frequencies, make it a suitable candidate for broadband antennas.

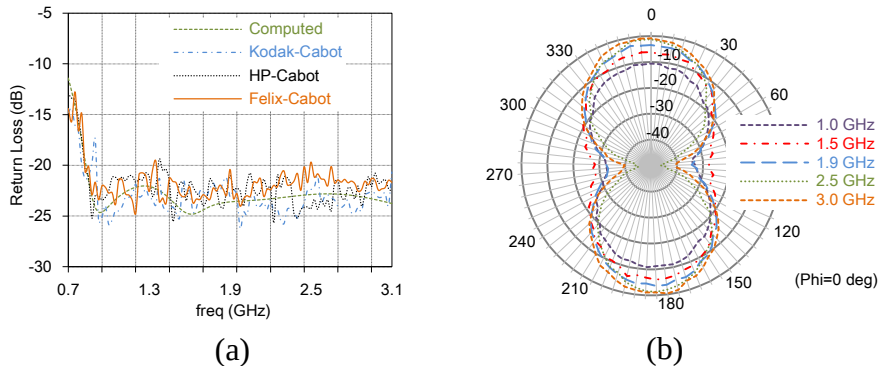

Figure 5.10: (a) Measured & computed return loss, (b) measured 2D far-field radiation plots. (Reproduced courtesy of Taylor & Francis [14])

The measured normalized radiation patterns (of antenna printed on Kodak photopaper) at characteristic frequencies of (1.0, 1.5, 1.9, 2.5) & 3.0GHz are plotted in Figure 5.10(b). The radiation patterns show extreme similarity between computations and measurements, and are in coherence with previously published results [53].

5.4 Two-Arm Sinuous Antenna

5.4.1 Antenna Structure and Design

Several design parameters of a two-arm sinuous-spiral antenna are optimized in a sense that RFID tag needs to be read in any orientation. The integrated wireless applications within the proposed multi-module tag require a wideband antenna

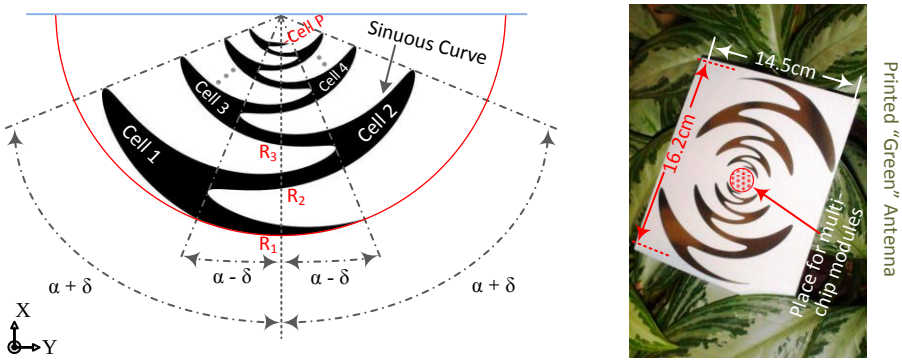

Figure 5.11: Design, dimensions of proposed antenna. (Reproduced courtesy of Taylor & Francis [15])

element that offers the orthogonal senses of polarization. Simultaneous polarization ability such as vertical and horizontal or right and left circular from a same aperture with coincident phase centers is of particular significance [99]. The proposed design needs to be in accordance with the manufacturing constrains because only single side of paper substrate is available for full integration of modules alongside the antenna.

In designing a planar structure, the starting point for the evaluation process is set to attain an optimal structure with a self-complementary geometry. As explained in the past, self-complementary structures have better impedance and pattern properties than non-self-complementary ones [99]. Interestingly, for this particular type of indistinct phasing, self-complementary structure is not a good option if low axial ratio is required. In this study, numerous self-complementary two-arm sinuous structures are investigated by varying growth rate while maintaining a fixed radiating aperture size. In order to do this, the number of sinuous segments or cells of the antenna are varied. However, it is observed, there is no improvement in the axial ratio at the circularly polarized bands regardless of the geometry and growth rate. The axial ratio improvement is possible if one deviates away from the self-complementary principle. Thus, this is done by changing the variables α and δ in Equation (5.19) and the final optimized design is achieved showed in Figure 5.11.

In accordance with appropriate log-periodic practice, the sinuous curve is defined solely by angles and the growth rate (expansion ratio τ). As mentioned in Figure 5.11, the curve is a set of cells starting with cell 1 at the outer radius R_1 (the proposed structure has eight cells). R_p defines the outer radius of cell p, and α_p with τ_p determine the angular width and ratio of the inside-to-outside radius for each cell. The Equation for the pth cell is provided by:

$$\phi = (-1)^p \alpha_p sin\left(\frac{180\ ln(r/R_p)}{ln\tau_p}\right) \qquad R_{p+1} \leq r \leq R_p \tag{5.19}$$

where r and ϕ are the polar coordinates of the curve. The radii R_p are related by:

$$R_p = \tau_{p-1} R_{p-1} \tag{5.20}$$

The design parameters τ_p and α_p may possibly be independent of p and log-periodic structure that is a periodic function of the logarithm of the radius r. The proposed structure in Figure 5.11 has α of 45^o and angle δ is 22.5^o with an outer radius of 8.4cm. One sinuous arm of the proposed structure is formed by rotating the curve of Equation 5.19 by plus and minus an angle δ around the origin as showed in Figure 5.11. Thus, the complete aperture is developed by the angular rotation of the single arm through 180 degree increment to create a two-arm structure. The directly printable proposed antenna is intended for cardboard cartons-level tagging, where size is not an issue but high performance with increased functionality at low cost is desired so that valuable goods can be tracked in any orientation and transported safely.

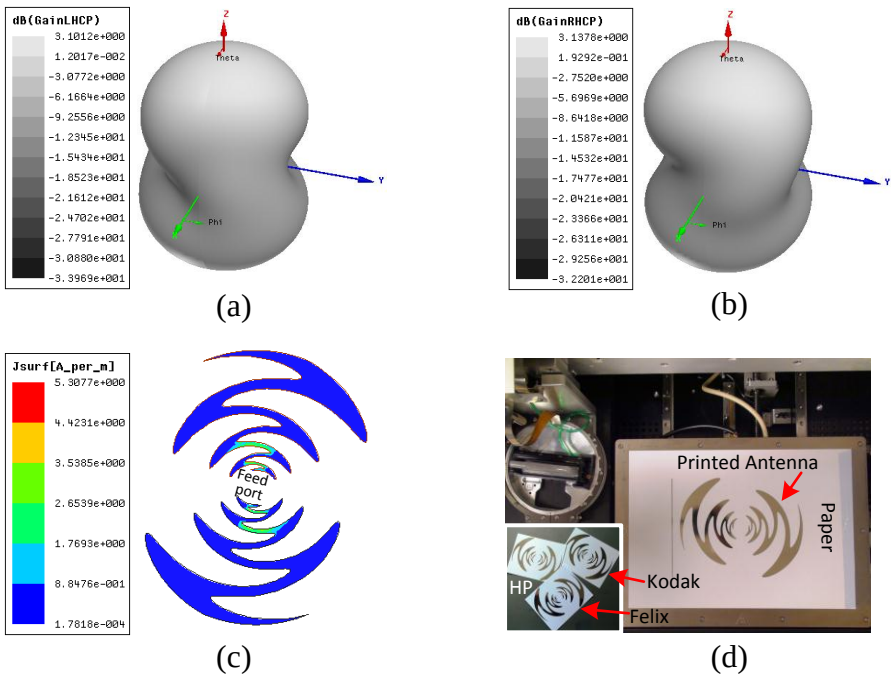

Figure 5.12: Simulated 3D gain: (a) LHCP, (b) RHCP; (c) current distribution at 1.9GHz; (d) inkjet printing setup & antennas printed on paper substrates. (Reproduced courtesy of Taylor & Francis [15])

Figures 5.12(a) & (b) show the LHCP and RHCP gain of the proposed antenna, respectively. It is observed that the proposed structure exhibits better performance

throughout the operational range from 0.8–3.0GHz, than other configurations experienced to achieve this optimal design. Figure 5.12(c) shows the current distribution plot of the proposed antenna. Moreover, the projected structure is optimized without enlarging the antenna's physical aperture.

5.4.2 Results and Discussions

As a first step, five identical structures are printed on each paper substrate. For measurements infinite balun (Dyson) feed [68] is used for excitation. A 1.2mm flexible UTiFORM coaxial cable is fixed between the sinuous arms starting from the outside. UTiFORM coaxial cable is bonded to the test terminal with CW2400 silver conductive epoxy, cured at 24°C for 4 hours to gain maximum conductivity and adhesion. Furthermore, the bend radii of the coaxial turns are below the maximum tolerable value of 2.54mm [137].

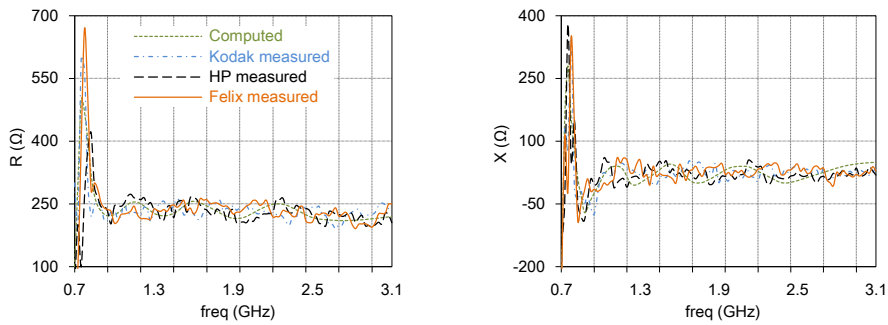

Figure 5.13: Input: (a) resistance variation, (b) reactance variation. (Reproduced courtesy of Taylor & Francis [15])

It is observed that by not having a self-complementary structure, the stability of the input impedance is deteriorated, as showed in Figure 5.13. The resistance of the proposed antenna showed in Figure 5.13 (a) varies between 210–250Ω throughout the frequency band of interest and exhibits consistent behavior. However, the antenna printed on Felix paper showed a higher degree of uncertainty between the two extremes and the antenna printed on Kodak paper followed more steady behavior. Nevertheless, exceptionally small variation is detected among the curves of all antennas and this behavior is stable over a much larger frequency range in coherence with the published results [42]. The reactance part of the impedance, as showed in Figure 5.13(b), follows positive values between 0–45Ω with exceedingly small variation with frequency. Moreover, relatively constant agreement exists between the computed and measured results.

In accordance with other log-periodic antennas, the center frequencies of the bands are directly linked to the geometric growth rate observed in Equation 5.19.

This states that ratio of the adjacent band frequencies is equal to the growth rate. This observance is of greater importance when specific bands are targeted. It ought to be noteworthy that bands toward the low and high operating limits of the antenna will be affected due to the finite size of the aperture, and are slightly different from the growth rate. Analogous to the planar structure, the linearly polarized bands, are positioned between circularly polarized bands, and they have orientations which wobble about two orthogonal directions aligned with opposite tips of the sinuous segments. It is realistic to anticipate that the performance can be further enhanced by optimisation [42]. The computed and measured return loss of the proposed geometry are presented in Figure 5.14(a). A good agreement is achieved between measurements and computations which are fairly coherent with published results [130]. The measured return loss of the sinuous antenna is below –15dB from 0.8–3GHz. The difference between computations and measurements is due to the difficulty to realize a perfect alignment of Balun structure especially on extremely flexible paper substrate.

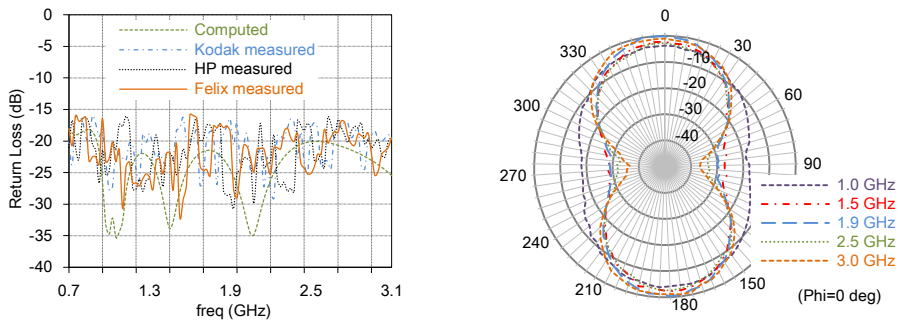

Figure 5.14: (a) Measured & computed return loss, (b) measured 2D far-field radiation plots. (Reproduced courtesy of Taylor & Francis [15])

Moreover, the proposed antenna is capable of exhibiting extended read range under conjugately impedance matching conditions which also depends upon the ASIC used for RFID. The conjectural calculations after substituting measured values results into 15–16m read range. The antenna exhibits high gain values on paper substrate (mentioned in Table 2.1), and above all in direct contrast to most of the presently available RFID tags its superior performance in any orientation makes it an ideal choice for transportation applications. The measured normalized radiation patterns of antenna printed on Kodak photopaper at significant characteristic frequencies are plotted in Figure 5.14(b). The measured radiation patterns have extreme coherence with computed values, and are in pursuant with previously published results [42, 199] that validates the detection of proposed multifunctional wireless tag in any orientation.

5.5 RFID Antenna with Embedded Sensor & Calibration Functions

RFID is an emerging and disruptive compact wireless technology for the identification of physical objects and is reckoned as an eminent candidate, for the realization of ubiquitous wireless sensor networks [34, 116]. The prima challenges which are presently hampering the effective RFID implementation are: cost, reliability, and environmental-friendliness that could countenance for the implementation of "green" and "robust" RFID solutions. The employment of additional RFID tags [34] or sensing material [74, 131] to develop a sensor module has extended the ambit of RFID practice in assorted segments of industrial applications. This concept gets "green" by integrating paper substrate with conductive ink [18], and multiple set of discrete components to accomplish RFID-enabled sensor tags [116]. These sensor based solutions either involve additional tag, sensing material or components in accession to RFID tag, which not only increases the overall size but also cost effectiveness is an issue. Furthermore, the capability of customizable calibration is a prime aspect for an efficient sensor-enabled solution [205].

In this section, an RFID tag antenna which has incorporated humidity sensor functionality along with calibration mechanism due to distinctiveness of its structural behavior, is presented. The sensor-enabled antenna is directly printed on paper substrate using inkjet printing technology for realizing the eco-friendly and ultra-low cost wireless sensor network (WSN) module. The antenna has reduced profile that paves the way for small item-level tagging and monitoring. The effect of humidity on paper-based antenna characteristics along with other electromagnetic parameters is investigated to evaluate the antenna performance under realistic operating conditions. The proposed antenna exhibits wider operational bandwidth and extended read range while at the same time provides an additional degree of freedom for sensor calibration.

5.5.1 Antenna as a Sensor Design

The antenna has to counter the dielectric variations of the substrate in a precise, controlled mode while demonstrating linear parametric change for realizing humidity sensor and its calibration relative to specified humidity levels without being undetected. Consequently, the antenna is composed of four classifiable elements which provide stability as well as variability in order to exhibit sensory and radiating physiognomies. The substrate adopted is Kodak photopaper of 250μm thickness (280gm/m^2) printed with Cabot ink (CCI-300), and NXP UCODE G2XM RFID Al strap is selected (@915MHz is 13.3-j122Ω). However, the principle of operation for the proposed antenna is not IC dependent.

The novel progressive ladder contours (Figure 5.15) play the important role for customizing the sensor calibration by varying the lengths of *D–H* segments. It is observed that the coupling between electromagnetic characteristics of the paper substrate and radiating elements is significantly aided by these contours. The

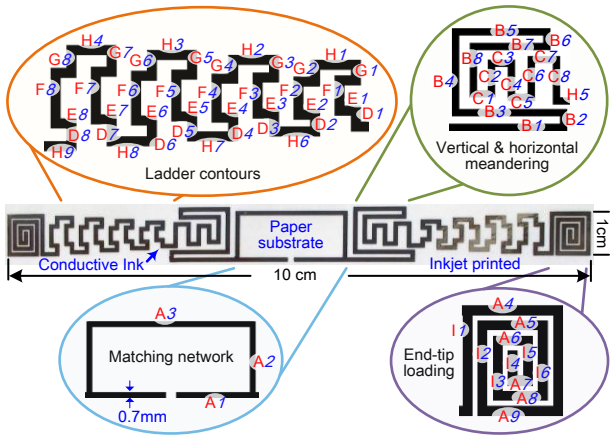

Figure 5.15: Geometry & structural components of RFID sensor antenna.

coupling features and stabilized performance in the far-field region are likewise alleviated by quadrangular end-tip loading by adjusting the length and spacing of segments from *A4–A9* & *I*. Moreover, the length of segments (*B–C*) forming the progressive & horizontal meandering structure is optimized to improve the input impedance matching in collaboration with series and shunt stubs (*A1–A3*). The dimensions of the proposed antenna are optimized (Table 5.2) and calibrated for measuring every 20% RH change.

Table 5.2: Dimensions of antenna for sensing every 20% RH change.

(mm)	A	B	C	D	E	F	G	H	I
1	9.50	12.1	2.42	0.40	1.85	2.8	0.39	3.55	6.30
2	8.40	0.70	2.22	0.46	1.85	3.0	0.46	3.55	5.25
3	18.8	11.0	2.60	0.53	1.85	3.2	0.53	3.50	3.15
4	7.01	7.00	2.56	0.60	1.80	3.4	0.60	3.50	1.75
5	4.90	9.40	2.60	0.67	1.80	3.6	0.67	3.10	2.10
6	2.80	0.70	2.90	0.74	1.80	3.8	0.74	3.55	4.20
7	1.75	7.70	3.10	0.81	1.80	4.0	0.81	3.55	
8	3.85	3.80	3.24	0.88	1.80	4.2	0.88	3.50	
9	5.95							3.50	

5.5.2 Experimental Verification of Antenna Performance

Firstly, the antenna characteristics are measured standalone in an anechoic chamber setup with Impinj's UHF RFID reader kit in order to verify the standard commu-

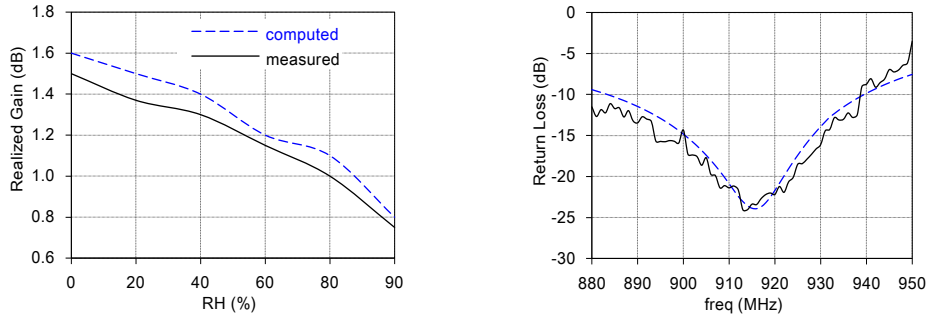

Figure 5.16: (a) Resistance and reactance variation, (b) radiation patterns of RFID sensor antenna at 915MHz.

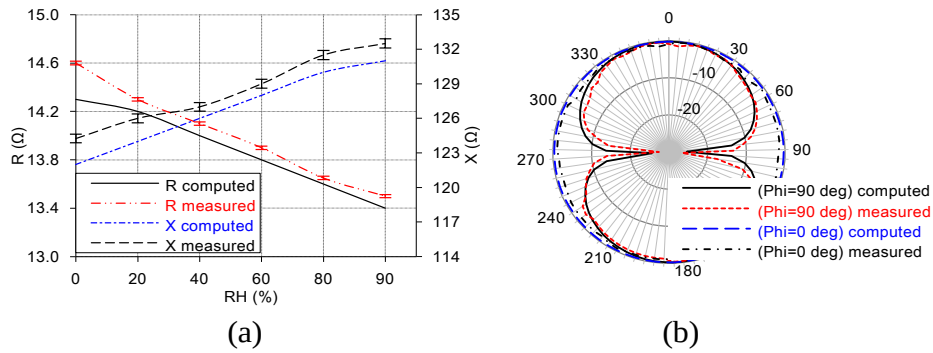

Figure 5.17: (a) Gain variation due to change in humidity level, (b) measured and computed return loss.

nication characteristics of the proposed RFID tag. The impedance is measured by using S-parameter method [160] whereas the return loss, and radiation patterns are measured by employing Half Mirror method to achieve ameliorated measurement accuracy. The effect of humidity on antenna is foremost characterized using climate chamber (Weiss Technik WK 11-180), and then for demonstrating results under normal room conditions, measurements are carried out in the anechoic chamber by deploying humidifier and hygrometer while maintaining the fixed distance between the reader and the sensor tag. The computed and measured impedance variations of the antenna against distinct humidity levels are shown in Figure 5.16(a). The resistance and reactance exhibit controlled linear curves of overall 9% and 7% variation, respectively. The measurements are reiterated several times for extracting reliability parameters and corroborating the sensor functionality.

Secondly, the calibration mechanism on the tag side alleviates in enforcing un-

pretentious and more reliable modes to formulate the entire humidity sensing system. The gain of the antenna varies with respect to ambient humidity levels as showed in Figure 5.17(a), and as a result, the received backscattered power (while placed in boresight) to the reader varies, which is conveniently scaled to determine the relative humidity (RH%) change. Figure 5.17(b) shows the return loss which is better than –15dB in the complete FCC RFID ISM band. The distortion is possibly due to the effect of metal ground fixture used for half mirror method. The normalized computed and measured radiation pattern, which are almost uniform (omnidirectional) at 915MHz, are plotted in Figure 5.16(b). A good agreement is observed between the computations and measurements, which can also be verified for other frequencies within the antenna's bandwidth. The proposed sensor tag exhibits extended portable read range of 11m and fixed 6.5m as a standalone RFID tag and with full humidity sensing capability, respectively. Moreover, the gain of sensor antenna can be improved by increasing the size depending upon the particular application.

5.6 Summary

During the numerical and experimental analysis of planar, non-self-complementary, wideband spiral antennas, it is observed that by adjusting the gap between the adjacent tracks to create the spiral arms leads to a larger number of turns within the same aperture size. All the previously published relevant work in contrast to the proposed approaches are focused on complex techniques, to make such antennas using nonflexible or contaminated substrates, which neither can be implemented with roll-to-roll printing nor suitable for eco-friendly applications. Furthermore, these antennas exhibit superior impedance matching capability, improved return loss and wider bandwidths for all realized bands. Although the presented research is specific to inkjet printed Archimedean spiral, Log-spiral and Sinuous antennas, the same approach can be applied to other antennas made of printed strips, to form modules for green electronics.

Lastly, an RFID tag antenna which has instinct characteristics of a humidity sensor and potentiality of customizable calibration, is designed, fabricated and validated. It is observed that the explicit incorporation of ink and paper substrate is crucial for igniting the destabilisation effect, which is exploited in a regulated mechanism by the structural alignment of the proposed antenna. The design flexibility of the antenna resourcefully provides the effective calibration of the humidity sensor in accordance with defined requirements. In addition, this structure is eco-friendly, flexible and ultra-low cost, thus making this antenna well suited for realizing ubiquitous wireless sensor networks.

Chapter 6

Conclusion and Future Work

6.1 Conclusions

In recent years, the recognition of radio frequency identification (RFID) technology has greater than before and comprehensively integrated into modern society applications, ranging from remote monitoring and sensing to more demanding operational conditions in logistics, healthcare and access control. In this research passive UHF RFID tags and emerging concept of integrating RFID with sensors along with other wireless applications by using single tag antenna is implemented, by fabricating proposed antennas using state-of-the-art printing technologies on commercially available substrates as mentioned in Chapter 2. The design and fabrication challenges mentioned in Chapter 1, are addressed categorically in the presented antennas which are summarized in Figure 6.1 and concluded as follows:

Meander Line Antennas RFID tag antennas for EU and NA bands are achieved by design evolution process. The evolution process is applied to get robust tags, which must show less sensitivity to the variation of dielectric permittivity environment. In the first stage, novel meander line antennas are developed which are a natural choice when the size and tuning is considered. Unique progressive meandering technique is deployed to realize the antenna for 866–868MHz band as discussed in Chapter 3. The proposed antenna exhibits read range of up to 4 meters whereas, the whole structure measures only 9cm×0.8cm. In the second evolution stage, narrow-band antennas for EU and NA bands are realized which exhibit higher stability against environmental effects. The foremost challenge resolved at this stage is by achieving high gain and smaller size while improving the stability factor. The other ingredient, that governed the design modifications is the low ink usage to reduce the manufacturing cost. Thus, an innovative technique of also meandering the matching stub is introduced to rectify the issues of low gain, stability and matching. Furthermore, rigorous optimization is performed which is resulted into two distinctive antenna structures which exhibit exceptional read range from 5.5–

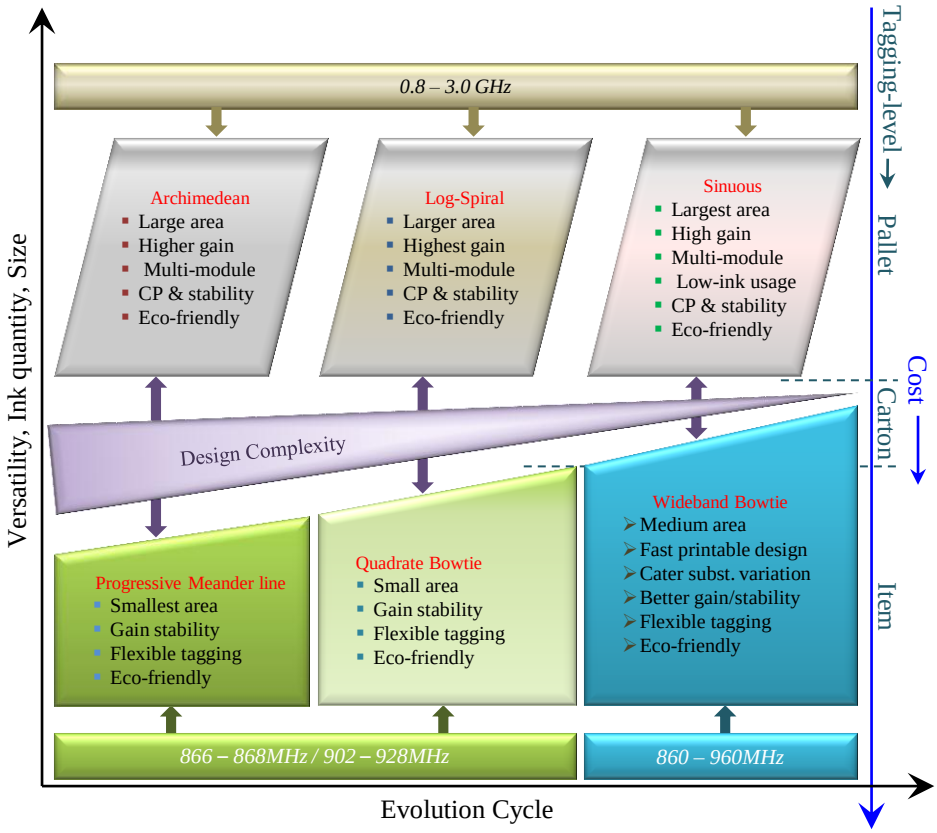

Figure 6.1: Presented research stages and evolution cycle.

6.5 meters having directivity around 2.1dBi with different manufacturing combinations as presented in Chapter 2. These compact antennas are extremely suitable for tags attached to articles which are prone to be bent or folded several times during their life cycle.

Narrow-band Bowtie Antennas Innovative quadrate bowtie passive RFID tag antennas for EU and NA bands are presented with the introduction of impedance matching approach to improve the reliability against environmental diversities as well as increase the maximum reading distance. The quadrate bowtie antenna profile modification by addressing the concept of antenna effective aperture and T-matching network are used to match the antenna input impedance to tag's chip impedance. The proposed antennas have surpassed read range from 6.5–7.0 meters depending upon which substrate is utilized. Moreover, the effects of metal and water on the proposed antennas are also categorically investigated as discussed

in Chapter 3. The antennas exhibit exceptional operational characteristics when stumble upon metal and water containing objects. The use of the inkjet printing process in the development of these proficient RFID antennas on different types of paper has also been demonstrated, verifying that paper-based inkjet printing topologies offer a remarkably low-cost, green solution to system-level packaging for UHF, wireless, and microwave applications.

Wideband T-Matched Bowtie Antennas The second phase of the evolution process is discussed in Chapter 4, thorough analysis of novel rounded-corner bowtie passive RFID tag antennas, which are fabricated on various ultra-low-cost substrates in combination with the state-of-the-art printing technologies that are mentioned in Chapter 2. The implementation of T-match arms for matching of these antennas to the integrated circuit (IC) is introduced that improves the reliability against environmental diversities as well as increase the maximum reading distance up to 9m from 860–960MHz. The bandwidth of the proposed antenna is 197MHz, corresponding to 23% around the center frequency 855MHz; so it covers the common worldwide UHF RFID bands and can cater greater degree of environmental disparities.

Wideband Hole-Matched Bowtie Antennas One of the critical observations made while field testing (in supply chain industry) of antennas having thinner traces used for matching network, is that the effect of even minor scratches on those tracks can cause loss of RFID tags during transportation. Therefore, it led towards the realization of a structure which can eliminate such risk factors while exhibiting better performance. This motivated the evolution cycle towards rounded & straight corner bowtie antenna structures as mentioned in Chapter 4. The implementation of pattern holes is responsible for matching of the antenna impedance to that of the IC through the fine tuning of their location and size which is discussed in Chapter 4. The experimental characterization of the proposed antennas validates extended read range of up to 10.1 meter, while exhibiting return loss of better than –15dB over a wide frequency range (860–960MHz) to cover any manufacturing disparities. This work also gives a unique insight into evaluating sustainability of the specified antenna, which validates the potential for ultra-low cost mass production of RFID tags for green electronics.

Sensor-Enabled Wireless Tag Antennas Numerous design topologies of Log-spiral, Archimedean spiral and two-arm Sinuous antennas along with comprehensive numerical and experimental analysis are presented in Chapter 5 to demonstrate the emerging concept of integrating RFID functionalities along with sensors and other wireless applications for green electronics. These are extensively, used circularly polarized wideband antennas that brought them to focus in recent literature. In distinction to the previously reported antennas, the proposed antennas are manufactured by effectively exploiting inkjet printing technology to manufacture

ulta-low cost multi-module equipped wireless tags to operate from 0.8–3.0GHz, on extremely biodegradable paper substrates. The conjectural calculations after substituting measured values results into stable read range of up to 15–16 meters, which depends upon the ASIC used for RFID. These directly printable antennas are intended for cardboard cartons or pallets-level tagging, where size is not an issue but high performance with increased functionality at low cost is desired so that valuable goods can be tracked in any orientation and transported safely. Future development is intended to optimize the designs to provide additional modules within the same antenna size.

RFID Tag Antenna as Humidity Sensor Ultimately, An RFID tag antenna which has instinct characteristics of a humidity sensor and potentiality of customizable calibration, is designed, fabricated and validated. It is observed that the explicit incorporation of ink and paper substrate is essential for enkindling the destabilisation effect, which is exploited in a systematized mechanism by the structural arrangement of the proposed antenna. The design flexibility of the antenna resourcefully provides the effective calibration of the humidity sensor in accordance with specified requisites. In addition, the structure is eco-friendly, flexible and ultra-low cost, therefore, making this antenna well suited for realizing ubiquitous wireless sensor networks.

6.2 Future Work

The new discoveries in RFID research promise to incorporate it in aggrandized dynamic solutions, which will be part of anticipated seamless integration of electronics in everyday life. Multi-disciplinary research is responsible for advancements in RFID eminently in flexible and organic tags. In persuasion of future work on RFID antennas, there is a desideratum to cognize the market dynamics as the prospect evolution of R&D Models is market driven [202].

6.2.1 Research Potential in RFID Tags

The world renowned research and consulting firm Gartner has formulated a phenomenon designated as the hype cycle as showed in Figure 6.2, which has become the benchmark for all technology spectators in the information services business. The logic of the 'hype cycle' is that every technology firstly ascends to the peak of inflated expectations and then certainly slides into a trough of disillusionment. After this survival cycle, only the transcendant technologies move gradually towards maturity (slope of enlightenment) where adoption happens across a wide cross section of customers. The internet of things (IoT) has the potential to overcome the hype cycle phenomenon and truly get relevant-to governments, communities and the IT industry without any slackening of pace [76].

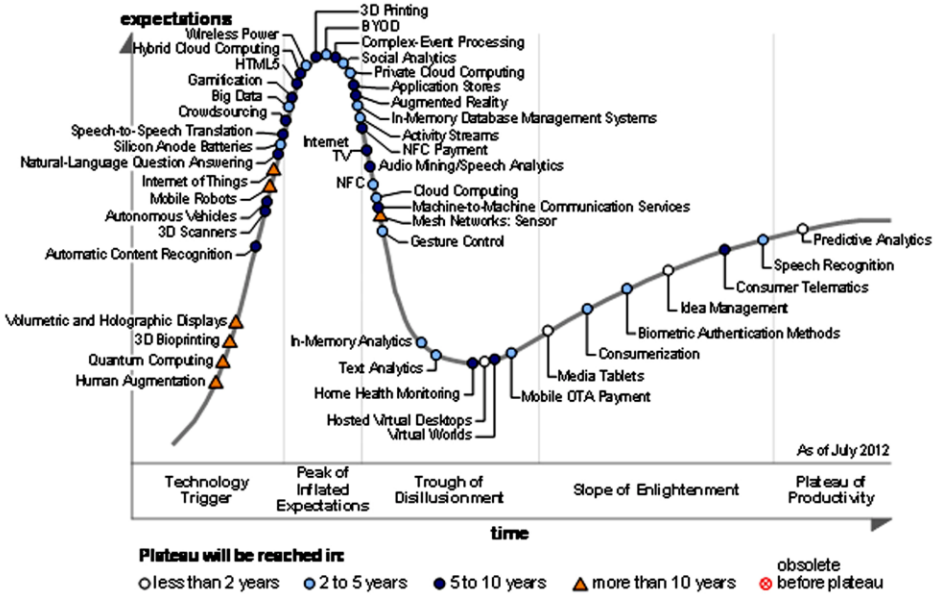

Figure 6.2: Gartner's 2012 Hype Cycle for emerging technologies. (Figure adopted from [76])

Logically the aboriginal application of IoT was in the logistics area and the implementation of RFID tagging for promoting trustworthy inventory management, route outlining and preclusion of losses in retail and distribution [97, 218]. Passive RFID due to extensive research and market potential survived the hype cycle and is now in maturity stages, thus paving the way for realizing IoT in the near future. In this context, there is the need to appraise the potential of several key component technologies for realization of future flexible, green and durable RFID tags that will aggregate the building blocks of IoT.

6.2.2 Dynamics of Printed Electronics

The printing industry is increasingly interlocked with the electronics industry, and this fusion of capabilities resulted into many applications of flexible and organic electronics. It is observed that there are numerous printing mechanisms that will print electronic circuitry, with gravure and flexography as the most persuasive contenders [86, 105] and in the near future for medium scale industrial applications inkjet printing will prevail with its distinct capabilities [19].

In the recent report, IDTechEx finds that the market for printed and thin film electronics will be $9.46 billion in 2012; 42.5% of that will be predominately organic electronics. At first photovoltaics, OLED and e-paper displays flourish swiftly,

followed by thin film transistor circuits, sensors and batteries. By 2022, the market will be worth $63.28 billion, with 45% printed and 33% on flexible substrates. Thus in the near future, more efficient commercial substrates for RFID tags will be available [62]. These substrates will constitute more flexible, durable tags that can sustain in extreme, harsh environments. Moreover, better sensors will be realized with high performance substrates.

6.2.3 Advancements in Conductive Inks

Conductive inks are a uncomplicated and unglamorous layer, but they will constitute a substantial $2.86 billion market in 2012. This market is foreseen to rise to $3.36 billion in 2018, with $735 million captured by new silver and copper nanostructure inks [104].

The conductive inks find use in a great variety of RFID applications ranging from flexible, green and robust RFID tags. The multiplicity of market requirements has resulted in the availability of several types of inks, each offering their own set of characteristics and unique segment of applications. Innovation in the domain of nanotechnology has extensively enabled this high level of product differentiation. Assuredly, the market today consist of graphene, carbon nanotubes, silver and copper nanostructure (nanoparticle and nanowire) inks [41, 174], all of these have one or two dimensions in the nanoscale [38].

Silver flake inks are presently serving the largest and maturest markets. The emerging inks are leisurely perforating the market by either supplanting an existent product (e.g., indium tin oxide) and/or enabling brand-new markets based on their characteristics of higher conductivity, inkjet printability, versatility, and/or enhanced surface smoothness [104]. Therefore, these inks will significantly contribute in high performance RFID tags in future. The realization of extremely conductive and flexible inks will provide much freedom for RFID tag antennas design that will ultimately lead to more efficient tags.

6.3 Trends for RFID Future Tags

In recent VDC Research report, a leading market research and advisory services firm providing market intelligence, prognosticated in 2012 RFID will overwhelm on harsh environments and find its way into more user environments, actuating vertical and application solutions. With an average CAGR of 65 percent, as showed in Figure 6.3, EPC UHF transponders look to outpace high frequency transponders as RFID is utilized by plentiful industries as showed in Figure 6.4, and executing significant progress in deployment across markets as assorted as MRO, healthcare and energy [78].

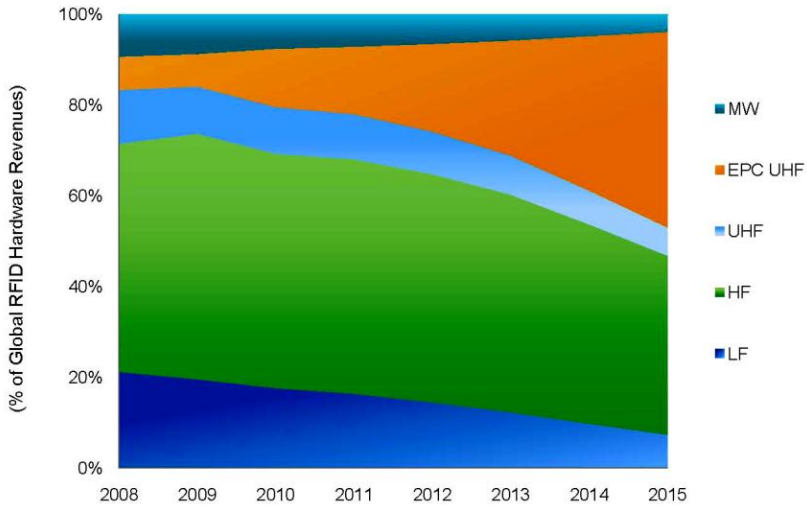

Figure 6.3: Global RFID hardware revenues by frequency. (Figure adopted from [78])

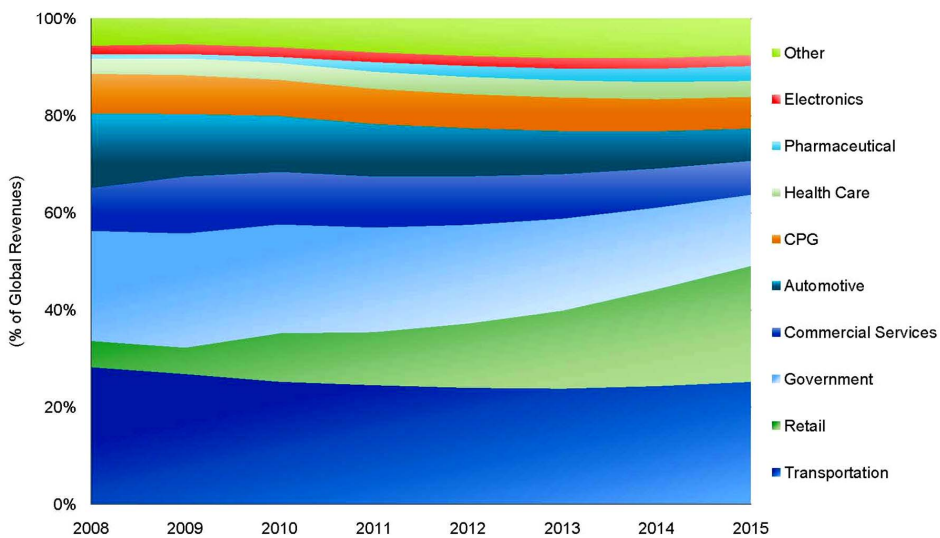

Figure 6.4: RFID solutions by vertical market. (Figure adopted from [78])

6.3.1 MRO Industry: Towards Drastic Changes

The advancements in RFID technology are propelling the research focus towards realizing new generation of rugged metal tags, which are small enough to be attached to individual assets such as working tools, and small machine parts that will extend the possibilities of RFID implementation into more robust and extreme environments.

Presently the technology has the capability for significantly improving the performance of critical assets in hazardous, higher risk conditions which has paved the way for adoption of RFID for MRO (maintenance, repair, and overhaul) in rugged and harsh environments [203, 217] (more confident usage in military applications) [222]. The implementation of RFID is now moving beyond basic identification applications into the era of creating "smart" assets which can convey key product specifications, maintenance, installation, supply chain, and other useful data with them as they are transported from place to place, throughout the world. These applications demand lightweight substrates along with the plausibility of being eco-friendly in the near future as repair and overhaul are norm for day to day business applications. There is growing pursuit for RFID enabled sensors, which can transmit information about the condition of the specific item so that it can be fixed before its malfunctioning. RFID antennas, which can offer higher performance against metal contacts will be more adoptive in this area of application.

6.3.2 Transportation Industry: Improving Efficiency

This covers product movement from the point of production through the store floor that includes travel and logistics - not only, continues to account for the majority of the reader and tags usage, but remains a leading adopter of hybrid (i.e. more than one frequency or technology) solutions. Main applications of RFID within the transportation in reference to tag type include:

- supply chain management [77, 153]–(robust and higher read range tags),
- asset tracking [43]–(small-size and durable tags),
- ticketing [83]–(low-cost and green tags),
- baggage handling [138]–(low-cost and green tags for low carbon emission),
- and security/access control [210, 4]–(reliable and robust tags).

6.3.3 Oil and Gas Industry: Towards Smooth Operations

More and more oil and gas companies are now adopting RFID because of its economic, and security benefits as it has proven to meet the extreme applications required by the industry [70, 127]. The tags that can be embedded in to custom carrier and in the near future the embedded sensor tags into the assets themselves;

the industry is choosing and implementing RFID at a large scale almost in every product segment.

In the future, the industry will increasingly demand new ruggedized RFID solutions that will open a new horizon for research and development in RFID tags. These tags will be adopted for a full range of products and services in order to provide real-time and errorless visibility to spare parts/components. The embedded tags will be used to track crucial consignments of components and supplies to off-shore oil platforms, improve visibility of supply chain in order to eliminate theft and losses, elevate efficiencies in tracking processes by reducing paper work, better manage and maintain their rental assets with automated inventory, and keep strict and timely maintenance records on key components (including premises of oil rigs and oil refinery) to make sure the whole process perpetuates to run smoothly.

6.3.4 Healthcare: Advanced Patient Monitoring and Asset Tracking

The implementation of RFID, both active and especially passive technologies, have seen a growing trend in the healthcare sector in the past several years. The RFID applications realized in this domain are commonly classified in two segments, patient and hospital assets tracking within the hospital premises [44, 179]. In case of patient tracking it emphasis primarily on identification and for assets, it deals with location of the particular item. Thus, currently, RFID is tagged differently to patients and equipment and so on [176, 157], but the future vision of RFID is that all of these will be linked in one way or another, hence increasing efficiency.

In the aftertime, the extensive research in RFID based embedded sensors radically develops this sector by not only providing the identification or location info but also the condition of the equipment along with additional services as inferred in Figure 6.5. Supplementary information about the equipment will be available because of RFID ASIC improvements such as; when was it last inspected, cleaned, date of last maintenance or calibration, number of used cycles, state of warranty or service agreement, manufacturer, model number, etc.

Furthermore, in the futurity there is much research opening for passive UHF RFID tags that are small and rugged enough to be attached or bonded to individual surgical instruments. This implementation will not only improve the asset tracking and asset management but also critical surgical instruments will be handled more effectively and efficiently.

6.3.5 Aircraft Manufacturers Industry: Towards Safe Environment

Aircraft manufacturers have created high memory RFID standards for flyable aircraft parts which are mentioned in Aviation Transportation Association Spec2000, Chapter 9 [183] that provides the standard formats for automatic identification and data capture with RFID. Airbus' new A350 XWB (extra-wide body) project is

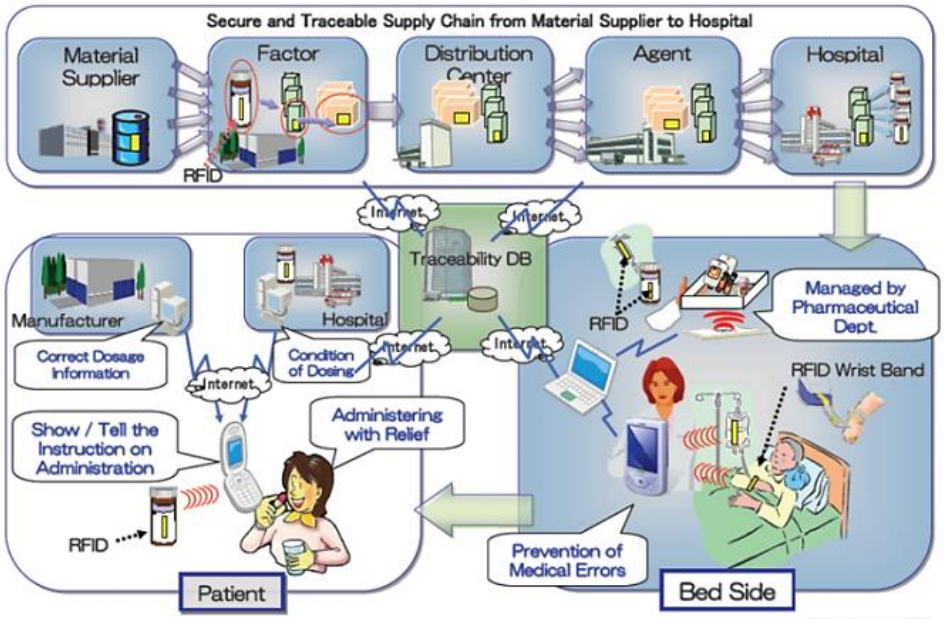

Figure 6.5: Future vision of RFID application in healthcare. (Figure adopted from [92])

already implementing this standard in which Airbus has mandated that thousands of pressurized and non-pressurized parts, and components use high memory RFID tags [129]. In a similar fashion, Boeing is implementing a solution that can provide customers with Fujitsu's RFID tags, designed specifically for aerospace applications, as well as integration and maintenance services from Fujitsu and Boeing [140].

As these projects, as well as other new builds, get under way, it is expected to offer wide scale adoption of high memory RFID in the industry. These opportunities require extensive research to achieve RFID tags that can demonstrate reliable performance especially when attached to metallic objects. Furthermore, all of these industries are proceeding towards low carbon emission ambitions there is much research potential for tags that can have eco-friendly characteristics. These future tags are supposed to provide inventory control, tracking assets without network access, recording high value asset life histories, and sensor recording and monitoring.

Bibliography

[1] S. Agrawal and M.L. Das. Internet of things — a paradigm shift of future internet applications. In *Proc. Nirma University Int Engineering (NUiCONE) Conf*, pages 1–7, 2011.

[2] V. Akan and E. Yazgan. New analytical input impedance calculation for fast design of printed narrow slot antenna. *International Journal of Electronics*, 98(9):1229–1237, 2011.

[3] J. Al-Kassab and W.-C. Rumsch. Challenges for rfid cross-industry standardization in the light of diverging industry requirements. *IEEE Systems Journal*, 2(2):170–177, 2008.

[4] M. Al-Zewairi, J. Alqatawna, and O. Al-Kadi. Privacy and security for rfid access control systems: Rfid access control systems without back-end database. In *Proc. IEEE Jordan Conf. Applied Electrical Engineering and Computing Technologies (AEECT)*, pages 1–6, 2011.

[5] A.V. Alejos, M. Garcia Sánchez, I. Cuinas, and J.C.G. Valladares. Sensor area network for active rtls in rfid tracking applications at 2.4 ghz. *Progress In Electromagnetics Research*, 110:43–58, 2010.

[6] UHF Alien Technology Corporation. Gen2 rfid tags. *Online: www.alientechnology.com.*

[7] F. Alimenti, M. Virili, G. Orecchini, P. Mezzanotte, V. Palazzari, M.M. Tentzeris, and L. Roselli. A new contactless assembly method for paper substrate antennas and uhf rfid chips. *IEEE Transactions on Microwave Theory and Techniques*, 59(3):627–637, 2011.

[8] P. Alitalo, A.E. Culhaoglu, A.V. Osipov, S. Thurner, E. Kemptner, and S.A. Tretyakov. Experimental characterization of electromagnetic cloaking structures with bistatic measurements at x-band. In *Antennas and Propagation (EUCAP), 2012 6th European Conference on*, pages 1682–1686. IEEE, 2012.

[9] O. Aluf. Active rfid tags system analysis of energy consumption as excitable linear bifurcation system. In *Proc. IEEE Int. Conf. Microwaves, Communications, Antennas and Electronics Systems COMCAS 2009*, pages 1–9, 2009.

[10] Y. Amin, Q. Chen, H. Tenhunen, and L.-R. Zheng. Evolutionary versatile printable rfid antennas for “green” electronics. *Journal of Electromagnetic Waves and Applications*, 26(2-3):264–273, 2012.

[11] Y. Amin, Q. Chen, H. Tenhunen, and L.-R. Zheng. Performance-optimized quadrate bowtie rfid antennas for cost-effective and eco-friendly industrial applications. *Progress In Electromagnetics Research*, 126:49–64, 2012.

[12] Y. Amin, Q. Chen, L.-R. Zheng, and H. Tenhunen. Design and fabrication of wideband archimedean spiral antenna based ultra-low cost“green”modules for rfid sensing and wireless applications. *Progress In Electromagnetics Research*, 130:241–256, 2012.

[13] Y. Amin, Q. Chen, L.-R. Zheng, and H. Tenhunen. Development and analysis of flexible uhf rfid antennas for "green" electronics. *Progress In Electromagnetics Research*, 130:1–15, 2012.

[14] Y. Amin, Q. Chen, L.-R. Zheng, and H. Tenhunen. “green” wideband log-spiral antenna for rfid sensing and wireless applications. *Journal of Electromagnetic Waves and Applications*, 26(14-15):2043–2050, 2012.

[15] Y. Amin, Q. Chen, L.-R. Zheng, and H. Tenhunen. Two-arm sinuous antenna for rfid ubiquitous sensors and wireless applications. *Journal of Electromagnetic Waves and Applications*, 26(17-18):2365–2371, 2012.

[16] Y. Amin, R.K. Kanth, P. Liljeberg, Q. Chen, L.-R. Zheng, and H. Tenhunen. Green wideband rfid tag antenna for supply chain applications. *IEICE Electronics Express*, 9(24):1861–1866, 2012.

[17] Y. Amin, R.K. Kanth, P. Liljeberg, Q. Chen, L.-R. Zheng, and H. Tenhunen. Performance-optimized printed wideband rfid antenna and environmental impact analysis. *ETRI Journal, submitted for publication*, 2012.

[18] H. Andersson, A. Manuilskiy, T. Unander, C. Lidenmark, S. Forsberg, and H. Nilsson. Inkjet printed silver nanoparticle humidity sensor with memory effect on paper. *IEEE Sensors Journal*, 12(6):1901–1905, 2012.

[19] B. Ando and S. Baglio. Inkjet-printed sensors: a useful approach for low cost, rapid prototyping [instrumentation notes]. *IEEE Instrumentation & Measurement Magazine*, 14(5):36–40, 2011.

[20] J. Appel-Hansen. Centers of structures in electromagnetism–a critical analysis. *IEEE Transactions on Antennas and Propagation*, 30(4):606–610, 1982.

[21] J.S. Aronson. Making it a positive force in environmental change. *IT Professional*, 10(1):43–45, 2008.

[22] Organic Electronics Association *et al.* Oe-a roadmap for organic and printed electronics. *White Paper*, 2009.

[23] M.M. Aung, Y.S. Chang, and J.U. Won. Emerging rfid/usn applications and challenges. *International Journal of RFID Security and Cryptography*, 1(1/2): 3–8, 2012.

[24] A. Babar, L. Ukkonen, and L. Sydanheimo. Dual uhf rfid band miniaturized multipurpose planar antenna for compact wireless systems. In *Proc. Int Antenna Technology (iWAT) Workshop*, pages 1–4, 2010.

[25] A. Ali Babar, J. Virtanen, V.A. Bhagavati, L. Ukkonen, A.Z. Elsherbeni, P. Kallio, and L. Sydanheimo. Inkjet-printable uhf rfid tag antenna on a flexible ceramic- polymer composite substrate. In *Proc. IEEE MTT-S Int. Microwave Symp. Digest (MTT)*, pages 1–3, 2012.

[26] J.H. Bae, W.K. Choi, C.W. Park, C.S. Pyo, and K.T. Kim. Design of reader baseband receiver structure for demodulating backscattered tag signal in a passive rfid environment. *ETRI Journal*, 34(2):147–158, 2012.

[27] C.A. Balanis. *Antenna theory: analysis and design*. Wiley-Interscience, New York, 2005.

[28] M. Balde, F. Jacquemoud-Collet, B. Charlot, P. Combette, and B. Sorli. Microelectronic technology on paper substrate. In *Proc. Symp. Design, Test, Integration and Packaging of MEMS/MOEMS (DTIP)*, pages 140–143, 2012.

[29] R. Barnett, G. Balachandran, S. Lazar, B. Kramer, G. Konnail, S. Rajasekhar, and V. Drobny. A passive uhf rfid transponder for epc gen 2 with -14dbm sensitivity in 0.13μm cmos. In *Proc. Digest of Technical Papers. IEEE Int. Solid-State Circuits Conf. ISSCC 2007*, pages 582–623, 2007.

[30] S. Basat, S. Bhattacharya, A. Rida, S. Johnston, L. Yang, M.M. Tentzeris, and J. Laskar. Fabrication and assembly of a novel high-efficiency uhf rfid tag on flexible lcp substrate. In *Proc. 56th Electronic Components and Technology Conf*, 2006.

[31] S.S. Basat, Kyutae Lim, J. Laskar, and M.M. Tentzeris. Design and modeling of embedded 13.56 mhz rfid antennas. In *Proc. IEEE Antennas and Propagation Society Int. Symp*, volume 4, pages 64–67, 2005.

[32] C. Beelen-Hendrikx. Trends in ic packaging. In *Proc. European Microelectronics and Packaging Conf. EMPC 2009*, pages 1–8, 2009.

[33] J.M. Bell and M.F. Iskander. A low-profile archimedean spiral antenna using an ebg ground plane. *IEEE Antennas and Wireless Propagation Letters*, 3 (1):223–226, 2004.

[34] R. Bhattacharyya, C. Floerkemeier, and S. Sarma. Low-cost, ubiquitous rfid-tag-antenna-based sensing. *Proceedings of the IEEE*, 98(9):1593–1600, 2010.

[35] T. Bjorninen, A.Z. Elsherbeni, and L. Ukkonen. Low-profile conformal uhf rfid tag antenna for integration with water bottles. *IEEE Antennas and Wireless Propagation Letters*, 10:1147–1150, 2011.

[36] T. Bjorninen, M. Lauri, L. Ukkonen, R. Ritala, A.Z. Elsherbeni, and L. Sydanheimo. Wireless measurement of rfid ic impedance. *IEEE Transactions on Instrumentation and Measurement*, 60(9):3194–3206, 2011.

[37] J.C. Bolomey and F.E. Gardiol. *Engineering applications of the modulated scatterer technique*. Artech House Publishers, 2001.

[38] A. Bonea, A. Brodeala, M. Vladescu, and P. Svasta. Electrical conductivity of inkjet printed silver tracks. In *Proc. 35th Int Electronics Technology (ISSE) Spring Seminar*, pages 1–4, 2012.

[39] I. Bose and S. Yan. The green potential of rfid projects: A case-based analysis. *IT Professional*, 13(1):41–47, 2011.

[40] C. Boyer and S. Roy. Coded qam backscatter modulation for rfid. *IEEE Transactions on Communications*, 60(7):1925–1934, 2012.

[41] A. Brodeala, A. Bonea, C. Ionescu, M. Vladescu, and P. Svasta. Physical properties of silver inkjet printed circuits. In *Proc. 35th Int Electronics Technology (ISSE) Spring Seminar*, pages 114–116, 2012.

[42] M.C. Buck and D.S. Filipovic. Two-arm sinuous antennas. *IEEE Transactions on Antennas and Propagation*, 56(5):1229–1235, 2008.

[43] B. Calio, D. Wyskida, and M. Frissora. Integrating rfid technology to improve it asset management controls, playing an integral part in datacenter relocation. In *Proc. 8th Int Emerging Technologies for a Smarter World (CEWIT) Conf. & Expo*, pages 1–6, 2011.

[44] L. Catarinucci, R. Colella, and L. Tarricone. Integration of rfid and sensors for remote healthcare. In *Proc. 3rd Int Applied Sciences in Biomedical and Communication Technologies (ISABEL) Symp*, pages 1–5, 2010.

[45] H. Chaabane, E. Perret, and S. Tedjini. Towards uhf rfid robust design tag. In *Proc. IEEE Int RFID Conf*, pages 223–229, 2010.

[46] H. Chaabane, E. Perret, and S. Tedjini. A methodology for the design of frequency and environment robust uhf rfid tags. *IEEE Transactions on Antennas and Propagation*, 59(9):3436–3441, 2011.

[47] J. Chang, T. Ge, and E. Sanchez-Sinencio. Challenges of printed electronics on flexible substrates. In *Proc. IEEE 55th Int Circuits and Systems (MWSCAS) Midwest Symp*, pages 582–585, 2012.

[48] A.X. Chen, T.H. Jiang, Z.D. Chen, and D. Su. A novel low-profile wideband uhf antenna. *Progress In Electromagnetics Research*, 121:75–88, 2011.

[49] J. Chen, G. Fu, G.-D. Wu, and S.-X. Gong. A novel broadband circularly polarized irregular slot antenna. *Journal of Electromagnetic Waves and Applications, 24*, 2(3):413–421, 2010.

[50] P.-Y. Chen, P.-H. Wu, W. J. Ong, Y.-J. Huang, W.-C. Lin, and T.-L. Pan. Development of a brand new system using rfid combining with wireless sensor network (wsns) for real-time doze alarm. In *Proc. 3rd Int. Conf. Anti-counterfeiting, Security, and Identification in Communication ASID 2009*, pages 197–201, 2009.

[51] S.-L. Chen. A miniature rfid tag antenna design for metallic objects application. *IEEE Antennas and Wireless Propagation Letters*, 8:1043–1045, 2009.

[52] S.-L. Chen, S.-K. Kuo, and C.-T. Lin. A metallic rfid tag design for steel-bar and wire-rod management application in the steel industry. *Progress In Electromagnetics Research*, 91:195–212, 2009.

[53] T.-K. Chen and G.H. Huff. Stripline-fed archimedean spiral antenna. *IEEE Antennas and Wireless Propagation Letters*, 10:346–349, 2011.

[54] Y.-S. Chen, S.-Y. Chen, and H.-J. Li. Analysis of antenna coupling in near-field communication systems. *IEEE Transactions on Antennas and Propagation*, 58(10):3327–3335, 2010.

[55] J.S. Choi, Mingon Kang, R. Elmasri, and D.W. Engels. Investigation of impact factors for various performances of passive uhf rfid system. In *Proc. IEEE Int RFID-Technologies and Applications (RFID-TA) Conf*, pages 152–159, 2011.

[56] K. Chomkhamsri and N. Pelletier. Analysis of existing environmental footprint methodologies for products and organizations: Recommendations, rationale and alignment. Technical report, European Commission joint research centre, Institute of Environment and sustainability, Ispra, Italy, 2011.

[57] C. Chung, Y.-H. Kim, T.-H. Ki, K. Bae, and J. Kim. Fully integrated ultra-low-power passive uhf rfid transponder ic. In *Proc. IEEE Int Radio-Frequency Integration Technology (RFIT) Symp*, pages 77–80, 2011.

[58] Anritsu Company. Ms2026b. *Online: http://www.anritsu.com.*

[59] Cabot Corporation. Conductive ink: Cci-300. *Online: http://www.cabot-corp.com/.*

[60] Sun Chemical Corporation. *Online: http://www.sunchemical.com/.*

[61] R. Das and P. Harrop. Printed, organic & flexible electronics forecasts, players & opportunities 2009-2029, 2009.

[62] R. Das and P. Harrop. Printed, organic & flexible electronics forecasts, players & opportunities 2012-2022, printed and potentially printed - the complete picture, 2012.

[63] G. De Vita and G. Iannaccone. Design criteria for the rf section of uhf and microwave passive rfid transponders. *IEEE Transactions on Microwave Theory and Techniques*, 53(9):2978–2990, 2005.

[64] D.M. Dobkin. *The RF in RFID: passive UHF RFID in practice.* Newnes, 2007.

[65] A. Dohr, R. Modre-Opsrian, M. Drobics, D. Hayn, and G. Schreier. The internet of things for ambient assisted living. In *Proc. Seventh Int Information Technology: New Generations (ITNG) Conf*, pages 804–809, 2010.

[66] L. Dong-Sheng, Z. Xue-Cheng, Z. Fan, and D. Min. Embeded eeprom memory achieving lower power - new design of eeprom memory for rfid tag ic. *IEEE Circuits and Devices Magazine*, 22(6):53–59, 2006.

[67] DuPont. Dupont microcircuit materials. *Online: www.dupont.com/.*

[68] J. Dyson. The equiangular spiral antenna. *IRE Transactions on Antennas and Propagation*, 7(2):181–187, 1959.

[69] G.B. Education. Handbook for life cycle assessment (lca). *Using the GaBi Education Software Package, PE International*, 2011.

[70] H.M.G. E.-D.M. El-Anzeery, M.A. E.-A.S. El-Bagouri, and R. Guindi. Novel radio frequency energy harvesting model. In *Proc. IEEE Int. Power Engineering and Optimization Conf. (PEDCO) Melaka, Malaysia*, pages 209–213, 2012.

[71] D.S. Filipovic and J.L. Volakis. Broadband meanderline slot spiral antenna. *IEE Proceedings Microwaves, Antennas and Propagation*, 149(2):98–105, 2002.

[72] P.R. Foster and R.A. Burberry. Antenna problems in rfid systems. In *Proc. IEE Colloquium RFID Technology (Ref. No. 1999/123)*, 1999.

[73] B. Gao, K.C.H. Cheung, C.K.T. Wong, M.M.F. Yuen, and R.D. Murch. Ultrathin low cost electromagnetic band gap (ebg) materials as uhf rfid tag substrate. In *Proc. Int. Conf. Electronic Materials and Packaging EMAP 2006*, pages 1–4, 2006.

[74] J. Gao, J. Siden, and H.-E. Nilsson. Printed electromagnetic coupler with an embedded moisture sensor for ordinary passive rfid tags. *IEEE Electron Device Letters*, 32(12):1767–1769, 2011.

[75] J.A. Garcia, L. Cabria de Juan, R. Marante, L. Rizo, and A. Mediavilla. An unbiased dual-mode mixing antenna for wireless transponders. *Progress In Electromagnetics Research*, 102:1–14, 2010.

[76] Inc. Gartner. Gartner's 2012 hype cycle for emerging technologies identifies "tipping point" technologies that will unlock long-awaited technology scenarios. *Online: http://www.gartner.com.*

[77] G.M. Gaukler. Item-level rfid in a retail supply chain with stock-out-based substitution. *IEEE Transactions on Industrial Informatics*, 7(2):362–370, 2011.

[78] VDC Research Group. Competing and complementary frequencies changing global rfid landscape. *Online: http://www.vdcresearch.com/.*

[79] F. Guidi, N. Decarli, D. Dardari, C. Roblin, and A. Sibille. Performance of uwb backscatter modulation in multi-tag rfid scenario using experimental data. In *Proc. IEEE Int Ultra-Wideband (ICUWB) Conf*, pages 484–488, 2011.

[80] L. Guo, W. Fang, G. Wang, and L. Zheng. Intelligent traffic management system base on wsn and rfid. In *Proc. Int Computer and Communication Technologies in Agriculture Engineering (CCTAE) Conf. On*, volume 2, pages 227–230, 2010.

[81] A.R. Guraliuc, R. Caso, P. Nepa, and J.L. Volakis. Numerical analysis of a wideband thick archimedean spiral antenna. *IEEE Antennas and Wireless Propagation Letters*, 11:168–171, 2012.

[82] H.A.U. Haes. Life-cycle assessment and the use of broad indicators. *Journal of Industrial Ecology*, 10(3):5–7, 2008.

[83] M.F.M. Hasan, G. Tangim, M.K. Islam, M.R.H. Khandokar, and A.U. Alam. Rfid-based ticketing for public transport system: Perspective megacity dhaka. In *Proc. 3rd IEEE Int Computer Science and Information Technology (ICCSIT) Conf*, volume 6, pages 459–462, 2010.

[84] T. Hassan and S. Chatterjee. A taxonomy for rfid. In *Proc. 39th Annual Hawaii Int. Conf. System Sciences HICSS '06*, volume 8, 2006.

[85] C. He, M.E. Kiziroglou, D.C. Yates, and E.M. Yeatman. A mems self-powered sensor and rf transmission platform for wsn nodes. *IEEE Sensors Journal*, 11(12):3437–3445, 2011.

[86] E. Hrehorova, M. Rebros, A. Pekarovicova, B. Bazuin, A. Ranganathan, S. Garner, G. Merz, J. Tosch, and R. Boudreau. Gravure printing of conductive inks on glass substrates for applications in printed electronics. *Journal of Display Technology*, 7(6):318–324, 2011.

[87] H.-T. Hsu, F.-Y. Kuo, and C.-H. Chang. Application of quasi log-periodic antenna for uhf passive rfid tag design featuring constant power transmission coefficient over broadband operation. *Journal of Electromagnetic Waves and Applications, 24*, 5(6):575–586, 2010.

[88] R.-C. Hua and T.-G. Ma. A printed dipole antenna for ultra high frequency (uhf) radio frequency identification (rfid) handheld reader. *IEEE Transactions on Antennas and Propagation*, 55(12):3742–3745, 2007.

[89] S.-R. Huang, G.-J. Horng, and G.-J. Jong. Intelligent hospital space platform combined with rfid and wireless sensor network. In *Proc. IIHMSP '08 Int Intelligent Information Hiding and Multimedia Signal Processing Conf*, pages 1001–1004, 2008.

[90] Y. Huang and K. Boyle. *Antennas: from theory to practice*. Wiley, 2008.

[91] UHF Impinj Inc. Gen2 rfid products. *Online: www.impinj.com*.

[92] EPC Global Inc. *Online: http://www.gs1.org/epcglobal*.

[93] T. Jaakola, M. Lahti, J. Petaja, K. Kautio, K. Ronka, and J. Lenkkeri. Low cost printed flexible multilayer substrates. In *Proc. 10th Electronics Packaging Technology Conf. EPTC 2008*, pages 344–349, 2008.

[94] P.C. Jain and K.P. Vijaygopalan. Rfid and wireless sensor networks. *Proceedings of ASCNT–2010, CDAC, Noida, India*, pages 1–11, 2010.

[95] M.F. Jamlos, T.B.A. Rahman, M.R.B. Kamarudin, P. Saad, O. Abdul Aziz, and M.A. Shamsudin. Adaptive beam steering of rlsa antenna with rfid technology. *Progress In Electromagnetics Research*, 108:65–80, 2010.

[96] M.F. Jamlos, T.B.A. Rahman, M.R.B. Kamarudin, P. Saad, M.A. Shamsudin, and A.M.M. Dahlan. A novel adaptive wi-fi system with rfid technology. *Progress In Electromagnetics Research*, 108:417–432, 2010.

[97] X. Jia, Q. Feng, T. Fan, and Q. Lei. Rfid technology and its applications in internet of things (iot). In *Proc. 2nd Int Consumer Electronics, Communications and Networks (CECNet) Conf*, pages 1282–1285, 2012.

[98] H. Jingyuan, H. Jiale, Z. Zheming, C. Haibin, and W. Jingshen. Reliability optimization for multilayer active rfid tags on rigid and flexible substrates. In *Proc. 12th Int Electronic Packaging Technology and High Density Packaging (ICEPT-HDP) Conf*, pages 1–6, 2011.

[99] R.C. Johnson and H. Jasik. Antenna engineering handbook. *New York, McGraw-Hill Book Company, 1984, 1356 p. No individual items are abstracted in this volume.*, 1, 1984.

[100] U. Karthaus and M. Fischer. Fully integrated passive uhf rfid transponder ic with 16.7-μw minimum rf input power. *IEEE Journal of Solid-State Circuits*, 38(10):1602–1608, 2003.

[101] S. Kawdungta, C. Phongcharoenpanich, and D. Torrungrueng. Design of flat spiral rectangular loop gate antenna for hf-rfid systems. In *Proc. Asia-Pacific Microwave Conf. APMC 2008*, pages 1–4, 2008.

[102] PolyIC GmbH & Co. KG. *Online: http://www.polyic.com/.*

[103] A. Khaleghi. Diversity techniques with parallel dipole antennas: Radiation pattern analysis. *Progress In Electromagnetics Research*, 64:23–42, 2006.

[104] G. Khasha and Z. Harry. Conductive ink markets 2012-2018, silver & copper inks & pastes and beyond, 2012.

[105] C.H. Kim, J. Jo, and S.-H. Lee. Design of roll-to-roll printing equipment with multiple printing methods for multi-layer printing. *Rev Sci Instrum*, 83(6): 065001, 2012.

[106] J. Kim, W.K. Choi, and G.Y. Choi. Small proximity coupled ceramic patch antenna for uhf rfid tag mountable on metallic objects. *Progress In Electromagnetics Research C*, 4:129–138, 2008.

[107] M. Kim, K. Kim, and N. Chong. Rfid based collision-free robot docking in cluttered environment. *Progress In Electromagnetics Research*, 110:199–218, 2010.

[108] Inc. Kovio. *Online: http://www.kovio.com/.*

[109] B.A. Kramer, C.-C. Chen, M. Lee, and J.L. Volakis. Fundamental limits and design guidelines for miniaturizing ultra-wideband antennas. *IEEE Antennas and Propagation Magazine*, 51(4):57–69, 2009.

[110] B.A. Kramer, C.-C. Chen, and J.L. Volakis. Size reduction of a low-profile spiral antenna using inductive and dielectric loading. *IEEE Antennas and Wireless Propagation Letters*, 7:22–25, 2008.

[111] B.A. Kramer, S. Koulouridis, C.-C. Chen, and J.L. Volakis. A novel reflective surface for an uhf spiral antenna. *IEEE Antennas and Wireless Propagation Letters*, 5(1):32–34, 2006.

[112] B.A. Kramer, M. Lee, C.-C. Chen, and J.L. Volakis. Design and performance of an ultrawide-band ceramic-loaded slot spiral. *IEEE Transactions on Antennas and Propagation*, 53(7):2193–2199, 2005.

[113] C.M. Kruesi, R.J. Vyas, and M.M. Tentzeris. Design and development of a novel 3-d cubic antenna for wireless sensor networks (wsns) and rfid applications. *IEEE Transactions on Antennas and Propagation*, 57(10):3293–3299, 2009.

[114] S.-K. Kuo, S.-L. Chen, and C.-T. Lin. An accurate method for impedance measurement of rfid tag antenna. *Progress In Electromagnetics Research*, 83: 93–106, 2008.

[115] S.-K. Kuo, J.-Y. Hsu, and Y.-H. Hung. Analysis and design of an uhf rfid metal tag using magnetic composite material as substrate. *Progress In Electromagnetics Research*, 24:49–62, 2010.

[116] V. Lakafosis, A. Rida, R. Vyas, Li Yang, S. Nikolaou, and M.M. Tentzeris. Progress towards the first wireless sensor networks consisting of inkjet-printed, paper-based rfid-enabled sensor tags. *Proceedings of the IEEE*, 98 (9):1601–1609, 2010.

[117] S. Laybros and P.F. Combes. On radiating-zone boundaries of short, $\lambda/2$, and λ dipoles. *IEEE Antennas and Propagation Magazine*, 46(5):53–64, 2004.

[118] A. Lazaro, D. Girbau, and R. Villarino. Effects of interferences in uhf rfid systems. *Progress In Electromagnetics Research*, 98:425–443, 2009.

[119] J.-W. Lee, D.H.T. Vo, Q.-H. Huynh, and S.H. Hong. A fully integrated hf-band passive rfid tag ic using 0.18-μm cmos technology for low-cost security applications. *IEEE Transactions on Industrial Electronics*, 58(6):2531–2540, 2011.

[120] M. Lee, B.A. Kramer, C.-C. Chen, and J.L. Volakis. Distributed lumped loads and lossy transmission line model for wideband spiral antenna miniaturization and characterization. *IEEE Transactions on Antennas and Propagation*, 55 (10):2671–2678, 2007.

[121] K.S. Leong, M.L. Ng, and P.H. Cole. Investigation of rf cable effect on rfid tag antenna impedance measurement. In *Proc. IEEE Antennas and Propagation Society Int. Symp*, pages 573–576, 2007.

[122] K.S. Leong, M.L. Ng, and P.H. Cole. Miniaturization of dual frequency rfid antenna with high frequency ratio. In *Proc. IEEE Antennas and Propagation Society Int. Symp*, pages 5475–5478, 2007.

[123] W.M. Li, Y.C. Jiao, L. Zhou, and T. Ni. Compact dual-band circularly polarized monopole antenna. *Journal of Electromagnetic Waves and Applications, 25*, 14(15):2130–2137, 2011.

[124] X. Li, J. Liao, Y. Yuan, and D. Yu. Eye-shaped segmented reader antenna for near-field uhf rfid applications. *Progress In Electromagnetics Research*, 114:481–493, 2011.

[125] D.-B. Lin, I.-T. Tang, and C.-C. Wang. Uhf rfid h-shaped tag antenna using microstrip feed design on metallic objects. *Journal of Electromagnetic Waves and Applications*, 25(13):1828–1839, 2011.

[126] H. Liu, M. Bolic, A. Nayak, and I. Stojmenovic. Taxonomy and challenges of the integration of rfid and wireless sensor networks. *IEEE Network*, 22(6): 26–35, 2008.

[127] S. Liu, H. Zheng, H. Meng, H. Hu, J. Wu, and C. Li. Study on quality safety traceability systems for cereal and oil products. In *Proc. WRI World Congress Software Engineering WCSE '09*, volume 1, pages 163–166, 2009.

[128] H. Makimura, Y. Watanabe, K. Watanabe, and H. Igarashi. Evolutional design of small antennas for passive uhf-band rfid. 47(5):1510–1513, 2011.

[129] V. Mancini, M. Pasquali, and M.M. Schiraldi. Opportunities for using rfid in the aircraft production process. *International Journal of RF Technologies: Research and Applications*, 3(4):243–255, 2012.

[130] A. Manna, P. Baldonero, and F. Trotta. Novel uwb low-profile sinuous slot antenna. In *Proc. 5th European Conf. Antennas and Propagation (EUCAP)*, pages 783–786, 2011.

[131] S. Manzari, C. Occhiuzzi, S. Nawale, A. Catini, C. Di Natale, and G. Marrocco. Humidity sensing by polymer-loaded uhf rfid antennas. *IEEE Sensors Journal*, 12(9):2851–2858, 2012.

[132] G. Marrocco. The art of uhf rfid antenna design: impedance-matching and size-reduction techniques. *IEEE Antennas and Propagation Magazine*, 50(1): 66–79, 2008.

[133] L.J. Martin, S. Ooi, D. Staiculescu, M.D. Hill, C.P. Wong, and M.M. Tentzeris. Effect of permittivity and permeability of a flexible magnetic composite material on the performance and miniaturization capability of planar antennas for rfid and wearable wireless applications. *IEEE Transactions on Components and Packaging Technologies*, 32(4):849–858, 2009.

[134] Q. Meng and J. Jin. Design of low-power active rfid tag in uhf band. In *Proc. Int Control, Automation and Systems Engineering (CASE) Conf*, pages 1–4, 2011.

[135] Y.S. Meng and Y.H. Lee. Investigations of foliage effect on modern wireless communication systems: A review. *Progress In Electromagnetics Research*, 105:313–332, 2010.

[136] S.L. Merilampi, T. Björninen, A. Vuorimäki, L. Ukkonen, P. Ruuskanen, and L. Sydänheimo. The effect of conductive ink layer thickness on the functioning of printed uhf rfid antennas. *Proceedings of the IEEE*, 98(9):1610–1619, 2010.

[137] Technical Specification Micro-Coax. *Hand-formable Coaxial Cable, UT-047-FORM.*

[138] R. Miesen, R. Ebelt, F. Kirsch, T. Schafer, G. Li, H. Wang, and M. Vossiek. Where is the tag? *IEEE Microwave Magazine*, 12(7), 2011.

[139] R. Mittra. Challenges in antenna designs and some novel techniques for meeting them. In *Proc. Loughborough Antennas and Propagation Conf. LAPC 2007*, pages 1–4, 2007.

[140] K. Miyazawa. Fujitsu's approach to cloud computing. *FUJITSU Sci. Tech. J*, 47(4):371–377, 2011.

[141] H. Nakano. A meander spiral antenna. In *Proc. IEEE Antennas and Propagation Society Int. Symp*, volume 3, pages 2243–2246, 2004.

[142] H. Nakano, R. Satake, and J. Yamauchi. Extremely low-profile, single-arm, wideband spiral antenna radiating a circularly polarized wave. *IEEE Transactions on Antennas and Propagation*, 58(5):1511–1520, 2010.

[143] K.F. Navarro and E. Lawrence. Wsn applications in personal healthcare monitoring systems: A heterogeneous framework. In *Proc. Second Int. Conf. eHealth, Telemedicine, and Social Medicine ETELEMED '10*, pages 77–83, 2010.

[144] P.V. Nikitin and K.V.S. Rao. Reply to "comments on 'antenna design for uhf rfid tags: A review and a practical application'". *IEEE Transactions on Antennas and Propagation*, 54(6):1906–1907, 2006.

[145] P.V. Nikitin and K.V.S. Rao. Antennas and propagation in uhf rfid systems. In *Proc. IEEE Int RFID Conf*, pages 277–288, 2008.

[146] P.V. Nikitin, K.V.S. Rao, and S. Lazar. An overview of near field uhf rfid. In *Proc. IEEE Int RFID Conf*, pages 167–174, 2007.

[147] E. Nilsson, B. Nilsson, L. Bengtsson, B. Svensson, P. Wiberg, and U. Bilstrup. A low power-long range active rfid-system consisting of active rfid backscatter transponders. In *Proc. IEEE Int RFID-Technology and Applications (RFID-TA) Conf*, pages 26–30, 2010.

[148] H.-E. Nilsson, J. Siden, T. Olsson, P. Jonsson, and A. Koptioug. Evaluation of a printed patch antenna for robust microwave rfid tags. *IET Microwaves, Antennas & Propagation*, 1(3):776–781, 2007.

[149] J. Norman and P. Joseph. Secure neighbour authentication in wireless sensor networks. In *Proc. 2nd Int Wireless Communication, Vehicular Technology, Information Theory and Aerospace & Electronic Systems Technology (Wireless VITAE) Conf*, pages 1–4, 2011.

[150] UHF NXP Semiconductors. Gen2 rfid products. *Online: http://www.nxp.com*.

[151] C. Occhiuzzi and G. Marrocco. The rfid technology for neurosciences: Feasibility of limbs' monitoring in sleep diseases. *IEEE Transactions on Information Technology in Biomedicine*, 14(1):37–43, 2010.

[152] H. Ohashi. Role of green electronics in low carbonated society toward 2030. In *Proc. 14th Int. Power Electronics and Motion Control Conf. (EPE/PEMC)*, 2010.

[153] O. Ondemir, M.A. Ilgin, and S.M. Gupta. Optimal end-of-life management in closed-loop supply chains using rfid and sensors. *IEEE Transactions on Industrial Informatics*, 8(3):719–728, 2012.

[154] G. Orecchini, F. Alimenti, V. Palazzari, A. Rida, M.M. Tentzeris, and L. Roselli. Design and fabrication of ultra-low cost radio frequency identification antennas and tags exploiting paper substrates and inkjet printing technology. *IET Microwaves, Antennas & Propagation*, 5(8):993–1001, 2011.

[155] J.R. Panda and R.S. Kshetrimayum. A printed 2.4 ghz/5.8 ghz dual-band monopole antenna with a protruding stub in the ground plane for wlan and rfid applications. *Progress In Electromagnetics Research*, 117:425–434, 2011.

[156] Inc. Plextronics. *Online: http://www.plextronics.com*.

[157] A.C. Polycarpou, A. Dimitriou, A. Bletsas, P.C. Polycarpou, L. Papaloizou, G. Gregoriou, and J.N. Sahalos. On the design, installation, and evaluation of a radio-frequency identification system for healthcare applications [wireless corner]. *IEEE Antennas and Propagation Magazine*, 54(4):255–271, 2012.

[158] S. Pranonsatit, D. Worasawate, and P. Sritanavut. Affordable ink-jet printed antennas for rfid applications. *IEEE Transactions on Components, Packaging and Manufacturing Technology*, 2(5):878–883, 2012.

[159] D. Preuveneers and Y. Berbers. *Internet of things: A context-awareness perspective*. Auerbach, 2008.

[160] X. Qing, C.K. Goh, and Z.N. Chen. Impedance characterization of rfid tag antennas and application in tag co-design. *IEEE Transactions on Microwave Theory and Techniques*, 57(5):1268–1274, 2009.

[161] S.W. Qu and C.L. Ruan. Effect of round corners on bowtie antennas. *Progress In Electromagnetics Research*, 57:179–195, 2006.

[162] M.J. Radway, T.P. Cencich, and D.S. Filipovic. Pattern purity of coiled-arm spiral antennas. *IEEE Transactions on Antennas and Propagation*, 59(3): 758–766, 2011.

[163] A. Rahmati, L. Zhong, M. Hiltunen, and R. Jana. Reliability techniques for rfid-based object tracking applications. In *Proc. 37th Annual IEEE/IFIP Int. Conf. Dependable Systems and Networks DSN '07*, pages 113–118, 2007.

[164] A. Ramos, A. Lazaro, D. Girbau, and R. Villarino. Time-domain measurement of time-coded uwb chipless rfid tags. *Progress In Electromagnetics Research*, 116:313–331, 2011.

[165] K.V.S. Rao, P.V. Nikitin, and S.F. Lam. Antenna design for uhf rfid tags: a review and a practical application. *IEEE Transactions on Antennas and Propagation*, 53(12):3870–3876, 2005.

[166] A. Rawa and N.C. Karmakar. A novel l-shaped rfid tag antenna. In *Proc. European Conf. Wireless Technologies*, pages 245–248, 2007.

[167] D. Raychaudhuri and N.B. Mandayam. Frontiers of wireless and mobile communications. *Proceedings of the IEEE*, 100(4):824–840, 2012.

[168] D. Redinger, S. Molesa, Shong Yin, R. Farschi, and V. Subramanian. An ink-jet-deposited passive component process for rfid. *IEEE Transactions on Electron Devices*, 51(12):1978–1983, 2004.

[169] A. Rida, Li Yang, R. Vyas, and M.M. Tentzeris. Conductive inkjet-printed antennas on flexible low-cost paper-based substrates for rfid and wsn applications. *IEEE Antennas and Propagation Magazine*, 51(3):13–23, 2009.

[170] ROHACELL. ROHACELL HF 51. `www.rohacell.com`, 2012. [Online; accessed 19-July-2012].

[171] D. Ruffieux, M. Contaldo, J. Chabloz, and C. Enz. Ultra low power and miniaturized mems-based radio for ban and wsn applications. In *Proc. ESSCIRC*, pages 71–80, 2010.

[172] H.-K. Ryu and J.-M. Woo. Miniaturisation of rectangular loop antenna using meander line for rfid tags. *Electronics Letters*, 43(7):372–374, 2007.

[173] H.K. Ryu, J.M. Woo, and S. Lim. Miniaturization of a folded, inverted-f antenna for container rfid tag applications. In *Proc. IEEE Antennas and Propagation Society Int. Symp. APSURSI '09*, pages 1–4, 2009.

[174] B. Salam, W.L. Lai, L.C.W. Albert, and L.B. Keng. Low temperature processing of copper conductive ink for printed electronics applications. In *Proc. IEEE 13th Electronics Packaging Technology Conf. (EPTC)*, pages 251–255, 2011.

[175] R. Sanchez-Montero, S. Salcedo-Sanz, J.A. Portilla-Figueras, and R. Langley. Hybrid pifa-patch antenna optimized by evolutionary programming. *Progress In Electromagnetics Research*, 108:221–234, 2010.

[176] A. Sani, M. Rajab, R. Foster, and Y. Hao. Antennas and propagation of implanted rfids for pervasive healthcare applications. *Proceedings of the IEEE*, 98(9):1648–1655, 2010.

[177] L. Schreider, X. Begaud, M. Soiron, B. Perpere, and C. Renard. Broadband archimedean spiral antenna above a loaded electromagnetic band gap substrate. *IET Microwaves, Antennas & Propagation*, 1(1):212–216, 2007.

[178] B. Shao, Q. Chen, R. Liu, and L.-R. Zheng. Linearly-tapered rfid tag antenna with 40ultra-low-cost applications. In *Proc. IEEE Int RFID (RFID) Conf*, pages 45–49, 2011.

[179] S.-T. Shih, C.-M. Hsu, and C.-Y. Chao. Self healthcare management system based on rfid technology. In *Proc. 7th Int Networked Computing and Advanced Information Management (NCM) Conf*, pages 252–255, 2011.

[180] F.E.M. Silveira and J.A.S. Lima. Skin effect from extended irreversible thermodynamics perspective. *Journal of Electromagnetic Waves and Applications, 24*, 2(3):151–160, 2010.

[181] Z.W. Sim, R. Shuttleworth, M.J. Alexander, and B.D. Grieve. Compact patch antenna design for outdoor rf energy harvesting in wireless sensor networks. *Progress In Electromagnetics Research*, 105:273–294, 2010.

[182] M.R. Souryal, D.R. Novotny, D.G. Kuester, J.R. Guerrieri, and K.A. Remley. Impact of rf interference between a passive rfid system and a frequency hopping communications system in the 900 mhz ism band. In *Proc. IEEE Int Electromagnetic Compatibility (EMC) Symp*, pages 495–500, 2010.

[183] Spec2000. *Online: http://www.spec2000.com/.*

[184] V. Subramanian, J.M.J. Frechet, P.C. Chang, D.C. Huang, J.B. Lee, S.E. Molesa, A.R. Murphy, D.R. Redinger, and S.K. Volkman. Progress toward development of all-printed rfid tags: Materials, processes, and devices. *Proceedings of the IEEE*, 93(7):1330–1338, 2005.

[185] L. Sun, Y.-H. Huang, J.-Y. Li, and Q.-Z. Liu. A wideband circularly polarized candy-like patch antenna. *Journal of Electromagnetic Waves and Applications, 25*, 8(9):1113–1121, 2011.

[186] D. Sung, A. de la Fuente Vornbrock, and V. Subramanian. Scaling and optimization of gravure-printed silver nanoparticle lines for printed electronics. *IEEE Transactions on Components and Packaging Technologies*, 33(1):105–114, 2010.

[187] H. Tanaka and F. Okada. Precise measurements of dissipation factor in microwave printed circuit boards. *IEEE Transactions on Instrumentation and Measurement*, 38(2):509–514, 1989.

[188] Z. Tang, Y. He, Z. Hou, and B. Li. The effects of antenna properties on read distance in passive backscatter rfid systems. In *Proc. Int. Conf. Networks Security, Wireless Communications and Trusted Computing NSWCTC '09*, volume 1, pages 120–123, 2009.

[189] Agilent Technologies. 8562e portable spectrum analyzer. *Online: http://www.home.agilent.com.*

[190] PulseForge Technology. *Online: www.novacentrix.com.*

[191] J. Thaysen, K.B. Jakobsen, and J. Appel-Hansen. A wideband balun-how does it work? *Applied Microwave and Wireless*, 12(10):40–51, 2000.

[192] V.M. Thomas. Environmental implications of rfid. In *Proc. IEEE Int. Symp. Electronics and the Environment ISEE 2008*, pages 1–5, 2008.

[193] J.J. Tiang, M.T. Islam, N. Misran, and J.S. Mandeep. Circular microstrip slot antenna for dual-frequency rfid application. *Progress In Electromagnetics Research*, 120:499–512, 2011.

[194] J.J. Tiang, M.T. Islam, N. Misran, and J.S. Mandeep. Slot loaded circular microstrip antenna with meandered slits. *Journal of Electromagnetic Waves and Applications*, 25(13):1851–1862, 2011.

[195] D. Tobjörk and R. Österbacka. Paper electronics. *Advanced Materials*, 23 (17):1935–1961, 2011.

[196] M.S. Trotter and G.D. Durgin. Range estimation for passive rfid systems that use power-optimized waveforms. In *Proc. IEEE Int RFID (RFID) Conf*, pages 102–109, 2012.

[197] L. Ukkonen, D. Engels, A. Sydanheimo, and M. Kivikoski. Reliability of passive rfid of multiple objects using folded microstrip patch-type tag antenna. In *Proc. IEEE Antennas and Propagation Society Int. Symp*, volume 2, pages 341–344, 2005.

[198] International Telecommunication Union. Itu internet reports 2005: The internet of things 2005, 7th ed. Technical report, International Telecommunication Union, Geneva, Switzerland., November 2005.

[199] M. Vahdani and X. Begaud. A directive ultra wideband sinuous slot antenna. In *Proc. First European Conf. Antennas and Propagation EuCAP 2006*, pages 1–6, 2006.

[200] N. Vaidya and S.R. Das. Rfid-based networks: exploiting diversity and redundancy. *ACM SIGMOBILE Mobile Computing and Communications Review*, 12(1):2–14, 2008.

[201] J.L. Volakis, G. Mumcu, K. Sertel, C.-C. Chen, M. Lee, B. Kramer, D. Psychoudakis, and G. Kiziltas. Antenna miniaturization using magnetic-photonic and degenerate band-edge crystals. 48(5):12–28, 2006.

[202] M. Von Zedtwitz and O. Gassmann. Market versus technology drive in r&d internationalization: four different patterns of managing research and development. *Research policy*, 31(4):569–588, 2002.

[203] H. Wang, X. Du, F. Zhang, and W. Li. Application of rfid technology in elevator maintenance supervision. In *Proc. Int Computer Science and Service System (CSSS) Conf*, pages 2112–2115, 2011.

[204] J.J.H. Wang. Spiral antennas in rfid and their size reduction and performance enhancement. In *Proc. IEEE Int Anti-counterfeiting, Security, Identification Workshop*, pages 44–47, 2007.

[205] Y.I. Wang, C.J. Simonson, R.W. Besant, and W. Shang. Transient humidity measurements–part i: Sensor calibration and characteristics. *IEEE Transactions on Instrumentation and Measurement*, 56(3):1074–1079, 2007.

[206] Z. Wang, S. Fang, S. Fu, and S. Jia. Single-fed broadband circularly polarized stacked patch antenna with horizontally meandered strip for universal uhf rfid applications. *IEEE Transactions on Microwave Theory and Techniques*, 59 (4):1066–1073, 2011.

[207] R. Want. Enabling ubiquitous sensing with rfid. *Computer*, 37(4):84–86, 2004.

[208] R. Want. An introduction to rfid technology. *IEEE Pervasive Computing*, 5 (1):25–33, 2006.

[209] Y. Watanabe, K. Watanabe, and H. Igarashi. Optimization of meander line antenna considering coupling between nonlinear circuit and electromagnetic waves for uhf-band rfid. *IEEE Transactions on Magnetics*, 47(5):1506–1509, 2011.

[210] D.-L. Wu, W.W.Y. Ng, P.P.K. Chan, H.-L. Ding, B.-Z. Jing, and D.S. Yeung. Access control by rfid and face recognition based on neural network. In *Proc. Int Machine Learning and Cybernetics (ICMLC) Conf*, volume 2, pages 675–680, 2010.

[211] J. Xi, H. Zhu, and T.T. Ye. Platform-tolerant pifa-type uhf rfid tag antenna. In *Proc. IEEE Int RFID Conf*, pages 174–180, 2010.

[212] Z. Xiong, F. Sottile, M.A. Spirito, and R. Garello. Hybrid indoor positioning approaches based on wsn and rfid. In *Proc. 4th IFIP Int New Technologies, Mobility and Security (NTMS) Conf*, pages 1–5, 2011.

[213] L. Yang, D. Staiculescu, R. Zhang, C.P. Wong, and M.M. Tentzeris. A novel "green" fully-integrated ultrasensitive rfid-enabled gas sensor utilizing inkjet-printed antennas and carbon nanotubes. In *Proc. IEEE Antennas and Propagation Society Int. Symp. APSURSI '09*, pages 1–4, 2009.

[214] C.-C. Yen, A.E. Gutierrez, D. Veeramani, and D. van der Weide. Radar cross-section analysis of backscattering rfid tags. *IEEE Antennas and Wireless Propagation Letters*, 6:279–281, 2007.

[215] W.S. Yeoh, K.L. Wong, and W.S.T. Rowe. Wideband miniaturized half bowtie printed dipole antenna with integrated balun for wireless applications. *IEEE Transactions on Antennas and Propagation*, 59(1):339–342, 2011.

[216] W.-J. Yoon, S.-H. Chung, S.-J. Lee, and Y.-S. Moon. Design and implementation of an active rfid system for fast tag collection. In *Proc. 7th IEEE Int. Conf. Computer and Information Technology CIT 2007*, pages 961–966, 2007.

[217] L. Yuan, L. Jiani, S. Zhengping, and S. Xin. Development of the equipment overhaul management system based on rfid. In *Proc. IEEE Symp. Robotics and Applications (ISRA)*, pages 939–941, 2012.

[218] K. Zhang, Z. Ao, C. Tang, Y. Wang, W. Zhu, and B. Feng. Application of internet of things in combined operation logistics support. In *Proc. Fourth Int Computational and Information Sciences (ICCIS) Conf*, pages 388–391, 2012.

[219] Y. Zhang and B.R. Bakshi. Statistical evaluation of input-side metrics for life cycle impact assessment of emerging technologies. In *Electronics & the Environment, Proceedings of the 2007 IEEE International Symposium on*, pages 117–122. IEEE, 2007.

[220] F. Zhao. Sensors meet the cloud: Planetary-scale distributed sensing and decision making. In *Proc. 9th IEEE Int Cognitive Informatics (ICCI) Conf*, 2010.

[221] W. Zhao, Y.-J. Zhao, and H.-B. Qin. Calibration of the three-port vna using the general 6-term error model. *Journal of Electromagnetic Waves and Applications, 24*, 2(3):319–326, 2010.

[222] D. Zhijian, T. Guangcai, and W. Min. Application of rfid technology in u.s. logistics and the enlightenment for our army. In *Proc. 2nd Int Artificial Intelligence, Management Science and Electronic Commerce (AIMSEC) Conf*, pages 2825–2828, 2011.

[223] Y. Zhou. A novel slot antenna for uhf rfid tag. In *Proc. IET 3rd Int Wireless, Mobile and Multimedia Networks (ICWMNN 2010) Conf*, pages 254–257, 2010.

[224] M. Zorzi, A. Gluhak, S. Lange, and A. Bassi. From today's intranet of things to a future internet of things: a wireless- and mobility-related view. 17(6): 44–51, 2010.

[225] Y. Zuo. Survivable rfid systems: Issues, challenges, and techniques. *IEEE Transactions on Systems, Man, and Cybernetics, Part C: Applications and Reviews*, 40(4):406–418, 2010.

Appendix A

Included Papers

Paper I–Evolutionary Versatile Printable RFID Antennas for "Green" Electronics

Y. Amin, Q. Chen, H. Tenhunen, and L.-R. Zheng, *Journal of Electromagnetic Waves and Applications*, vol. 26, nos. 2-3, pp. 264-273, 16 Apr 2012

Available online at: http://www.tandfonline.com/10.1163/156939312800030901

J. of Electromagn. Waves and Appl., Vol. 26, 264–273, 2012

EVOLUTIONARY VERSATILE PRINTABLE RFID ANTENNAS FOR "GREEN" ELECTRONICS

Y. Amin*, Q. Chen, H. Tenhunen, and L. R. Zheng

iPack VINN Excellence Center, Royal Institute of Technology (KTH), Stockholm, SE-16440, Sweden

Abstract—The development of low cost directly printable RFID tag antennas is essential for item level tracking. We present evolutionary design approach to achieve robust extremely versatile RFID antennas on paper/flexible substrates which allow a simple integration directly on, e.g., paperboard in a roll-to-roll production line. Fully integrated printed tags for "green" electronics are designed for operability in frequencies 866–868 MHz & 902–928 MHz. We present benchmarking results for various challenges of antennas in terms of ruggedness, reliability and flexing performance.

1. INTRODUCTION

In recent years, the concepts "internet of things" [1] and "green" electronics [2] have attracted tremendous attention. For the last decade or so, predictions have stated an exponential increase in the revenue of RFID. However, so far mainly cost insensitive niche areas have utilized this new technology [3, 4]. The requirement for RFID tags to survive against harsh environments adds further complexity to the implementation horizon [5]. The material of the objects on which the tags are attached can influence the capacitive characteristics and radiation pattern of the tag antenna [6, 7]. Some experience has suggested that we need to take precautionary measures to prevent the likely negative results from the final disposal of RFID labels [8]. Currently, RFID tags are neither biodegradable [9] nor recyclable [10].

In this paper, we propose an evolution of novel RFID tag antennas. The design and computations are performed using ANSYS HFSS^{TM}. These antennas are printed on several substrates using state-of-the-art

Received 2 December 2011, Accepted 4 January 2012, Scheduled 11 January 2012

* Corresponding author: Yasar Amin (ysar@kth.se).

printing technologies (screen printing, flexography and inkjet printing). The measurements are carried out in an anechoic chamber owing to an experimental set up dedicated to antenna characterization. The small size, low cost, convenient aspect ratio and exceptional read range of these proposed antennas make them an ideal choice for far-field case, carton and pallet applications. The focus is extended to eco-friendly tags which can be a milestone for the next generation of printable "green" electronics.

2. ANTENNAS DESIGN EVOLUTION & GEOMETRY

The paramount design and print parameters that an RFID tag can accommodate are investigated in design evolution process which is proposed in Figure 1. Each antenna is designed for flexible and "green" electronics utilizing most commonly available substrates (Table 1). Several conductive inks are used for trial printing of these antenna structures which are summarized in Table 2. The evolution process is applied to get robust tags which must show less sensitivity to the variation of dielectric permittivity environment. The objective

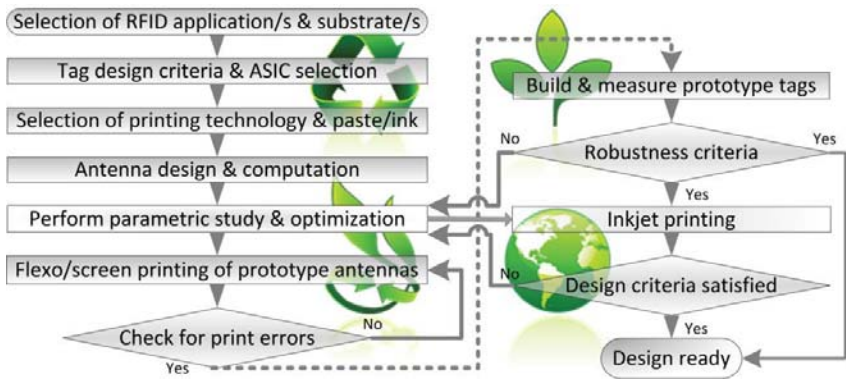

Figure 1. Evolution process for robust & "green" RFID tags.

Table 1. Substrate parameters.

Substrate	Permittivity (ε_r)	Loss Tangent
Paper (Korsnäs) (375 µm)	3.3 (average)	0.077 1 GHz@25°C
Paper (p_e: smart)/(250 µm)	3.2 (average)	0.077 1 GHz@25°C
Teonex Q51 (25 µm)	2.9	0.005 1 GHz@25°C
Kapton HN (125 µm)	3.5	0.0026 1 KHz@25°C

is to stabilize the antenna behavior on the entire frequency band of interest. The variations of the environment inevitably impact the tag performance [11], e.g., usage on metallic objects; however, even if it is not possible to eliminate it completely [12], it is made possible in the proposed antennas to strongly limit this phenomenon. The NXP ucode g2xm (TSSOP8, e.g., the target IC impedance at 915 MHz is $22 - j191\,\Omega$) is selected in flip-chip package. The main goal of optimization at each stage is to maximize the feeding power to the load (RFID IC) while at the same time the antenna area is minimized

Table 2. Printing technology/ink/substrate/speed combinations.

Screen Printing *Asahi Paste (LS-411AW)*	**Flexo Printing** *Asahi Paste (LS-411AW)*	**Inkjet Printing** *Cabot Ink CCI-300, Harima Ink NPS-JL*
Paper (375 µm)	Paper (375 µm)	Paper (250 µm)
Teonex Q51 (25 µm)	Teonex Q51 (2 m/min)	Paper (p_e: smart)
Kapton HN (125 µm)	Teonex Q51 (4 m/min)	-

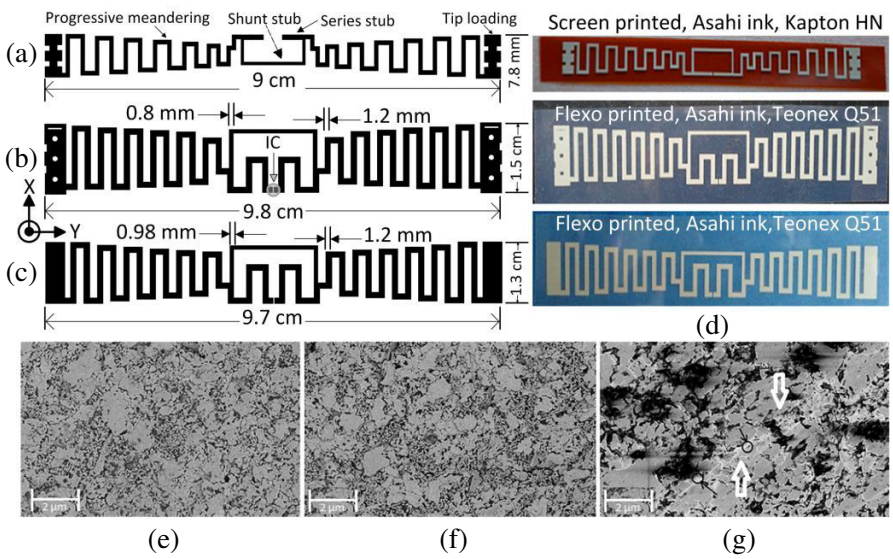

Figure 2. (a) The smallest proposed antenna, (b) enhanced EU band antenna, (c) optimized NA band antenna, (d) antennas printed on flexible substrates, (e) SEM of asahi printed antenna trace, (f) SEM after bending 50 times, (g) SEM after scratch test.

in order to employ these tags on small objects.

In the first phase, novel meander line antenna is developed which is a natural choice when the size and tuning is considered [13]. Unique progressive meandering technique is deployed to realize the antenna for 866–868 MHz band showed in Figure 2(a). The whole structure measures only 9 cm × 0.8 cm and is smaller than previously published results [5, 14, 15].

In the second evolution phase, the antennas with higher stability against environmental effects are realized. The major challenge at this stage is to maintain the gain and smaller size while improving the stability factor. The other ingredient that governed the design modifications is the low ink usage to reduce the manufacturing cost. Thus an innovative technique of also meandering the matching stub is introduced to rectify the issues of low gain, stability and matching. Furthermore, rigorous optimization is performed which is resulted into two distinctive antenna structures presented in Figures 2(b) & (c) cover EU and North American UHF RFID band respectively. These compact antennas are extremely suitable for tags attached to articles which are prone to be bent or folded several times during their life cycle and are far more superior than formerly published results [5, 14, 15]. The final evolution stage comprises of realizing these antennas on different types of paper substrate as showed in Figure 3(f).

3. RESULTS AND DISCUSSION

3.1. Antenna Fabrication

During transportation, it is likely that items get scratches. Therefore, for solving this problem antennas are manufactured using flexo and screen printing with Asahi paste in order to exploit its outstanding mechanical performance [16]. We have tested the mechanical toughness after printing these antennas showing excellent scratch resistance, i.e., no change in conductivity or antenna efficiency. Figures 2(e) & (g) show scanning electron microscope (SEM) photos of antenna traces before and after getting scratches (by metal object of sharp edge 400 µm × 100 µm with an applied force of one Newton) respectively. These proposed antennas are extremely flexible and perform without retardation after being bent several times and results are shown in Figures 3 & 4 along with bending test setup in Figure 3(d).

The first step in the process of evolutional development of the "green" tags involves inkjet printing utilizing DMP2800 inkjet printer which is a table-top printer available from Dimatix Inc and is shown in Figure 3(f). To ensure good RF properties, an in-house recipe was developed. The print head is adjusted to achieve high print resolution,

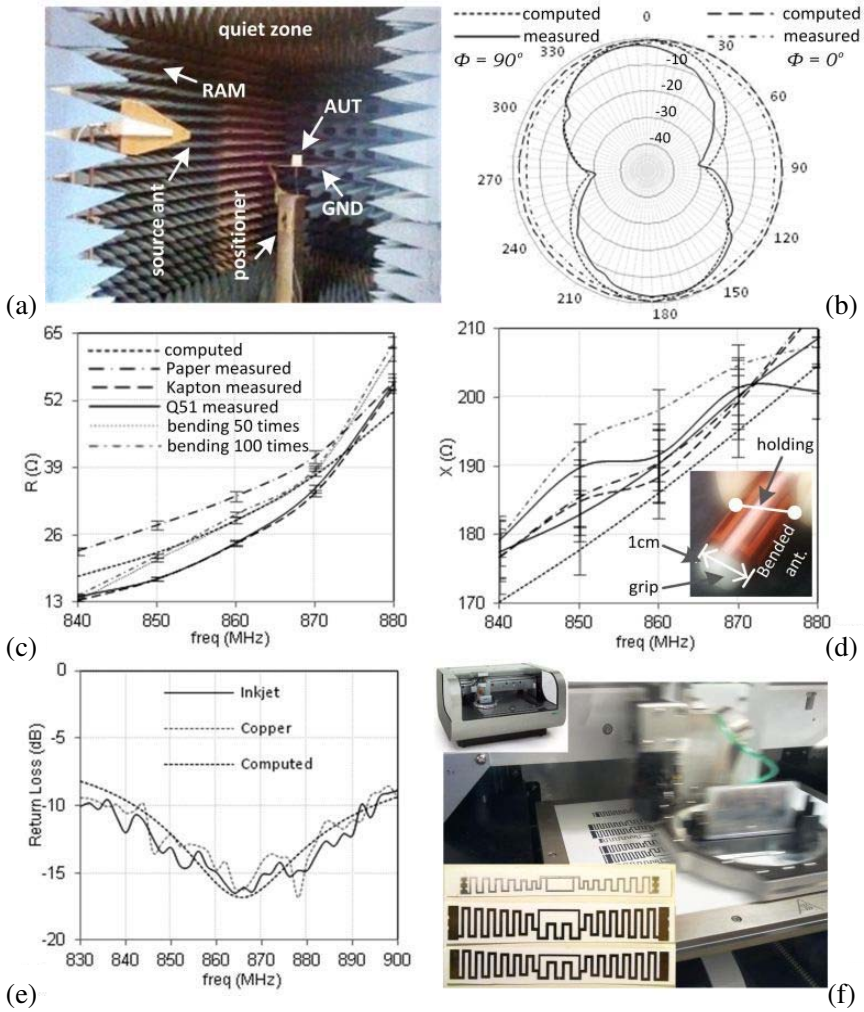

Figure 3. (a) Experiment setup in the anechoic chamber, (b) 2D far-field radiation plots, (c) input resistance variation, (d) input reactance variation & bending test setup, (e) return loss analysis, (f) inkjet printing setup & antennas printed on paper substrate.

which ensures good RF conductivity throughout the frequency band of interest. The silver nanoparticle based ink mentioned in Table 2, is then jetted at a temperature of 40°C, while the paper substrate mentioned in Table 1 (p_e: smart from Felix Schoeller & 280 gm photopaper) is maintained at 60°C (cabot ink) & at 30°C (harima ink). In order to achieve better conductivity each structure is printed with

multi-layers [17], e.g., 3–4 layers to provide better analysis about the printing technique. Each printed structure is then cured in a thermal oven for two hours at 120°C (cabot ink) and for 1.5 hours at 90°C (harima ink).

In the final step, these "green" tags are realized with roll-to-roll printing arrangement (using Korsnäs flexo printing paper of 375 µm thickness) to add tremendous scale of industrial usage for these antennas. The measurement analysis in Figures 3 & 4 illustrate surpassing performance of these environmentally friendly tags.

3.2. Parametric Analysis

RFID Tags (based on far-field communication and the physical property of backscattering or "reflected" power), with different sizes, presented in Figures 2(a)–(d) with manufacturing combinations mentioned in Table 2, are measured in a rigorous measurement approach. Firstly for each antenna structure ten identical prototypes are printed (with same combination of printing material & technology)

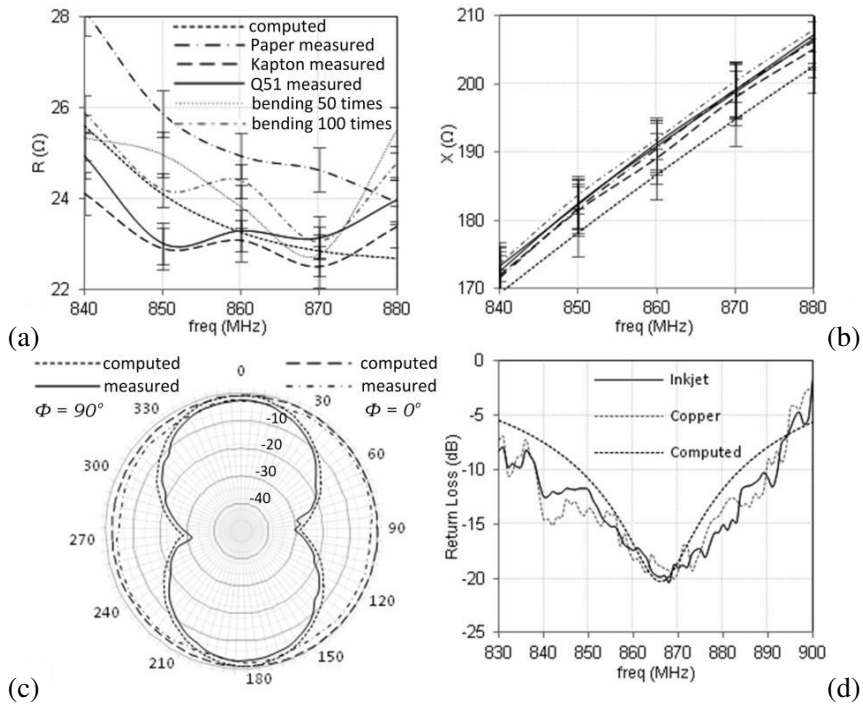

Figure 4. (a) Input resistance variation, (b) input reactance variation, (c) 2D far-field radiation plots, (d) return loss analysis.

and are measured across the frequency band of interest using half mirror method. Maximum deviated value at a particular point among ten samples is reported here which provides in depth view for worst case analysis to project more realistic data. This technique is adopted to thoroughly investigate the reliability criteria of each designed structure.

One of the most important tag performance characteristics is read range. Read range is also sensitive to the tag orientation, the material which the tag is placed on, and to the propagation environment. The read range can be obtained from the Friis equation as explained in [15], but it gives the maximum distance at which RFID reader can read the tag in free space. Thus this calculation of read range is invalid at near field distances. In most UHF RFID systems, this distance extends well into the far field zone. While some tag application scenarios involve near field tag scanning, it can be expected that in most cases the tag which can operate in the far field should receive more than adequate power to operate when brought closer to RFID reader antenna into the near field. Hence, the read range of most UHF RFID tags is determined by the tag performance in far field [18]. The read range of the proposed antenna of Figure 2(a) is from 3.5 m (paper/inkjet)–4m (optimal). However, the optimized antennas of Figures 2(b) and (c) exhibits exceptional read range from 5.5 m–6.5 m with different manufacturing combinations which is better in comparison with reported results [5, 14, 15].

Moreover, the near-field performance testing is carried out inside the anechoic chamber with Impinj's UHF RFID reader kit. The transition from near-field to far-field is not abrupt and the far-field distance is determined by $(2D^2/\lambda)$. The D (maximum dimension of the radiating structure) of reader antenna used is 0.3 m (1 foot), thus in one of the measurement cases the far-field distance at 915 MHz ($\lambda = 0.33$ m) is estimated to be 0.56 m. The proposed antennas exhibit flawless readability with in reactive near-field region. It is worth noting in this region, that the antenna pattern is taking shape but is not fully formed, and the antenna gain measurements vary with distance.

Impedance measurements are taken using vector network analyzer (MS2026B, Anritsu). The standard calibration method short-open-load (SOL) is used. The impedance variation of antenna in Figure 2(a) is shown in Figures 3(c) & (d). It is depicted from Figure 3(c) that the antenna has maintained the resistance around 35 Ω in a linear manner with frequency. This design has the constrain of higher resistance value which evolutes towards the design showed in Figure 2(b), so that the resistance can be maintained closer to the desired value of around 23 Ω. Figures 4(a) & (b) show the impedance analysis of the proposed

antenna in Figure 2(b). There is very small variation observed among the curves for different antennas which is elaborated in Figure 4(a).

The reactance of antenna in Figure 2(a) is shown in Figure 3(d) which features a positive value but with disparities among different curves. If this design is realized with different combinations mentioned in Table 1 instead of only one combination then these disparities have adverse effects on reliability. Figures 2(b) & 3(f) show more robust proposed structures which have linear and stable reactance behavior despite the variation especially in the dielectric constant of substrate material which is shown in Figure 4(b). This pertained to an inductance that conjugately matched or, equivalently, canceled the effect of the IC capacitance. Fairly good agreement is found between the computed and measured results.

In order to verify the performance of the inkjet printed RFID antennas of Figure 3(f), measurements are also executed on standard copper clad antenna prototypes. These have the same dimensions and fabricated using lpkf ProtomatC30. The return loss results of antennas in Figures 2(a) & (b) are shown in Figures 3(e) & 4(d) respectively. It is pragmatic that the return loss of the inkjet printed antennas is vaguely larger than the return loss of copper antenna. However, by analyzing the results in Figure 4(d) the optimized antenna structure in Figure 2(b) has better return loss agreement with computed values. Overall, good agreement between the standard copper based and the inkjet printed antennas is observed, regardless of the higher metal loss of the silver based conductive ink. The distortion is possibly due to the effect of metal ground fixture used for half mirror method [19].

Finally, the radiation pattern of antennas is measured in an anechoic chamber setup [20] that simulates infinite free space which is presented in Figure 3(a). The antenna under test (AUT) is placed in the center of the chamber and a continuous-wave (CW) signal excites the antenna, and the AUT is rotated by a positioner to obtain a 360° radiation pattern. The antennas with paper substrate are attached to the test terminal with CW2400 silver conductive epoxy, cured at 24°C for 4 hours to get maximum conductivity and adhesion. The normalized computed radiation pattern and the microwave chamber measurement, are plotted. As shown in Figures 3(b) & 4(c), the radiation patterns are almost uniform (omnidirectional) at 866 MHz, with directivity around 1.9 dBi (for antenna in Figure 2(a))–2.1 dBi (for antennas in Figures 2(b) & (c)). They show very good agreement between computations and measurements, which also could be verified for other frequencies within the antenna's bandwidth. Similar parametric behavior is depicted by antennas for North American band which are photographed in Figures 2(c) & 3(f).

4. CONCLUSION

The development of extremely versatile eco-friendly antennas for a high robustness level with respect to mechanical stresses and dielectric environment is demonstrated. The low-ink consumption in the proposed antennas provides a significant step towards the dream to achieve affordable multipurpose "green" tags. Future development is aimed to optimize the design to allow additional read ranges, bandwidth increase and design flexibility.

ACKNOWLEDGMENT

This work was financially supported by Vinnova (The Swedish Governmental Agency for Innovation Systems) through the Vinn Excellence centers program.

REFERENCES

1. Mayordomo, I., et al., "Emerging technologies and challenges for the internet of things," *2011 IEEE 54th International Midwest Symposium on Circuits and Systems, MWSCAS*, 1–4, 2011.
2. Ohashi, H., "Role of green electronics in low carbonated society toward 2030," *2010 14th International Power Electronics and Motion Control Conference, EPE/PEMC*, K-20–K-25, 2010.
3. Occhiuzzi, C. and G. Marrocco, "The RFID technology for neurosciences: Feasibility of limbs'monitoring in sleep diseases," *IEEE J. ITBM*, Vol. 14, No. 1, 37–43, 2010.
4. Tiang, J. J., M. T. Islam, N. Misran, and J. S. Mandeep, "Slot loaded circular microstrip antenna with meandered slits," *Journal of Electromagnetic Waves and Applications*, Vol. 25, No. 13, 1851–1862, 2011.
5. Chaabane, H., et al., "A methodology for the design of frequency and environment robust UHF RFID tags," *IEEE J. AP*, Vol. 59, No. 9, 3436–3441, 2011.
6. Kim, J.-S., W.-K. Choi, and G.-Y. Choi, "Small proximity coupled ceramic patch antenna for UHF RFID tag mountable on metallic objects," *Progress In Electromagnetics Research C*, Vol. 4, 129–138, 2008.
7. Tang, I.-T. and C.-C. Wang, "UHF RFID H-shaped tag antenna using microstrip feed design on metallic objects," *Journal of Electromagnetic Waves and Applications*, Vol. 25, No. 13, 1828–1839, 2011.

8. Thomas, V. M., "Environmental implications of RFID," *IEEE International Symposium on Electronics and the Environment, 2008, ISEE 2008*, 1–5, 2008.
9. Aronson, J. S., "Making IT a positive force in environmental change," *IEEE IT Pro.*, Vol. 10, No. 1, 43–45, 2008.
10. Bhattacharyya, R., et al., "Low-cost, ubiquitous RFID-tag-antenna-based sensing," *IEEE J. PROC*, Vol. 98, No. 9, 1593–1600, 2010.
11. Hsu, H.-T., et al., "Application of quasi log-periodic antenna for UHF passive RFID tag design featuring constant power transmission coefficient over broadband operation," *Journal of Electromagnetic Waves and Applications*, Vol. 24, Nos. 5–6, 575–586, 2010.
12. Chen, S.-L., S.-K. Kuo, and C.-T. Lin, "A metallic RFID tag design for steel-bar and wire-rod management application in the steel industry," *Progress In Electromagnetics Research*, Vol. 91, 195–212, 2009.
13. Watanabe, Y., et al., "Optimization of meander line antenna considering coupling between nonlinear circuit and electromagnetic waves for UHF-band RFID," *IEEE J. MAG*, Vol. 47, No. 5, 1506–1509, 2011.
14. Marrocco, G., et al., "The art of UHF RFID antenna design: Impedance-matching and size-reduction techniques," *IEEE M AP*, Vol. 50, No. 1, 66–79, 2008.
15. Rao, K. V. S., et al., "Antenna design for UHF RFID tags: A review and a practical application," *IEEE J. AP*, Vol. 53, No. 12, 3870–3876, 2005.
16. Jaakola, T., et al., "Low cost printed flexible multilayer substrates," *10th Electronics Packaging Technology Conference, 2008, EPTC 2008*, 344–349, 2008.
17. Merilampi, S. L., et al., "The effect of conductive ink layer thickness on the functioning of printed UHF RFID antennas," *IEEE J. PROC*, Vol. 98, No. 9, 1610–1619, 2010.
18. Tikhov, Y., "Comments on "Antenna design for UHF RFID tags: A review and a practical application"," *IEEE J. AP*, Vol. 54, No. 6, 2006.
19. Kuo, S.-K., S.-L. Chen, and C.-T. Lin, "An accurate method for impedance measurement of RFID tag antenna," *Progress In Electromagnetics Research*, Vol. 83, 93–106, 2008.
20. Khaleghi, A., "Diversity techniques with parallel dipole antennas: Radiation pattern analysis," *Progress In Electromagnetics Research*, Vol. 64, 23–42, 2006.

Paper II–Performance-Optimized Quadrate Bowtie RFID Antennas for Cost-Effective and Eco-Friendly Industrial Applications

Y. Amin, Q. Chen, H. Tenhunen, and L.-R. Zheng, *Progress in Electromagnetics Research*, vol. 126, pp. 49-64, 2012

Available online at: http://www.jpier.org/pier/pier.php?paper=12020805

Progress In Electromagnetics Research, Vol. 126, 49–64, 2012

PERFORMANCE-OPTIMIZED QUADRATE BOWTIE RFID ANTENNAS FOR COST-EFFECTIVE AND ECO-FRIENDLY INDUSTRIAL APPLICATIONS

Y. Amin[1,*], Q. Chen, H. Tenhunen, and L. R. Zheng

iPack VINN Excellence Center, Royal Institute of Technology (KTH), Stockholm SE-16440, Sweden

Abstract—Fully integrated printed RFID antennas show potential solution for item level labeling applications. In order to accommodate the antenna during the package printing process, it is vastly preferred that antenna structures are printed on paper substrates. However, the electromagnetic properties and thickness of paper substrates are susceptible to change due to various environmental effects. Thus, adequately consistent in performance and material insensitive printed Quadrate Bowtie RFID antennas are proposed. This paper presents an in-depth efficient optimization for high performance tag antenna designs for operability in frequencies 866–868 MHz & 902–928 MHz. It is demonstrated that the proposed antennas can tolerate a considerable variation in the permittivity on thin paper substrates, and present benchmarking results when n across metal and water containing objects.

1. INTRODUCTION

As an ingredient of rapidly emerging technologies in automatic identification and data capture (AIDC) industries, radio frequency identification (RFID) has been increasingly used in many applications such as supply chain management, inventory control, security management, and logistics [1]. To meet the requirements for these applications, RFID tags need to be attached on various objects [2, 3] with different shapes and material properties. Therefore, an RFID tag antenna attached on a target object plays a crucial role in determining the overall performance of an RFID system. Presently much effort is dedicated to the development of RFID antennas by implementing

Received 8 February 2012, Accepted 1 March 2012, Scheduled 8 March 2012

* Corresponding author: Yasar Amin (ysar@kth.se).

Table 1. Substrate parameters evaluated for proposed antennas.

Substrate	Thickness (μm)	Permittivity (ε_r)	Loss Tangent
Kodak Photopaper	280	3.2 (average)	0.077 (1 GHz@25°C)
HP Photopaper	280	3.2 (average)	0.04 (1 GHz@25°C)
Paper (p_e:smart)	250	3.2 (average)	0.077 (1 GHz@25°C)
Metal coated PET	50	3.3	0.003 (0.9 GHz@25°C)

various technologies [4–6]; however, the development area appears deserted while encountering the issues interconnected to the field of economic and eco-friendly tags comprising of paper substrate.

It often overlooked while mentioning the paper printed RFID tags that use of paper defines the entirely new era of electrical performance, which encounters from, new set of issues [7, 8]. The polymer-covered paper substrates have been used to demonstrate electrochemical displays. While these paper coatings compromise the low cost and recyclability, this might still be acceptable for relatively high-value electronic applications that require relatively expensive materials, several processing steps, and encapsulation [9]. Paper substrates offer many advantages for printing RFID antennas, not only is paper widely available and affordable, it is lightweight, biodegradable and can be rolled or folded into 3D configurations [10, 11].

In this paper, novel quadrate bowtie passive RFID tag antennas on paper/PET substrates are presented with the introduction of impedance matching approach to improve the reliability against environmental diversities as well as increase the maximum reading distance. The quadrate bowtie antenna [12] profile modification and T-matching network are used to match the antenna input impedance to tag's chip impedance, and the effects of metal and water on the proposed antennas are also categorically investigated. The European and North American UHF RFID bands are preferred and all simulations are performed using ANSYS HFSS^{TM}. These antennas are printed on different substrates (Table 1) using state-of-the-art printing technologies (**D**ry **P**hase **P**atterning & Inkjet Printing). The measurements are carried out in an anechoic chamber along with the reader setup dedicated to antenna characterization for metal, and water containing objects and proposed antennas are also compared with that of a commercial RFID tag. The ruggedness, eco-friendliness, flexibility and exceptionally long read range of these proposed antennas make them an ideal choice for far-field cases, carton (containing water & metal objects) and (wood or metal) pallet industrial applications.

2. ANTENNA DIMENSIONS AND PARAMETRIC OPTIMIZATION

The proposed quadrate bowtie antennas are optimized on a methodical basis for minimizing the effects of environmental adversities on RFID tags. The main purpose of enhancement is to maximize the feeding power to the load and reduce the antenna area, while realizing the highly efficient structures on paper substrate for eco-friendly tags. Figure 1 shows the Thevenin equivalent circuit of the IC tag, from which the consumption power at the load is evaluated assuming the incident plane waves. In Figure 1, v_o is received open voltage, $Z_a = R_a + jX_a$ the input impedance of the tag antenna, $Z_c = R_c + jX_c$ the impedance of the load, I the current flowing at the load. I and the consumption power of the load P_c are obtained from (1) & (2):

$$I = \frac{v_o}{Z_a + Z_c} \tag{1}$$

$$P_c = Re\{Z_c I I^*\} \tag{2}$$

It is worth mentioning here that throughout the text onwards whenever input impedance of antenna is referred it will be meant that the real part R_a of the antenna input impedance Z_a consists of the radiation resistance and the antenna losses or loss resistance. Hence, one of the optimization criteria is defined as (3),

$$kP_c + \left(1 - \frac{S}{S_{\max}}\right) \to \max \tag{3}$$

where S is the antenna size and $S_{\max}$ the maximum size, and k in the first term is the weighting constant to offset the first and second terms. If the effect of the second term in the objective function is trivial, the impedance matching between Z_a and Z_c will stand for the optimal antenna, that is, Z_a of the optimized antenna will be the complex conjugate of Z_c. Note that the input voltage v_o depends on the

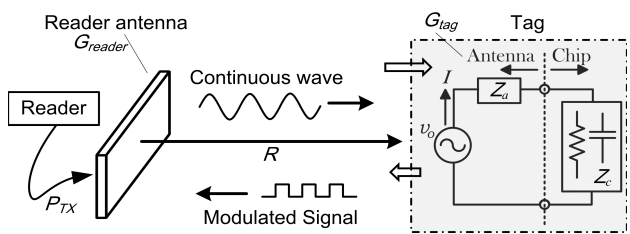

Figure 1. Far-field RFID mechanism & equivalent circuit of an IC tag.

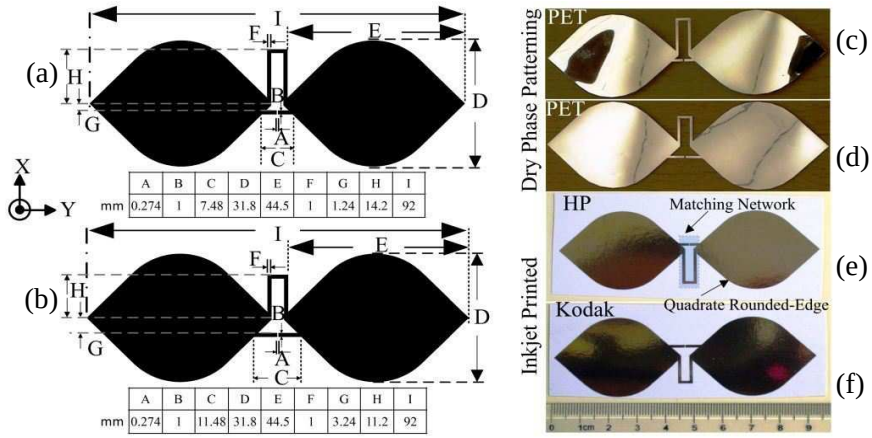

Figure 2. The geometry of RFID antenna for: (a) EU band, (b) NA band; DPP of antenna on PET for: (c) EU band, (d) NA band; inkjet printed antenna on: (e) HP photopaper for EU band, (f) Kodak photopaper for NA band.

antenna structure in this problem [11]. Thus, it requires a conjugate matching technique such as series or parallel stubs. The matching network of the tag has to ensure the maximum power delivered to the chip. To achieve these design goals, a T-matched quadrate bowtie antenna (half wavelength dipole antenna) with rounded corners, is designed and fabricated. This design is used for the matching of the passive antenna terminals to the NXP ucode g2xm (TSSOP8, e.g., the target IC impedance at 915 MHz is 22-j191Ω). The prototype antenna structures for UHF RFID European (EU) band and North American (NA) is shown along with dimensions in Figures 2(a) & (b) respectively. The T-match arms are liable for impedance matching of the antenna terminals to that of the RFID chip through the fine tuning of the series and shunt stubs.

2.1. Antenna Effective Aperture

A commonly disregarded issue about an (RFID) antenna is how directivity and gain are correlated to its physical dimensions. Since the field/current, on the antenna aperture is not uniform, the concept of antenna effective aperture is established to serve this purpose. The effective aperture A_e is less than the physical aperture A_p [13]. The directivity D can also be articulated in expressions of the aperture size

and aperture efficiency η_{ap}:

$$D = \frac{4\pi}{\lambda^2} A_e = \frac{4\pi}{\lambda^2} \eta_{ap} A_p \tag{4}$$

where λ is the wavelength of the radio waves. By knowing the power density S at the receiving antenna, we can approximate the received power P_r:

$$P_r = S A_e \tag{5}$$

Thus during optimization course of action, much effort is devoted to improving the effective aperture to increase the gain while maintaining the low profile of the proposed antennas showed in Figure 2.

2.2. Skin Depth Effect and Antenna Performance

The skin depth and ohmic losses of the printed conductive layer set the boundary conditions for the manufacturing methods, and parameters such as the amount of silver ink and the thickness of the printed layers. Skin depth is one of the significant factors that lead to achieve a certain thickness of the conductive layer/s. Due to the skin effect at high frequencies, e.g., at UHF, the current density is crowded in the region near the surface of a good conductor. More precisely the skin depth is the depth below the surface of the conductor at which the amplitude of the incident electric field decays to 0.37% of the amplitude at the surface of the conductor. Mathematically, the skin depth δ in case of a good conductor is, therefore [13], expressed as:

$$\delta \approx \sqrt{\frac{1}{\pi f \mu \sigma}} \tag{6}$$

where f is the frequency, μ is the permeability and σ is the conductivity of the conductor material. Thus from above we can deduce three key conclusions that surround the manufacturing process of the proposed antennas:

(i) The higher the frequency, (in this particular case, 860–960 MHz), the smaller the skin depth.

(ii) The higher the permeability (in case, it is not that high, which needs attention while printing process), the smaller the skin depth. However for a good conductor, the permittivity has little effect on the skin depth.

(iii) The higher the conductivity (in case, the conductivity of the printed structure is almost 5 times lower than that of bulk silver due to several parametric constrains in manufacturing), the smaller the skin depth.

3. DPP AND INKJET PRINTING: CONDUCTIVE FEATURES

The standard antenna structures for comparison and validation of the concept are fabricated using Dry Phase Patterning (DPP). It is a single step method for patterning metal or polymer layers on most flexible substrates. The laminate of Aluminum (10 μm layer)/PET is patterned for proposed antennas showed in Figures 2(c) & (d) in one single step, unlike in a wet etching process that involves 6–8 steps to achieve the same pattern. Acreo AB has reported patterning resolution of as small as 200 μm and speed up to 150 m/min, which made it a better choice for cost effective RFID tags.

In addition to cutting down on waste and providing an all-in-one substitute to cleanroom deposition technologies, inkjet printing characteristics with regards to accuracy and form make it an exceptionally pleasant contestant for RF circuits. The practicability of inkjet printing for applications at UHF frequencies has been well covered under [9]. The Cabot conductive ink (CCI-300) by Cabot Corp., is used to print these proposed antennas, which contains 19–21% weight of nano-silver particles of less than 20 nm diameter. The large ratio of the area to volume of these nano-silver particles exhibit the significantly lower melting point even less than 100°C. The inkjet printing is carried out utilizing DMP2800 inkjet printer, as showed in Figure 3(a) which is a table-top printer available from Dimatix Inc. To realize substantial RF properties, the printing resolution of 1000 dpi (Dimatix 10 pL cartridge) −2540 dpi (Dimatix 1 pL cartridge) is achieved by adjusting the print head and it is figured out that using this technique a printing resolution of 1000 dpi is suitable for frequencies in the UHF range. Figure 3(b) shows the surface profile of an RFID antenna printed using cartridges jetting out ink droplets. The ink is then jetted at a temperature of 40°C, while the paper substrate mentioned in Table 1 is maintained at 60°C. In all print setups, the substrate is kept at a distance of 0.5 mm from the print head. To ensure reliable RF conductivity, three layers of ink are printed which results in a thickness of around 3 μm while using a heat gun to anneal in between each re-printing cycle.

After printing, the deposited ink also needs to be annealed to ensure adjacent silver nanoparticles in the jetted ink to coagulate with neighbors, allowing for a smoother path for electron flow particularly at high frequencies. Each printed structure is cured in a thermal oven for two hours at 120° resulting into a consistent, measured DC conductivity in the range 9×10^6 [S/m] -1.1×10^7 [S/m]. The conductivity of the printed structure can also be further increased

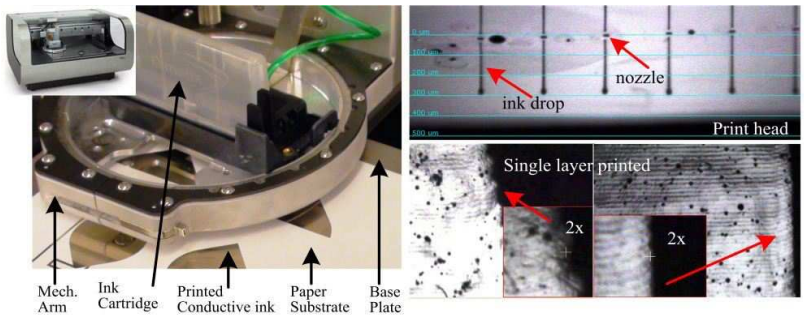

Figure 3. (a) Inkjet printing setup, (b) drop watcher view (top) showing ink printed out of nozzles & images by Fiducial camera of DMP-2800 for inspection of printed ink layer.

by using a higher print resolution setting on the printer. Antenna traces with exceptionally meritorious conductivity and the pitches are accurately fabricated using this inkjet printing process, and is shown by the close-up of a printed trace in Figure 3(b).

4. RESULT ANALYSIS AND DISCUSSION

Passive RFID tags for European and North American UHF RFID bands are manufactured with different substrates mentioned in Table 1, are measured across the frequency band of interest using half mirror method to investigate the reliability aspects of the proposed antennas for commercial grade practices. Ten identical prototypes of proposed structures are manufactured on an each paper substrate in order to determine the worst case analysis ingredients. Thus, each curve in Figure 4 represents the highest deviated values at a certain point among identical samples.

Impedance measurements are taken using vector network analyzer (MS2026B, Anritsu). The standard calibration procedure short-open-load (SOL) is adopted for accuracy of results. In order to verify the performance of the inkjet printed antennas of Figures 2(e) & (f), measurements are also executed using standard antenna prototypes fabricated on Aluminum coated PET substrate as showed in Figures 2(c) & (d). These standard prototypes have the same dimensions as that of proposed antennas and are fabricated using DPP (Dry Phase Patterning) process at Acreo AB. The impedance variation of antenna in Figure 2(a) is shown in Figures 4(a) & (b). Whereas, input impedance plots of antenna in Figure 2(b) are shown

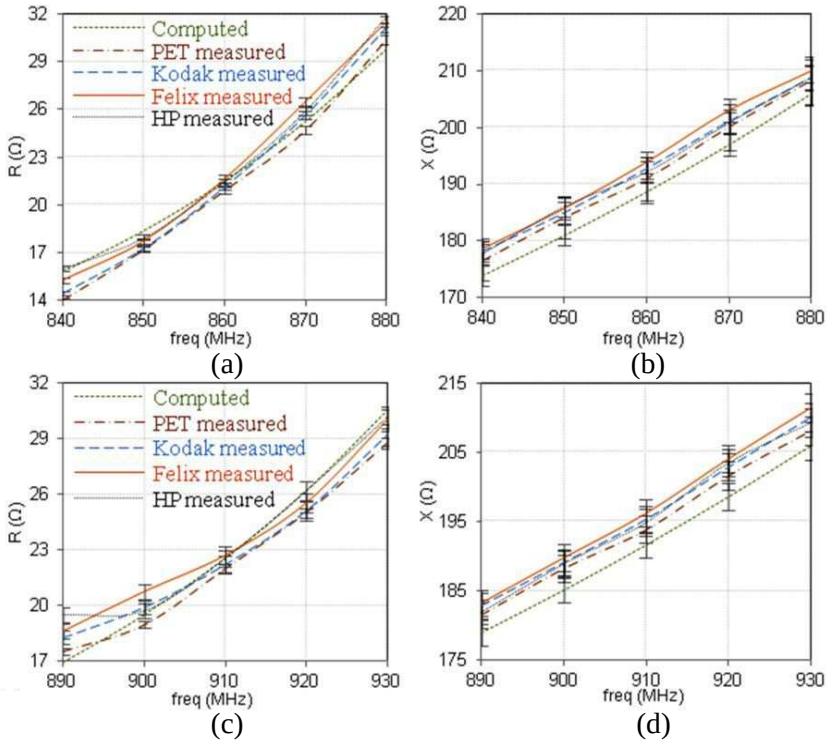

Figure 4. EU band's antenna input: (a) (radiation & loss) resistance variation, (b) reactance variation; NA band's antenna input: (c) (radiation & loss) resistance variation, (d) reactance variation.

in Figures 4(c) & (d). The resistive parts of impedance as showed in Figures 4(a) & (c) for EU and NA band antennas respectively, printed on different photopapers demonstrate consistency to the DPP antennas & simulated results throughout frequency band of interest which is a primary concern for antennas stable behavior. However, slightly greater drift is observed in the resistive part of the antennas printed on paper (p_e:smart) from Felix Schoeller as compared to the others but the difference remains within the acceptable range. Similarly, fairly coherent trend of reactance curves is depicted in Figures 4(b) & (d) for both proposed structures. The formation of round corners is used to obtain wider impedance band. Round corners at the sharp vertexes decreases the reflection of incident current near the edges and changes the current distribution on radiation surfaces. Thus, flatter impedance within the frequency band of interest with much stable real

and imaginary parts is demonstrated in Figure 4.

Using the Friis equation, the read range which is one of the most dominant tag performance characteristics can be estimated by Equation (7) defining forward-link-limited range and Equation (8) defining reverse-link-limited range. Read range is also susceptible to the tag orientation, the object which the tag is placed on, path loss, spatial and temporal fading statistics of the propagation environment [14].

$$R_{forward} = \left(\frac{\lambda}{4\pi}\right)\sqrt{\frac{P_{TX}G_{reader}G_{tag}}{P_{\min,tag}}} \tag{7}$$

and defining the minimum signal power for demodulation at the reader as $P_{\min,rdr}$ we obtain the reverse-link-limited range:

$$R_{reverse} = \left(\frac{\lambda}{4\pi}\right)\sqrt[4]{\frac{P_{TX,reader}T_bG_{reader}^2G_{tag}^2}{P_{\min,rdr}}} \tag{8}$$

where the output power of the reader is P_{TX}, the gain of the reader antenna is G_{reader}, and the gain of the tag antenna is G_{tag}. λ is the wavelength in free space at the operating frequency, $P_{\min}$ is the minimum power required to turn on the tag chip and T_b is backscatter transmission loss.

The read range from Equations (7) & (8) gives the maximum distance at which RFID reader can interpret the tag in free space. Thus, this statement of read range is invalid at near-field distances. In the near-field region, the E and H-fields are not orthogonal so anything within this region couples with the antenna and distort the pattern; thus, the antenna gain is not a valid parameter here. Therefore, the near-field performance testing is carried out inside the anechoic chamber with Impinj's UHF RFID reader kit. The far-field distance is calculated by $(2D^2/\lambda)$, and it is observed as an estimate because the transition from near-field to far-field is not instantaneous. The D (maximum dimension of the radiating structure) of the reader antenna used is 0.3 m (1foot), thus in measurements which are taken at 915 MHz ($\lambda = 0.33$ m) the far-field distance is estimated to be 0.56 m. The proposed antennas exhibit superior readability within reactive near-field region. It is observed that, in the near-field region the antenna pattern is taking shape but is not fully formed, and the antenna gain measurements vary with distance.

In most UHF RFID systems, the reading distance obtained by Equations (7) & (8) extends well into the far-field region. When there is an implementation of tag which can operate in the far-field also involves near-field tag scanning. It can be expected that, in almost all

cases, the tag gets more than sufficient power to operate when brought closer to RFID reader antenna. Hence, the read range of most UHF RFID tags is determined by the tag working in the far-field [15]. The proposed antennas have surpassed read range from 6.5 m (HP) – 7.0 m depending upon which substrate is utilized. Furthermore, the detailed analysis of read range variation is presented in Tables 2 & 3.

The return loss results of antennas in Figures 4(a) & (b) is shown in Figures 5(a) & (b) respectively. It is pragmatic that the return loss of the inkjet printed antennas is slightly higher than the return loss of standard PET substrate antennas. Overall, good agreement between the standard PET-based, and the inkjet printed antennas is observed, regardless of the higher metal loss of the silver based conductive ink. The distortion is possibly due to the effect of metal ground fixture used for half mirror method [16].

The most challenging in measurement steps, the radiation pattern of antennas is measured in an anechoic chamber setup that replicate absolute free space which is presented in Figure 6. The antenna under test (AUT) is mounted over the positioner assembly in the

Table 2. Analysis of effect by metal on the proposed tag at 915 MHz.

Measured → • Computed → ∗	Input impedance (Ω)•	Radiation efficiency (%)∗	Trans. coeff. (dB)∗	Directivity (dBi)∗	Gain (dBi) ∗	Reading range, R (m)•
Free space	24.42 + j194.92	83.64	−1.07	1.85	1.97	6.50
$d = 1$ mm	4.31 + j152.13	1.02	−13.57	7.96	−10.37	0.31
$d = 5$ mm	5.76 + j173.06	6.61	−9.97	8.26	−1.12	1.14
$d = 10$ mm	7.75 + j186.55	18.02	−3.53	8.29	0.58	3.22
$d = 15$ mm	10.17 + j193.10	30.67	−0.67	8.28	2.92	8.10

Table 3. Analysis of effect by water on the proposed tag at 915 MHz.

Measured → • Computed → ∗	Input impedance (Ω)•	Radiation efficiency (%)∗	Trans. coeff. (dB)∗	Directivity (dBi)∗	Gain (dBi)∗	Reading range, R (m)•
Free space	24.42 + j194.92	83.64	−1.07	1.85	1.97	6.50
$d = 1$ mm	129.27 + j330.00	8.77	−9.51	4.12	−7.51	0.61
$d = 5$ mm	23.61 + j201.20	6.29	−1.32	2.67	−10.05	1.15
$d = 10$ mm	13.77 + j189.04	20.26	−0.33	2.81	−3.02	3.23
$d = 15$ mm	12.20 + j189.90	27.64	−0.15	3.73	−1.13	4.37
$d = 20$ mm	10.21 + j190.82	38.31	−0.08	4.93	−0.12	5.26

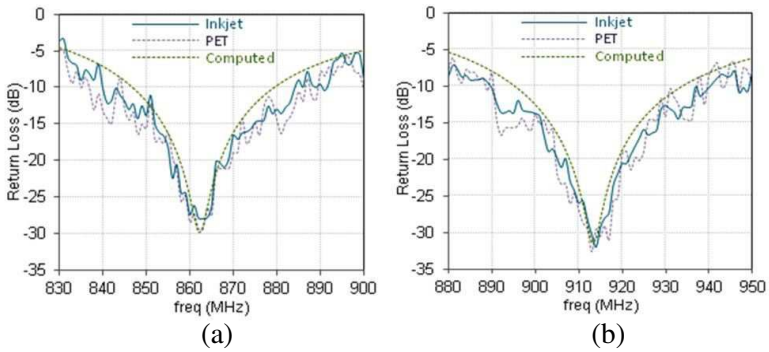

Figure 5. Return loss of antennas for: (a) EU band, (b) NA band.

Figure 6. The anechoic chamber & instruments used.

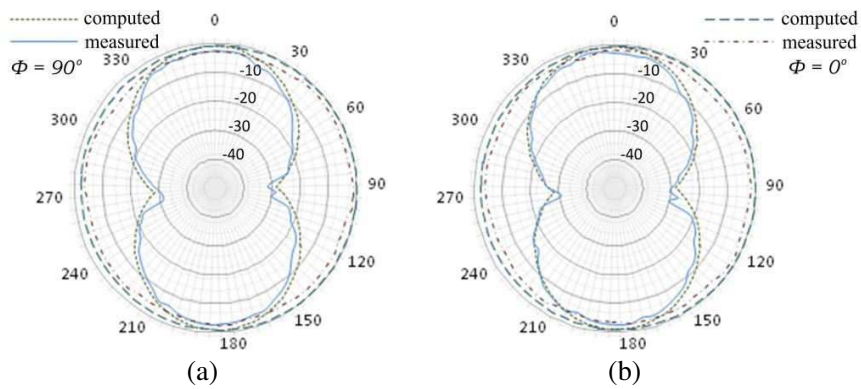

Figure 7. Measured & computed 2D far-field radiation plots of antennas for: (a) EU band, (b) NA band.

center of the chamber which is set to rotate the antenna in small steps of 5 degrees to obtain a 360° radiation pattern. A continuous-wave (CW) signal from the signal generator excites the AUT. The receiver antenna is connected to the spectrum analyzer (Agilent HP 8562E) and a PC running the test automation software controls the measurement setup. Soft soldering is avoided to fix the AUT to the test fixture since it requires heating the filler metal above 250°C to achieve proper soldering, but this temperature severely damages the printed traces on paper substrates. Thus, antennas are attached to the test terminal with CW2400 silver conductive epoxy, cured at 24°C for 4 hours to reach maximum conductivity and adhesion. The normalized computed radiation pattern and the microwave chamber measurements are plotted in Figure 7. The radiation patterns are nearly uniform (omnidirectional) at 915 MHz. They show remarkably satisfactory agreement between computations and measurements. The same uniformity in antenna radiation pattern could be demonstrated for other frequencies within the antenna's bandwidth. Similar parametric behavior is depicted by proposed antennas for EU band, which are shown in Figures 2(a), (c) & (e).

5. ANALYSIS FOR INDUSTRIAL APPLICATIONS

5.1. Effects of Metal on Tag Antenna Performance

The metal effect is limited in the tag antenna which has its own ground plane [17, 18]. However, the antenna which does not have a ground plane, such as quadrate bowtie, the radiation characteristics and input impedance of the antenna, are distorted when the tag is placed on or near a metal object. Whenever there is an encounter with metal objects these variations certainly impact the tag performance [5]; however, even if it is not possible to eliminate it completely [3]; it is made possible in the proposed antennas to, strongly limit this phenomenon.

The comprehensive data on the metal effect on the proposed RFID tag antenna placed close to a metal plate and reading distance at 915 MHz is summarized in Table 2. The antenna is positioned parallel to and below a metal plate measuring 30 cm × 30 cm. The directivity, radiation efficiency, gain, and input impedance, are examined for the different distances from the metal plate. Considering the worst case, i.e., when the antenna is placed extremely close to the metal plate ($d = 1$ mm), the directivity of the antenna enhances significantly to around 8 dBi. However, the radiation efficiency plunges drastically to 1.02%, which results in remarkably low gain of -10.37 dBi at 915 MHz. Particularly, the real part of the input impedance varies severely, as well. This variation in impedance outcome in deprived impedance

matching with the RFID tag chip (circuit showed in Figure 1), resulting in a transmission loss of −13.57 dB at 915 MHz. The gain reduction and poor impedance matching results in the reading distance reducing to 0.31 m. However, the proposed antenna still exhibited superior reading distance when placed so closer to the metal object in coherence with previously published results [3, 18].

The directivity of the antenna remains virtually unchanged, by moving the antenna further away from the metal plate. In the meantime, the radiation efficiency shows an escalating drift, which domino result in increasing antenna gain. The real part of the input impedance shows modest change, whereas the imaginary part inclined to values close to those in free space. An increasing trend is observed in the reading distance; when the tag is moved away from the metal plate. When the tag is moved to $d = 5$ mm, the reading distance exhibits higher value than that of in free space because the metal plate acts as a reflector which ultimately boosts the tag antenna gain. In conclusion, although the metal object degrades the reading range of the tag significantly when it is directly attached or is placed real close to it, but the proposed antennas are even capable of reasonably communicating under these critical testing conditions.

5.2. Effects of Water on Tag Antenna Performance

Table 3 shows the complete characteristic analysis of the proposed antenna which is placed close to a water cuboid. The antenna is placed parallel to and above a water cuboid which is measuring 30 cm × 8 cm × 8 cm; whereas, $\varepsilon_r = 77.3$ and $\delta \tan = 0.048$ [19] of water is adopted in this experimentation. The input impedance, radiation efficiency, directivity, and gain are inspected at different distances away from the water cuboid. When the proposed antenna is placed closer to water at a distance of $d = 1$ mm, the directivity of the antenna amplifies while the radiation efficiency reduces considerably, which domino effect in a decrease, in the antenna gain.

In dissimilarity with the metal plate effect, it is pragmatic that the water always causes a decrease in the gain regardless of the distance between the water and the proposed antenna. When the antenna is moved further away at a distance of $d = 15$–20 mm, the antenna gain achieves the value roughly equal to that in free space. The input impedance displays a smoother variant with the exception of the situation once the antenna is extremely close to the water, i.e.; $d = 1$ mm. If the tag antenna is placed extremely close to water (that means almost touching the cuboid), the reading distance reduces considerably to 0.61 m but not that much as observed in the case of metal plate. When the tag is moved further away, the effect of the

water is declined; resulting in read range enhancement. Therefore, exhibiting the graceful degradation in functionality for suitability in high performance industrial applications. The proposed antennas exhibit improved performance and are in accordance with commercially available RFID tags and previously published results [20].

Furthermore, the metallic plate and water do not degrade the bandwidth of the proposed antennas to such an extent that they become unreadable until the tag is placed closer than $d = 1\,\text{mm}$. The bandwidth degradation behavior is constant, in case the tag is brought nearer to the water containing objects, but in case of metallic plate, the bandwidth degradation is more serious particularly within $d = 5\,\text{mm}$. The proposed antennas are designed with reasonably wideband in order to demonstrate readable bandwidth at the expense of read range (bandwidth vs. read range trade-off) which limits their usage to narrow bandwidth operations, i.e., either for EU band or NA band. The stabilization of bandwidth can further be achieved by reducing the effect of matching network, but that will induce instability against dielectric variation of paper substrate, so it is trade-off always among optimum values depending upon the applications.

6. CONCLUSION

The novel quadrate bowtie antennas for UHF RFID industrial applications have been proposed and fabricated on paper and PET substrates, using inkjet printing and DPP technology respectively. In addition to categorical optimization of antenna profile, a T-matching network is introduced to develop a novel compact, RFID tag, featuring outstanding overall performance. The antennas exhibit exceptional operational characteristics when stumble upon metal and water containing objects. The use of the inkjet printing process in the development of these proficient RFID antennas on different types of paper has also been demonstrated, verifying that paper-based inkjet printing topologies offer a remarkably low-cost, "green" solution to system-level packaging for UHF, wireless, and microwave applications.

ACKNOWLEDGMENT

The author would like to thank Peter Fuks in school of electrical engineering at KTH who generously provided measurement facilities. This work was financially supported by Vinnova (The Swedish Governmental Agency for Innovation Systems) through the Vinn Excellence centers program and by the EU project CLIP of grant number 243557 through EU FP7-SME-2008-2.

REFERENCES

1. Zuo, Y., "Survivable RFID systems: Issues, challenges, and techniques," *IEEE J. SMCC*, Vol. 40, No. 4, 406–418, 2010.
2. Tiang, J.-J., M. T. Islam, N. Misran, and J. S. Mandeep, "Circular microstrip slot antenna for dual-frequency RFID application," *Progress In Electromagnetics Research*, Vol. 120, 499–512, 2011.
3. Chen, S.-L., S.-K. Kuo, and C.-T. Lin, "A metallic RFID tag design for steel-bar and wire-rod management application in the steel industry," *Progress In Electromagnetics Research*, Vol. 91, 195–212, 2009.
4. Panda, J. R. and R. S. Kshetrimayum, "A printed 2.4 GHz/5.8 GHz dual-band monopole antenna with a protruding stub in the ground plane for WLAN and RFID applications," *Progress In Electromagnetics Research*, Vol. 117, 425–434, 2011.
5. Hsu, H.-T., F.-Y. Kuo, and C.-H. Chang, "Application of quasi log-periodic antenna for UHF passive RFID tag design featuring constant power transmission coefficient over broadband operation," *Journal of Electromagnetic Waves and Applications*, Vol. 24, Nos. 5–6, 575–586, 2010.
6. Jamlos, M. F., T. A. Rahman, M. R. Kamarudin, P. Saad, M. A. Shamsudin, and A. M. M. Dahlan, "A novel adaptive Wi-Fi system with RFID technology," *Progress In Electromagnetics Research*, Vol. 108, 417–432, 2010.
7. Alimenti, F., M. Virili, G. Orecchini, P. Mezzanotte, V. Palazzari, M. M. Tentzeris, and L. Roselli, "A new contactless assembly method for paper substrate antennas and UHF RFID chips," *IEEE Transactions on Microwave Theory and Techniques*, Vol. 59, No. 3, 627–637, 2011.
8. Lazaro, A., D. Girbau, and R. Villarino, "Effects of interferences in UHF RFID systems," *Progress In Electromagnetics Research*, Vol. 98, 425–443, 2009.
9. Tobjërk, D. and R. Österbacka, "Paper electronics," *Adv. Mater.*, Vol. 23, No. 17, 1935–1961, 2011.
10. Bose, I. and S. Yan, "The green potential of RFID projects: A case-based analysis," *IEEE IT Pro.*, Vol. 13, No. 1, 41–47, 2011.
11. Makimura, H., Y. Watanabe, K. Watanabe, and H. Igarashi, "Evolutional design of small antennas for passive UHF-band RFID," *IEEE J. MAG*, Vol. 47, No. 5, 1510–1513, 2011.
12. Qu, S.-W. and C.-L. Ruan, "Effect of round corners on bowtie antennas," *Progress In Electromagnetics Research*, Vol. 57, 179–

195, 2006.

13. Huang, Y. and K. Boyle, *Antennas from Theory to Practice*, John Wiley & Sons Ltd., New York, 2008.
14. Nikitin, P. V. and K. V. Rao, "Antennas and propagation in UHF RFID systems," *IEEE International Conference on RFID*, 277–288, 2008.
15. Tikhov, Y., "Comments on 'antenna design for UHF RFID tags: A review and a practical application," *IEEE J. AP*, Vol. 54, No. 6, 2006.
16. Kuo, S.-K., S.-L. Chen, and C.-T. Lin, "An accurate method for impedance measurement of RFID tag antenna," *Progress In Electromagnetics Research*, Vol. 83, 93–106, 2008.
17. Sanchez-Montero, R., S. Salcedo-Sanz, J. A. Portilla-Figueras, and R. Langley, "Hybrid pifa-patch antenna optimized by evolutionary programming," *Progress In Electromagnetics Research*, Vol. 108, 221–234, 2010.
18. Lin, D. B., I.-T. Tang, and C.-C. Wang, "UHF RFID H-shaped tag antenna using microstrip feed design on metallic objects," *Journal of Electromagnetic Waves and Applications*, Vol. 25, No. 13, 1828–1839, 2011.
19. Xi, J., H. Zhu, and T. T. Ye, "Platform-tolerant PIFA-type UHF RFID tag antenna," *International IEEE Conference on RFID*, 174–180, 2010.
20. Bjorninen, T., A. Z. Elsherbeni, and L. Ukkonen, "Low-profile conformal UHF RFID tag antenna for integration with water bottles," *IEEE J. AWPL*, Vol. 10, 1147–1150, 2011.

Paper III–Development and Analysis of Flexible UHF RFID Antennas for "Green" Electronics

Y. Amin, Q. Chen, L.-R. Zheng, and H. Tenhunen, *Progress in Electromagnetics Research*, vol. 130, pp. 1-15, 2012

Available online at: http://www.jpier.org/pier/pier.php?paper=12060609

Progress In Electromagnetics Research, Vol. 130, 1–15, 2012

DEVELOPMENT AND ANALYSIS OF FLEXIBLE UHF RFID ANTENNAS FOR "GREEN" ELECTRONICS

Y. Amin*, Q. Chen, L.-R. Zheng, and H. Tenhunen

iPack VINN Excellence Center, Royal Institute of Technology (KTH), Stockholm SE-16440, Sweden

Abstract—In this paper, novel Bowtie antennas which cover complete UHF RFID band (860–960 MHz), fabricated on various ultra-low-cost substrates using state-of-the-art printing technologies are investigated as an approach that aims to accommodate the antenna during the package printing process whilst faster production on commercially available paper. The proposed antenna structures are evaluated in reference to circuit and field concepts, to exhibit extreme degree of functional versatility. These antennas are developed to cater the variations which appear in electromagnetic properties and thickness of paper substrate due to various environmental effects. Computed (simulated) and well-agreed measurement results confirm a superior performance of the tag modules while stepping towards next generation of "green" tags.

1. INTRODUCTION

In recent years, the recognition of radio frequency identification (RFID) technology has greater than before and comprehensively integrated into modern society applications, ranging from remote monitoring sensing to more demanding operational conditions in logistics, healthcare and access control [1–4]. Ultra-High frequency (UHF) RF identification (RFID) systems employing modulated backscatter communication links, such as those based on the widely deployed ISO18000-6c or EPC Global Class 1 Generation 2 specification [5], have traditionally been analyzed using techniques first developed to analyze radar systems. Compared to conventional identification method or barcodes, RFID technology offers several advantages, such as the ability for simultaneously reading a number of tags, higher reading range, and faster data transfer [6].

Received 6 June 2012, Accepted 9 July 2012, Scheduled 13 July 2012

* Corresponding author: Yasar Amin (ysar@kth.se).

Passive RFID tags do not have any internal source of energy, such as a battery, to support the functioning. Passive tags get all the energy needed for functioning from the electromagnetic radiation emitted by the reader. Communication between the reader and the tag is based on backscattering principle in which reader transmits energy to activate the tag, and then the tag responds by backscattering its identification information to the reader. In general, an RFID tag consists of an antenna and an application-specific integrated circuit chip (strap or RFIC). For low-cost and reliable production of RFID tags, the fabrication methods and materials for antennas are considered to be challenges [7–9]. Moreover, the research area appears deserted while addressing the new rising issues interrelated to the field of economic and eco-friendly tags comprising of paper substrate [10, 11]. Paper substrates offer numerous advantages for manufacturing RFID tags, not only is paper extensively available, and inexpensive it is lightweight, recyclable and can be rolled or folded into 3D configurations [12, 13].

This paper presents a thorough analysis of novel rounded-corner bowtie passive RFID tag antennas, which are fabricated on various ultra-low-cost substrates (characterized & evaluated for the proposed antenna in Table 1 in combination with the state-of-the-art printing technologies (Screen Printing, Rotary Printing (Flexo), Inkjet printing & (Dry Phase Patterning) mentioned in Table 2. The implementation of T-match arms for matching of the antenna to the integrated circuit (IC) is introduced that improves the reliability against environmental diversities as well as increase the maximum reading distance. The design and simulations are performed using ANSYS HFSS^{TM} whereas; the measurements are carried out in an anechoic chamber along with the reader setup dedicated to antenna characterization. The proposed antenna operates from 860–960 MHz, thus expands to the

Table 1. Characterized/evaluated substrate parameters.

Substrate	Thickness (μm)/ Permittivity (ε_r)/Loss Tangent	Applications
Kodak U-P Photopaper	250/3.3 (avg.)/0.077 (1 GHz@25°)	Packaging
HP Adv. Photopaper	250/3.3 (avg.)/0.04 (1 GHz@25°)	Packaging
Paper (p_e:smart)	250/3.2 (avg.)/0.077 (1 GHz@25°)	Packaging
Paper (Korsnäs)	375/3.3 (avg.)/0.077 (1 GHz@25°)	Packaging
Teonex Q51	25/2.9/0.005 (1 GHz@25°)	Harsh environment
Kapton HN	125/3.5/0.0026 (1 kHz@25°)	Harsh environment
Metal coated PET	50/3.3/0.003 (0.9 GHz@25°)	Fully wrapable

Table 2. Printing technology/ink/substrate/speed combinations.

Inkjet Printing	**Rotary Printing**	**Screen Printing**	**DPP**
Cabot Ink	*Asahi*	*Asahi*	*Al Coated*
CCI-300	*Paste (LS-411AW)*	*Paste (LS-411AW)*	
Kodak Photopaper	Kapton HN	Kapton HN	PET
HP Photopaper	Teonex Q51 (2 & 4 m/min)	Paper (Korsnäs)	
Paper (p_e:smart)	Paper (Korsnäs)		

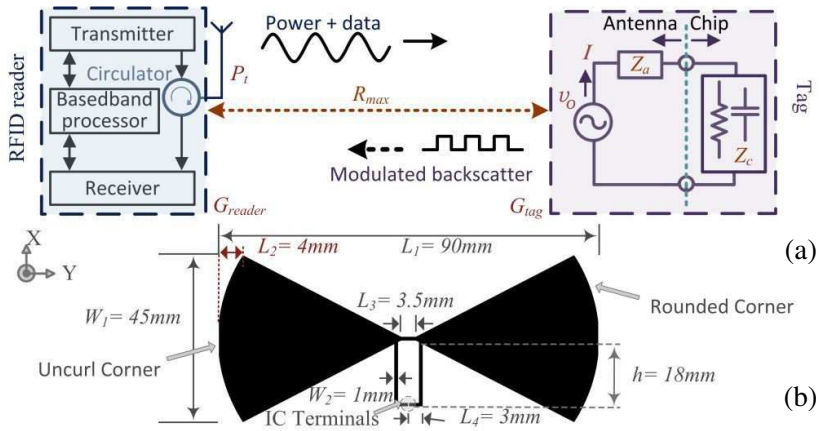

Figure 1. (a) Far-field RFID mechanism & equivalent circuit of an IC tag, (b) T-match folded rounded-corner bowtie RFID tag module configuration.

global usage of this tag. The robustness, eco-friendliness, flexibility and outstandingly read range of the proposed antennas make them an absolute choice for far-field industrial applications (a few mentioned in Table 1).

2. ANTENNA DIMENSIONS AND PARAMETRIC OPTIMIZATION

The main purpose of optimization is to maximize the feeding power to the load to achieve the maximum possible read range while preserving the multifaceted nature of the proposed antenna. The NXP ucode g2xm (SOT1040AB2 (Al strap), e.g., the target IC impedance at 915 MHz is $13.3 - j122\,\Omega$) is selected. Figure 1(a) shows the Thevenin equivalent circuit of the IC tag, from which we can calculate the

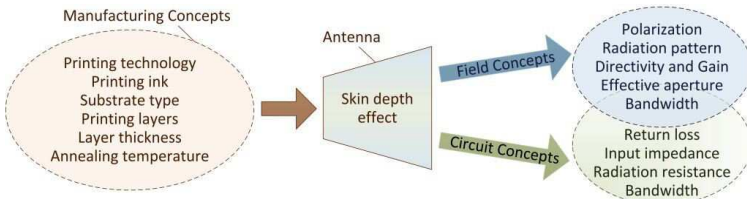

Figure 2. An outline of key antenna development parameters.

key design criteria. Antenna input impedance Z_a is expressed as the impedance offered by an antenna at its terminals or the ratio of the voltage to current at its terminals. Mathematically, it is calculated as:

$$Z_a = \frac{v_o}{I} = R_a + jX_a \tag{1}$$

where v_o is the input voltage and I the current at the antenna input. The input impedance is a complex number, and the real part further consists of two components. So, it is worth mentioning here that throughout the text onwards whenever input impedance of antenna is referred it will be meant that the real part R_a of the antenna input impedance Z_a consists of the radiation resistance and the antenna losses or loss resistance.

The proposed antenna structure is shown in Figure 1(b) along with dimensions and IC terminals placed in the center of the T-match arms. The T-match arms are also responsible for the matching of the antenna impedance to that of the IC through the fine tuning of the length L_4, height h, and width W_2. In the proposed tag, antenna is directly connected to a source (IC or strap) of impedance $Z_c = R_c + jX_c$, for a matched load the following condition should be met:

$$Z_c = Z_a^* = R_a - jX_a \tag{2}$$

Thus, the impedance matching between Z_a and Z_c will stand for the optimal antenna. This ultimate goal defines the essence of antenna design in order to control the current distribution, which in turn determines the radiation pattern and input impedance. Therefore, to assess development process thoroughly all relevant parameters of antenna are analysed here, which are categorized from the manufacturing, circuit and field point of views as summarized in Figure 2.

2.1. Antenna Effective Aperture and Aperture Efficiency

In the proposed antenna, conscientious effort has been carried out to optimize antenna dimensions. Since the field/current, on the antenna

aperture is not uniform, the concept of antenna effective aperture is established. In achieving high performance while keeping the minimum antenna size, an established concept that the effective aperture A_e is less than the physical aperture A_p is accomplished [14]. Thus, the aperture efficiency is mathematically expressed as the ratio of these two terms. For a good antenna structure, this parameter should be in the range of 50–80%. The effective aperture is proportional to the directivity of the antenna, and the directivity can also be expressed in terms of the aperture size and aperture efficiency:

$$D = \frac{4\pi}{\lambda^2} A_e = \frac{4\pi}{\lambda^2} \eta_{ap} A_p \tag{3}$$

By knowing the power density S at the receiving antenna, we can estimate the received power by using the following equation:

$$P_r = SA_e \tag{4}$$

This optimization parameter enriched the key design criteria to save every drop of the manufacturing ink and material in order to make low-cost as well as environmental friendly tags.

2.2. Skin Depth Effect and Antenna Performance

The skin depth and ohmic losses of the printed conductive layer set the boundary conditions for the printing technologies, and parameters such as the amount of silver ink depending upon its conductivity and the thickness of the printed layers. Mathematically, the skin depth is, therefore, expressed as:

$$FieldConcept \dashrightarrow \left(\delta \approx \sqrt{\frac{1}{\pi f \mu \sigma}}\right) = CircuitConcept \dashrightarrow \left(J = J_0 e^{-z/\delta}\right) \tag{5}$$

and from circuit concept it is defined as the depth below the surface of the conductor at which the current density decays to *1/e* (about 37%) of the current density at the surface [14]. Equation (5) leads to the manufacturing parameters of the proposed antenna mentioned in Figure 2. In a good conductor, skin depth varies as the inverse square root of the conductivity. Thus, better conductors have a reduced skin depth, and this factor plays a key role in investigating optimal printing techniques for fabrication.

3. MANUFACTURING PARAMETRIC ANALYSIS

The manufacturing processes are analyzed primarily with a focus on low cost solutions available for industrial applications at present. In general, the comparison of the exact cost for each printing process

depend upon the number of factors which make such analysis out of scope of this article. However, relative comparison of cost per tag is carried out while implementing each technology and on the basis of this study each fabrication technology is given the scale value from (1) to (4), where (4) corresponds to the cheapest solution.

3.1. Screen Printing — (2)

One of the recent areas, where screen has made itself welcome is in the printing of RFID antennas. The technological advancements have made it possible to print antennas through the process of screen printing, by using conventional substrates or materials.

The proposed antennas are screen printed with the semiautomatic screen printer (Figure 3(a)) in VTT (Technical Research Centre of Finland) on Kapton HN and Korsnäs paper, as showed in Figures 3(b) & (c), respectively. The 25 µm thick layer is printed using Asahi paste in order to exploit its outstanding mechanical performance [15], while remarkably stable ink distribution all over the printed patterns is achieved. Robust proposed RFID tag antennas are achieved by this process, which can maintain their performance even being bent several times, this is demonstrated with detail in [16]. The characterization and measurements of the printed traces are carried out using Veeco profilometer, which are presented in Figures 3(d)–(f). The samples are post-annealed for 2 hours at 140°C to achieve improved conductivity.

3.2. Rotary Printing — (4)

Rotary printing, is a finer resolution printing (flexo) technology, it is rapidly gaining importance by RFID antenna printing providers as a manufacturing choice that offers higher throughput than screen printing.

The rotary screen printing of antennas is studied here using VTT's ROKO pilot line showed in Figure 4(a). PEN, polyimide and paper substrates are used with two silver PTF — (Polymer Thick Film) inks and one silver nanoparticle ink. Additionally, the printing screen mesh size is varied in these test runs to study its effects on, e.g., layer thickness. A hot air drying oven having length of 4 m is used. The performance of rotary printed antennas showed in Figures 4(b)–(d) depend on several parameters. The line thickness is typically 10–15 µm, and sheet resistance 50 mΩ/square, which can be further decreased to 30 mΩ/square by additional oven drying. The best print quality is obtained using a printing speed of 2 m/min.

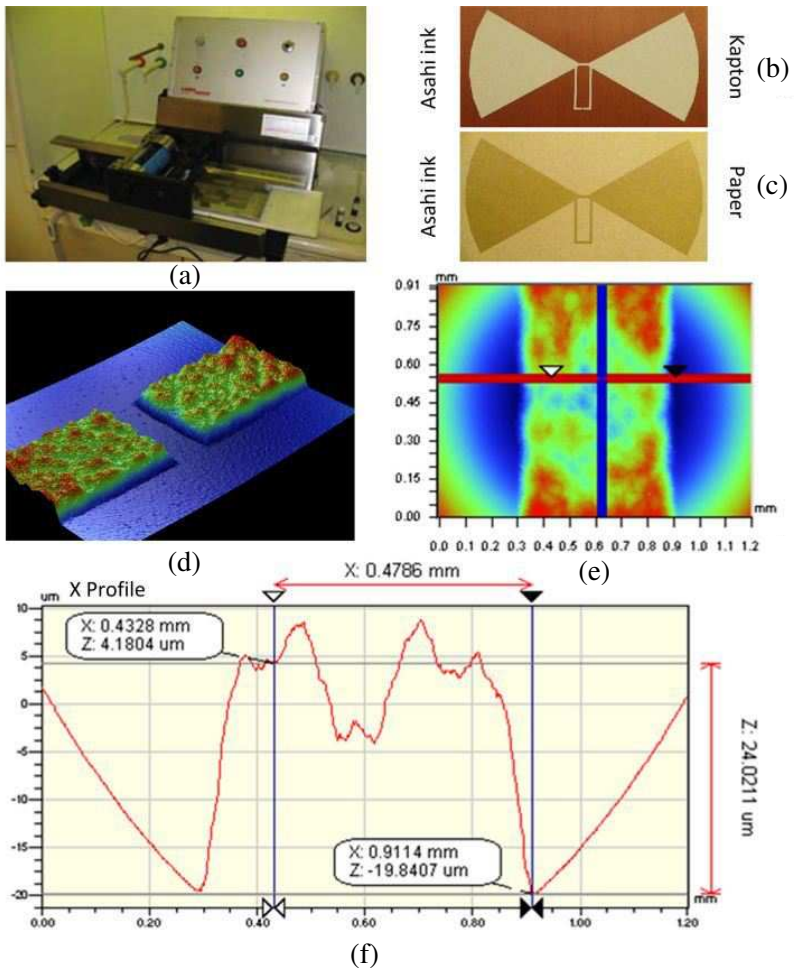

Figure 3. (a) Screen printing setup; Screen printed antenna on: (b) Kapton HN, (c) Korsnäs paper; Profilometer measurement of printed layer: (d) roughness, (e) surface topography, (f) thickness.

3.3. Dry Phase Patterning — (3)

The Proposed antennas are also developed using Dry Phase Patterning (DPP) for comparison and validation of the concept (in Acreo AB, Sweden), a method for patterning metal layers on flexible substrates. The laminate of Aluminum/PET is patterned for proposed antennas showed in Figure 5(c). Process speed up to 150 m/min and line pitch down to 250 µm has been demonstrated, which made DPP a better choice for cost effective RFID tags.

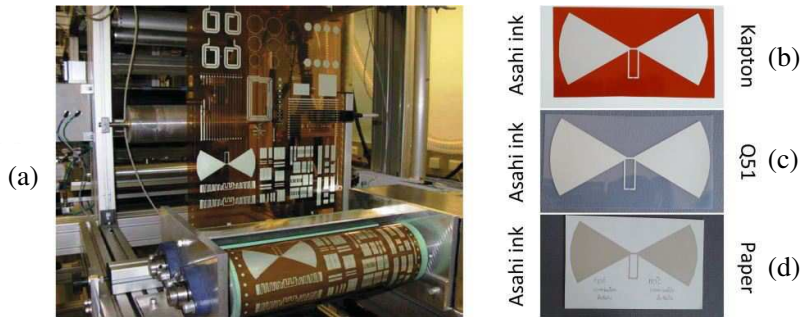

Figure 4. (a) Rotary printing setup; Rotary printed antenna on: (b) Kapton HN, (c) Q51, (d) Korsnäs paper.

Figure 5. (a) DPP setup at Acreo, (b) antenna patterning, (c) aluminum patterned antenna on PET.

Laboratory production line showed in Figures 5(a) & (b) is used for the test trials. One of the main benefits of employing DPP method for the fabrication of proposed antennas is the reduced load on the environment which embraces the concept of "green" tags. This is mainly because of reduced energy consumption; no washing, brushing or drying is required. Since, no chemicals are used, the residual product is in a dry and easily recyclable form.

3.4. Inkjet Printing — (1)

Inkjet printing is a direct-write mechanism by which the desired design outline is transferred directly to the (flexible) substrate. This technology requires no masks compared with the conventional etching technique, which has been commonly used in industry. During inkjet printing, the single ink droplet is jetted from the nozzle to the desired position, therefore, creating no waste, ensuing in an economical and eco-friendly production choice.

The inkjet printing setup used in the present research is showed in Figure 6(a) and is based on a Fujifilm Dimatix DMP2800 printer. It uses one user fillable piezo-based inkjet print cartridge with 16 nozzles in a single row and 254 µm nozzle spacing, to eject 1 pl or 10 pl drops (depending upon the choice of cartridge). The printed structures on Kodak photopaper and (p_e:smart) from Felix Schoeller are showed in Figures 6(b) & (c), respectively. These are printed using 10 pL cartridge (DMC-11610) filled with Cabot conductive Ink (CCI-300 from Cabot Corp.), having viscosity of 11–15 cp, with silver solid loading of 19–21 wt% and density of 1.23–1.24 g/ml is jetted with printing resolution of 1270 dpi. The printing was carried out in a standard laboratory environment to determine the extent to which useable devices could be fabricated on a commercial scale printing method.

After the silver nanoparticle droplets are deposited to the substrate, the sintering process is carried out for 2 hr at 150°C for sufficiently curing, to remove the excess solvent and material impurities from the depositions. The characterization of the printed structures is carried out under ULTRA-55 Field Emission Scanning Electron Microscope from Carl Zeiss NTS showed in Figures 6(d) & (e). Figures 6(f) & (g) show the SEMs for elaborating the

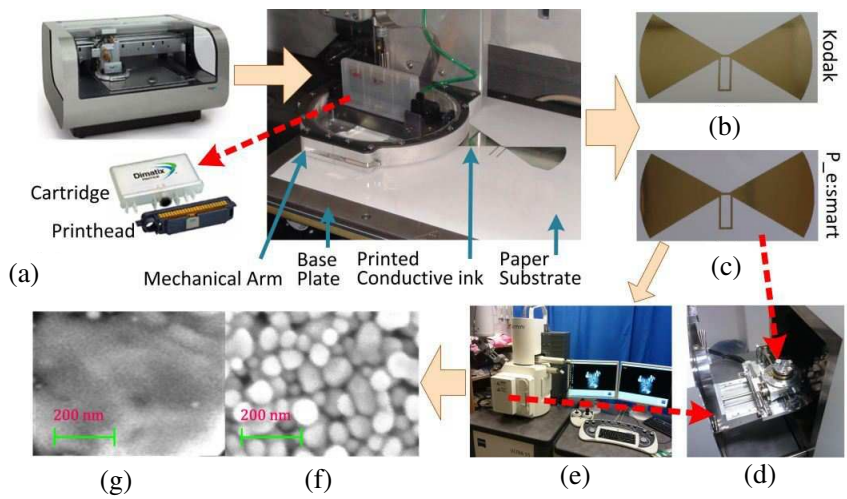

Figure 6. (a) Inkjet printing setup; Inkjet printed antenna on: (b) Kodak photopaper, (c) Felix Schoeller paper; (d) SEM sample holder, (e) ULTRA-55 FESEM Carl Zeiss setup; SEM images of three layers of printed silver nanoparticle ink, after curing 2 hr at: (f) 100°C, (g) 150°C.

difference between the heating temperature after a 2 hr curing at 100°C and 150°C respectively. At high temperature, an almost solid metal conductor is formed so providing a percolation channel for the conduction of electrons throughout the material without obstruction. The sintering process also presents the derived benefit of increasing the bonding of the deposition with the paper substrate.

4. FIELD & CIRCUIT CONCEPTS PARAMETRIC ANALYSIS

During the printing process of the proposed antennas, attention is given to fabricate five identical structures with the same combination of printing material, ambient conditions & technology. These prototypes are then measured across the UHF frequency band using half mirror method. Half mirror method is adapted instead of balun usage to eliminate the possibility of error [17]. Furthermore, maximum deviated data value at a frequency among five prototypes is reported here, which provides an in-depth view for the worst case analysis. Moreover, this technique provides the thorough investigation of reliability parameters for each printing technology.

Figures 7(a) & (b) show the impedance plots. Impedance measurements are taken using vector network analyzer (MS2026B, Anritsu). The standard calibration method short-open-load (SOL) is used. As showed in Figure 7(a), the computed resistance for the antenna in the UHF RFID frequency range maintains a value close to 14 Ω between the two successive peaks. There is extremely small variation observed among the curves for different antennas, and it can be well illustrated from the Figure 7(a), that all the prototype antennas have maintained the resistance around 14 Ω in a linear fashion with frequency. The reactance part of the impedance, as showed in Figure 7(b), follows a positive value with a linear variation with frequency, pertaining to an inductance that conjugately matches or, equivalently, cancels the effect of the 1.42 pF input capacitance (parallel) of the IC. It is observed that a relatively constant concurrence is found between the computed and measured results.

The RFID IC/strap is attached to the IC terminals on printed structures with CW2400 silver conductive epoxy, cured at 24°C for 4 hours or 70°C for 10 minutes to achieve maximum conductivity and adhesion. The reading range of the proposed antenna is measured in response to Impinj's UHF RFID kit and reader antennas in an anechoic chamber, to validate the feasibility for commercial RFID system. The computations are carried out in accordance with the following Friis

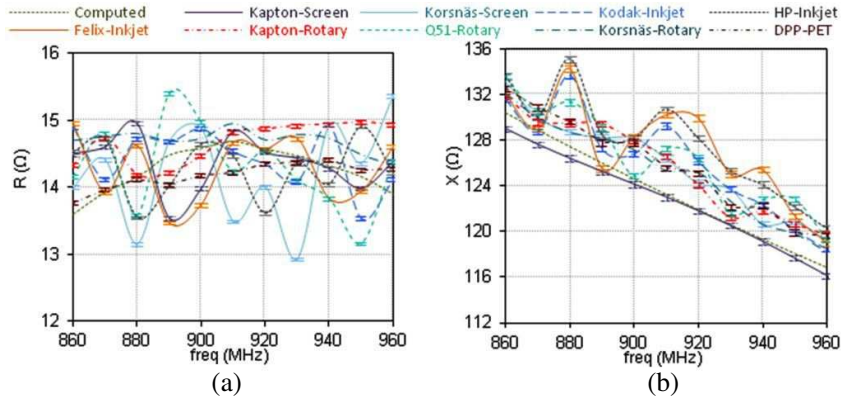

Figure 7. Antenna input: (a) resistance variation, (b) reactance variation.

equation:

$$R_{\max} = \sqrt[4]{\frac{P_t G_{tag}^2 G_{reader}^2 p^2}{P_{system}} \left(\frac{\lambda}{4\pi}\right)^4} \tag{6}$$

where the output power of the reader is P_t, p the polarization efficiency, G_{tag} the realized gain of the tag antenna (including the mismatch between the tag antenna and the tag chip), G_{reader} the gain of the reader antenna, λ the wavelength in free space at the operating frequency, and P_{system} the sensitivity of the reader system in detecting the backscattered signal from the tag. It is observed that the read range can be influenced by the reader antenna in use. The measured and computed results are in close agreement, and the maximum read range achieved is 9 meters. The complete comparison of read range of different printed antennas is analysed in Figure 8(a), which exhibits the improved performance than previously published results [6, 18].

However, the read range is also susceptible to the tag orientation, the object which the tag is attached to, path loss, spatial and temporal fading statistics of the propagation environment [19]. In most UHF RFID systems, the reading distance obtained by Equation (6) extends well into the far-field region. When there is realization of tag which can operate in the far-field also involves near-field tag scanning. It can be projected that, in almost all cases, the tag gets more than sufficient power to operate when brought closer to RFID reader antenna. Hence, the read range of most UHF RFID tags is determined by the tag operational in the far-field [20].

The return loss of the antenna structure is calculated based on the power reflection coefficient. The computed return loss is showed

along with measured values of the rotary, screen, DPP & inkjet printed antennas in Figure 8(b). On the whole, a good agreement among the computed, and the manufactured antennas is pragmatic despite the higher metal loss of the silver-based conductive ink. Moreover, it is deduced from Figures 8(a) & (b) that the proposed antenna design can gracefully cater the variations in the properties of different substrates mentioned in Table 1. The characteristics of the bowtie profile of the half-wavelength dipole antenna body allows for a broadband operation. The bandwidth of the proposed antenna is 197 MHz, corresponding to 23% around the center frequency 855 MHz; so it covers the worldwide UHF RFID bands and can cater greater degree of environmental disparities. Furthermore, each calculation at a frequency is carried out by considering the variation of the IC reactance, which varies from 130–116 Ω from 850–960 MHz, respectively. In general, it is sufficient by conjugately matching the antenna input impedance to those provided in the IC specifications by the manufacturer around the center frequency.

The radiation pattern is measured inside an anechoic chamber setup that replicates absolute free space, which is presented in Figure 9(a). The antenna under test (AUT) is mounted over the positioner assembly in the center of the chamber which is set to rotate the antenna in small steps of 5 degrees to obtain a 360° radiation pattern. A continuous-wave (CW) signal from the signal generator excites the AUT. The receiver antenna is connected to the spectrum analyzer (Agilent HP 8562E) and a PC running the test automation software controls the measurement setup. The normalized computed radiation pattern and the microwave chamber measurements

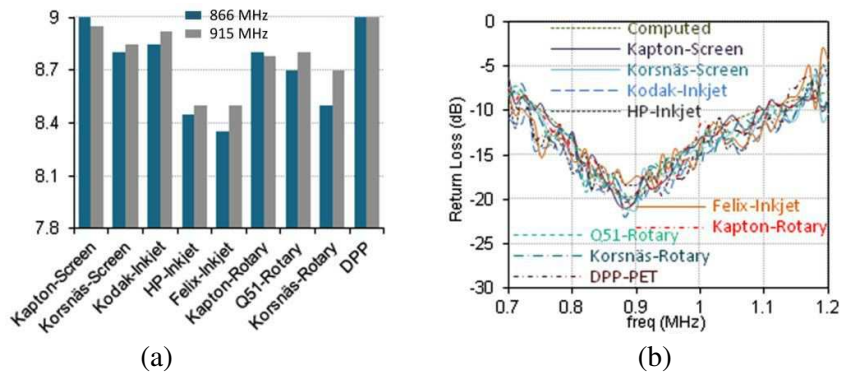

Figure 8. (a) Measured read range, (b) measured and computed return loss.

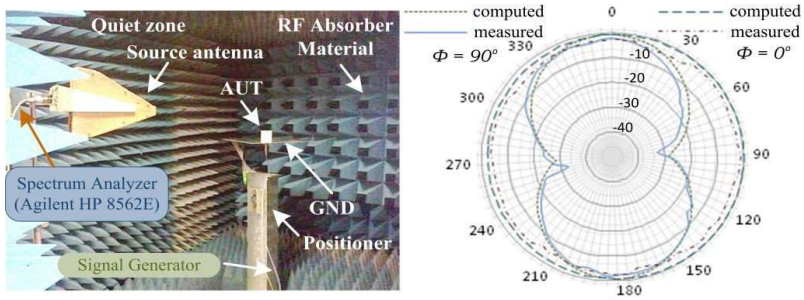

(a) (b)

Figure 9. (a) The anechoic chamber setup, (b) measured & computed 2D far-field radiation plots.

are plotted in Figure 9(b). The radiation patterns are nearly uniform (omnidirectional) at 915 MHz with directivity around 2.1 dBi and show extreme agreement between computations and measurements, which can also be verified for other frequencies within the antenna bandwidth and are in coherence with previously published results [3, 6]. However, some distortion in the measurements is possibly due to the metal-plate structure [21], used for half mirror method which can be reduced by metal-plate fixture with curved edges [19].

5. CONCLUSION

In this paper, we introduced an innovative tag antenna capable of significantly increasing RFID reading range while being used on several substrates with different printing technologies. The proposed antenna has optimized effective aperture consisting of curled and uncurled corners along with T-matching network. The measured impedance bandwidth wholly covers the UHF RFID band and is capable of exhibiting long reading range of up to 9 m from 860–960 MHz, which is measured with a commercial RFID system. Numerous design parameters are optimized using successive iterations to obtain a single design which can be manufactured by various combinations of fabrication technology, ink and substrate that are potential candidates for "green" electronics solutions.

ACKNOWLEDGMENT

This work was financially supported by Vinnova (The Swedish Governmental Agency for Innovation Systems) through the Vinn Excellence centers program.

REFERENCES

1. Marrocco, G., L. Mattioni, and C. Calabrese, "Multiport sensor RFIDs for wireless passive sensing of objects-basic theory and early results," *IEEE Transactions on Antennas and Propagation*, Vol. 56, No. 8, 2691–2702, 2008.
2. Tiang, J.-J., M. T. Islam, N. Misran, and J. S. Mandeep, "Circular microstrip slot antenna for dual-frequency RFID application," *Progress In Electromagnetics Research*, Vol. 120, 499–512, 2011.
3. Chen, S.-L., S.-K. Kuo, and C.-T. Lin, "A metallic RFID tag design for steel-bar and wire-rod management application in the steel industry," *Progress In Electromagnetics Research*, Vol. 91, 195–212, 2009.
4. Zuo, Y., "Survivable RFID systems: Issues, challenges, and techniques," *IEEE Transactions on Systems, Man, and Cybernetics*, Vol. 40, No. 4, 406–418, 2010.
5. Thomas, S. J., E. Wheeler, J. Teizer, and M. S. Reynolds, "Quadrature amplitude modulated backscatter in passive and semipassive UHF RFID systems," *IEEE Transactions on Microwave Theory and Techniques*, Vol. 60, No. 4, 1175–1182, 2012.
6. Rida, A., L. Yang, R. Vyas, and M. M. Tentzeris, "Conductive inkjet-printed antennas on flexible low-cost paper-based substrates for RFID and WSN applications," *IEEE Antennas and Propagation Magazine*, Vol. 51, No. 3, 13–23, 2009.
7. Panda, J. R. and R. S. Kshetrimayum, "A printed 2.4 GHz/5.8 GHz dual-band monopole antenna with a protruding stub in the ground plane for WLAN and RFID applications," *Progress In Electromagnetics Research*, Vol. 117, 425–434, 2011.
8. Hsu, H.-T., F.-Y. Kuo, and C.-H. Chang, "Application of quasi log-periodic antenna for UHF passive RFID tag design featuring constant power transmission coefficient over broadband operation," *Journal of Electromagnetic Waves and Applications*, Vol. 24, Nos. 5–6, 575–586, 2010.
9. Jamlos, M. F., T. A. Rahman, M. R. Kamarudin, P. Saad, M. A. Shamsudin, and A. M. M. Dahlan, "A novel adaptive Wi-Fi system with RFID technology," *Progress In Electromagnetics Research*, Vol. 108, 417–432, 2010.
10. Alimenti, F., et al., "A new contactless assembly method for paper substrate antennas and UHF RFID chips," *IEEE Transactions on Microwave Theory and Techniques*, Vol. 59, No. 3, 627–637, 2011.
11. Lazaro, A., D. Girbau, and R. Villarino, "Effects of interferences

in UHF RFID systems," *Progress In Electromagnetics Research*, Vol. 98, 425–443, 2009.

12. Bose, I. and S. Yan, "The green potential of RFID projects: A case-based analysis," *IEEE IT Pro.*, Vol. 13, No. 1, 41–47, 2011.
13. Makimura, H., et al., "Evolutional design of small antennas for passive UHF-band RFID," *IEEE Journals and Magazines*, Vol. 47, No. 5, 1510–1513, 2011.
14. Huang, Y. and K. Boyle, *Antennas from Theory to Practice*, John Wiley & Sons Ltd., New York, 2008.
15. Jaakola, T., et al., "Low cost printed flexible multilayer substrates," *10th Electronics Packaging Technology Conference, EPTC 2008*, 344–349, 2008.
16. Amin, Y., Q. Chen, H. Tenhunen, and L. R. Zheng, "Evolutionary versatile printable RFID antennas for "Green" electronics," *Journal of Electromagnetic Waves and Applications*, Vol. 26, Nos. 2–3, 264–273, 2012.
17. Leong, K. S., M. L. Ng, and P. H. Cole, "Investigation of RF cable effect on RFID tag antenna impedance measurement," *IEEE Antennas and Propagation Society Int.' Symposium*, 573–576, 2007.
18. Bjorninen, T., A. Z. Elsherbeni, and L. Ukkonen, "Low-profile conformal UHF RFID tag antenna for integration with water bottles," *IEEE Antennas and Wireless Propagation Letters*, Vol. 10, 1147–1150, 2011.
19. Amin, Y., Q. Chen, H. Tenhunen, and L. R. Zheng, "Performance-optimized Quadrate bowtie RFID antennas for cost-effective and eco-friendly industrial applications," *Progress In Electromagnetics Research*, Vol. 126, 49–64, 2012.
20. Tikhov, Y., "Comments on 'antenna design for UHF RFID tags: A review and a practical application'," *IEEE Transactions on Antennas and Propagation*, Vol. 54, No. 6, 2006.
21. Kuo, S.-K., S.-L. Chen, and C.-T. Lin, "An accurate method for impedance measurement of RFID tag antenna," *Progress In Electromagnetics Research*, Vol. 83, 93–106, 2008.

Paper IV–Design of Novel Paper-Based Inkjet Printed Rounded Corner Bowtie Antenna for RFID Applications

Y. Amin, J. Hållstedt, H. Tenhunen, and L.-R. Zheng, *Sensors & Transducers Journal*, vol. 115, no. 4, pp. 160-167, 2010

Available online at: http://www.sensorsportal.com/HTML/DIGEST/P_609.htm

Sensors & Transducers Journal, Vol. 115, Issue 4, April 2010, pp. 160-167

www.sensorsportal.com

Sensors & Transducers

ISSN 1726-5479

http://www.sensorsportal.com

Design of Novel Paper-based Inkjet Printed Rounded Corner Bowtie Antenna for RFID Applications

Yasar AMIN, Julius HÅLLSTEDT, Hannu TENHUNEN, Li-Rong ZHENG
iPack Vinn Excellence Center, School of Information and Communication Technology,
KTH (Royal Institute of Technology), Forum 120, 164 40, Stockholm-Kista, Sweden,
Tel.: +46-8-7904132, fax: +46-8-7511793
E-mail: ysar@kth.se

Received: 18 July 2009 /Accepted: 20 April 2010 /Published: 27 April 2010

Abstract: This paper presents a novel inkjet printed rounded corner bowtie antenna with T-matching stubs on paper substrate which is the cheapest and widest available substrate. The antenna exhibits compact size with outstanding read range and complete coverage of UHF RFID band (860-960 MHz). The results show extreme immunity of proposed antenna against paper dielectric constant variation. *Copyright © 2010 IFSA.*

Keywords: Bowtie antenna, Inkjet printing, UHF-RFID, Paper substrate, Dielectric variation

1. Introduction

UHF systems generally use far-field coupling, when the antennas of the reader and tag operate in a more conventional way: the forward and reverse link limited read range can be obtained by using Friis equation as [1].UHF far-field systems typically have greater range than LF and HF systems. Thus they are often used in systems where higher than normal levels of performance are required.

$$R_{forward} = \left(\frac{\lambda}{4\pi}\right)\sqrt{\frac{P_{TX} G_{reader} G_{tag}}{P_{\min,tag}}} \tag{1}$$

$$R_{reverse} = \left(\frac{\lambda}{4\pi}\right)\sqrt[4]{\frac{P_{TX} T_b G_{reader}^2 G_{tag}^2}{P_{\min,rdr}}}, \tag{2}$$

where λ is the wavelength, P_{TX} is the reader transmitted power, G_{reader} is the gain of the reader antenna, G_{tag} the gain of the tag antenna, $P_{min,tag}$ is the minimum threshold power required to turn on the tag chip and T_b is the backscatter transmission loss respectively. From equation (1) & (2) it is deduced that the changeable parameter is only the gain of the tag antenna when the reader measurements and tag IC are fixed.

Systems with carrier frequencies above 100 MHz generally operate by transferring power in the far field. The most commonly used frequency bands are in the region of 900 MHz, although the ISM band centered at 2.45 GHz is also used (this band is sometimes termed microwave rather than UHF) [2].

The emerging trend towards low cost, flexible and high performance electronics for automated identification of objects is leading to complex integration techniques. Three major challenges exist in today's RFID technologies. One is the design of small-size tag antennas with very high efficiency and effective impedance matching for IC chips with typically high capacitive reactance. In RFID system it is essential to optimize the antenna for power performance, especially for passive or semi-active configurations, where the only energy source is the incoming reader energy. Another major challenge is the existence of various different UHF frequency bands ranging from 860 to 960 MHz for Europe (866-868 MHz), Asia (864-954 MHz) and US (902-928 MHz). The universal operation of the RFID necessitates the use of wideband antennas covering all three bands. The third obstacle is the realization of ultra-low-cost RFID tags, with a cost requirement for individual tags below one cent [3]. This is only possible by using ultra low cost substrate and small sized antenna structures so that less amount of ink is used for their inkjet printing.

Antenna as shown in Fig. 1 is Inkjet printed on paper substrate of 270 μm thickness using printer from Fujifilm Dimatix, Inc. [4]. In this inkjet process the thickness of printed structures is less than 1-2 μm and significant higher thickness cannot be possible even by printing multiple layers. The fine sized inkjet nozzle cannot work with micrometer sized particle inks used in flexographic and screen printing processes so nano particle based inks from Sun Chemicals and Cabot are used in this printing process, conductivity of the ink-resultant film 12.5×10^6 S/m and $4\text{-}25\times10^6$ S/m respectively, which are lower than that of bulk silver conductivity.

Fig. 1. UHF RFID tag antenna with T-matching stubs.

2. Tag Design Challenges

A key consideration for RFID is the frequency of operation. RFID systems use different bands for communication, the choice of frequency affects several characteristics of any RFID system, the frequency band of interest for presented tag is 860-960 MHz and the choice criteria along with design challenges is discussed below [5].

2.1. Read Range

In the lower frequency bands, the read ranges of passive tags are no more than a couple feet, due to primarily poor antenna gain. (At low frequencies, electromagnetic wavelengths are very high, on the order of several miles sometimes, and much longer than the dimensions of the antennas integrated into RFID tags. Antenna gain is directly proportional to antenna size relative to wavelength. Hence, antenna gain at these frequencies is very low.) At higher frequencies, the read range typically increases. However, because the high frequency bands pose some health concerns to humans, most regulating bodies, such as the FCC, have posed power limits on UHF and microwave systems and this has reduced the read range of these high frequency systems to 10 to 30 feet on average in the case of passive tag which is realized in this project while maintaining the minimum size.

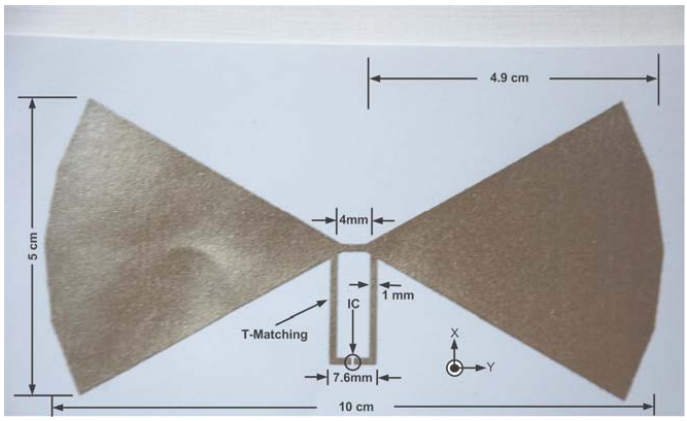

Fig. 2. Printed UHF RFID tag antenna with measurements.

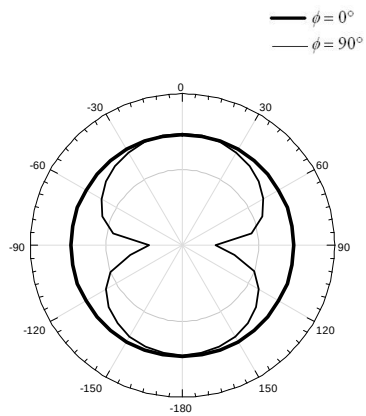

Fig. 3. 2D Radiation pattern.

2.2. Liquids and Metals

The performance of RFID systems will be adversely affected by water or wet surfaces. Signals in the high frequency bands are more likely to be absorbed in liquid. Metal is an electromagnetic reflector and radio signals cannot penetrate it. As a result, metal will not only obstruct communication if placed between a tag and an interrogator, but just the near presence of metal can have adverse affects on the operation of a system; when metal is placed near any antenna the characteristics of that antenna are changed and a deleterious effect called de-tuning can occur. The high frequency bands are affected by metal more so than the lower frequency bands. In order to tag objects made of metal, liquid bearing containers, or materials with high dielectric permittivity, special precautions have to be taken, which ultimately drives up costs. In the presented work the requirement is low cost with integrated capabilities to with stand against these adverse effects to some extent.

2.3. Data Rate

RFID systems operating in the LF band have relatively low data rates, on the order of Kbits/s. Data rates increase with frequency of operation, reaching the Mbit/s range at microwave frequencies [5]. RFID tags in UHF band see the widest use due to their higher data transfer rate (currently 640 kbps for Gen 2 RFID Standard).

2.4. Antenna Size and Type

Due to the long wavelengths of low frequency radio signals, the antennas of LF and HF systems have to be made much larger than UHF and microwave antennas in order to achieve comparable signal gain. This conflicts with the goal of making RFID tags small and cheap. Frequency of operation also dictates the type of antenna used in an RF system. At LF and HF, inductive coupling and inductive antennas are used, which are usually loop-type antennas. At UHF and microwave frequencies, capacitive coupling is used and the antennas are of the dipole type which leads to the selection of proposed rounded corner bowtie antenna (shown in Fig. 2) in our design.

2.5. Size and Price of Tags

Early RFID systems used primarily the LF band, due to the fact that LF tags are the easiest to manufacture. They have many drawbacks, however, such as a large size, as mentioned previously, which translates into a higher price at volume. The HF band is currently the most prevalent worldwide, because HF tags are typically less expensive to produce than LF tags. The UHF band represents the present state of the art. Recent advances in chip technology have brought prices for UHF tags down. The largest barrier to RFID growth is tag cost. Production costs for RFID tags can be broken down as follows

- Silicon die production (1/3)
- Die placement on printed circuit board (1/3)
- Antenna/adhesive packaging (1/3)

This indicates antenna cost plays vital role in production expenses. More complex RFID tags can cost tens of dollars. By the selection of cheapest substrate and printing area reduction by implementing innovative techniques in antenna design, low cost tag is realized here.

2.6. Reliability

RFID tag must be a reliable device that can sustain variations due to temperature, humidity, stress, and survive such processes as label insertion, printing and lamination.

3. Design Process

RFID tag antenna performance strongly depends on the frequency dependent complex impedance presented by the chip. Tag read range must be closely monitored in the design process in order to satisfy design requirements. Since antenna size and frequency of operation impose limitations on maximum attainable gain and bandwidth compromises have to be made to obtain optimum tag performance to satisfy design requirements [6].

RFID tag antenna design process is illustrated on a flow chart shown in Fig. 4. At first the RFID application is selected then system requirements can be translated into tag/antenna design criteria. After these requirements selection of ink for inkjet printing is carried out. The impedance value across the frequency band of interest (860 - 960 MHz) of the selected ASIC (NXP UCODE G2XM) in a chosen RF package (flip chip) to which antenna will be matched can be measured with a network analyzer and verified with datasheet provided by the manufacturer. Antenna parametric study and optimization is performed until design requirements are met in simulation. Like most antennas, RFID tag antennas (derivatives of dipole antenna) tend to be too complicated for analytical solution as they can be used in complex environment. Tag antennas are usually analyzed with electromagnetic modeling and simulation tools, typically with method of moments (MoM) for planar designs (e.g. thin flexible tags) and with finite-element method (FEM) or finite-difference time-domain method (FDTD) for more complicated three-dimensional designs (e.g. thick metal mounted tags). Fast EM analysis tools are crucial for efficient tag design, state of the art CAD tool Ansoft® HFSS is used in this design.

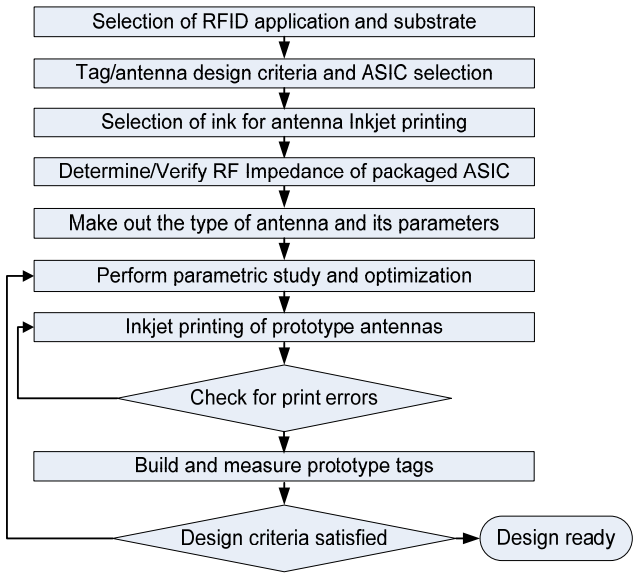

Fig. 4. Inkjet printed RFID tag antenna design process.

In a typical design process, modeling and simulation tools can be benchmarked against measurements. Read range calculation can be implemented directly in EM software by the aid of equations. Tag antenna is first modeled, simulated, and optimized on a computer by monitoring the tag range, antenna gain, return loss and impedance which give to a designer a better understanding of the antenna behavior. In the final two step of the design process, prototype antennas are first Inkjet printed and checked for printing errors and after passing this stage prototype tags are built and their performance is measured extensively. If design requirements are satisfied, the antenna design is ready. If not, the design is further modified and optimized until requirements are met [6].

3. Results and Analysis

The matching with ASIC is achieved by T-matching using stubs as shown in Fig. 2. Good antennas maintain -15 to -20 dB return loss across the entire band of interest [7]. The return loss variation due to

change in paper dielectric constant of proposed antenna is shown in Fig. 5 which shows good agreement with already published results. As required in RFID applications the proposed antenna exhibits a uniform quasi-omnidirectional radiation pattern as shown in Fig. 3 which is mostly the requirement in most of RFID applications. The radiation pattern is in good agreement with the literature [8, 9, 10]. The designed antenna structure is well resistant to variation in paper dielectric constant. Fig. 6 shows the stability of the antenna realized gain against variations, which validates an absolute surpassing performance of this proposed structure cross over the band of interest.

The tag antenna gain is an important parameter for the reading distance. The range is largest in the direction of maximum gain which is fundamentally limited by the size, radiation patterns of the antenna, and the frequency of operation. For a small dipole-like omnidirectional antenna, the gain is about 0-2 dBi [11]. The proposed antenna has demonstrated high gain across the complete UHF RFID band even under critical constrains of size reduction and paper dielectric variations which is in close relation with published results [8, 10]. Fig. 7 shows the simulated impedance variation plots of the antenna, indicating good matching conditions across the frequency band of interest regardless of the variation in paper dielectric constant.

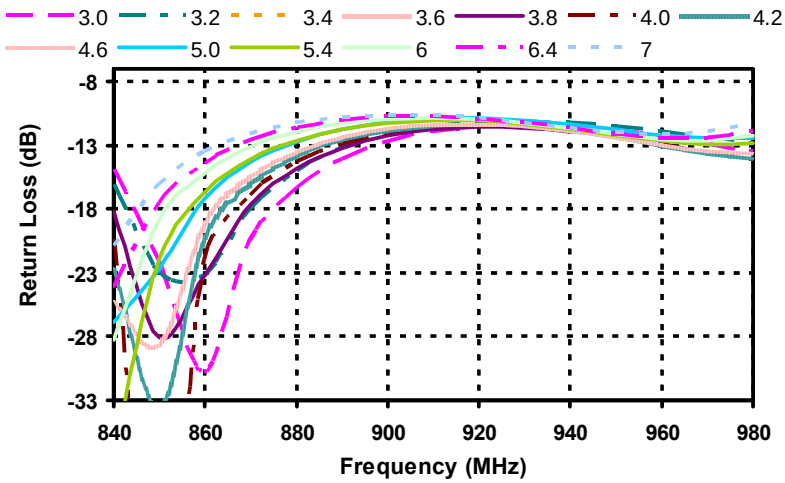

Fig. 5. Return Loss variation (Cabot Ink).

Both lossy and metallic objects may considerably degrade the performance of far-field tag antennas. These objects primarily lower the radiation efficiency of the antenna, and also distort the impedance matching when the tag is placed very close to the objects. In the presented design this effect is also minimized as much possible to a certain extent. The other way is to adopt antennas which have their own ground plane. However, such antennas are usually bulky in size and their multilayer structures are not cost-effective for mass production [11]. The proposed antenna is quite compact in size as well and it occupies only 10 cm x 5 cm. This size is smaller than previously published results [9].

Note that for worldwide operation in the region of 900 MHz, a wide frequency range – approximately 860 to 960 MHz –is required. This means that the antenna must be relatively wideband, with a fractional bandwidth of approximately 11 %. Because of this, the antenna Q is limited, leading to a limited voltage at the tag IC. Importantly, this indicates that there is a trade-off between bandwidth of operation and range [2].

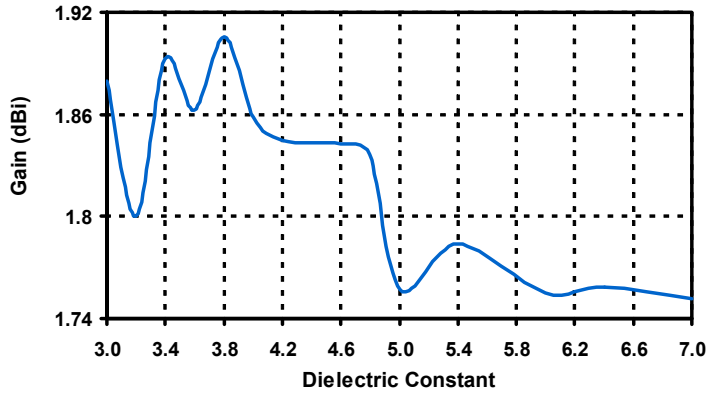

Fig. 6. Antenna Gain Stability (Cabot Ink).

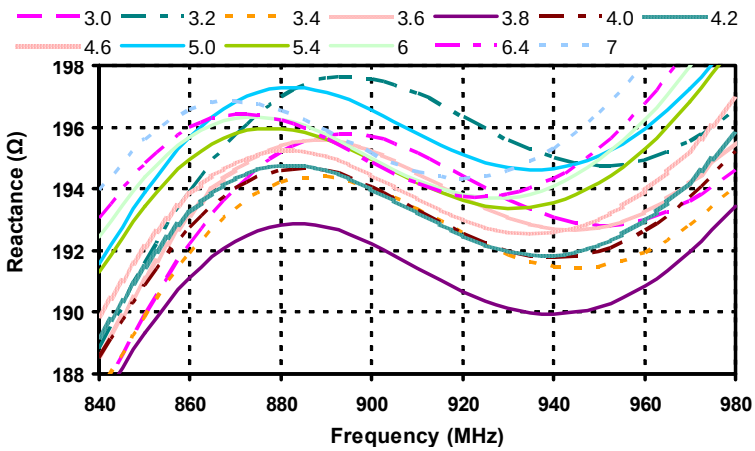

(a)

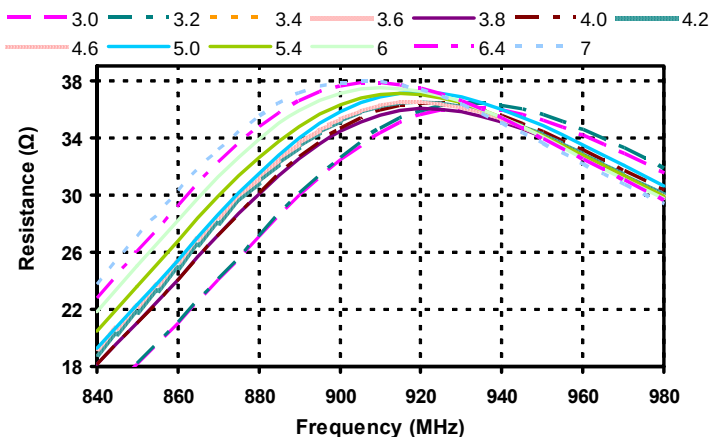

(b)

Fig. 7. (a) Reactance variation (Cabot Ink); (b) Resistance variation (Cabot Ink).

5. Conclusions

The development of low cost directly printable RFID tag antennas is essential in order to enable item level RFID tracking. The proposed antenna readable across the world due to its coverage of complete UHF RFID band (860–960 MHz) and has significant prospective to be used in small, extremely cheap solutions where read range and/or high data transfer rate is essential. In this paper we have presented extremely versatile antenna with outstanding reading distance of 3.8 meter. We discussed design criteria, challenges outlined generic design process with focus on Inkjet printing and analyzed the results due to variation in paper dielectric constant. The antenna has a wider bandwidth for catering the fabrication disparity. The versatility of this design of the RFID tag is most useful for applications where durability in read range is required, even in the presence of environment which can change the dielectric constant of the substrate. The proposed antenna allows a simple integration directly on e.g. paperboard in a roll-to-roll production line.

Acknowledgements

This work was financially supported by Vinnova (The Swedish Governmental Agency for Innovation Systems) through the Vinn Excellence centers program

References

[1]. Rao, K. V. S., Nikitin, P. V., Lam, S. F., Antenna design for UHF RFID tags: a review and a practical application, *IEEE Transactions on Antennas and Propagation,* Vol. 53, No. 12, Dec. 2005, pp. 3870–3876.
[2]. Yi Huang, Kevin Boyle, Antennas from Theory to Practice, *John Wiley,* United Kingdom, 2008.
[3]. Li Yang, Rida, A., Jiexin Li, Tentzeris, M. M., *Proc. of IEEE*, 2007, pp. 2040-2041.
[4]. Fujifilm Dimatix, Inc., (www.dimatix.com).
[5]. V. Daniel Hunt, Albert Puglia, Mike Puglia, RFID-A guide to radio frequency identification*, Wiley*, 2007.
[6]. Rao, K. V. S., Nikitin, P. V., Lam, S. F., *IEEE Trans. on Antennas and Propagation,* Vol. 53, No. 12, Dec. 2005, pp. 3870-3876.
[7]. Daniel M. Dobkin, The RF in RFID: passive UHF RFID in practice, *Newnes*, 2007.
[8]. Rida, A., Li Yang, Vyas, R., Bhattacharya, S., Tentzeris, M. M., in *Proc. of the IEEE Microwave Conf. European,* 2007, pp. 724-727.
[9]. Li Yang Rida, A. Vyas, R. Tentzeris, M. M., *IEEE Trans. on Microwave Theory and Technology*, Vol. 55, No. 12, Dec. 2007, pp. 2894-2901.
[10].Rida, A., Li Yang, Tentzeris, M. M., in *Proc. of the IEEE Antennas and Propagation Inter. Symposium,* 2007, pp. 2749-2752.
[11].Zhi Ning Chen, Antennas for Portable Devices, England, *John Wiley*, 2007.

Paper V–Performance-Optimized Printed Wideband RFID Antenna and Environmental Impact Analysis

Y. Amin, R. K. Kanth, P. Liljeberg, Q. Chen, L.-R. Zheng, and H. Tenhunen, *ETRI Journal*, submitted for publication, 2012

Performance-Optimized Printed Wideband RFID Antenna and Environmental Impact Analysis

Yasar Amin, Rajeev Kumar Kanth, Pasi Liljeberg, Qiang Chen, Li-Rong Zheng, and Hannu Tenhunen

This paper presents performance optimized RFID tag antenna, developed by using commercially accessible paper substrates and advanced inkjet printing process to guarantee mechanical flexibility and ultra-low production costs. The proposed antenna structure can endure the variations which emerge in electromagnetic properties of paper substrate due to varying environmental effects. Hole-matching technique is implemented to eliminate the matching network for reducing the consumption of conductive ink. The proposed structure is uniquely evaluated by demonstrating, sustainability and environmental impact analysis that validate the potential for ultra-low cost mass production of RFID tags for future generation of organic electronics. The antenna performance is assessed for cardboard cartons exclusively containing metal cans and water bottles. The experimental characterization of the proposed antenna endorses the wider bandwidth to cover UHF RFID ISM band (860-960MHz), which empowers its usage throughout the globe for supply chain applications. The improved design effectuates return loss of better than -15dB over a wide frequency range while exhibiting outstanding readability from 10.1 meters.

Keywords: RFID antenna, paper substrate, inkjet printing, organic electronics, sustainability analysis

Manuscript received ; revised ; accepted accepted_date.

This work was financially supported by Vinnova (The Swedish Governmental Agency for Innovation Systems) through the Vinn Excellence centers program.

Yasar Amin (phone: +46 8 790 4132, email: ysar@kth.se), Qiang Chen (email: qiangch@kth.se), Li-Rong Zheng (email: lirong@kth.se), and Hannu Tenhunen (email: hannu@kth.se) are with iPack VINN Excellence Center, Royal Institute of Technology (KTH), Stockholm, Sweden.

Rajeev Kumar Kanth (email: rajkan@utu.fi), and Pasi Liljeberg (email: pakrli@utu.fi), are with Turku Centre for Computer Science, Department of Information Technology, University of Turku, Turku, Finland.

I. Introduction

In the recent years, radio-frequency identification (RFID) technology has been widely integrated into modern society applications, ranging from barcode successor to retail supply chain [1], remote monitoring [2], detection and healthcare [3], for instance. Compared to traditional identification systems or barcodes, RFID technology offers several advantages [4], such as the capability of simultaneously reading a number of tags and faster data transfer [5]. In general, an RFID tag or transponder is composed of an antenna and an application-specific integrated circuit chip [6]. In passive UHF RFID systems, the communication between the transponder tag and the reader is established by modulating the radar cross section (RCS) of the transponder tag [7]. The modulation is set up by changing the input impedance of the transponder IC related to the data stream to be transmitted e.g. the EPC (electronic product code) value [8]. The need for flexible RFID tags has recently been increased enormously [9]; particularly the RFID tags for the UHF band ensure the widest use but in the meantime face considerable challenges of cost [10], reliability and environmental friendliness. In a similar fashion, the substrate material and the associated integration techniques are becoming more than a basic research topic, due to the ever growing demand for affordable and power-efficient broadband wireless electronics virtually in a ubiquitous manner [11].

In this study, a UHF RFID tag antenna using an innovative technique of pattern holes for conjugate impedance matching with the RFID strap, while at the same time saving the expensive ink is proposed. The antenna is designed by eliminating the matching network in order to achieve wideband characteristics and reliability against environmental multifariousness. We have revisited the manufacturing technique in order to achieve extra degree of enhancement in electrical characteristics while utilizing the state-of-the-art inkjet printing technology. The proposed antenna is directly printed on different commercially available paper substrates

which are characterized for flexible printed electronics (Table 1) for an ultra-low cost, flexible and highly integrated tag module. The ANSYS HFSS™ tool is used to design and predict the performance of the proposed antenna in terms of radiation pattern and input impedance, whereas the measurements are performed in an anechoic chamber along with the reader setup dedicated to antenna characterization. The proposed structure exhibits benchmarking results all over the frequency band of interest (860-960MHz). Furthermore, an in-depth sustainability and life cycle analysis is provided, which reveals that the proposed tag is an excellent choice for far-field industrial applications due to its organic nature, flexibility and outstanding read range, especially for large items level tracking in supply chain (cardboard cartons containing water & metal objects) and goods (wood or metal pallet) transportation.

Table 1. Characterized substrate parameters.

Substrate	Thickness μm	Permittivity ε_r	Loss Tangent @1GHz/25°C
Kodak U-P Photopaper	250	3.3 (average)	0.077
HP Adv. Photopaper	250	3.3 (average)	0.04
Felix Schoeller Paper (p_e:smart)	250	3.2 (average)	0.077

II. Antenna Design and Optimization

The proposed antenna is optimized in an organized approach for maximizing the read range while minimizing the ink consumption and effects of environmental harsh conditions on RFID tag. One of the critical observations made while field testing (in supply chain industry) of antennas having thinner traces used for matching network, is that the effect of even minor scratches on those tracks can cause loss of RFID tags during transportation. Therefore, it led towards the realization of a structure which can eliminate such risk factors while exhibiting better performance.

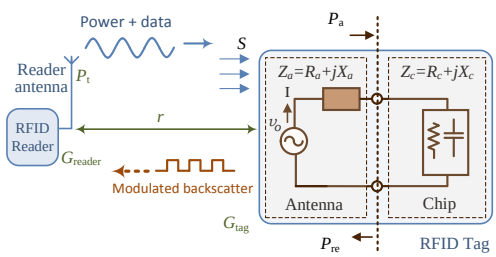

Fig. 1. Far-field RFID mechanism & tag equivalent circuit.

The main purpose of iterations and parametric enhancements is to maximize the feeding power to the load (RFID IC) and reduce the antenna area, in order to demonstrate highly efficient antenna structure on paper substrate for eco-friendly tags. The NXP UCODE G2XM (SOT1040AB2 (Al strap), for instance the goal IC impedance at 915MHz is 13.3 - j122Ω) is preferred. It is noteworthy here that the proposed design and technique is not restricted to the above mentioned RFID IC and it can be realized with any other commercially available RFID straps to produce optimum results accordingly. RFID radar cross section is important for reflecting passive tags. In this case, the RFID contains a resonating structure that reradiates when illuminated by the reader. The detectability of the tag depends on the RCS (or backscattered field) returned by the tag. The RFID reacts to the incident power density generated by the reader:

$$S = \frac{P_t G_{reader}}{4\pi r^2} \quad (1)$$

Here S is the power density in Watts/m^2, P_t is the total transmitted power by the reader, G_{reader} is the reader's antenna gain, and r is the distance between the reader and the RFID tag. If the tag's antenna has an effective aperture, A_e, its received power at the antenna terminals is then $P_a = SA_e$. This becomes the input power to the circuit powering the tag's circuit. Thus, one of the optimization factors is to achieve optimal antenna effective aperture in contrast to previous approaches in which one dimensional methodology is adapted to simply improve the antenna gain. As we are impending towards eco-friendly tags, every drop of ink saved in manufacturing process plays a vital role. Referring to the tag's equivalent circuit (Figure 1), the reradiated power P_{re} due to P_a can then computed as:

$$P_{re} = KP_aG_{tag} = \frac{4R_a^2}{|Z_a + Z_c|} \cdot P_aG_{tag} \quad (2)$$

Where, G_{tag} is the tag's antenna gain and K is the ratio of reradiated to incident energy with $R_a = \Re\{Z_a\}$, where Z_a is the complex antenna input impedance:

$$Z_a = \frac{v_o}{I} = R_a + jX_a \quad (3)$$

Here v_o is the input voltage, and I is current at the antenna input. The input impedance is a complex number, and in addition its real part, is composed of two components. It is observed that a short circuited tag ($Z_c = 0$) reradiates 4 times more power than a conjugate matched one ($Z_a = Z_a^*$). It is also noted that, in the case of conjugate matching, the tag absorbs and reradiates equal amounts of power. In general, the tag radar cross section, σ, is used to measure the radiation effectiveness. Specifically, in evaluating the RFID's effectiveness, the ratio of the returned to transmitted power is of interest. This is also the formal definition of the RCS, σ:

$$\sigma = \frac{P_{re}}{S} = KA_eG_{tag} \quad (4)$$

$$= \frac{\lambda^2 G_{tag} G_{reader} R_a^2}{\pi |Z_a + Z_c|^2} \left| \hat{p}_{reader} \cdot \hat{p}_{tag} \right|^2$$

Here $\hat{p}_{reader}$ and $\hat{p}_{tag}$ refer to the corresponding antenna polarizations. Clearly, the tag antenna gain plays a major factor; therefore, several iterations are carried out to address this challenge for achieving an efficient tag antenna design as showed in Figure 2.

The proposed rounded corner bowtie antenna structure is shown in Figure 2(a), and the printed antenna integrated with RFID strap forming an RFID tag in Figures 2(b) & (c). The implementation of pattern holes is responsible for matching of the antenna impedance to that of the IC through the fine tuning of their location and size which is mentioned in Figure 2(a). It is observed that earlier efforts to reduce the ink usage led towards lower gain and as a result, the scope of those tags is limited in supply chain industry. In the proposed approach for achieving multidimensional performance benefits, the pattern holes suite these requirements effectively. It is noticed that the inner holes positions (B-D) are more persuasive towards antenna efficiency whereas, the outer hole positions (E-I) assist more towards fine tuning the impedance. The vertical holes positions (J-P) are critical towards current distribution. Moreover, it is observed that the insertion of more pattern holes can cause the performance degradation.

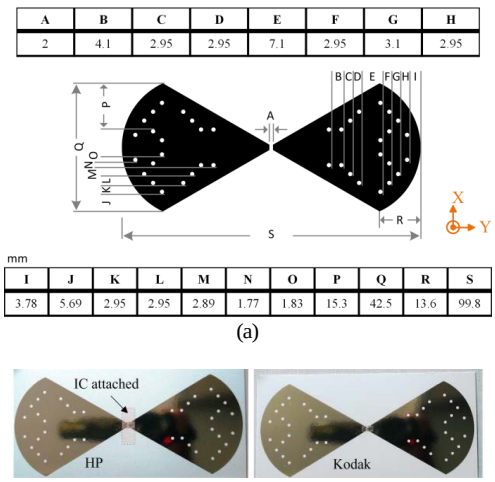

Fig. 2. (a) The geometry & dimensions of RFID antenna; inkjet printed RFID tag on: (b) HP, (c) Kodak; photopaper.

Consequently, the impedance matching between Z_a and Z_c will stand for the optimal antenna. This ultimate goal defines the quintessence of antenna structure in order to control the current distribution, which in turn determines the radiation pattern and input impedance. In the proposed antenna, diligent attempt has been carried out to optimize antenna dimensions. Because the field or current, on the antenna aperture is not uniform, the concept of antenna effective aperture is recognized. In achieving extended read range while keeping minimum antenna size as possible, an established concept that the effective aperture is less than the physical aperture is accomplished [12], which resulted in predilection of rounded corner structure.

The effect of annealing temperature is also analyzed to achieve better curing while, at the same time due to green nature of the proposed antenna, lowest possible energy should be consumed to accomplish optimum manufacturing objectives. After rigorous iterations, it is concluded that each type of paper substrate should be annealed at different temperature in order to attain better conductivity, in spite of the fact that all antennas under test are printed with same conductive ink (CCI-300 from Cabot Corp.). It is observed under appropriate annealing conditions (150°C /120min, 120°C /120min, 110°C /90min for Kodak, HP and Felix papers, respectively), an almost solid metal conductor with measured RF conductivity in the range $9x10^6$-$1.1x10^7$ [S/m] is formed, so providing a percolation channel for the conduction of electrons throughout the material without obstacle.

III. Field and Circuit Concepts Parametric Analysis

The measurements are carried out in a multidimensional approach for not only finding out the impedance, return loss, radiation pattern and read range but also determine the reliability parameters, which are extracted by repeatability. Thus, for worst case analysis five identical antennas with the selfsame combination of printing material, ambient conditions and inkjet technology are fabricated. The purpose of using several paper substrates is to verify the performance matrix on a rational basis, because paper substrates from different manufacturers significantly differ in properties exploited by printed electronics. In order to get a better understanding of antenna behavior when printed on paper substrate, maximum deviated data value at a frequency among five prototypes is reported hither.

The impedance is measured using S-parameter method (which is the most accurate method reported till date), in which the antenna is connected to the two ports of a vector network analyzer through a test fixture [13]. The principle governing this method is shown in Figure 3(a), which shows a distinctive asymmetrical balanced dipole antenna, with two arms of different lengths and excited differentially. The positive and negative ports of the source with a voltage of V are connected

to the input terminals of the radiators of the antenna, respectively. As showed in Figure 3(b), the driven voltage can be split as V_1 and V_2 with a virtual ground plane without any disturbance of the current distribution on the antenna. Hence, each terminal of the antenna radiators and the ground plane can be regarded as a "port", which is showed in Figure 3(c). The antenna can be equivalent to a "two-port" network, as showed in Figure 3(d). The impedance of the antenna is thusly associated to the network parameters of the corresponding two-port network, and can be characterized by measuring the network parameters such as S-parameters [13]. From Figure 3(d), the normalized impedance of the antenna can be expressed as follows:

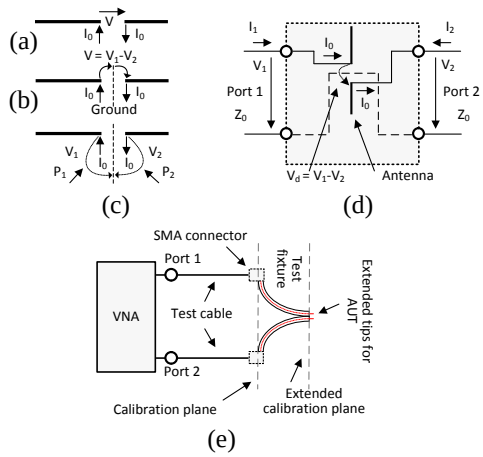

Fig. 3. Input: (a) resistance variation, (b) reactance variation.

$$\tilde{Z}_d = \frac{V_d}{I_0} = \frac{V_1 - V_2}{I_0} \tag{5}$$

Using the impedance matrix, the equations of a linear two ports (relating voltages and currents) are:

$$V_1 = Z_{11} I_1 + Z_{12} I_2 \tag{6}$$

$$V_2 = Z_{21} I_1 + Z_{22} I_2 \tag{7}$$

If the two ports are driven by current source i.e., $I_1 = I_0$ and $I_2 = -I_0$, the differential voltage V_d is given by:

$$V_d = V_1 - V_2 = (Z_{11} - Z_{21} - Z_{12} + Z_{22}) I \tag{8}$$

And the impedance is given by:

$$\tilde{Z}_d = \frac{V_d}{I_0} = \frac{V_1 - V_2}{I_0} = (Z_{11} - Z_{21} - Z_{12} + Z_{22}) I \tag{9}$$

Now by transforming the Z-parameters as a function of S-parameters and taking into account $Z_d = Z_0 \cdot \tilde{Z}_d$, we get:

$$Z_d = \frac{2\, Z_0 (1 - S_{11}S_{22} + S_{12}S_{21} - S_{12} - S_{21})}{(1 - S_{11})(1 - S_{22}) - S_{21}S_{12}} \tag{10}$$

Where Z_0 is the reference impedance, which is mostly 50Ω for measurement systems. Thus, in case of the symmetrical balanced antenna, where $S_{11} = S_{22}$ *and* $S_{12} = S_{21}$. By substituting these values in (10), to get a simplified expression:

$$Z_d = \frac{2\, Z_0 (1 - S_{11}^2 + S_{21}^2 - 2S_{12})}{(1 - S_{11})^2 - S_{21}^2} \tag{11}$$

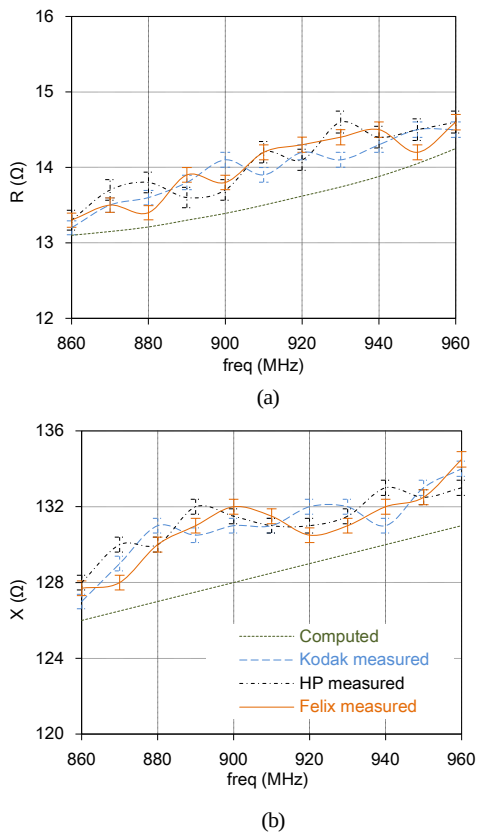

Fig. 4. Input: (a) resistance variation, (b) reactance variation.

The constellation of the measurement system is illustrated in Figure 3(e). The measurement is carried out by using a two-port VNA (MS2026B, Anritsu) and a test fixture. The test fixture is constructed by using two semi-rigid coaxial cables having a length of 100 mm with an outer conductor diameter of 2.2 mm. The outer conductors of the coaxial cables are

shorted by jointly soldering with the corresponding gap between the tips to accommodate between the two terminals of the antenna. One end of the fixture is with two SMA connectors, which is connected to the VNA through the test cables. The other end of the fixture is opened with the small extension (1.5mm) of inner conductors in order to form the tips for connecting the antenna under test (AUT). Soft soldering is avoided to fix the AUT to the test fixture since it requires heating the filler metal above 250°C to acquire proper soldering, but this temperature seriously damages the printed traces on paper substrates. Therefore, antenna is attached to the test fixture tips with CW2400 silver conductive epoxy, cured at 24°C for 4 hours for achieving maximum conductivity and adhesion.

In order to increase the accuracy of the measurements, all internal VNA errors after the sampler and the cables must be removed. This is exercised by shifting the reference plane to the tips of the measuring cable by applying the standard calibration method short-open-load-through (SOLT) and short-open-load (SOL) for S-parameter method (Figure 3) and Half-mirror method (Figure 6), respectively.

It is observed from Figure 4(a) the computed and measured resistance for the antenna from 860-960MHz maintains a value around 14Ω all over the curves. It is noteworthy, that the proposed structure and design technique are well suitable for adequate tuning of the matching characteristics as depicted in Figure 1. The reactance part of the impedance, as showed in Figure 4(b), exhibits a positive value with a linear variation with frequency, and slight fluctuation within acceptable values is pragmatic, pertaining to an inductance that conjugately matches or equivalently cancels the effect of the 1.42-pF capacitance of the RFID strap. It is noticed that a reasonably good harmony exists between the computed and measured results. Moreover, in-depth analysis reveals that the measurement fixture asserts certain amount of impedance, which can be eliminated or minimized by exercising two probe method [13].

The critical parameter, which determines the performance of an RFID tag antenna, is the read range [14]. The effective isotropic radiated power referenced for both the RFID reader and reader antenna, or equivalent isotropically radiated power *(EIRP)*, is set to 3.2W and 4W according to ETSI and FCC RFID standards, respectively. The maximum read range can be obtained theoretically from Friis free-space formula [15]:

$$r_{max} = \left(\frac{\lambda}{4\pi}\right)\sqrt{\frac{(EIRP)G_{tag}\tau}{P_{min,tag}}} \qquad (12)$$

Where (as showed in Figure 1) G_{tag} is the gain of the tag antenna, τ is the power transmission coefficient, λ is the wavelength in free space at the operating frequency, $P_{min,tag}$ is the minimum power required to turn on the tag chip.

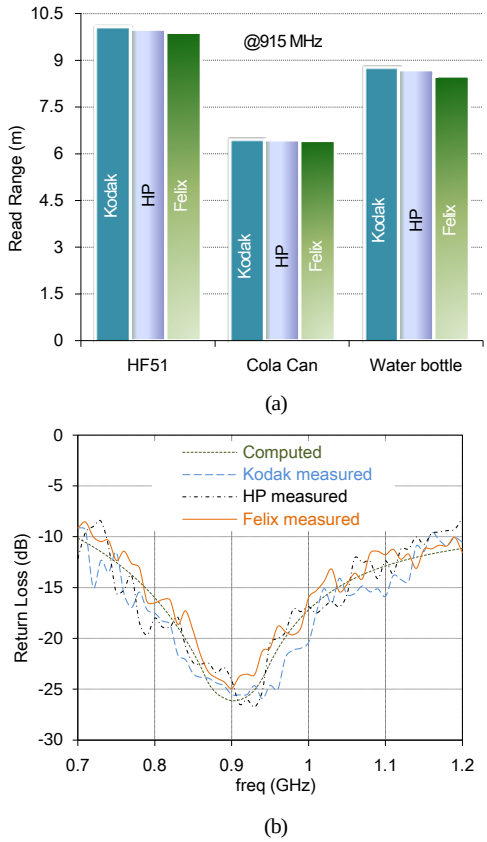

Fig. 5. (a) Measured read range, (b) measured and computed return loss.

The read range performance testing is conducted with Impinj's UHF RFID reader Kit and in order to make the measurement more edifying, the proposed tag is bonded on a closed-cell rigid foam HF51 from ROHACELL's with 90mm thickness [16]. The foam is based on polymethacrylimide (PMI) chemistry and has extremely low dielectric constant of 1.057@2.5GHz, resembling that of the free space and is especially designed for antenna applications. This setup facilitates to determine the tag read range variation when placed on different objects, as analyzed in Figure 5(a) for cardboard cartons exclusively containing cola cans and plastic water bottles. The measured read range validates the exceptional performance of the proposed RFID tag and is in

coherence with the calculated values by (12).

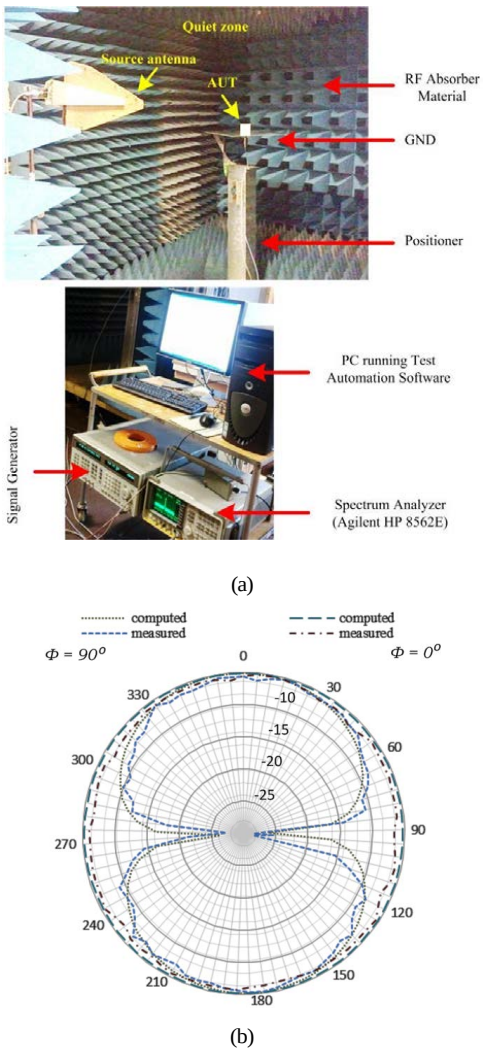

Fig. 6. (a) The anechoic chamber & instruments used, (b) 2D measured and computed far-field radiation plots.

The return loss of the antenna is calculated based on the power reflection coefficient on the basis of the data acquired by Half-Mirror method [17]. Figure 5(b) shows the measured and computed return loss of the proposed antenna. The distortion in the measured values is due to the ground plate fixture used for half-mirror method, which can be reduced or eliminated by using ground plate with more curved edges. It can be deduced that a fair agreement exists between the computed and measured results, in spite of the higher metal loss of the silver-based conductive ink.

The radiation patterns are measured inside an anechoic chamber arrangement as showed in Figure 6(a), that replicates absolute free space [13]. The antenna under test (AUT) is placed in the center of the chamber, and a continuous-wave (CW) signal excites the antenna, and the AUT is rotated by a positioner to obtain a 360° radiation pattern. The 2D measured and computed normalized radiation patterns of antenna printed on Kodak photopaper at characteristic frequency of 915MHz are plotted in Figures 6(b). The antenna exhibits stable gain values throughout the frequency band of interest with directivity of 2.3dBi. The radiation patterns are almost uniform (omnidirectional) at 915MHz and show tremendous match between computations and measurements, which can also be demonstrated for other frequencies (860-960MHz) within the antenna bandwidth, and are in consistency with earlier published results [5], [12].

Table 2 provides the parametric comparison of proposed RFID antenna along with best available previously reported paper-based T-matched bowtie antennas for operational frequency from 860MHz – 960MHz. It can be seen that the proposed antenna has better return loss, 52% improvement in bandwidth and 10% higher gain. As a result, higher read range is obtained. The proposed antenna is also smaller in size than the [5]. Moreover, hole-matching technique leads to less ink consumption as compared to relatively smaller structure of [12].

Table 2. Comparison of antenna parameters.

Substrate	Propose Antenna Hole-Matching	[5] T-Matching	[12] T-Matching
Return Loss (dB)	-15 to -26	-15 to-25	-15 to -21
BW (MHz)	290	190	197
Size	100 x 43	122.2 x 50	90 x 45
Gain (dBi)	2.3	2.1	2.1
Read Range (m)	10.1	-	9

IV. Sustainability & Environmental Impacts Analysis

Nanotechnology (nano-particle based ink) offers a variety of

benefits over traditional materials and enables the development of innovative applications and products. However, there are often concerns about the safety aspects and to what extent these have been investigated. High-quality measurements are the basis for reliable safety assessments, process improvement, quality control and the development of new nanotechnology applications. Thus, at present it is unreasonable to use silver nano-particle based ink products directly on food items [18].

This section emphasis on sustainability and environmental impacts analysis for the proposed antenna to validate that it has the potential to be used in various RFID-based eco-friendly applications. Figure 2 explicitly shows the dimension of the antenna which leads to determine the area required to accommodate antenna on the substrate that is 10cm x 4.3cm. Inkjet printing is considered for tracing the pattern on the substrate. The environmental impacts model is created a (Figure 7) by using life cycle assessment software "GaBi" [19].

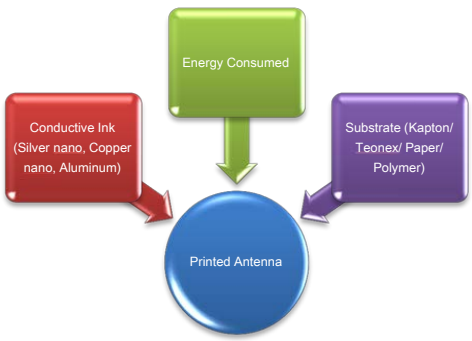

Fig. 7. Parametric model required for sustainability analysis.

Inkjet printing is accomplished by using Fujifilm Diamatix printer which is operated at 230V AC, 50Hz with maximum power consumed at any moment is 375Watt. The estimated time required for printing a pattern is approximately 15 minutes. If the printer operates at its maximum power rating, the energy required to print 1 million patterns is 337500 Mega Joules i.e. $(375 \times 15 \times 60 \times 10^6)$. The substrate under test is high gloss inkjet photo paper with standard weight of 280g/m^2 and thus for 1 million tags the required weight of paper substrate is 975.545kg $(230 \times 99.8 \times 42.5 \times 10^{-3})$. The capability of the printer to produce the antenna trace on paper substrate is 4000 structures with 1000ml (1kg) of conductive ink. Therefore, the estimated amount of conductive ink consumed for production of 1 million tags is 250kg. The mass of each component for manufacturing 1 million proposed RFID antennas is summarized in Table 3.

The Institute for Environment and Sustainability, European Commission Joint Research Centre, has published the research report [20] that recommends a preferred methodological approach which aims to calculate the environmental footprints of the products and organizations. For product environmental footprint, "ISO 14044: Environmental management- Life Cycle Assessment" is a recommended method. This method is employed to analyze the environmental footprint sustainability analysis of the proposed printed antenna. Life cycle approach takes into consideration the spectrum of resources flows and environmental interventions associated with the product, service, or organization from a supply chain perspective, including all phases from raw material acquisitions through processing, distribution, use and end of life processes. There are different methods such as TRACI (Tools for reduction and Assessment of Chemical and other Environmental Impacts) and CML (Centre for Environmental Studies, University of Leiden) that are employed to perform life cycle impact assessment. In this study, LCIA-CML methodology is considered to achieve the projected research analysis.Based on the modeling parameters possible environmental impacts are explored in terms of global warming potential ($KGCO_2$ equivalent), acidification potential ($KGSO_2$ equivalent), ozone layer depletion potential and human toxicity potentials.

Table 3. Mass of each component specified in the model and quantitative comparison for producing 1 million tags.

Substrate	Ink Consumed (kg)	Substrate Consumed (kg)	Energy Consumed (MJ)
Proposed Antenna	250	976	337500
[5]	270	982	495000
[12]	260	975	405000

Figure 8 shows the potential environmental impacts in the manufacturing process of the proposed printed antenna. Four main environmental impacts are demonstrated and in each emission profile, there are four columns that correspond to the quantity of emissions caused by a specific component such as substrate, conductive ink or the associated energy consumptions in manufacturing 1 million printed antennas. $KGCO_2$ and $KGSO_2$ are carbon dioxide and sulphur dioxide equivalent emissions while ozone layer depletion and human toxicity potentials are computed by the release of trichlorofluoromethane (CFC-11, also known as R11) and dichlorobenzene (DCB), respectively.

The proposed antenna is compared with standard already

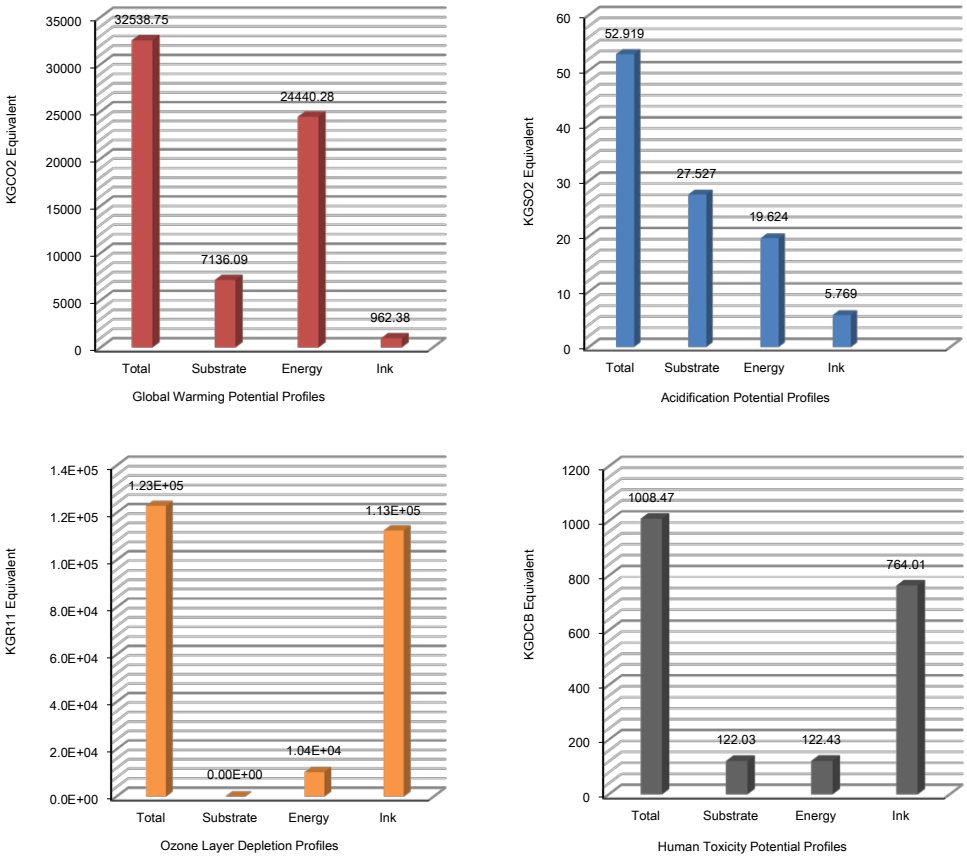

Fig. 8. Environmental Emissions Profiles.

published antennas which have exhibited superior performance than any other topology, in terms of read range and reliability to some extent when stumble upon metal or water containing objects. Table 3 provides the quantitative analysis for manufacturing 1 million structures of standard antennas in comparison with the proposed structure. It is obvious that the proposed antenna is rather more eco-friendly than previously realized structures as it consumes fewer quantities while exhibiting more exalted performance, which substantiates widespread acceptability of hole-matching technique in fusion with rounded corner structures in imminent circuits of organic electronics.

V. Conclusion

In this paper, several key deign parameters of bowtie antenna are reconsidered for their optimization in order to realize on commercial paper substrates while significantly increasing RFID read range up to 10.1 meters. The rigorous optimization criteria resulted into implementation of all the new hole-matching technique for improving the reliability against mechanical scratches by eliminating the extra matching pattern. This technique in combination with rounded corners resulted into wider bandwidth of operation and smaller structural dimensions, which paves the way for saving manufacturing ingredients. The proposed antenna is a perfect choice for roll-to-roll fabrication of ultra-low cost, flexible organic tags. The sustainability and environmental impacts reckoning for the printed antennas can be applied as a manufacturing yield benchmark for future productions.

References

[1] J. H. Bae, W. K. Choi, C. W. Park, C. S. Pyo, and K. T. Kim, "Design of Reader Baseband Receiver Structure for Demodulating

Backscattered Tag Signal in a Passive RFID Environment," *ETRI Journal*, vol. 34, no. 2, 2012, pp. 147-158.

[2] R. Bhattacharyya, C. Floerkemeier, and S. Sarma, "Low-Cost, Ubiquitous RFID-Tag-Antenna-Based Sensing," *Proceedings of the IEEE*, vol. 98, no. 9, 2010, pp. 1593-1600.

[3] S. J. Hwang, Y. Han, S. W. Kim, and J. O. Kim, "Streaming RFID: Robust Stream Transmission over Passive RFID," *ETRI Journal*, vol. 33, no. 3, 2011, pp. 382-392.

[4] T.-W. Koo, D. Kim, J.-I. Ryu, H.-M. Seo, J.-G. Yook, and J.-C. Kim, "Design of a Label-Typed UHF RFID Tag Antenna for Metallic Objects," *IEEE Antennas and Wireless Propagation Letters*, vol. 10, 2011, pp. 1010-1014.

[5] A. Rida, L. Yang, R. Vyas, and M. M. Tentzeris, "Conductive Inkjet-Printed Antennas on Flexible Low-Cost Paper-Based Substrates for RFID and WSN Applications," *IEEE Antennas and Propagation Magazine*, vol. 51, no. 3, 2009, pp. 13-23.

[6] D. M. Dobkin, *The RF in RFID: passive UHF RFID in practice*. Newnes, 2007.

[7] Y.-S. Chen, S.-Y. Chen, and H.-J. Li, "A Novel Dual-Antenna Structure for UHF RFID Tags," *IEEE Transactions on Antennas and Propagation*, vol. 59, no. 11, 2011, pp. 3950-3960.

[8] H. B. Kang, S. K. Hong, Y. W. Song, M. Y. Sung, B. Choi, J. Chung, and J. W. Lee, "High Security FeRAM-Based EPC C 1 G 2 UHF(860 MHz-960 MHz) Passive RFID Tag Chip," *ETRI journal*, vol. 30, no. 6, 2008, pp. 826-832.

[9] H.-W. Son, H.-G. Jeon, and J.-H. Cho, "Flexible wideband UHF RFID tag antenna for curved metal surfaces," *Electronics Letters*, vol. 48, no. 13, 2012, pp. 749-750.

[10] S. Myong, S. Mo, H. Yang, J. Cha, H. Lee, and D. Seo, "Location Error Analysis of an Active RFID-Based RTLS in Multipath and AWGN Environments," *ETRI Journal*, vol. 33, no. 4, 2011, pp. 528-536.

[11] G. Orecchini, F. Alimenti, V. Palazzari, A. Rida, M. M. Tentzeris, and L. Roselli, "Design and fabrication of ultra-low cost radio frequency identification antennas and tags exploiting paper substrates and inkjet printing technology," *IET Microwaves, Antennas & Propagation*, vol. 5, no. 8, 2011, pp. 993-1001.

[12] Y. Amin, Q. Chen, L. R. Zheng, and H. Tenhunen, "Development and Analysis of Flexible UHF RFID Antennas for 'Green' Electronics," *Progress In Electromagnetics Research*, vol. 130, 2012, pp. 1-15.

[13] X. Qing, C. K. Goh, and Z. N. Chen, "Impedance Characterization of RFID Tag Antennas and Application in Tag Co-Design," *IEEE Transactions on Microwave Theory and Techniques*, vol. 57, no. 5, 2009, pp. 1268-1274.

[14] S. Pranonsatit, D. Worasawate, and P. Sritanavut, "Affordable Ink-Jet Printed Antennas for RFID Applications," *IEEE Transactions on Components, Packaging and Manufacturing Technology*, vol. 2, no. 5, 2012, pp. 878-883.

[15] K. V. S. Rao, P. V. Nikitin, and S. F. Lam, "Antenna design for UHF RFID tags: a review and a practical application," *IEEE Transactions on Antennas and Propagation*, vol. 53, no. 12, 2005, pp. 3870-3876.

[16] ROHACELL, "ROHACELL HF 51." 2012.

[17] C. A. Balanis, *Antenna theory: analysis and design*. Wiley-Interscience, New York, 2005.

[18] FrogHeart, "Figuring out our knowledge gaps (European Agency for Safety and Health at Work) and fillng them ," *Online: www.frogheart.ca/?tag=nanomaterials*.

[19] G. B. Education, "Handbook for Life Cycle Assessment (LCA)," *Using the GaBi Education Software Package, PE International*, 2011.

[20] Chomkhamsri K. and P. N., "Analysis of Existing Environmental Footprint Methodologies for Products and Organizations: Recommendations, Rationale and Alignment," 2011.

Paper VI–Green Wideband RFID Tag Antenna for Supply Chain Applications

Y. Amin, R. K. Kanth, P. Liljeberg, Q. Chen, L.-R. Zheng, and H. Tenhunen, *IEICE Electronics Express*, vol. 9, no. 24, pp. 1861-1866, 2012

ELectronics EXpress

LETTER

IEICE Electronics Express, Vol.9, No.24, 1861–1866

Green wideband RFID tag antenna for supply chain applications

Yasar Amin[1a)], **Rajeev Kumar Kanth**[2], **Pasi Liljeberg**[2], **Qiang Chen**[1], **Li-Rong Zheng**[1], **and Hannu Tenhunen**[1,2]

[1] *iPack VINN Excellence Center, Royal Institute of Technology (KTH) Isafjordsgatn 39, Stockholm, SE-16440, Sweden*

[2] *TUCS, Department of Information Technology,University of Turku Turku-20520, Finland*

a) *ysar@kth.se*

Abstract: In this paper, we demonstrate for the first time an RFID tag antenna manufactured by advanced inkjet printing technology on paper substrate using novel hole-matching technique for reducing the consumption of substrate material and conductive ink while attaining green RFID tags. In-depth electromagnetic analysis is performed methodologically for optimizing the parameters that effectuate the antenna dimensions. The antenna design is optimized for consistent wideband performance and extended read range throughout the complete UHF RFID band (860–960 MHz), while exhibiting benchmarking results when n across cardboard cartons filled with metal or water containing objects.

Keywords: RFID tag, wideband antenna, inkjet printing, paper substrate, green electronics

Classification: Microwave and millimeter wave devices, circuits, and systems

References

[1] Y. Zuo, "Survivable RFID systems: issues, challenges, and techniques," *IEEE Trans. Syst. Man, Cybern. C, Appl. Rev.*, vol. 40, no. 4, pp. 406–418, July 2010.

[2] G. M. Gaukler, "Item-level RFID in a retail supply chain with stock-out-based substitution," *IEEE Trans. Ind. Informat.*, vol. 7, no. 2, pp. 362–370, May 2011.

[3] K. V. S. Rao, P. V. Nikitin, and S. F. Lam, "Antenna design for UHF RFID tags: a review and a practical application," *IEEE Trans. Antennas Propag.*, vol. 53, no. 12, pp. 3870–3876, Dec. 2005.

[4] I. Bose and S. Yan, "The green potential of RFID projects: a case-based analysis," *IT Professional*, vol. 13, no. 1, pp. 41–47, Jan.-Feb. 2011.

DOI: 10.1587/elex.9.1861
Received November 25, 2012
Accepted November 29, 2012
Published December 21, 2012

1 Introduction

Passive radio frequency identification (RFID) has recently engrossed much attention from retailers and manufacturers in all areas of the supply chain [1, 2]. It is a contactless identification technique that transmits data from an identification tag to a reader device via electromagnetic waves by obeying backscattering principle [3]. Presently majority of the RFID circuits are fabricated on nonbiodegradable substances i.e., FR-4 or PET. In order for businesses to minimize their impact on the environment, there is a need to limit this adversely challenging factor [4].

This paper presents eco-friendly wideband (860–960 MHz) RFID tag antenna inkjet printed on commercially available paper substrate. We have addressed the newfangled set of parameters emerging in RFID antennas while entering the era of green RFID revolution by evaluating and optimizing the key design parameters which are affected by the utilization of paper substrate. The proposed antenna uses innovative technique of square pattern holes for conjugately impedance matching with the RFID chip, thus eliminating the use of matching network and reduces the ink usage. The proposed tag is a perfect choice for far-field industrial applications especially for large items-level tracking in supply chain (cardboard cartons containing water & metal objects) and freight (wood or metal pallet) transportation.

2 Antenna design analysis and optimization

The proposed antenna is optimized in an organized approach for maximizing the read range while minimizing the ink consumption. One of the critical observations made while field testing (in supply chain industry) of antennas having thinner traces used for matching network, is that the effect of even minor scratches on those tracks can cause loss of RFID tags during transportation. Therefore, it led us towards the realization of a structure which can eliminate such risk factors while exhibiting better performance. Design computations and optimizations are performed using ANSYS HFSS^{TM} for the target IC NXP UCODE G2XM (13.3-j122 Ω@915 MHz). The substrate adopted is Kodak photopaper of 250 μm thickness (280 gm/m^2) with dielectric permittivity of $\varepsilon_r = 3.2$, and loss tangent tan $\delta = 0.077$, characterized at 1 GHz@25°C. The primary aim of parametric optimization is to maximize the feeding power to the load (IC). An often neglected issue during designing an (RFID) antenna is how directivity and gain are related to its physical dimensions. In view of the fact that the field/current, on the antenna aperture is not uniform, the parametric optimization of antenna effective aperture is carried out, as the effective aperture A_e is less than the physical aperture A_p. The directivity in terms of the aperture size and aperture efficiency is:

$$D = \frac{4\pi}{\lambda^2} A_e = \frac{4\pi}{\lambda^2} \eta_{ap} A_p \tag{1}$$

It is observed that η_{ap} is generally 50 to 80%. By knowing the power density S at the receiving antenna, we have estimated the received power at the tag:

$$P_r = S A_e \tag{2}$$

DOI: 10.1587/elex.9.1861
Received November 25, 2012
Accepted November 29, 2012
Published December 21, 2012

Hence during optimization strategy, much effort is devoted for improving the effective aperture in order to boost the antenna gain which consequently increases the amount of power delivered to the chip.

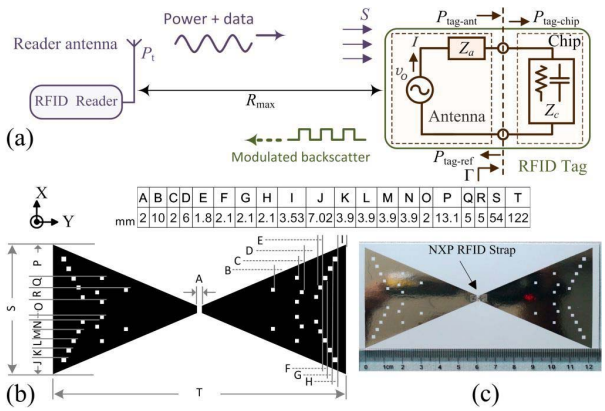

Fig. 1. (a) Far-field RFID mechanism & tag equivalent circuit; (b) geometry & dimensions of proposed antenna; (c) printed tag on paper.

Now by achieving maximum effective aperture A_{e-max} of the tag antenna located in the field of the reader antenna with the power density S as showed in Fig. 1(a). The tag antenna receives the power from the wave and delivers it to the RFID chip (strap) with load impedance Z_c. Fraction of the power received by the tag antenna is delivered to the chip whereas the remaining portion of power is reflected and re-radiated by the antenna. Thus, the power transmission coefficient, τ is used to calculate the power delivered to the RFID chip. Mathematically, it is expressed as:

$$P_{tag-chip} = \tau P_{tag-ant} \tag{3}$$

where $P_{tag-ant}$ is the power antenna received from the incident wave, and $P_{tag-chip}$ is the power delivered to the chip. The power transmission coefficient, τ, is determined by the impedance matching between the tag antenna and the chip. Therefore, good impedance matching between antenna and chip is of paramount importance. In the Thevenin equivalent circuit of the tag showed in Fig. 1(a), $Z_c = R_c + jX_c$ is the complex chip impedance and $Z_a = R_a + jX_a$ is the complex antenna impedance. The Z_c takes in the effects of strap and chip package parasitics. It is worth mentioning here that both Z_a and Z_c are frequency-dependent. Power wave reflection coefficient Γ is defined to evaluate the transmission of the power waves as:

$$\Gamma = \frac{Z_c - Z_a^*}{Z_c + Z_a}, \quad 0 \le |\Gamma| \le 1 \tag{4}$$

Thus, the power delivered to the chip is:

$$P_{tag-chip} = \left(1 - |\Gamma|^2\right) P_{tag-ant} \tag{5}$$

DOI: 10.1587/elex.9.1861
Received November 25, 2012
Accepted November 29, 2012
Published December 21, 2012

Therefore, the power transmission coefficient is calculated by:

$$\tau = \frac{P_{tag-chip}}{P_{tag-ant}} = 1 - |\Gamma|^2 = \frac{4R_aR_c}{(R_a+R_c)^2 + (X_a+X_c)^2}, \quad 0 \le \tau \le 1 \qquad (6)$$

From Eq. (5) maximum power is transferred when the antenna is conjugately matched to the chip, i.e. $R_c = R_a$ and $X_c = -X_a$, then $|\Gamma| = 0$, $\tau = 1.0$. After rigorously going through iterations based on this numerical analysis, we have achieved 20% compact structure than its counterpart T-matched design, and Eq. (2) takes the form:

$$P_{tag-chip-max} = P_{tag-ant} = SA_{e-max} \qquad (7)$$

The skin depth is evaluated through:

$$\delta = \sqrt{\frac{1}{\pi f \mu \sigma}} \qquad (8)$$

Thus, at UHF in accordance with Eq. (8), the conductive traces are made to obtain a thickness of the same order of magnitude as the skin depth. However, it is observed that in case the thickness is equal to or thinner than the skin depth, the total resistance of a printed conductive trace with fixed trace width is proportional to the overall trace length and inversely proportional to the conductor thickness.

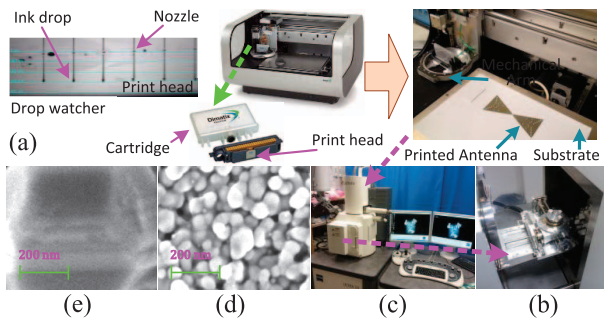

Fig. 2. (a) Inkjet printing setup; (b) SEM sample holder; (c) SEM setup; SEM images of three layers of printed silver nanoparticle ink, after curing 2hr at: (d) 100°C, (e) 150°C.

In previously reported results cavities were used in the antenna arms for either brand identification or ink saving, but in both cases this practice terminates into inferior current distribution in the antenna arms. However in the proposed antenna, the induction of pattern holes is effective for matching of the antenna impedance to that of the IC through the fine tuning of their location and size which is mentioned in Fig. 1(b) without deteriorating the current distribution. It is observed that earlier efforts to reduce the ink usage also led towards lower gain and as a result, the scope of those tags is limited

DOI: 10.1587/elex.9.1861
Received November 25, 2012
Accepted November 29, 2012
Published December 21, 2012

in supply chain industry. In the proposed procedure for achieving multidimensional performance benefits, the pattern holes suite these requirements effectively. It is noticed that the inner holes positions (B-D) are more persuasive towards antenna efficiency whereas, the outer hole positions (E-I) assist more towards fine tuning the impedance. The vertical holes positions (J-P) are critical towards current distribution. Therefore, this efficient technique in combination with above mentioned optimizing method not only fulfilled the matching criteria, but also reduced the conductive ink consumption by 35% without performance degradation.

The proposed structure is inkjet printed on paper substrate with print resolution of 1270 dpi by using silver nano-particle based ink (CCI-300 from Cabot Corp.) with Fujifilm Dimatix DMP 2800 printer as showed in Fig. 2(a). The resultant thickness of single layer of the printed trace is around 600 nm, which goaded to print three layers of the proposed antenna pattern (showed in Fig. 1(c)) in reference to limit the skin depth effect. After annealing, the characterization of the printed antenna structures is carried out under ULTRA-55 FESEM from Carl Zeiss NTS showed in Figures 2(b) & (c). Figures 2(d) & (e) show the SEMs for elaborating the difference between the heating temperatures. It is pragmatic under suitable annealing conditions 150°C/120 min, an almost solid metal conductor with measured conductivity of $9x10^6$–$1.1x10^7$ [S/m] is formed.

3 Field and circuit concepts parametric analysis

The characterization of reliability and repeatability is conducted by employing worst case analysis. Thus, for this reason maximum deviated values at a certain frequency are reported in impedance graphs. Impedance measurements are carried out with handheld (VNA) vector network analyzer (MS2026B, Anritsu) by using S-parameter measurement method. Figures 3(a) & (b) show the impedance plots. It is observed from Fig. 3(a) the computed and measured resistance for the antenna from 860–960 MHz varies between two extremes, from 13–15 Ω with mostly measured values maintain around 14 Ω. The reactance part of the impedance, as showed in Fig. 3(b), exhibits a positive value with a linear variation against frequency. The return loss of the proposed antenna is calculated based on the power reflection coefficient by using Eq. (4). Fig. 3(c) shows the measured and computed return loss of the proposed antenna with the measured bandwidth of the antenna in the worst case is 260 MHz, corresponding to 28% around the center frequency 910 MHz; so it covers the global UHF RFID bands and can cater greater degree of environmental disparities.

The read range measured by using Impinj's UHF RFID reader Kit validated that proposed tags exhibit consistent reading distance 7.5 meters and 9.3 meters while attached to cardboard cartons exclusively containing cola cans, and plastic water bottles, respectively. The radiation patterns are measured inside an anechoic chamber setup that replicates absolute free space. The antenna gain measurements are carried out by employing rigorous

DOI: 10.1587/elex.9.1861
Received November 25, 2012
Accepted November 29, 2012
Published December 21, 2012

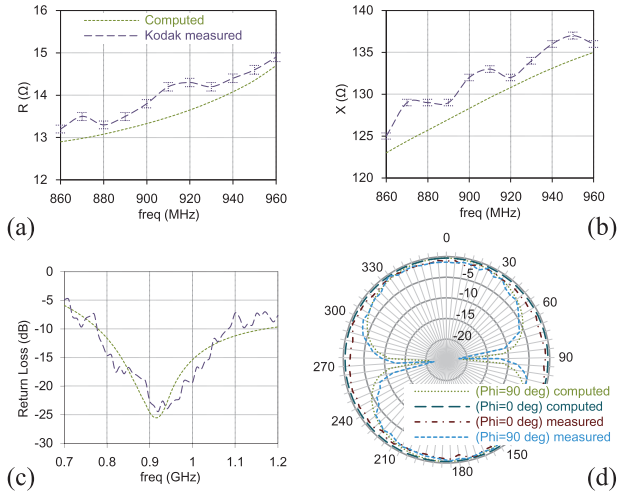

Fig. 3. (a) Resistance variation; (b) reactance variation; (c) measured & computed return loss; (d) 2D measured & computed far-field radiation plots.

three antennas measurement method, which proves surpassing directivity of 2.2 dBi despite the reduction in size and ink consumption. Fig. 3(d) shows the 2D measured normalized radiation patterns of antenna at characteristic frequency of 866 MHz. It is observed that radiation patterns are nearly uniform (omnidirectional) and show substantial concurrence between computations and measurements, which can also be established for other frequencies within the antenna bandwidth.

4 Conclusion

To the best of our knowledge, this is the first time novel hole-matching technique is realized in combination with antenna effective aperture optimization method for enhancing the RFID tag performance on paper substrate. The intended meticulous optimization approach resulted into extended read range of up to 9.3 meters, 20% compact antenna size while cutting down the ink consumption by 35%. Thus, this approach will be a milestone for future development of green RFID tags. The proposed antenna is a perfect choice for roll-to-roll printing of ultra-low cost flexible tags for supply chain applications.

Acknowledgments

This work was financially supported by Vinnova (The Swedish Governmental Agency for Innovation Systems) through the Vinn Excellence centers program.

DOI: 10.1587/elex.9.1861
Received November 25, 2012
Accepted November 29, 2012
Published December 21, 2012

Paper VII–Design and Fabrication of Wideband Archimedean Spiral Antenna Based Ultra-Low Cost "Green" Modules for RFID Sensing and Wireless Applications

Y. Amin, Q. Chen, L.-R. Zheng, and H. Tenhunen, *Progress in Electromagnetics Research*, vol. 130, pp. 241-256, 2012

Available online at: http://www.jpier.org/pier/pier.php?paper=12070807

Progress In Electromagnetics Research, Vol. 130, 241–256, 2012

DESIGN AND FABRICATION OF WIDEBAND ARCHIMEDEAN SPIRAL ANTENNA BASED ULTRA-LOW COST "GREEN" MODULES FOR RFID SENSING AND WIRELESS APPLICATIONS

Y. Amin*, Q. Chen, L. R. Zheng, and H. Tenhunen

iPack VINN Excellence Center, Royal Institute of Technology (KTH), Stockholm, SE-16440, Sweden

Abstract—A parametric analysis is performed for a wideband Archimedean spiral antenna in recognition of an emerging concept to integrate RFID along with several applications by using a single antenna. The antenna is fabricated using state-of-the-art inkjet printing technology on various commercially available paper substrates to provide the low-cost, flexible RF modules for the next generation of "green" electronics. The effects on electromagnetic characteristics of the planar Archimedean spiral antenna, due to the use of paper are investigated besides other parameters. The proposed antenna is evaluated and optimized for operational range from 0.8–3.0 GHz. It exhibits exceptional coverage throughout numerous RFID ISM bands so do for other wireless applications.

1. INTRODUCTION

RFID (Radio Frequency Identification) is considered an emerging leading technology in future telecommunications [1, 2], automatic identification and data capture (AIDC) industries [3]. The RFID market has grown in a two-dimensional trend one side constitutes standalone RFID systems which are commonly found at present [4–6]. On the other hand, more ultramodern approach is paving its way, in which RFID needs to be integrated with broad operational array of distinct applications [7, 8] for performing different functions including navigation, broadcasting, and personal communication [9–11], to mention a few. Using different antennas to include all communication

Received 8 July 2012, Accepted 13 August 2012, Scheduled 14 August 2012

* Corresponding author: Yasar Amin (ysar@kth.se).

bands is a straightforward approach, but at the same time, it leads to increasing cost, weight, more surface area for installation, and above all electromagnetic compatibility issues [12]. Thus, there is the need for wide-bandwidth antennas [13, 14]. The espousal of a single, small-sized wideband antenna is certainly more attractive because RFID is replacing other identification methods by whistling about cost-effective more efficient solutions [15, 16].

Spirals are extensively used circularly polarized wideband antennas [17]. The wideband features of spiral antenna brought it to the limelight in recent literature, particularly for miniaturization. The fundamental inspiration for miniaturization is to slow down the wave traveling within the antenna structure. Numerous approaches have been pursued to achieve it, which includes dielectric or magneto-dielectric loading, artificial materials, spiral arm shaping, distributed reactive loading and arm orienting vertically [12]. Conversely, when using the popular dielectric loading approach, the input impedance is also lowered. On the other hand, when the wave velocity is reduced by meandering of metalized arms, the axial ratio also deteriorates [17]. It has been established that coiling of the spiral arms provides for impedance control [12, 18]. The vast majority of circuits fabricated on PCB use FR-4 [19–22]; thus this volumetric design or miniaturization is weighty, whereas PET is commonly found in RFID inlays and tags. Furthermore, both FR-4, which is a ceramic-based material [23], and polyethylene terepthalate (PET) are nonbiodegradable substances that may take decades to decompose in landfills largely contributing to the bulk of annually generated electronic waste.

This paper presents parametric analysis of a flexible, wideband Archimedean antenna, which is fabricated by utilizing an exceptionally efficient and low-cost inkjet printing technique to print "green" conformal electronic circuits on paper substrate. Paper is extremely eco-friendly requiring a few months to decompose organically in landfills. Organic materials do tend to be more lossy at higher frequencies, due to their affinity to water. However, by using the correct paper type and printing process, adequate radio frequency performance is achieved on paper-based RF circuit designs. We demonstrate the successful use of the proposed inkjet printed antenna for operational range from 0.8–3.0 GHz. The design and simulations are performed using ANSYS HFSS^{TM}, whereas; the measurements are performed in an anechoic chamber dedicated to antenna characterization. The proposed antenna successfully operates throughout the operational range of interest, thus expanding the scope of simultaneously integrating several wireless modules while developing eco-friendly industrial solutions.

2. "GREEN" ANTENNAS EVOLUTION

The innovative concept of "green" broadband antennas perpetuated new set of parameters that constitute the proposed design stages mentioned in Figure 1. In contrast to traditional design flow, each stage of "green" evolution is loaded with a unique matrix of factors which need to be evaluated for integration with electronic devices. It is evident from the proposed evolution stages that the degree of

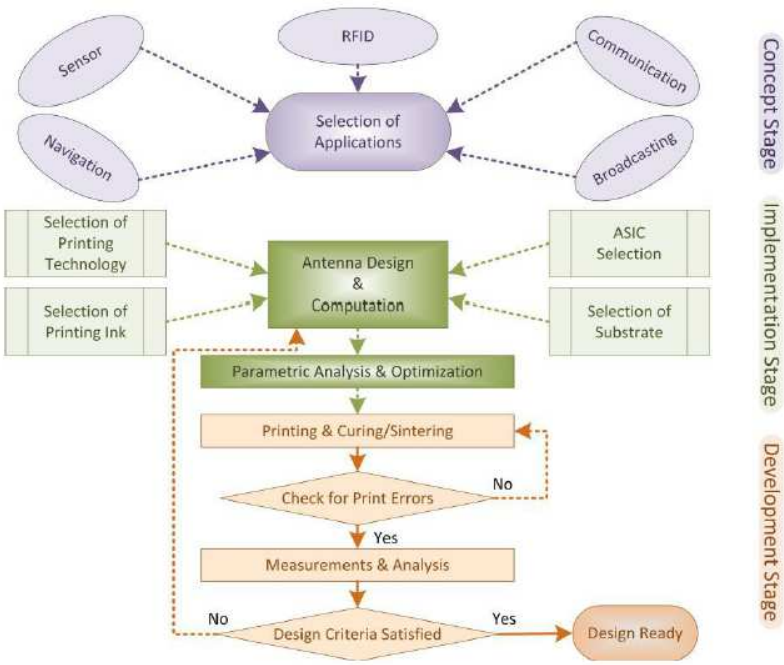

Figure 1. Evolution process of "Green" antennas for multi-module applications.

Table 1. Characterized/evaluated substrate parameters.

Substrate	Thickness (μm)	Permittivity (ε_r)	Loss Tangent
Kodak U-P Photopaper	250	3.3 (average)	0.077 (1 GHz@25°C)
HP Adv. Photopaper	250	3.3 (average)	0.04 (1 GHz@25°C)
Felix Schoeller Paper (p_e:smart)	250	3.2 (average)	0.077 (1 GHz@25°C)

freedom at the concept level, limits the choices at the implementation phase than development. Therefore, much effort is devoted to the implementation stage and design parameters are investigated and optimized categorically. Two types of conductive inks, CCI-300 from Cabot Corp. and Nano-AG-120I from Xerox Corp. are evaluated by trial printing in combination with three different types of commercially available paper substrates mentioned in Table 1. The key concept encapsulating the entire adaptation process is to achieve robust broadband antennas, which must show less sensitivity to the environmental variations that affect the paper dielectric constant.

3. SYNTHESIS OF THE ANTENNA TOPOLOGY

In order to achieve stable broadband multimode feature [24] multimode feature in far and near fields planar Archimedean spiral antenna structure is realized. Three designs of a two-arm Archimedean spiral antenna are assessed. The in-depth research proves that the Archimedean spiral is not a frequency-independent antenna structure because the spacing between the arms is specified by a constant, not an angle [25]. However, this is a contentious point because fundamentally frequency-independent performance is achieved over 10 : 1 bandwidths. The following numerical calculations are exploited to construct the proposed antenna structure in Figure 2. The centerline of the proposed Archimedean antenna is defined by:

$$r = a\phi = r_0 + (E)\phi^{(1/S)} \tag{1}$$

where,

$$a = \frac{1}{K}\frac{dK}{dC} \tag{2}$$

and C is the angle of rotation which depends on K. If the antenna is to be scaled to a frequency that is K times lower than the original

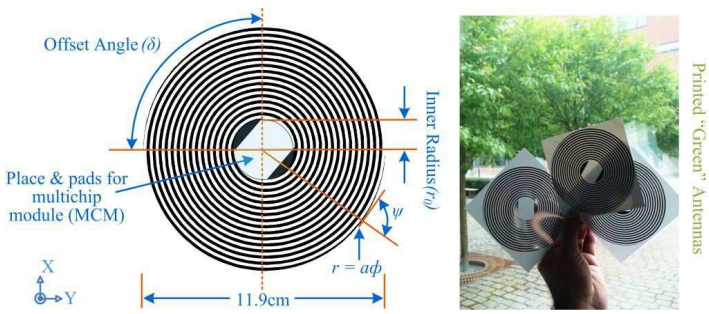

Figure 2. Dimensions & "green" theme of proposed antennas.

frequency, the antenna's physical surface must be made K times greater to maintain the same electrical dimensions [26]. The Expansion coefficient (E) and the Spiral coefficient (S) of the proposed antenna are 1 whereas, r_0 is the inner radius which is 1.6 cm. The pitch angle ψ varies with radius as:

$$\tan\psi = \frac{r}{a} \tag{3}$$

When r is large, then the pitch angle approaches 90°. An equivalent design ratio τ_{eq}, which varies with radius, may be defined for the Archimedean spiral that has the same pitch angle ψ at radius r. Therefore,

$$\tau_{eq}(r) = e^{-2\pi/|\tan\psi|} = e^{-2\pi|a/r|} \tag{4}$$

It is worth noting here that τ_{eq} approaches 1 for large value of r. The sides of a strip may be defined in terms of the rotation angle ϕ of Figure 2 and the angle δ (offset angle is 90° of the proposed structure) to get:

$$r = a\left(\phi \pm \frac{\delta}{2}\right) \tag{5}$$

The radial width of the antenna strip W_r is a constant, which is independent of radius and is obtained by:

$$W_r = a\delta \tag{6}$$

The actual width of the antenna strip varies to some extent with radius and is calculated by:

$$W = a\delta\sin\psi \tag{7}$$

The spacing S_r between the centerlines of the adjacent turns for one arm is specified by:

$$S_r = 2\pi a \tag{8}$$

Furthermore, the actual spacing is given by:

$$S = S_r\sin\psi = 2\pi a\sin\psi \tag{9}$$

The two-arm spiral antenna proposed in Figure 2 for frequency band 0.8–3 GHz is self complementary when $W/S = 1/4$ or $\delta = \pi/2$ [26]. Given that the strip widths and spacings are defined by constants rather than by angles, Archimedean spiral antenna does not conform to either the frequency-independent or log-periodic principles [25]. Thus, this antenna gives autonomy to those ASIC manufacturers [27, 28] which have frequency dependent modules. In practice, it is observed that frequency independent characteristics are obtained if τ is large enough in the active region (i.e., radiation region), wherein the circumference of the radiation ring is about one

length. Alas, diminutive information has been published [12, 29] on the degradation of gain and patterns versus τ. Some published results indicate the loosely wound log-spiral performs as well as the tightly wound Archimedean spirals; however, this analysis is out of scope of this article.

4. MANUFACTURING PARAMETRIC ANALYSIS

4.1. Skin Depth Effect and Antenna Performance

It is well established that the thickness of the printed design needs to be larger or closer to the value of skin depth in order to achieve optimal performance [3, 30]. For a normal conductor, the skin depth can be computed as [31]:

$$\delta = \sqrt{\frac{1}{\pi f \mu \sigma}} \tag{10}$$

where f is the frequency, σ the conductivity, and μ the permeability of the conducting material. The conductivity of the printed traces of silver nano-particle based inks used in this research, after curing, is high enough (for Xerox ink $\approx 0.7 \times 10^7$ S/m and for Cabot ink $\approx 0.9 \times 10^7$ S/m) to be considered as a good conductor, but not as high as bulk silver. The skin depth for traces of the proposed antenna with operational frequency at 800 MHz is evaluated using Equation (10). The thickness of the printed single layer of ink from the printer used is around 200 nm (Nano-AG-120I)–600 nm (CCI-300). It has been found after careful iterations that at least three layers of printing by Cabot ink and four layers of printing by Xerox ink, are sufficient to achieve better performance under the limits imposed by various design factors.

From Figures 3(e) & (f), it is obvious that the proposed antenna with 7.5-turns has improved LHCP (Figure 3(e)) and RHCP (Figure 3(f)) gain, than antennas with 6.5-turns (Figures 3(a) & (b)), and 7-turns (Figures 3(c) & (d)). This performance criterion is achieved without enlarging the antenna's physical aperture. Specifically, the antenna with 7.5-turns at approximately 1.9 GHz exhibits a 4.7-dB, 4.5-dB and 4.4-dB gain on Kodak, HP and Felix Schoeller paper(p_e:smart) respectively, by printing with Cabot ink. Whereas, by printing with Xerox ink the gain achieved at 1.9 GHz is 4.7-dB, 4.6-dB and 4.6-dB on Kodak, HP and Felix Schoeller paper respectively. It is depicted from Figure 3 that by further increasing the number of spiral turns, the gain improves at lower frequencies. It is observed that the antenna impedance also decreases with the increase in number of turns.

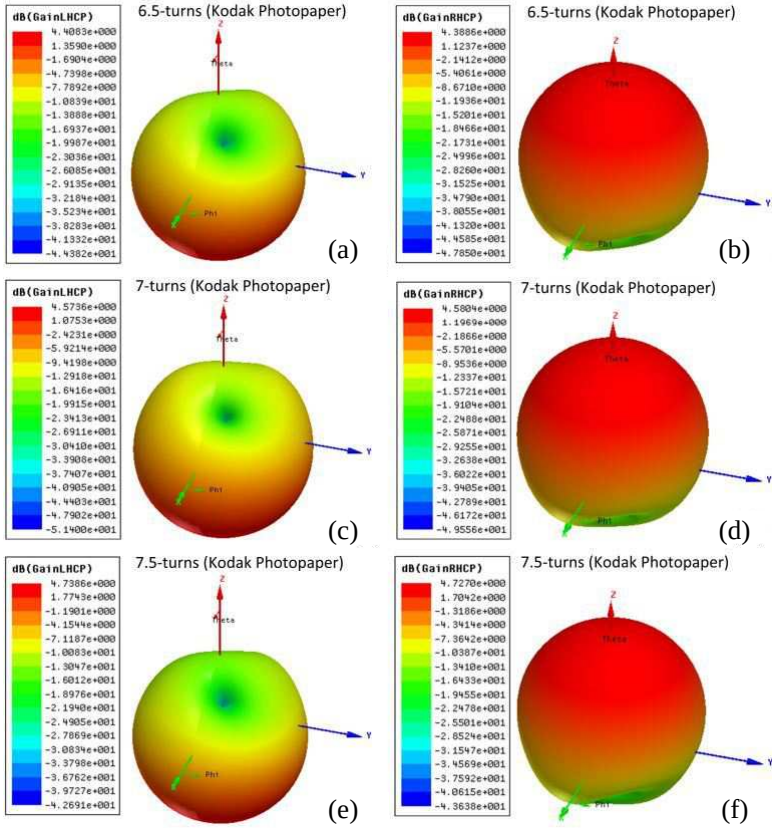

Figure 3. Simulated 3D LHCP & RHCP gain radiation patterns of antennas with 6.5, 7 and 7.5-turns.

On the other hand if the number of turns are reduced, the gain of the antenna decreases to a value which violates the design requirements because these tags are proposed for large items level tacking and information gathering. So it is mandatory for the antenna to exhibit better gain to achieve higher read range while at the same time providing readability in the near field region. Moreover, due to the consumption of expensive conductive ink, the size of the antenna has to be within economical limits for its possible realization on industrial scale. Therefore, the optimal design pattern is achieved while considering the size limits along with other performance factors for attaching to large items in the working range from 0.8–3.0 GHz is realized with 7.5-turns, and its current distribution plot is shown in Figure 4.

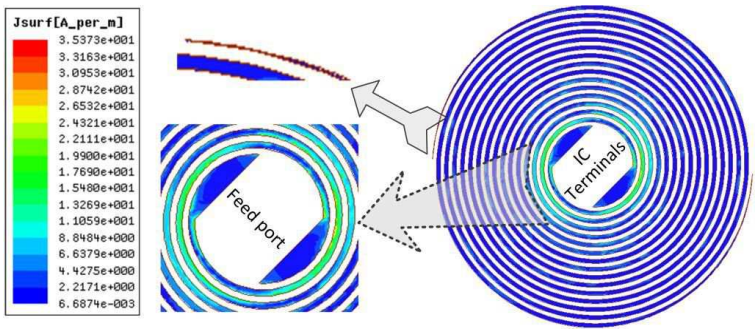

Figure 4. The current distribution of proposed antenna at 1.9 GHz.

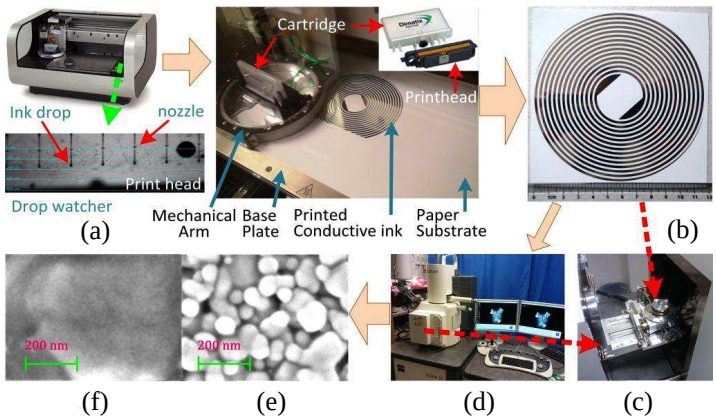

Figure 5. (a) Inkjet printing setup, (b) inkjet printed antenna on Felix Schoeller paper, (c) SEM sample holder, (d) ULTRA-55 FESEM Carl Zeiss setup; SEM images of three layers of printed silver nanoparticle ink, after curing 2 hr at: (e) 100°C, (f) 150°C.

4.2. Inkjet Printing

Inkjet printing is based on the drop-on-demand (DOD) mechanism by which the desired design is transferred directly to the (flexible) substrate. This technology requires no masks compared with the conventional etching technique, which has been commonly used in production, therefore, creating no waste, ensuing in an economical and eco-friendly manufacturing choice. Whereas, the proposed structure, utilizes more ink than [3, 15], but this cost is fully justified for exceptional degree of functionalities offered by the structure. The inkjet printer used in this research is Fujifilm Dimatix DMP2800 which

is a tabletop printer as showed in Figure 5(a). It employs one user fillable piezo-based inkjet print cartridge that has 16 nozzles in a single row with the spacing between two consecutive nozzles is 254 µm, and the substrate is held by vacuum plate. Figure 5(a) also shows the drop watcher view of ink drops of 10 pl in volume are ejecting out of DMC-11610 print cartridge which can be filled upto 1.5 ml.

The antenna structure on Felix Schoeller paper is showed in Figure 5(b) by using Cabot conductive ink having silver solid loading of 19–21 wt%. Furthermore, printing parameters are optimized for all the three paper substrate types using Xerox conductive ink having silver loading of 40 wt%. The optimized jetting voltage realized for both inks is 16–20 V with the velocity of around 5 m/s. The nozzle temperature is kept at room temperature, and the substrate vacuum plate, which is temperature controllable, is maintained at 40°C while printing with either ink. In order to keep the consistency for performing in-depth analysis, each combination is printed with 20 micron drop spacing and print resolution of 1270 dpi. The printer is equipped with Fiducial Camera, which provided the ease of substrate alignment using reference marks, and positioning a print origin or reference point to match substrate placement. Furthermore, it is used for evaluation of features and locations along with inspection and image capture of printed pattern or drops.

Two different sintering processes are evaluated after drying of ink on the substrate, first one is the prevalent method and the other is

Table 2. Annealing parameters for printed antennas.

Substrate	Xerox Ink Nano-AG-120I	Cabot Ink CCI-300	Temperature (°C)	Time (Minutes)
Kodak U-P Photopaper	√	-	140	30
Kodak U-P Photopaper	-	√	150	120
HP Adv. Photopaper	√	-	120	45
HP Adv. Photopaper	-	√	120	120
Felix Schoeller Paper	√	-	110	90
Felix Schoeller Paper	-	√	110	90

"PulseForge Technology" [32]. In the first approach sintering is carried out in the oven with ventilation system at different temperature and time (as mentioned in Table 2), depending upon the combination of ink and substrate, for sufficiently curing, removing the excess solvent and material impurities from the depositions.

The printed samples are also sintered through "PulseForge Technology" by Novacentrix USA, in order to demonstrate sintering and annealing for high-speed roll-to-roll manufacturing often in ambient air (and is capable of up to 1000 feet per minute). This approach enables the use of ultra low temperature and flexible substrates such as paper substrate, which cannot be annealed at high temperatures.

The characterization of the printed structures is carried out under ULTRA-55 Field Emission Scanning Electron Microscope from Carl Zeiss NTS showed in Figures 5(c) & (d). Figures 5(e) & (f) show the SEMs for elaborating the difference between the heating temperatures. At high temperature or by "PulseForge Technology", an almost solid metal conductor is formed so providing a percolation channel for the conduction of electrons throughout the material without obstruction. The sintering process also provides the derived benefit of increasing the bonding of the deposition with the paper substrate.

5. FIELD & CIRCUIT CONCEPTS PARAMETRIC ANALYSIS

A set of precise and thorough methods for evaluation of the reliability parameters and characterization of the proposed fabricated antenna on different paper substrates are implemented. Firstly, five identical structures are printed for each arrangement of ink and paper substrate. Secondly, in this study, an experimental methodology for the characterization of the impedance of the balanced tag antenna is implemented along with the balun structure. The balanced tag antenna is considered as a two-port network and the impedance of the antenna is characterized using network parameters. The antenna is connected to the two ports of a vector network analyzer through a test fixture mentioned in detail in [33]. The influence of the test fixture is deembedded by using a port-extension technique and the antenna impedance can be extracted directly from the measured parameters. Whereas, the broadband balun transforms the unbalanced coaxial mode into balanced two-wire transmission line mode that fed the spiral antenna. The accuracy of the measurements is increased if all errors up to the measuring instrument tip are eliminated [34]. This includes internal VNA errors after the sampler, the cables along with their tips

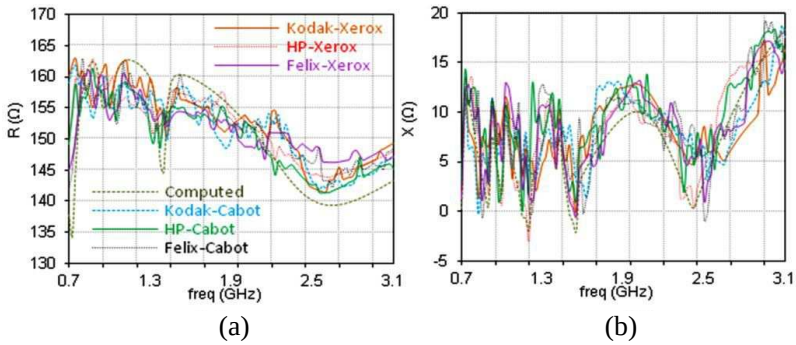

Figure 6. (a) Input resistance variation, (b) input reactance variation.

used to connect to the test structure. The reference plane is shifted to the tips by using the standard calibration methods SOLT (short-open-load-through) for two-ports technique and short-open-load (SOL) for balun structure.

Impedance measurements are carried out using handheld (VNA) vector network analyzer (MS2026B, Anritsu). The impedance graphs are presented in Figure 6 with the largest deviated value at a certain frequency which provides information for worst case analysis, in addition to exploration of performance parameters. This method helps in discovering potential variations that can take place due to the use of paper substrate, which is of critical significance. As showed in Figure 6(a), the measured resistance for the antenna between 1.1–1.4 GHz, fluctuates between 158–144 Ω and from 1.41–3.0 GHz, the variation of resistance is between 146–154 Ω but with much steady manner. However, exceptionally small deviation is pragmatic among the curves of all antennas and this behavior is stable over a much larger frequency range in accordance with published results for spiral structures in [12, 29]. The reactance part of the impedance, as showed in Figure 6(b), follows smaller positive values around 15 Ω with really small variation with frequency. Moreover, relatively constant harmony exists between the computed and measured results. This conforms to both frequency dependent & independent antennas in some extent; however, this behavior of impedance is deliberately achieved because most of the commercially available ASIC till date have also frequency dependence. More importantly, the impedance of the proposed antenna besides easier to match at lower frequencies.

The return loss of the antenna structure is calculated based on the power reflection coefficient. The computed return loss is showed along with measured values of the Xerox ink & Cabot ink printed antennas in Figure 7(a). From Figure 7(a), it is clear

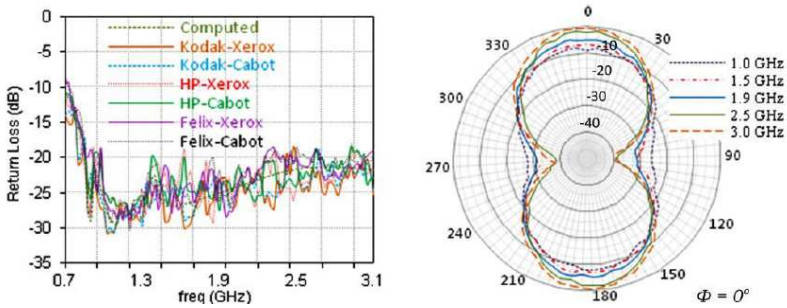

(a) (b)

Figure 7. (a) Measured & computed return loss, (b) measured & computed 2D far-field radiation plots.

that the proposed antenna has better return loss and is less than −15 dB throughout the frequency band of interest (and in eloquence with [35, 36]), which is the paramount requirement of antennas for optimal performance. Furthermore, the stable response of paper substrate at higher frequencies, (although with a certain amount of variations but within acceptable values) make it a suitable candidate for broadband antennas. Overall, a good agreement among the computed, Xerox ink printed, and the Cabot ink printed antennas is observed despite the higher metal loss of the silver-based conductive inks.

The radiation pattern is measured inside an anechoic chamber setup that replicates absolute free space [3] (however, half mirror method setup is used in [3]). The spiral antenna under test (AUT) is placed on a positioner assembly, which is set to rotate the antenna in small steps of 5 degrees to obtain a 360° radiation pattern. A continuous-wave (CW) signal from the signal generator excites the AUT. The receiver antenna is connected to the spectrum analyzer (Agilent HP 8562E) and a PC running the test automation software controls the measurement setup. The measured normalized radiation patterns (of antenna printed on Kodak photopaper using Cabot ink) at characteristic frequencies of (1.0, 1.5, 1.9, 2.5) & 3.0 GHz are plotted in Figure 7(b). It is observed that all of the radiation patterns have normal shape and show extreme similarity between computations and measurements, which can also be verified for other frequencies within the antenna bandwidth and are in coherence with previously published results [29]. Additionally, the measured radiation patterns exhibit a slight offset due to the feed line connecting to SMA. It can be depicted from Figure 7(b) that the radiation pattern does not deteriorate in the whole bandwidth from 0.8–3.0 GHz.

6. CONCLUSION

In this paper, it is the first time to propose wideband spiral antennas fabricated on paper substrate for simultaneously implementing a wide range of different modules in addition to, RFID tag. It is noted that adjusting the gap between the adjacent tracks to create the spiral arms leads to a larger number of turns within the same aperture size. All the previously published relevant work in contrast to the proposed approach, is focused on complex techniques, to make such antennas using nonflexible or contaminated substrates, which neither can be implemented with roll-to-roll printing nor suitable for eco-friendly applications. Although the presented research is specific to inkjet printed Archimedean spiral antennas, the same approach can be applied to other antennas made of printed strips, to form modules for "green" electronics.

ACKNOWLEDGMENT

The author would like to thank Peter Fuks in school of electrical engineering at KTH who generously provided research facilities. This work was financially supported by Vinnova (The Swedish Governmental Agency for Innovation Systems) through the Vinn Excellence centers program.

REFERENCES

1. Kim, M., K. Kim, and N. Chong, "RFID based collision-free robot docking in cluttered environment," *Progress In Electromagnetics Research*, Vol. 110, 199–218, 2010.
2. Garcia, J. A., L. Cabria de Juan, R. Marante, L. Rizo, and A. Mediavilla, "An unbiased dual-mode mixing antenna for wireless transponders," *Progress In Electromagnetics Research*, Vol. 102, 1–14, 2010.
3. Amin, Y., Q. Chen, H. Tenhunen, and L. R. Zheng, "Performance-optimized quadrate bowtie RFID antennas for cost-effective and eco-friendly industrial applications," *Progress In Electromagnetics Research*, Vol. 126, 49–64, 2012.
4. Tiang, J.-J., M. T. Islam, N. Misran, and J. S. Mandeep, "Circular microstrip slot antenna for dual-frequency RFID application," *Progress In Electromagnetics Research*, Vol. 120, 499–512, 2011.
5. Meng, Y. S. and Y. H. Lee, "Investigations of foliage effect on

modern wireless communication systems: A review," *Progress In Electromagnetics Research*, Vol. 105, 313–332, 2010.

6. Li, X., J. Liao, Y. Yuan, and D. Yu, "Eye-shaped segmented reader antenna for near-field UHF RFID applications," *Progress In Electromagnetics Research*, Vol. 114, 481–493, 2011.
7. Alejos, A. V., M. G. Sánchez, I. Cuinas, and J. C. G. Valladares, "Sensor area network for active RTLS in RFID tracking applications at 2.4 GHz," *Progress In Electromagnetics Research*, Vol. 110, 43–58, 2010.
8. Jamlos, M. F., A. R. B. Tharek, M. R. B. Kamarudin, P. Saad, O. A. Aziz, and M. A. Shamsudin, "Adaptive beam steering of RLSA antenna with RFID technology," *Progress In Electromagnetics Research*, Vol. 108, 65–80, 2010.
9. Panda, J. R. and R. S. Kshetrimayum, "A printed 2.4 GHz/5.8 GHz dual-band monopole antenna with a protruding stub in the ground plane for WLAN and RFID applications," *Progress In Electromagnetics Research*, Vol. 117, 425–434, 2011.
10. Sim, Z. W., R. Shuttleworth, M. J. Alexander, and B. D. Grieve, "Compact patch antenna design for outdoor RF energy harvesting in wireless sensor networks," *Progress In Electromagnetics Research*, Vol. 105, 273–294, 2010.
11. Jamlos, M. F., A. R. B. Tharek, M. R. B. Kamarudin, P. Saad, M. A. Shamsudin, and A. M. M. Dahlan, "A novel adaptive Wi-Fi system with RFID technology," *Progress In Electromagnetics Research*, Vol. 108, 417–432, 2010.
12. Guraliuc, A. R., R. Caso, P. Nepa, and J. L. Volakis, "Numerical analysis of a wideband thick archimedean spiral antenna," *IEEE Antennas and Wireless Propagation Letters*, Vol. 11, 168–171, 2012.
13. Ramos, A., A. Lazaro, D. Girbau, and R. Villarino, "Time-domain measurement of time-coded UWB chipless RFID tags," *Progress In Electromagnetics Research*, Vol. 116, 313–331, 2011.
14. Chen, A.-X., T.-H. Jiang, Z. D. Chen, and D. Su, "A novel low-profile wideband UHF antenna," *Progress In Electromagnetics Research*, Vol. 121, 75–88, 2011.
15. Amin, Y., Q. Chen, H. Tenhunen, and L. R. Zheng, "Evolutionary versatile printable RFID antennas for "Green" electronics," *Journal of Electromagnetic Waves and Applications*, Vol. 26, Nos. 2–3, 264–273, 2012.
16. Mahmoud, K. R., "Design optimization of a bow-tie antenna for 2.45 GHz RFID readers using a hybrid BSO-NM algorithm,"

Progress In Electromagnetics Research, Vol. 100, 105–117, 2010.

17. Filipovic, D. S. and J. L. Volakis, "Broadband meanderline slot spiral antenna," *2002 IEE Proceedings — Microwaves, Antennas and Propagation*, 98–105, 2002.
18. Zhu, Y.-Z. and J.-D. Xu, "Design of two-arm conical spiral antenna for low elevation angle communication," *Journal of Electromagnetic Waves and Applications*, Vol. 24, Nos. 5–6, 785–794, 2010.
19. Liao, W.-J., S.-H. Chang, and L.-K. Li, "A compact planar multiband antenna for integrated mobile devices," *Progress In Electromagnetics Research*, Vol. 109, 1–16, 2010.
20. Tze-Meng, O., K. G. Tan, and A. W. Reza, "A dual-band omni-directional microstrip antenna," *Progress In Electromagnetics Research*, Vol. 106, 363–376, 2010.
21. Secmen, M. and A. Hizal, "A dual-polarized wide-band patch antenna for indoor mobile communication applications," *Progress In Electromagnetics Research*, Vol. 100, 189–200, 2010.
22. Ou Yang, J., S. Bo, J. Zhang, and F. Yang, "A low-profile unidirectional cavity-backed log-periodic slot antenna," *Progress In Electromagnetics Research*, Vol. 119, 423–433, 2011.
23. De Cos, M. E., Y. Alvarez Lopez, R. C. Hadarig, and F. Las-Heras, "Flexible uniplanar artificial magnetic conductor," *Progress In Electromagnetics Research*, Vol. 106, 349–462, 2010.
24. Chen, J., G. Fu, G.-D. Wu, and S.-X., Gong, "A novel broadband circularly polarized irregular slot antenna," *Journal of Electromagnetic Waves and Applications*, Vol. 24, Nos. 2–3, 413–421, 2010.
25. Richard, C. J., *Antenna Engineering Handbook*, McGraw-Hill Inc., New York, 1992.
26. Balanis, C. A., *Antenna Theory*, John Wiley and Sons Inc., New Jersey, 2005.
27. Lin, D.-B., I.-T. Tang, and C.-C. Wang, "UHF RFID H-shaped tag antenna using microstrip feed design on metallic objects," *Journal of Electromagnetic Waves and Applications*, Vol. 25, No. 13, 1828–1839, 2011.
28. Hsu, H.-T., F.-Y. Kuo, and C.-H. Chang, "Application of quasi log- periodic antenna for UHF passive RFID tag design featuring constant power transmission coefficient over broadband operation," *Journal of Electromagnetic Waves and Applications*, Vol. 24, Nos. 5–6, 575–586, 2010.
29. Chen, T.-K. and G. H. Huff, "Stripline-fed archimedean spiral

antenna," *IEEE Antennas and Wireless Propagation Letters*, Vol. 10, 346–349, 2011.

30. Huang, Y. and K. Boyle, *Antennas from Theory to Practice*, John Wiley & Sons Ltd., New York, 2008.
31. Da Silveira, F. E. M. and J. A. S. Lima, "Skin effect from extended irreversible thermodynamics perspective," *Journal of Electromagnetic Waves and Applications*, Vol. 24, Nos. 2–3, 151–160, 2010.
32. PulseForge Technology, Available at www.novacentrix.com.
33. Kuo, S.-K., J.-Y. Hsu, and Y.-H. Hung, "Analysis and design of an UHF RFID metal tag using magnetic composite material as substrate," *Progress In Electromagnetics Research B*, Vol. 24, 49–62, 2010.
34. Zhao, W., Y.-J. Zhao, and H.-B. Qin, "Calibration of the three-port VNA using the general 6-term error model," *Journal of Electromagnetic Waves and Applications*, Vol. 24, Nos. 2–3, 319–326, 2010.
35. Schreider, L., X. Begaud, M. Soiron, B. Perpere, and C. Renard, "Broadband Archimedean spiral antenna above a loaded electromagnetic band gap substrate," *IET Microwaves, Antennas & Propagation*, Vol. 1, No. 1, 212–216, 2007.
36. Bell, J. M. and M. F. Iskander, "A low-profile Archimedean spiral antenna using an EBG ground plane," *IEEE Antennas and Wireless Propagation Letters*, Vol. 3, 223–226, 2004.

Paper VIII–"Green" Wideband Log-Spiral Antenna for RFID Sensing and Wireless Applications

Y. Amin, Q. Chen, L.-R. Zheng, and H. Tenhunen, *Journal of Electromagnetic Waves and Applications*, vol. 26, nos. 14-15, pp. 2043-2050, 11 Sep 2012

Available online at: http://www.tandfonline.com/10.1080/09205071.2012.724767

Journal of Electromagnetic Waves and Applications
Vol. 26, Nos. 14–15, October 2012, 2043–2050

Taylor & Francis
Taylor & Francis Group

"Green" wideband log-spiral antenna for RFID sensing and wireless applications

Y. Amin*, Q. Chen, L.R. Zheng and H. Tenhunen

iPack VINN Excellence Center, Royal Institute of Technology (KTH), Stockholm, SE 16440, Sweden

(*Received 15 July 2012; accepted 17 August 2012*)

The novel idea of integrating Radio Frequency Identification (RFID) with sensors along with other wireless applications by using single tag antenna is implemented, by fabricating proposed antenna using state-of-the-art inkjet printing technology on commercially available paper substrates. For the first time, a parametric analysis is performed for realization of the planar log-spiral antenna on paper for operational range from 0.8 to 3.0 GHz, which also exhibits excellent coverage throughout numerous RFID Industrial, Scientific and Medical (ISM) bands, and for other wireless applications. The ANSYS HFSS^{TM} tool is used to design and predict the performance of the proposed antenna in terms of radiation pattern and input impedance.

1. Introduction

As the modern society extends with the need for more information, many technologies for automatic identification materialized swiftly [1,2]. For several advantages over others [3], Radio Frequency Identification (RFID) is the most potential candidate [4] to be integrated in future communication systems but at the same time RFID is stepping into the sphere of influence where, there is much need of several integrated solutions [5]. In contrast to standalone solutions at present [6] for RFID tags, the future of RFID can constitute a brighter side of this technology by integrating tag with other wireless modules for broad operational range of different applications including, navigation, broadcasting, and personal communication [7,8], to mention a few. Thus, using separate antennas for each application module to cover the required communication band is a natural approach [9,10], but this approach not only increases the manufacturing cost, weight of the module, and the area for installation but also generate a complex set of electromagnetic compatibility issues. On the other side, the use of a single antenna for multiple applications will not only decrease the overall cost of the RF module but also more compact solutions can shift the paradigm of RFID industrial applications.

This paper presents electromagnetic analysis of a versatile, wideband planar log-spiral antenna, which is one of the extensively, used circularly polarized wideband antennas [11,12] that brought it to focus in the recent literature. In distinction to the previously reported antennas, the proposed antenna is manufactured by exploiting a remarkably effective and ultra-low-cost inkjet printing technology to print on extremely biodegradable paper substrates

*Corresponding author. Email: ysar@kth.se

ISSN 0920-5071 print/ISSN 1569-3937 online

http://dx.doi.org/10.1080/09205071.2012.724767
http://www.tandfonline.com

Table 1. Characterized/evaluated paper substrate parameters.

Substrate	Thickness (μm)	Permittivity (ε_r)	Loss tangent
Kodak U-P photopaper	250	3.3 (average)	0.077 (1 GHz@25 °C)
HP Adv. photopaper Felix Schoeller	250	3.3 (average)	0.04 (1 GHz@25 °C)
Paper (p_e:smart)	250	3.2 (average)	0.077 (1 GHz@25 °C)

mentioned in Table 1. We demonstrate the thriving use of the proposed inkjet-printed antenna from 0.8 to 3.0 GHz. The measurements are performed in an anechoic chamber devoted to antenna characterization. The proposed antenna exhibits exceptional performance throughout the operational range of significance, thus paving the way for developing eco-friendly multi-module RF industrial solutions.

2. Synthesis of the antenna topology

Numerous design topologies of a two-arm log-spiral antenna, which is one of the antenna configurations, that closely parallels the frequency independent concept are assessed. It is worth mentioning here that, the entire shape of proposed antenna cannot be entirely specified by angles it is not exactly frequency independent [13]. However, the construction of the proposed planar log-spiral structure is defined by the angles ψ and δ to obtain as much independence from frequency as possible within limits imposed by different factors mentioned throughout the text. The curve of the antenna in Figure 1(a) which has 1.25-turns is calculated by:

$$r = r_0 e^{a\phi} \tag{1}$$

where r_0 is the inner radius which is defined to be 1.36 cm in Figure 1(a) according to the area and space required for the multi-chip module/s package. The expansion coefficient a (which is governed by Equation (2)) of the proposed antenna is 2.88 and is related with the pitch angle ψ.

$$a = \frac{\ln(\tau)}{2\pi} \tag{2}$$

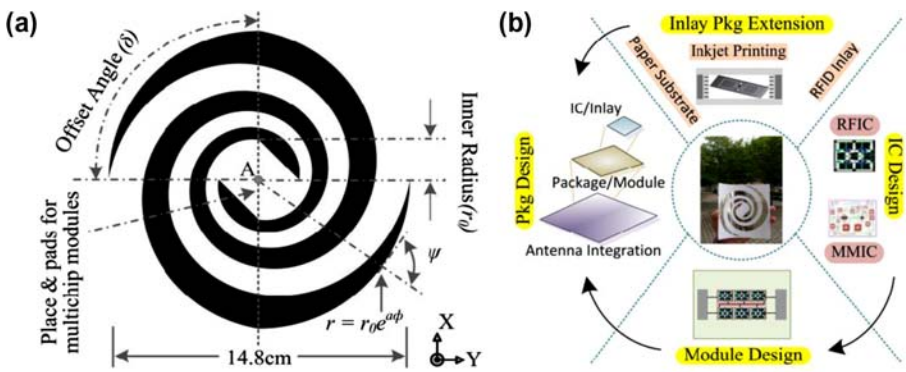

Figure 1. (a) Dimensions and (b) integration process of proposed antenna.

where expansion ratio (τ) is defined to be less than 1. The second arm of the proposed log-spiral antenna is obtained by rotating the first arm by 180° around the starting point A. The constant r_0 in Equation (1) can be resolute from the initial value of ϕ, which is arbitrary. The planar structure is self-complementary when $\delta = 90°$, and Babinet's principle [13] leads to the conclusion that the input impedance is $60\pi\ \Omega$ for free space (with no dielectric loading), and independent frequency [14].

3. Manufacturing parametric analysis

The conductivity of the printed traces achieved after annealing by silver nano-particle based ink (CCI-300 from Cabot Corp.) is $\approx 0.9 \times 10^7$ S/m. This parameter is also considered during the design stage of the proposed antenna in order to eliminate the impact of skin depth effect, which can limit the RF performance [15]. In order to optimize the manufactured structure with respect to skin depth effect, three layers of ink are printed each of which is approximately 600 nm thick. Figure 1(b) explains the integration and development process encapsulating the proposed wireless tag. The proposed structure is optimized without enlarging the antenna's physical aperture. Thus, it is evident from the Left Hand Circular Polarization (LHCP) (Figure 2(a)) and Right Hand Circular Polarization (RHCP) (Figure 2(b)) gain of the proposed antenna that it exhibits improved performance among several other configurations endeavored to achieve an optimal design. Therefore, the optimal design pattern for working range from 0.8 to 3.0 GHz is realized with 1.25-turns and its current distribution plot is shown in Figure 2(c).

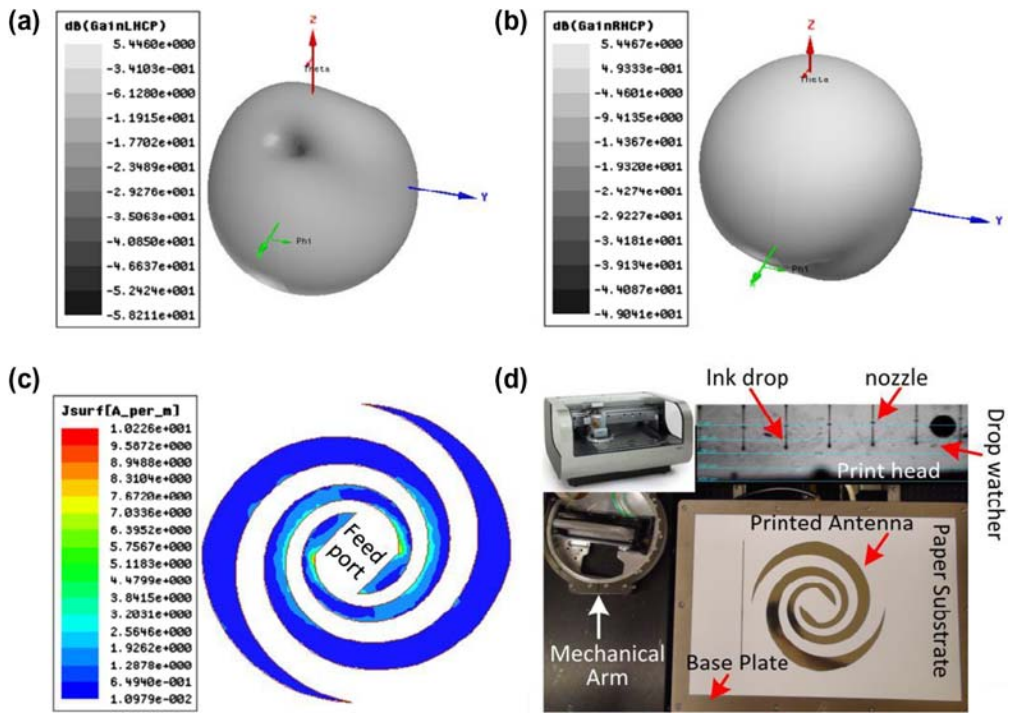

Figure 2. Simulated 3D gain: (a) LHCP, (b) RHCP, (c) current distribution at 1.9 GHz, and (d) inkjet printing setup and antenna printed on paper substrate.

In the small-scale electronics manufacturing industry, inkjet printing has proven to be more flexible, low-cost and more environmental friendly, than current manufacturing processes [16]. In this research, the inkjet printing showed in Figure 2(d) is carried out by utilizing the tabletop inkjet printer (DMP-2800) from Fujifilm Dimatix. Figure 2(d) also shows the drop watcher view of ink drops of 10 pl in volume that are ejecting out of the user fillable piezo-based DMC-11610 print cartridge. It is observed under appropriate curing conditions (150 °C/120 min, 120 °C/120 min, 110 °C/90 min for Kodak, HP and Felix paper, respectively), an almost solid metal conductor is formed.

4. Field and circuit concepts parametric analysis

A set of precise and thorough methods for analysis of the reliability parameters and characterization of the proposed fabricated antenna on different paper substrates is implemented. Firstly, five identical structures are printed on each paper substrate. The impedance is measured using *S*-parameter method (which is the most accurate method reported till data), in which the antenna is connected to the two ports of a vector network analyzer (VNA) through a test fixture [17,18].

The principle governing this method is shown in Figure 3(a), which shows a distinctive asymmetrical balanced dipole antenna, with two arms of different lengths and excited differentially. The positive and negative ports of the source with a voltage of V are connected to the input terminals of the radiators of the antenna, respectively. As showed in Figure 3(b), the driven voltage can be split as V_1 and V_2 with a virtual ground plane without any disturbance of the current distribution on the antenna. Hence, each terminal of the antenna radiators and the ground plane can be regarded as a "port," which is showed in Figure 3(c). The antenna can be equivalent to a "two-port" network, as showed in Figure 3(d). The impedance of the antenna is thusly associated to the network parameters of the corresponding two-port network, and can be characterized by measuring the network parameters such as *S*-parameters [17]. From Figure 3(d), the normalized impedance of the antenna can be expressed as follows:

$$\tilde{Z}_{\mathrm{d}} = \frac{V_{\mathrm{d}}}{I_0} = \frac{V_1 - V_2}{I_0} \tag{3}$$

Using the impedance matrix, the equations of a linear two ports (relating voltages and currents) are:

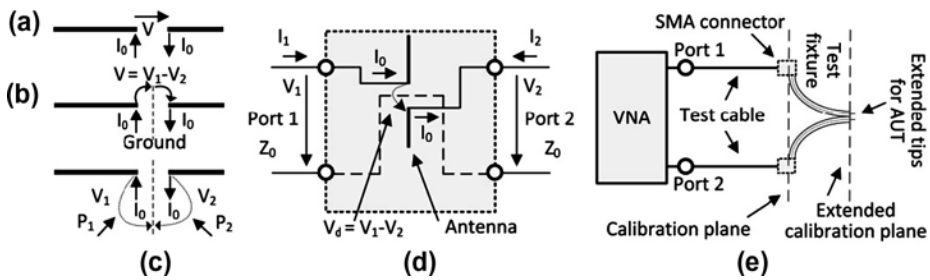

Figure 3. Asymmetrical balanced dipole antenna: (a) excitation, (b) virtual ground, (c) ports definition, (d) network representation of the asymmetrical dipole antenna, and (e) configuration of measurement setup.

$$V_1 = Z_{11}I_1 + Z_{12}I_2 \tag{4}$$

$$V_2 = Z_{21}I_1 + Z_{22}I_2 \tag{5}$$

If the two ports are driven by current source, i.e. $I_1 = I_0$ and $I_2 = -I_0$, the differential voltage V_d is given by:

$$V_{\mathrm{d}} = V_1 - V_2 = (Z_{11} - Z_{21} - Z_{12} + Z_{22})I \tag{6}$$

and the impedance is given by:

$$\tilde{Z}_{\mathrm{d}} = \frac{V_d}{I_0} = \frac{V_1 - V_2}{I_0} = (Z_{11} - Z_{21} - Z_{12} + Z_{22}) \tag{7}$$

Now by transforming the Z-parameters as a function of S-parameters and taking into account $Z_{\mathrm{d}} = Z_0 \cdot \tilde{Z}_{\mathrm{d}}$, we get:

$$Z_{\mathrm{d}} = \frac{2\ Z_0(1 - S_{11}S_{22} + S_{12}S_{21} - S_{12} - S_{21})}{(1 - S_{11})(1 - S_{22}) - S_{21}S_{12}} \tag{8}$$

where Z_0 is the reference impedance, which is mostly 50 Ω for measurement systems. Thus, in case of the symmetrical balanced antenna, where $S_{11} = S_{22}$ and $S_{12} = S_{21}$. By substituting these values in Equation (8), we get a simplified expression [17], which is as follows:

$$Z_{\mathrm{d}} = \frac{2\,Z_0(1 - S_{11}^2 + S_{21}^2 - 2S_{12})}{(1 - S_{11})^2 - S_{21}^2} \tag{9}$$

The constellation of the measurement system is illustrated in Figure 3(e). The measurement is carried out by using a two-port VNA (MS2026B, Anritsu) and a test fixture. The test fixture is constructed by using two semi-rigid coaxial cables having a length of 100 mm with an outer conductor diameter of 2.2 mm. The outer conductors of the coaxial cables are shorted by jointly soldering with the corresponding gap between the tips to accommodate between the two terminals of the antenna. One end of the fixture is with two SubMiniature version A (SMA) connectors, which is connected to the VNA through the test cables. The other end of the fixture is opened with the small extension (1.5 mm) of inner conductors in order to form the tips for connecting the antenna under test (AUT). Soft soldering is avoided to fix the AUT to the test fixture since it requires heating the filler metal above 250 °C to acquire proper soldering, but this temperature seriously damages the printed traces on paper substrates. Therefore, antenna is attached to the test fixture tips with CW2400 silver conductive epoxy, cured at 24 °C for 4 h for achieving maximum conductivity and adhesion.

The impedance graphs are presented in Figure 4 with the largest deviated value at a certain frequency which provides information for worst case analysis. As showed in Figure 4(a), the measured resistance for the antenna between 1.1 and 1.4 GHz fluctuates between 158 and 144 Ω and from 1.41 to 3.0 GHz, the variation of resistance is between 146 and 154 Ω but in much steady manner. However, exceptionally small deviation is pragmatic among the curves of all antennas and this behavior is stable over a much larger frequency range in accordance with the published results for spiral structures in [19]. The reactance part of the impedance, as showed in Figure 4(b), follows smaller positive values around 15 Ω with exceedingly

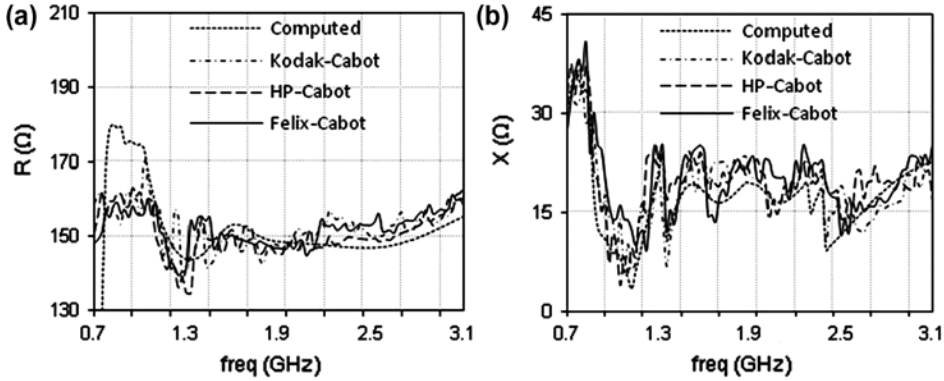

Figure 4. Input: (a) resistance variation and (b) reactance variation.

small variation with frequency. This performance relates to both frequency dependent and independent antennas to some extent. Moreover, relatively constant harmony exists between the computed and measured results.

The actual transformation between the unbalanced and the balanced mode is achieved by the balun which is exactly the same as well defined in [20], composed of the coplanar waveguide and the coplanar strip line which are only needed to connect the sender/receiver and the antenna. The balanced output from the balun is connected to the antenna using the balanced coplanar strip line. However, due to the additional complexity introduced by attaching the Balun using CW2400 and the feed line connecting to SMA, a slight offset/error and distortion is observed in the measured values. The measured return loss is showed along with computed values in Figure 5(a). It is clear that the proposed antenna has better return loss and is less than -15 dB throughout the frequency band of interest, which is the paramount necessity of antennas for optimal performance. Furthermore, the stable response of paper substrate at higher frequencies makes it a suitable candidate for broadband antennas. Overall, a good agreement among the computed and measured results is observed even though the silver-based conductive inks have higher metal loss.

The radiation pattern is measured inside an anechoic chamber setup that replicates absolute free space [16]. The measured normalized radiation patterns (of antenna printed on

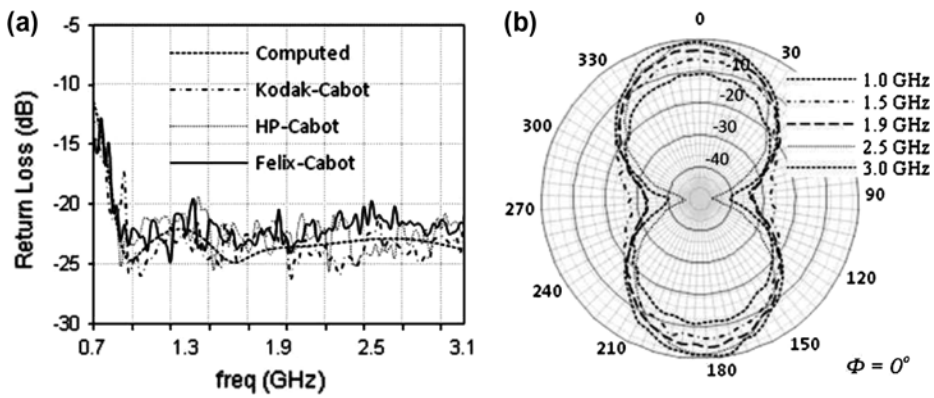

Figure 5. (a) Measured and computed return loss and (b) measured 2D far-field radiation plots.

Kodak photopaper) at characteristic frequencies of 1.0, 1.5, 1.9, 2.5, and 3.0 GHz are plotted in Figure 5(b). It is observed that all of the radiation patterns have normal shape and show extreme similarity between computations and measurements, which can also be verified for other frequencies within the antenna bandwidth and are in coherence with previously published results [19].

5. Conclusion

It is the first time the development and electromagnetic analysis of a log-spiral antenna printed on paper substrate are demonstrated to obtain affordable "green" tags. The wideband nature of the proposed antenna is exploited to accommodate several modules for sensing and wireless applications, in addition to an RFID tag. Future development is intended to optimize the design to provide additional modules within the same antenna size.

Acknowledgements

This work was financially supported by Vinnova (The Swedish Governmental Agency for Innovation Systems) through the Vinn Excellence centers program.

References

[1] Viani F, Salucci M, Robol F, Oliveri G, Massa A. Design of a UHF RFID/GPS fractal antenna tor logistics management. Journal of Electromagnetic Waves and Applications. 2012;26(4):480–92.
[2] Mohammad SR, Alyani I, Siti MS. Design and development of wireless communication transceiver to support RFID reader at UHF band. Journal of Electromagnetic Waves and Applications. 2010;24(14–15):2063–75.
[3] Lin D-B, Tang I-T, Wang C-C. UHF RFID H-shaped tag antenna using microstrip feed design on metallic objects. Journal of Electromagnetic Waves and Applications. 2011;25(13):1828–39.
[4] Lin D-B, Wang C-C, Chou J-H, Tang L-T. Novel UHF RFID loop antenna with interdigital coupled section on metallic objects. Journal of Electromagnetic Waves and Applications. 2012;26 (2–3):366–78.
[5] Tiang JJ, Islam MT, Misran N, Mandeep JS. Slot loaded circular microstrip antenna with meandered slits. Journal of Electromagnetic Waves and Applications. 2011;25(13):1851–62.
[6] Li X, Liao J, Yuan Y, Yu D. Eye-shaped segmented reader antenna for near-field UHF RFID applications. Progress in Electromagnetics Research. 2011;114:481–93.
[7] Xie K, Liu Y-M, Zhang H-L, Fu L-Z. Harvest the ambient AM broadcast radio energy for wireless sensors. Journal of Electromagnetic Wave and Applications. 2011;25(14–15):2054–65.
[8] Li Y, Sun S, Yang F, Jiang LJ. Design of dual-band slotted patch hybrid couplers based on PSO algorithm. Journal of Electromagnetic Waves and Applications. 2011;25(17–18):2409–19.
[9] Liao W-J, Chang S-H, Lee W-H. Beam scanning array using spatial diversity. Journal of Electromagnetic Waves and Applications. 2011;25(4):481–94.
[10] Hsu H-T, Kuo F-Y, Chang C-H. Application of quasi log-periodic antenna for UHF passive RFID tag design featuring constant power transmission coefficient over broadband operation. Journal of Electromagnetic Waves and Applications. 2010;24(5–6):575–86.
[11] Sun L, Huang Y-H, Li J-Y, Liu Q-Z. A wideband circularly polarized candy-like patch antenna. Journal of Electromagnetic Waves and Applications. 2011;25(8–9):1113–21.
[12] Li W-M, Jiao Y-C, Zhou L, Ni T. Compact dual-band circularly polarized monopole antenna. Journal of Electromagnetic Waves and Applications. 2011;25(14–15):2130–7.
[13] Balanis CA. Antenna theory. Hoboken (NJ): Wiley; 2005.
[14] Richard CJ. Antenna engineering handbook. New York (NY): McGraw-Hill; 1992.
[15] Silveira FEM, Lima JAS. Skin effect from extended irreversible thermodynamics perspective. Journal of Electromagnetic Waves and Applications. 2010;24(2–3):151–60.
[16] Amin Y, Chen Q, Tenhunen H, Zheng LR. Evolutionary versatile printable RFID antennas for "Green" electronics. Journal of Electromagnetic Waves and Applications. 2012;26(2–3):264–73.

[17] Qing X, Goh CK, Chen ZN. Impedance characterization of RFID tag antennas and application in tag co-design. IEEE Transactions on Microwave Theory and Techniques. 2009;57(5):1268–74.
[18] Kuo SK, Hsu JY, Hung YH. Analysis and design of an UHF RFID metal tag using magnetic composite material as substrate. Progress in Electromagnetics Research B. 2010;24:49–62.
[19] Chen T-K, Huff GH. Stripline-fed archimedean spiral antenna. IEEE Antennas and Wireless Propagation Letters. 2011;10:346–9.
[20] Thaysen J, Jakobsen K, Hansen JA. A wideband balun – how does it work? Applied Microwave and Wireless. 2000;12(10):40–50.

Paper IX–Two-Arm Sinuous Antenna for RFID Ubiquitous Sensors and Wireless Applications

Y. Amin, Q. Chen, L.-R. Zheng, and H. Tenhunen, *Journal of Electromagnetic Waves and Applications*, vol. 26, nos. 17-18, pp. 2365-2371, 11 Oct 2012

Available online at: http://www.tandfonline.com/10.1080/09205071.2012.734438

Journal of Electromagnetic Waves and Applications
Vol. 26, Nos. 17–18, December 2012, 2365–2371

Taylor & Francis
Taylor & Francis Group

Two-arm sinuous antenna for RFID ubiquitous sensors and wireless applications

Y. Amin*, Q. Chen, L.R. Zheng and H. Tenhunen

iPack VINN Excellence Center, Royal Institute of Technology (KTH), Stockholm, SE-16440, Sweden

(*Received 22 July 2012; accepted 18 September 2012*)

For the first time, two-arm planar sinuous antenna is demonstrated to realize the emerging concept of integrating RFID functionalities along with sensors and other wireless applications for "green" electronics. In-depth, parametric analysis is performed for the proposed antenna which is fabricated on a paper substrate using revolutionary inkjet printing technology to develop a system-level solution for ultra-low-cost mass production of multipurpose wireless tags in an approach that could be easily expanded to other microwave and wireless "cognition" applications. The proposed antenna exhibits excellent performance throughout several RFID ISM bands and for other wireless applications in its operational range from 0.8 to 3.0 GHz.

1. Introduction

Radio-frequency identification (RFID) is gaining a lot of influence as an effective method due to the growing demand [1] for reliable electronic identification systems [2,3], in view of the fact that it offers several advantages over conventional optical technologies such as barcodes in terms of range and non-line-of-sight operations [4]. There has been much research addressing the challenges to RFID adoption such as reducing transponder cost, standardizing RFID communication protocols, and implementing security measures [5,6]. In general, RFID can create a very low-cost integration platform of multifunctional capabilities [7]; thus an attractive research objective is to expand this well-developed infrastructure for wireless applications, which have an appetite for low-cost, robust, flexible, and reliable modules, for instance ubiquitous wireless sensing, navigation, broadcasting, and personal communication [8–10]. In order to accomplish these applications, separate antenna for each module to cover the corresponding frequency band is a common approach [11,12]. However, adaptation of this approach leads to higher manufacturing cost, weight, and the space required for installing such modules, and worst of all, it causes numerous electromagnetic compatibility issues which need to be addressed prior to deploying such solutions. Moreover, Flame Retardant 4 (FR-4) or Polyethylene Terepthalate (PET) is usually utilized in fabrication of prevailing RFID tags or wireless modules [13], which not only are nonbiodegradable but also have an adverse effect on economic factors involved in disposing off nonrecyclable waste.

In this paper, we propose a single wideband sinuous spiral antenna for simultaneously using in various applications, which not only reduces the cost and weight, but also decreases the electromagnetic intricacies. The ANSYS HFSS™ tool is used to design and simulate the proposed antenna, whereas the measurements are performed in an anechoic chamber

*Corresponding author. Email: ysar@kth.se

ISSN 0920-5071 print/ISSN 1569-3937 online

http://dx.doi.org/10.1080/09205071.2012.734438
http://www.tandfonline.com

Table 1. Substrates parameters used for design and fabrication.

Substrate	Thickness (μm)	Permittivity (ε_r)	Loss tangent
Kodak U-P Photopaper	250	3.3 (average)	0.077 (1 GHz @ 25 °C)
HP Adv. Photopaper	250	3.3 (average)	0.04 (1 GHz @ 25 °C)
Felix Schoeller Paper (p_e: smart)	250	3.2 (average)	0.077 (1 GHz @ 25 °C)

dedicated to antenna characterization. Comprehensive numerical and experimental analysis is presented from 0.8 to 3.0 GHz, for the proposed antenna, which exhibits exceptional performance. Paper material is one of the potential candidates that could make a breakthrough in the electronics world for its ultra-low cost and environmental friendly distinctiveness. The circular polarization of the proposed antenna, which is fabricated by utilizing an outstandingly efficient and extremely economical inkjet printing technology to print on commercially available paper substrates (Table 1), provides an optimal preference for future multimodule wireless tags with integrated RFID.

2. Antenna structure and design

Several design parameters of a two-arm sinuous-spiral antenna are optimized in a sense that RFID tag needs to be read in any orientation. The integrated wireless applications within the proposed multimodule tag require a wideband antenna element that offers the orthogonal senses of polarization. Simultaneous polarization ability such as vertical and horizontal or right and left circular from the same aperture with coincident phase centers is of particular significance [14]. The proposed design needs to be in accordance with the manufacturing constrains, because only a single side of paper substrate is available for full integration of modules alongside the antenna.

In designing a planar structure, the starting point for the evaluation process is set to attain an optimal structure with a self-complementary geometry. As explained in the past, self-complementary structures have better impedance and pattern properties than non-self-complementary ones [14]. Interestingly, for this particular type of indistinct phasing, self-complementary structure is not a good option if low axial ratio is required. In this study, numerous self-complementary two-arm sinuous structures are investigated by varying growth rate while maintaining a fixed radiating aperture size. In order to do this, the number of sinuous segments or cells of the antenna are varied. However, it is observed, there is no improvement in the axial ratio at the circularly polarized bands regardless of the geometry and growth rate. The axial ratio improvement is possible if one deviates away from the self-complementary principle. Thus, this is done by changing the variables α and δ in Equation (1) and the final optimized design achieved is shown in Figure 1.

In accordance with appropriate log-periodic practice, the sinuous curve is defined solely by angles and the growth rate (expansion ratio τ). As mentioned in Figure 1, the curve is a set of cells starting with cell 1 at the outer radius R_1 (the proposed structure has eight cells). R_p defines the outer radius of cell p, and α_p with τ_p determine the angular width and ratio of the inside-to-outside radius for each cell. The equation for the pth cell is provided by:

$$\phi = (-1)^p \alpha_p \sin\left(\frac{180 \ln(r/R_p)}{\ln \tau_p}\right) \quad R_{p+1} \le r \le R_p \tag{1}$$

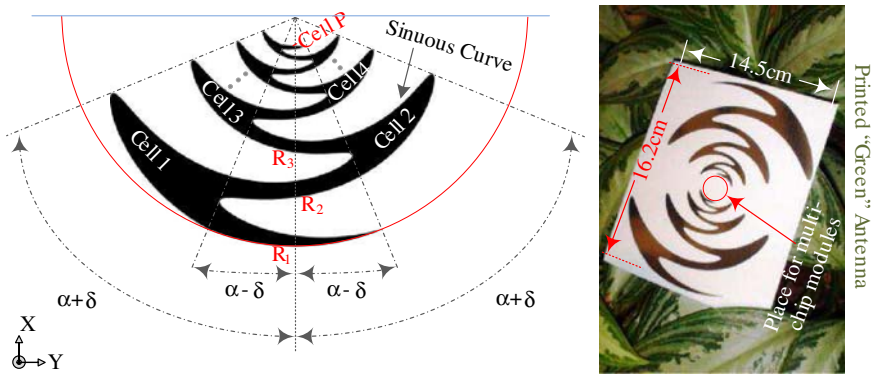

Figure 1. Design, dimensions and "green" theme of proposed antenna.

where r and ϕ are the polar coordinates of the curve. The radii R_p are related by:

$$R_p = \tau_{p-1} R_{p-1} \tag{2}$$

The design parameters τ_p and α_p may possibly be independent of p and log-periodic structure that is a periodic function of the logarithm of the radius r. The proposed structure in Figure 1 has α of 45° and angle δ is 22.5° with an outer radius of 8.4 cm. One sinuous arm of the proposed structure is formed by rotating the curve of Equation (1) by plus and minus an angle δ around the origin as shown in Figure 1. Thus, the complete aperture is developed by the angular rotation of the single arm through 180° increment to create a two-arm structure. The directly printable antenna proposed is intended for cardboard cartons level tagging, where size is not an issue but high performance with increased functionality at low cost is desired, so that valuable goods can be tracked in any orientation and transported safely.

3. Fabrication process

Figure 2(a) and (b) show the left hand circular polarization (LHCP) and right hand circular polarization (RHCP) gains of the proposed antenna, respectively. It is observed that the proposed structure exhibits better performance throughout the operational range from 0.8 to 3.0 GHz, than other configurations experienced to achieve this optimal design. Figure 2(c) shows the current distribution plot of the proposed antenna. Moreover, the projected structure is optimized without enlarging the antenna's physical aperture.

In contrast with etching, which is a subtractive process by removing undesirable metal from the surface of the substrate, inkjet printing jets the single ink droplet from the nozzle to the desired location, consequently, no waste is formed, ensuring an economical production solution. The ink used to fabricate the proposed antenna is sliver nano particle based CCI-300 manufactured by Cabot Corp. (USA), with a solid loading of about 19–21 wt.%, a viscosity of about 11–15 cP and a curing temperature of 100–350 °C according to the manufacturer. Prior to printing, the ink is degassed by placing in Bransonic 2510 ultrasonic cleaner for 5 min. Afterwards, the ink is injected into the fluid module of a user fillable DMC-11610, 10 pl piezoelectric drop-on-demand print-head cartridge with 16 nozzles. Droplet ejection and flight are optimized using the integrated stroboscopic drop-watching camera of the Fujifilm Dimatix DMP 2800 printer as shown in Figure 2(d).

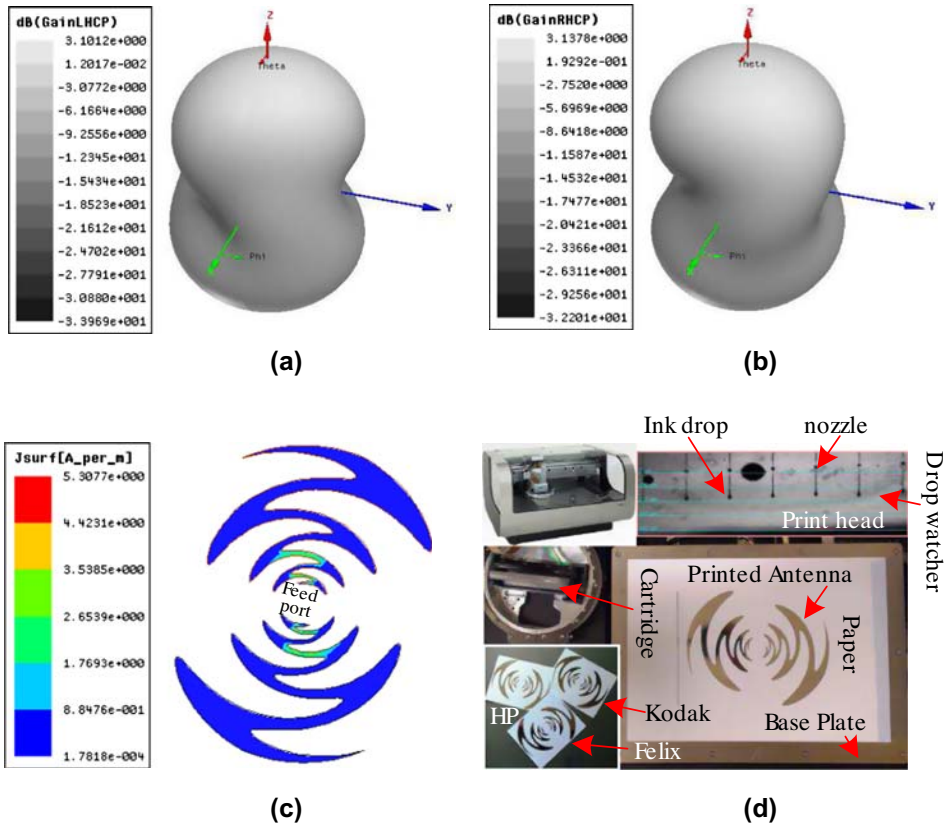

Figure 2. Simulated 3D gain: (a) LHCP, (b) RHCP; (c) current distribution at 1.9 GHz; and (d) inkjet printing setup and antennas printed on paper substrates.

The best printing parameters are achieved with a jetting frequency of 5 kHz and a meniscus set to 4 in. of H_2O. The voltages (18–21 V) is applied to the piezoelements of the print-head and are tuned to attain a velocity of 5 m/s. The print-head temperature is set to 40 °C and the substrate vacuum plate at 30–40 °C to avoid coffee ring effect [15]. The drop spacing is set to 20 μm to execute the print resolution of 1270 dpi, which resulted in smooth, printed edges. Considering the limits imposed by skin depth effect [16,17] for the frequency bands of interest, three layers of ink are printed, each of which is approximately 600 nm thick. The sintering/curing is carried out using high-tech ("PulseForge Technology" by Novacentrix USA) [18] in roll-to-roll sintering for mass-scale manufacturing, and the traditional method (oven with ventilation system) to estimate small-scale production. The optimal temperature/time observed for annealing are 150 °C/120 min, 120 °C/120 min, 110 °C/90 min for Kodak, HP, and Felix papers, respectively. The DC conductivity of $\approx 0.9 \times 10^7$ S/m of the printed pattern is attained after annealing which is measured by employing four-probe method and measurements carried out by profilometer. Hence, reasonably good conductivity is achieved by optimizing the printing procedure.

4. Results and discussion

An accurate and systematic approach is adopted for analysis of the reliability parameters and characterization of the proposed antenna manufactured on different paper substrates. As a first

step, five identical structures are printed on each paper substrate. For measurements, infinite balun (Dyson) feed [19] is used for excitation. A 1.2 mm flexible UTiFORM coaxial cable is fixed between the sinuous arms starting from the outside. Soft soldering is avoided to fix the UTiFORM coaxial cable since it needs heating the filler metal above 250 °C to attain proper soldering, but this temperature relentlessly damages the printed traces on paper substrates [20]. Consequently, cable is bonded to the test terminal with CW2400 silver conductive epoxy, cured at 24 °C for 4 h to gain maximum conductivity and adhesion. Furthermore, the bend radii of the coaxial turns are below the maximum tolerable value of 2.54 mm [21].

In order to execute worst-case analysis, impedance graphs in Figure 3 are plotted with the largest deviated values at a certain frequency. Therefore, rigorous information is looked into to achieve true understanding of reliability parameters, which have potential of variance due to the use of paper substrate. It is observed that by not having a self-complementary structure, the stability of the input impedance is deteriorated, as shown in Figure 3. The resistance of the proposed antenna shown in Figure 3(a) varies between 210 and 250 Ω throughout the frequency band of interest and exhibits consistent behavior. However, the antenna printed on Felix paper showed a higher degree of uncertainty between the two extremes and the antenna printed on Kodak paper followed more steady behavior. Nevertheless, exceptionally small variation is detected among the curves of all antennas and this behavior is stable over a much larger frequency range in coherence with the published results [22]. The reactance part of the impedance, as shown in Figure 3(b), follows positive values between 0 and 45 Ω with exceedingly small variation with frequency. Moreover, relatively constant agreement exists between the computed and measured results. Thus, such behavior of impedance corresponds to both frequency dependent and independent antennas to some degree, which is suitable for modern application-specific integrated circuit (ASIC) demands, where in most instances, chip impedance is frequency dependent.

In accordance with other log-periodic antennas, the center frequencies of the bands are directly linked to the geometric growth rate observed in Equation (1). This states that ratio of the adjacent band frequencies is equal to the growth rate. This observance is of greater importance when specific bands are targeted. It ought to be noteworthy that bands toward the low and high operating limits of the antenna will be affected due to the finite size of the aperture, and are slightly different from the growth rate. Analogous to the planar structure,

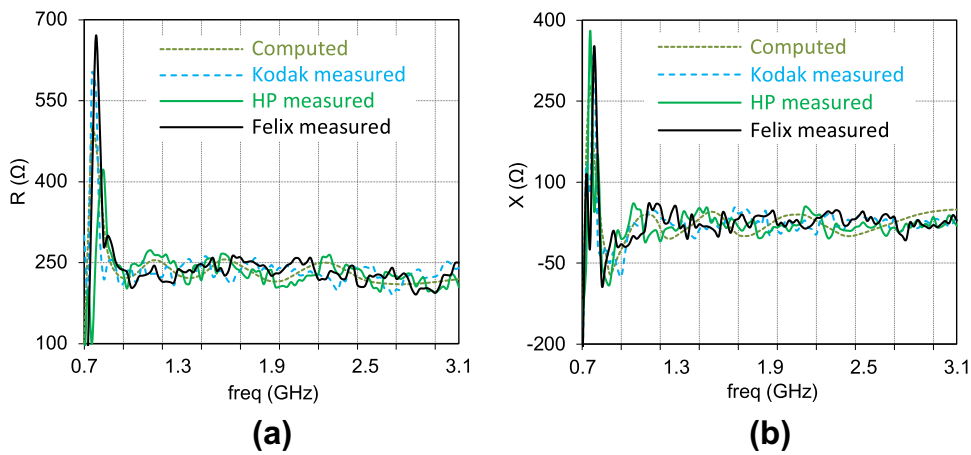

Figure 3. Input: (a) resistance variation and (b) reactance variation.

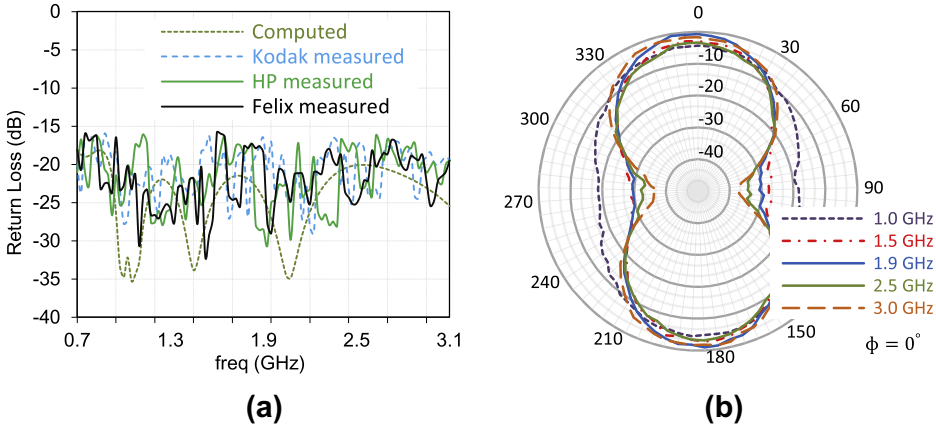

Figure 4. (a) Measured and computed return loss and (b) measured 2D far-field radiation plots.

the linearly polarized bands, are positioned between circularly polarized bands, and they have orientations which wobble about two orthogonal directions aligned with opposite tips of the sinuous segments. It is realistic to anticipate that the performance can be further enhanced by optimization [22]. The computed and measured return loss of the proposed geometry are presented in Figure 4(a). A good agreement is achieved between measurements and computations which are fairly coherent with published results [23]. The measured return loss of the sinuous antenna is below −15 dB from 0.8 to 3 GHz. The difference between computations and measurements is due to the difficulty to realize a perfect alignment of balun structure especially on extremely flexible paper substrate.

Moreover, the proposed antenna is capable of exhibiting extended read range under conjugately impedance matching conditions which also depend upon the ASIC used for RFID. The conjectural calculations after substituting measured values results into 15–16 m read range. The antenna exhibits high gain values on paper substrate (mentioned in Table 1) and above all, in direct contrast to most of the presently available RFID tags, its superior performance in any orientation makes it an ideal choice for transportation applications. The radiation patterns are measured inside an anechoic chamber, whose arrangement is mentioned in [17,20]. The measured normalized radiation patterns of antenna printed on Kodak photopaper at significant characteristic frequencies are plotted in Figure 4(b). The measured radiation patterns have extreme coherence with computed values and are in pursuant with previously published results [22] that validate the detection of proposed multifunctional wireless tag in any orientation.

5. Conclusion

The numerical analysis of a planar, non-self-complementary, two-arm sinuous antenna is presented. The antenna is manufactured on paper substrates utilizing inkjet printing technology to demonstrate the emergence of next generation of eco-friendly RFID tags, for ubiquitous sensing and wireless applications. Furthermore, the antenna exhibits superior impedance-matching capability, improved return loss, and wider bandwidths for all realized bands.

Acknowledgement

This work was financially supported by Vinnova (The Swedish Governmental Agency for Innovation Systems) through the Vinn Excellence centers program.

References

[1] Viani F, Salucci M, Robol F, Oliveri G, Massa A. Design of a UHF RFID/GPS fractal antenna tor logistics management. J. Electromagn. Waves Appl. 2012;26:480–492.

[2] Razalli MS, Mahdi MA, Ismail A, Shafie SM, Adam H. Design and development of wireless communication transceiver to support RFID reader at UHF band. J. Electromagn. Waves Appl. 2010;24:2063–2075.

[3] Lin D-B, Wang C-C, Chou J-H, Tang L-T. Novel UHF RFID loop antenna with interdigital coupled section on metallic objects. J. Electromagn. Waves Appl. 2012;26:366–378.

[4] Lin D-B, Tang I-T, Wang C-C. UHF RFID H-shaped tag antenna using microstrip feed design on metallic objects. J. Electromagn. Waves Appl. 2011;25:1828–1839.

[5] Amin Y, Chen Q, Tenhunen H, Zheng LR. Evolutionary versatile printable RFID antennas for "Green" electronics. J. Electromagn. Waves Appl. 2012;26:264–273.

[6] Krishna P, Husalc D. RFID infrastructure. IEEE M COM. 2007;45:4–10.

[7] Tiang JJ, Islam MT, Misran N, Mandeep JS. Slot loaded circular microstrip antenna with meandered slits. J. Electromagn. Waves Appl. 2011;25:1851–1862.

[8] Li X, Liao J, Yuan Y, Yu D. Eye-shaped segmented reader antenna for near-field UHF RFID applications. Prog. Electromagn. Res. 2011;114:481–493.

[9] Xie K, Liu Y-M, Zhang H-L, Fu L-Z. Harvest the ambient AM broadcast radio energy for wireless sensors. J. Electromagn. Waves Appl. 2011;25:2054–2065.

[10] Jamlos MFB, Tharek ARB, Kamarudin MRB, Saad P, Shamsudin MA, Dahlan AMM. A novel adaptive Wi-Fi system with RFID technology. Prog. Electromagn. Res. 2010;108:417–432.

[11] Liao W-J, Chang S-H, Lee W-H. Beam scanning array using spatial diversity. J. Electromagn. Waves Appl. 2011;25:481–494.

[12] Hsu H-T, Kuo F-Y, Chang C-H. Application of quasi log-periodic antenna for UHF passive RFID tag design featuring constant power transmission coefficient over broadband operation. J. Electromagn. Waves Appl. 2010; 24:575–586.

[13] Li W-M, Jiao Y-C, Zhou L, Ni T. Compact dual-band circularly polarized monopole antenna. J. Electromagn. Waves Appl. 2011;25:2130–2137.

[14] Richard CJ. Antenna engineering handbook. New York (NY): McGraw-Hill; 1992.

[15] Soltman D, Subramanian V. Inkjet-printed line morphologies and temperature control of the coffee ring effect. Langmuir. 2008;24:2224–2231.

[16] Silveira FEM, Lima JAS. Skin effect from extended irreversible thermodynamics perspective. J. Electromagn. Waves Appl. 2010;24:151–160.

[17] Amin Y, Chen Q, Zheng L-R, Tenhunen H. Development and analysis of flexible UHF RFID antennas for "green" electronics. Prog. Electromagn. Res. 2012;130:1–15.

[18] PulseForge Technology. Available from: www.novacentrix.com.

[19] Dyson J. The equiangular spiral antenna. IRE Trans. Antennas Propagation. 1959;7:181–187.

[20] Amin Y, Chen Q, Tenhunen H, Zheng L-R. Performance-optimized quadrate bowtie RFID antennas for cost-effective and eco-friendly industrial applications. Prog. Electromagn. Res. 2012;126:49–64.

[21] Technical Specification Micro-Coax, Hand-formable Coaxial Cable, UT-047-FORM. Available from: http://www.micro-coax.com

[22] Buck MC, Filipovic DS. Two-arm sinuous antennas. IEEE Trans. Antennas Propagation. 2008;56:1229–1235.

[23] Manna A, Baldonero P, Trotta F. Novel UWB low-profile sinuous slot antenna. In: Proceedings of the 5th European Conference on Antennas and Propagation (EUCAP); 2011 Apr. p. 783–786.

Paper X–RFID Antenna Humidity Sensor Co-Design for USN Applications

Y. Amin, Y. Feng, Q. Chen, L.-R. Zheng, and H. Tenhunen, *IEICE Electronics Express*, submitted for publication, 2013

RFID antenna humidity sensor co-design for USN applications

Yasar Amin[a)], **Yi Feng, Qiang Chen, Li-Rong Zheng, and Hannu Tenhunen**
iPack VINN Excellence Center, Royal Institute of Technology (KTH)
Isafjordsgatn 39, Stockholm, SE-16440, Sweden

a) *ysar@kth.se*

Abstract: We demonstrate for the first time an RFID tag antenna which itself is humidity sensor and also provides calibration functionality. The antenna is comprised of T-matching network and horizontally meandered lines for impedance matching and reliable near-field communication. The novel contour design provides humidity sensing, and calibration functions whilst concurrently acts as a radiating element along with quadrangular capacitive tip-loading with covered middle portion for far-field communication. The inkjet printed prototypes of the antenna provide effective ambient humidity sensing while demonstrating stable RFID communication. The antenna has a compact size of 1.1 × 10.2cm for 902–928MHz band.

Keywords: RFID antenna, humidity sensor, sensor calibration, inkjet printing, flexible electronics

Classification: Microwave and millimeter wave devices, circuits, and systems

References

[1] H. Andersson, A. Manuilskiy, T. Unander, C. Lidenmark, S. Forsberg, and H.-E. Nilsson, "Inkjet printed silver nanoparticle humidity sensor with memory effect on paper," *IEEE Sensors Journal*, vol. 12, no. 6, pp. 1901–1905, June, 2012.

[2] V. Lakafosis, A. Rida, R. Vyas, Li Yang, S. Nikolaou, and M. M. Tentzeris, "Progress towards the first wireless sensor networks consisting of inkjet-printed, paper-based RFID-enabled sensor tags," *Proceedings of the IEEE*, vol. 98, no. 9, pp. 1601–1609, Sep. 2010.

[3] R. Bhattacharyya, C. Floerkemeier, and S. Sarma, "Low-cost, ubiquitous RFID-tag-antenna-based sensing," *Proceedings of the IEEE*, vol. 98, no. 9, pp. 1593–1600, Sep. 2010.

[4] S. Manzari, C. Occhiuzzi, S. Nawale, A. Catini, C. Di Natale, and G. Marrocco, "Humidity sensing by polymer-loaded UHF RFID antennas," *IEEE Sensors Journal*, vol. 12, no. 9, pp. 2851–2858, Sep. 2012.

1 Introduction

In the Internet-of-Things paradigm (IoT), selective information from any item of a certain value is on the network in one form or another. Radio frequency IDentification (RFID) and sensor network technologies are giving fuel to this evolving standard. RFID faces several critical challenges of cost, reliability and eco-friendliness when evaluating, planning and implementing it for most exciting unfolding era of Ubiquitous Sensor Networks (USN). However, the present sensor-enabled RFID solutions downgrade their effectiveness on account of extra cost [1] by employing additional components or materials [2, 3, 4] to achieve sensor module. Likewise, the vast fated implementation of sensor nodes demands a design with the capability of customizable calibration function in order to replicate it without additional costs.

This paper presents an RFID tag antenna with embedded functionality as a humidity sensor along with calibration options realized through distinctive structural properties. The proposed compact antenna is directly printed on commercially available paper substrate for realizing the eco-friendly and ultra-low cost USN module. The accumulative effect of humidity on electromagnetic properties of paper substrate and conductive pattern, which constitute the RFID tag is explored to determine the antenna performance under various operating humidity levels. The proposed antenna has extended read range, and wider operational bandwidth for catering the manufacturing disparities while at the same time provides an extra level of liberty for sensor calibration.

2 Antenna design and optimization

The preeminent step in paper substrate usage is to characterize its properties, which varies considerably among commercially available papers. The substrate adopted is HP advanced photopaper of 250μm thickness (250gm/m^2) with dielectric constant and loss tangent of 3.2 and 0.077 respectively, extracted by using ring resonators method. NXP UCODE G2XM RFID Alstrap is selected, for instance the goal IC impedance at 915MHz is 13.3–j122Ω is preferred. However, the principle of operation for the proposed antenna is not IC dependent. RFID radar cross section is important for reflecting passive tags. In this case, the RFID contains a resonating structure that reradiates when illuminated by the reader. The detectability of the tag depends on the RCS (or backscattered field) returned by the tag. The RFID reacts to the incident power density generated by the reader:

$$S = \frac{P_t G_{reader}}{4\pi r^2} \tag{1}$$

Here S is the power density in Watts/m^2, P_t is the total transmitted power by the reader, G_{reader} is the reader's antenna gain, and r is the distance between the reader and the RFID tag. If the tag's antenna has an effective aperture, A_e, its received power at the antenna terminals is then $P_a = SA_e$. This becomes the input power to the circuit powering the tag's circuit. Thus, one of the optimization factors is to achieve optimal antenna

effective aperture in contrast to previous approaches in which one dimensional methodology is adapted to simply improve the antenna gain. As we are impending towards eco-friendly tags, every drop of ink saved in manufacturing process plays a vital role. The reradiated power P_{re} due to P_a can then computed as:

$$P_{re} = KP_aG_{tag} = \frac{4R_a^2}{|Z_a + Z_c|} \cdot P_aG_{tag} \tag{2}$$

Where, G_{tag} is the tag's antenna gain and K is the ratio of reradiated to incident energy with $R_a = \Re\ (Z_a)$, where Z_a is the complex antenna input impedance.

It is observed that a short circuited tag $(Z_c = 0)$ reradiates 4 times more power than a conjugate matched one $(Z_a = Z_a^*)$. It is also noted that, in the case of conjugate matching, the tag absorbs and reradiates equal amounts of power. In general, the tag radar cross section, σ, is used to measure the radiation effectiveness. Specifically, in evaluating the RFID's effectiveness, the ratio of the returned to transmitted power is of interest.

$$\sigma = \frac{P_{re}}{S} = KA_eG_{tag} = \frac{\lambda^2 G_{tag}G_{reader}{R_a}^2}{\pi|Z_a + Z_c|^2}|\hat{p}_{reader} \cdot \hat{p}_{tag}|^2 \tag{3}$$

Here $\hat{p}_{reader}$ and $\hat{p}_{tag}$ refer to the corresponding antenna polarizations. Clearly, the tag antenna gain plays a major factor; therefore, several iterations are carried out to address this challenge for achieving an efficient tag antenna design as showed in Fig. (1).

3 Antenna as a sensor design

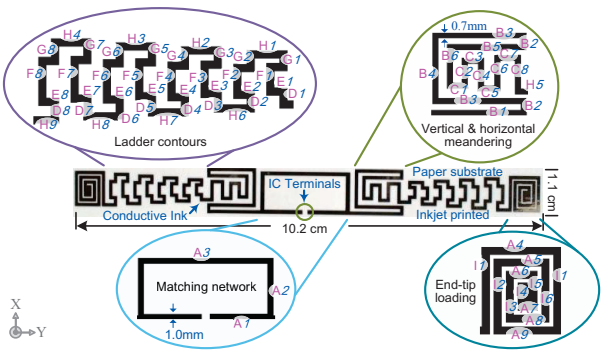

Fig. 1. Geometry of RFID sensor antenna.

In order to achieve humidity sensor, the proposed antenna has to demonstrate linear parametric changes in response to paper dielectric variations which in-turn corresponds to calibrated relative humidity levels. The main challenge at this stage is to realize an antenna structure which remains detectable in-spite of its parametric changes, which are eventually transformed

into sensor data. These limits motivated towards an antenna design, which has complex combination of five classifiable elements for providing stability as well as changeability in order to manifest sensory, and radiating characteristics simultaneously.

Table I. Antenna structural dimensions

(mm)	A	B	C	D	E	F	G	H	I
1	9.69	12.3	2.47	0.44	1.89	3.1	0.43	3.62	6.93
2	9.24	0.77	2.44	0.46	1.89	3.3	0.51	3.62	5.77
3	19.18	11.2	2.65	0.51	1.89	3.5	0.58	3.57	3.46
4	7.15	7.70	2.82	0.66	1.84	3.7	0.66	3.57	1.92
5	5.00	7.85	2.65	0.74	1.84	3.9	0.74	3.16	2.31
6	2.86	4.18	2.19	0.81	1.84	4.2	0.81	3.62	4.62
7	1.78		3.16	0.89	1.84	4.4	0.89	3.62	
8	3.93		3.56	0.97	1.84	4.6	0.97	3.57	
9	6.10							3.57	

The computer-aided design of the antenna is accomplished by using the commercial full-wave simulator ANSYS HFSS^{TM}. As showed in Fig. (1), the inner loop (composed of the series and shunt stubs) formed by T-matching network (*A1–A3*) is effective for stable near-field operation. It mainly optimizes and contributes to the input impedance matching in collaboration with progressive and horizontal meandering structures constituted by segments *B–C*. The novel progressive ladder contours formed by varying lengths of *D–H* segments, play the indispensable function of fine-tuning the slope of impedance curve in customizing the sensor calibration. It is discerned that the coupling between electromagnetic characteristics of the paper substrate and radiating elements is considerably aided by these contours. The coupling features and stabilized performance in the far-field region are likewise enhanced by quadrangular capacitive-tip loading, and the area of the middle plate structure by adjusting the length and spacing of segments from *A4–A9* & *I*. It is pragmatic, this added capacitance is approximately proportional to the perimeter of the loading shape rather than its area.

4 Fabrication process

The prototype antenna is directly printed on paper (Fig. 1) by using Fujifilm Dimatix DMP2800 tabletop printer by depositing silver nano particles based ink (CCI-300) by Cabot Corp., which has alcohol-based vehicle and contains 19-21% weight of nano-silver particles of less than 20nm diameter. This ink is selected due to the large ratio of the area to volume of its nano particles, which exhibit significantly lower melting point and provides stability against humidity effects. Each layer of printing at standard room conditions resulted in 600nm thickness; therefore, three layers are printed by considering skin depth effect and sheet resistance. After inkjet printing, a ventilated thermal oven sintering for two hours at 120°C provides a continuous metal conductor of around $9x10^6$ S/m conductivity, which is measured by deploying

Four Probe Method along with Profilometer measurements, thus providing a percolation channel for the conduction of electrons throughout the material without obstacles. The optimized dimensions of calibrated proposed antenna for measuring every 20% RH change are specified in Table I.

5 Experimental verification of antenna performance

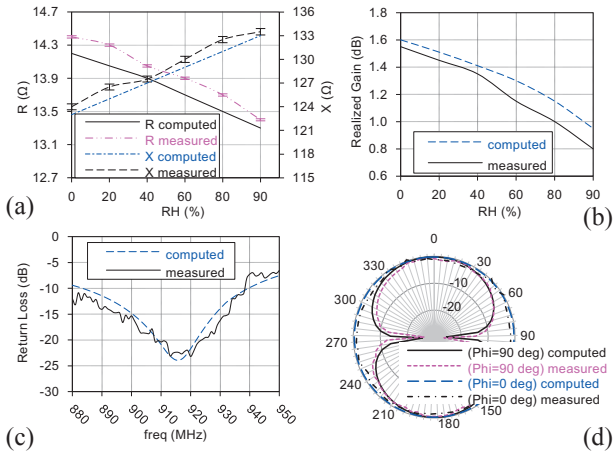

Fig. 2. (a) Resistance and reactance variation; (b) gain variation due to change in humidity level; (c) measured and computed return loss; (d) radiation patterns of RFID sensor antenna at 915MHz.

Firstly, the antenna's electromagnetic characteristics are measured standalone in an anechoic chamber setup in which impedance is measured by using S-parameter method (with SOLT calibration procedure), whereas the return loss and radiation patterns are measured by employing Half-Mirror method in combination with SOL calibration procedure for achieving elevated measurement accuracy. The near and far-field operational characteristics of the proposed RFID tag are verified using Impinj's UHF RFID reader kit. The effect of humidity variations on antenna parameters is characterized using climate chamber (Weiss Technik WK 11-180), and for validating results under normal room conditions, measurements are also carried out in the anechoic chamber by using humidifier and hygrometer while keeping the fixed distance between the RFID reader and the proposed sensor tag. The computed and measured impedance variations of the antenna in response to varying humidity levels are plotted in Fig. 2(a). The resistance and reactance show controlled linear behavior with overall 8% and 9% variation, respectively between two extremes. The measurements are repeated several times for extracting reliability parameters and validating the sensor functionality.

Furthermore, the calibration capability on the tag side in accordance with substrate for implementing self-effacing and more reliable procedures to for-

mulate the absolute humidity sensing system. The impedance variation with respect to relative humidity levels in-turn causes the variation in antenna gain, which is revealed in Fig. 2(b), and consequently, the backscattered power received while tag is placed in boresight of the RFID reader varies which is appropriately calibrated to ascertain the relative humidity (RH%) change. The antenna exhibits better return loss, which is larger than 15dB as showed in Fig. 2(c). The distortion is maybe due to the effect of metal ground fixture used for half-mirror method, and can be eliminated or significantly minimized by employing a metal plate with more rounded edges. Fig. 2(d) shows the normalized computed and measured 2D radiation patterns which are nearly uniform (omnidirectional) at 915MHz. Thus, a good agreement is pragmatic between the computations and measurements, which can similarly be substantiated for other frequencies within the antenna's bandwidth. The proposed sensor tag demonstrates extended portable read range of 11.1m and fixed 6.7m as a standalone RFID tag and with full humidity sensing functionality, respectively. Additionally, the gain and sensitivity against relative humidity level of the proposed antenna can be ameliorated by increasing the size depending upon particular industrial application.

6 Conclusion

An RFID tag antenna with incorporated humidity sensor characteristics, and has potential of customizable calibration, is designed, manufactured and validated. It is observed that paper type plays a pivotal role for response time in accordance with relative humidity level change. The integration of ink and paper substrate is critical for igniting the destabilization effect, which is utilized in a controlled mechanism by the structural configuration of the proposed antenna, and also inventively provides the effective calibration of the humidity sensor in accordance with defined desiderata. Likewise, the same phenomenon is achieved by using Kapton-HN as substrate which broadens the applicability of the proposed design. Furthermore, the proposed sensor-based RFID tag is eco-friendly, versatile and economical, thus making it well suited for realizing ubiquitous sensor networks.

Acknowledgments

This work was financially supported by Vinnova (The Swedish Governmental Agency for Innovation Systems) through the Vinn Excellence centers program.